Doctoral Dissertation

Control of Activity and Formation Mechanism of Non-Heme Iron(IV)-Oxo Complex

Yuma Morimoto

January 2013

Department of Material and Life Science

Graduate School of Engineering

Osaka University

Doctoral Dissertation

Control of Activity and Formation Mechanism of Non-Heme Iron(IV)-Oxo Complex

Yuma Morimoto

January 2013

Department of Material and Life Science

Graduate School of Engineering

Osaka University

Contents

General Introduction 1

Chapter 1. Crystal Structure of a Metal Ion-Bound Oxo-iron(IV) Complex and Implications for Biological Electron Transfer 16

Chapter 2. Metal Ion-Coupled Electron Transfer of a Nonheme Oxoiron(IV) Complex: Remarkable Enhancement of Electron-Transfer Rates by Sc^{3+} 40

Chapter 3. Mechanistic Borderline of One-Step Hydrogen Atom Transfer versus Stepwise Sc^{3+}-Coupled Electron Transfer from Benzyl Alcohol Derivatives to a Non-Heme Iron(IV)-Oxo Complex 59

Chapter 4. Proton-coupled electron transfer vs. metal ion-coupled electron transfer in electron-transfer reduction of an iron(IV)-oxo complex 96

Chapter 5. Effects of Proton Acceptors on Formation of a Non-Heme Iron(IV)-Oxo Complex via Proton-Coupled Electron Transfer 107

Chapter 6. Dioxygen Activation by a Non-Heme Iron(II) Complex: Formation of an Iron(IV)-Oxo Complex via C-H Activation by a Putative Iron(III)-Superoxo Species 126

Chapter 7. Autocatalytic radical chain pathway in formation of an iron(IV)-oxo complex by oxidation of an iron(II) complex with dioxygen and isopropanol 140

Concluding Remarks and Outlook 154

Publication List 157

Acknowledgment 161

General Introduction

The maintenance of our life, e.g. food and dioxygen and fossil fuels, depends upon the conversion of solar energy into chemical energy by biological photosynthesis, which has been performed by green plants and photosynthetic bacteria. In photosynthesis water and carbon dioxide are converted by using solar energy to dioxygen and carbohydrates that serve as food and fuel.[1–4] The process that requires solar energy in the photosynthesis is to take four electrons and four protons from water, which are used to reduce carbon dioxide to carbohydrates. The reverse process of the photosynthesis is the four-electron reduction of dioxygen with four protons to water, known as cellular respiration, which produce biochemical energy, adenosine triphosphate (ATP).[5–7] Because dioxygen is triplet in the ground state, the direct reaction of dioxygen with organic compounds is spin-forbidden. Thus, the four-electron reduction of dioxygen with four proton is only made possible by the spin-allowed electron-transfer reduction of dioxygen with transition metal complexes, which act as catalysts in cytochrome *c* oxidase.[5–7] There are metal-oxygen intermediates involved in the reduction of dioxygen as well as in the oxidation of water.[1–10]

Among many metal-oxygen intermediates, high-valent metal-oxo complexes play pivotal roles in both photosynthesis and respiration.[1–10] High-valent metal-oxo complexes are a collective term describing complexes with an unusually valences metal center from tetravalent to heptavalent coordinated by oxide ligand (O^{2-}), acting as strong electron acceptors as well as oxygen donors (Figure 1).[11] The biological water oxidation in the natural system is catalyzed by a $CaMn_4O_5(H_2O)_4$ cluster housed in the oxygen-evolving complex (OEC) in Photosystem II (PS II) (Figure 2a) where the Mn(V)-oxo intermediate oxidizes water.[1–4]

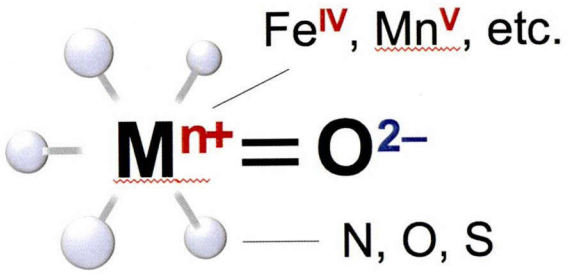

Key Features of High-Valent Metal-Oxo Complex

1. *Strong Electron Acceptor*
2. *Proton Acceptor*
3. *Oxygen Donor*

Figure 1. Structure of high-valent metal-oxo species.

Given broad fundamental interest and potential applications in artificial photosynthesis, the structure of this cluster and the mechanism of water oxidation to make dioxygen

have been the subject of extensive spectroscopic, computational, synthetic, crystallographic and biochemical studies.[10,12–16] However, the mechanism of dioxygen production is not well understood in particular with regard to the role of Ca^{2+} ion in the water oxidation although Ca^{2+} ion has been identified as an essential cofactor in water oxidation and the calcium-binding sites in PS II.[10,12–16] The synthesis of potentially biomimetic manganese oxide clusters as chemical models of the OEC has merited increasing attention.[17–22] The rational synthesis of a $[Mn_3CaO_4]^{6+}$ cubane that structurally models the trimanganese-calcium cubane subsite of the OEC5 has recently been reported by Agapie and coworkers (Figure 2b).[23] Structural and electrochemical comparison between Mn_3CaO_4 and a related Mn_4O_4 cubane alongside characterization of an intermediate calcium-manganese multinuclear complex has revealed potential roles of calcium in facilitating high oxidation states at manganese and in the assembly of the biological cluster.[23]

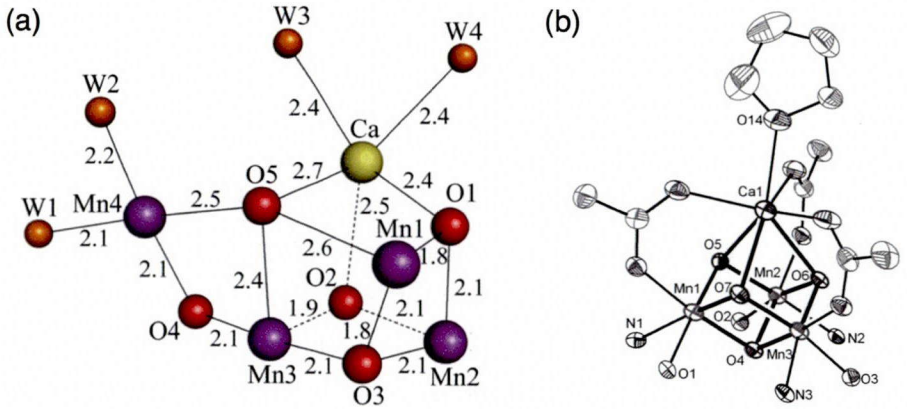

Figure 2. X-ray crystal structure of (a) the active site of OEC in PS II and (b) its structural model.

In the respiration, and an iron(IV)-oxo complex may be involved in the four-electron reduction of dioxygen in cytochrome *c* oxidase.[5–7] A catalytic cycle proposed using a model compound of cytochrome *c* oxygenases is shown in Scheme 1.[24] In the presence of acid, the Fe^{III}–O–Cu^{II} complex rapidly forms the Fe^{III}–Cu^{II} complex, releasing water and the catalytic cycle starts via a fast reduction of the heme and then the Cu to generate the reduced Fe^{II}–Cu^{I} complex. The O_2-binding in the next step is rate determining at room temperature. The Fe^{III}–O_2^{2-}–Cu^{II} complex thus generated undergoes a fast protonation to form the Fe^{III}–OOH^{-}–Cu^{II} complex. The O–O bond cleavage in the Fe^{III}–OOH complex upon the reduction by Fc with proton results in the four-electron reduction of O_2. However, the putative iron(IV)-oxo complex produced upon the O–O bond cleavage has yet to be identified.

Scheme 1. Catalytic Cycle for the Four-Electron Reduction of O_2 by a One-Electron Reductant (Fc: ferrocene) with a Cytochrome *c* Oxidase Model Compound.

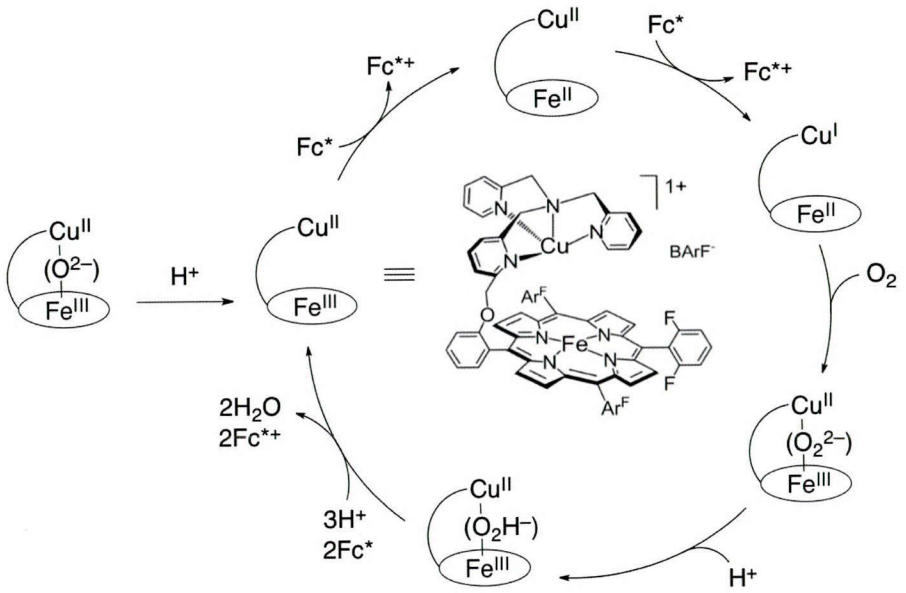

Nature also uses iron(IV)-oxo complexes in other essential transformations for metabolism of living organisms. For example, the cytochromes P450 are a versatile group of heme-based monooxygenases with vital functions for human health, including the biodegradation and metabolism of toxic compounds in the body as well as the biosynthesis of hormones.[25–29] They utilize dioxygen at a heme center with two electrons and two protons to produce high-valent iron-oxo intermediates, which are known as Compound I (Figure 3a) and Compound II.[25–29] Cytochrome P450 enzymes are found in broad spectrum of organisms, including bacteria, fungi, plants, insects, and mammals.[30]

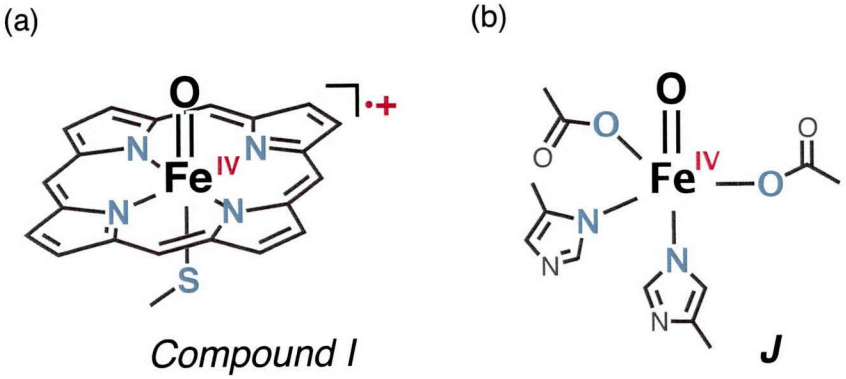

Figure 3. Structures of iron(IV)-oxo complexes served as active species of (a) cytochrome P450, Compound I and (b) taurine/α-ketoglutarate dioxygenase (TauD), **J**.

Meanwhile *Escherichia coli* which does not have P450 also utilize as a reactive species in their monooxygenases (Figure 3b) (vide infra). Compound I, which is iron(IV)-oxo porphyrin radical cation (Figure 3a), reacts via oxygen atom transfer to substrates (S), leading to C–H hydroxylation, C=C epoxidation, aromatic hydroxylation, and heteroatom oxidation.[25–29] The reaction mechanism to produce Compound I in the cytochrome P450 enzymes involves two distinct electron-transfer processes to activate oxygen (Scheme 2).[25–29] Compound I derived from horseradish peroxidase (HRP) has been produced by the reaction with H_2O_2 and well characterized.[30] On the other hand, the use of synthetic model systems has provided valuable mechanistic insight into the molecular catalytic mechanism of P450.[31–36]

Scheme 2. Catalytic cycle of Oxygenation Reaction Proceeds in P450

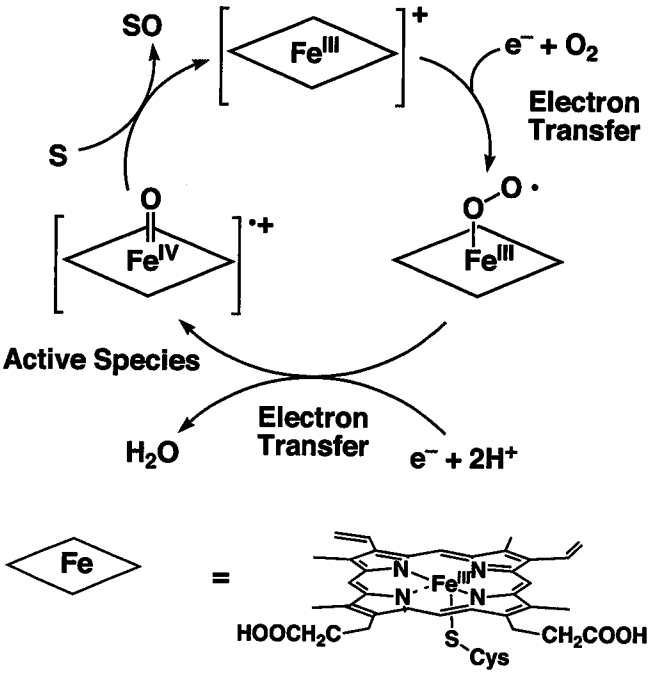

Mononuclear nonheme iron centers are also found in a superfamily of enzymes, that activate O_2 with two electrons and two protons to perform metabolically vital oxidative transformations like cytochromes P450.[37–40] Within the last ten years, iron(IV)-oxo intermediates have been characterized for taurine/α-ketoglutarate dioxygenase (TauD), prolyl 4-hydroxylase, and the halogenase CytC3, monoiron enzymes that require α-ketoglutarate as a cosubstrate. Enzymes requiring another electron donors for O_2 activation include the commonly used reductant NADH, tetrahydrobiopterin, and ascorbate are also though to have cycle through a common catalytic mechanism that involves formation of a substrate oxidizing oxoiron(IV) species, whereas some enzymes

such as the extradiol dioxygenases, isopenicillin *N*-synthase (IPNS), 4-hydroxymandelate synthase and (4-hydroxy-phenyl)pyruvate dioxygenase (HPPD), which effect distinct four-electron oxidations of their common substrate.[37–40] Most of these enzymes utilize an iron center coordinated to a 2-His-1-carboxylate facial triad motif to catalyze substrate oxidations, including alkyl/aromatic hydroxylation, alcohol oxidation, halogenation, desaturation/cyclization, and epoxidation (scheme 3).[37–40]

Scheme 3. Oxidation Reactions Proposed to Be Mediated by Iron(IV)-Oxo Intermediates in Non-heme Iron Enzymes.

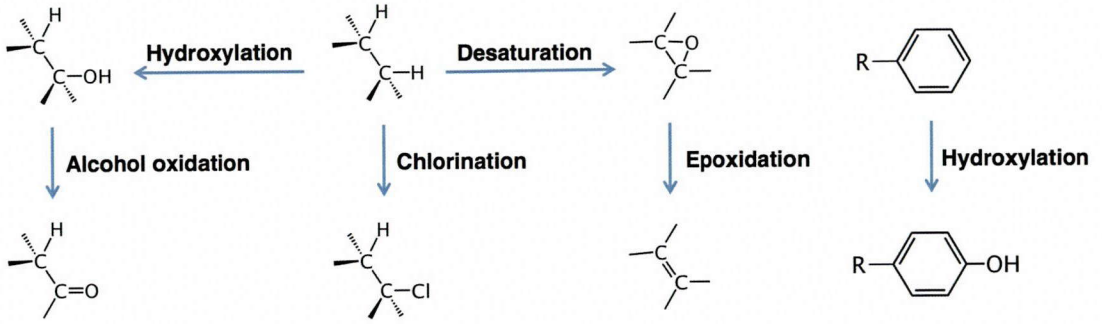

Figure 3b shows the structure of iron(IV)-oxo complex found in TauD in *Escherichia coli*. That is the first nonheme iron(IV)-oxo complex directly observed spectroscopically by Martin Bollinger, Jr., Carsten Krebs, and co-workers in 2003.[6b] An iron(IV)-oxo species is the oxidant most commonly postulated for these enzymes, while a *cis*-HO-iron(V)-oxo oxidant is proposed for the Rieske dioxygenases that catalyze *cis*-dihydroxylation of arene double bonds.[41] Extensive efforts have been devoted to synthesize these enzymatic model iron(IV)-oxo complexes.[38,42–44] The high-yield synthesis of $[Fe^{IV}(O)(TMC)(NCMe)]^{2+}$ (TMC = 1,4,8,11-tetramethyl-1,4,8,11-tetra-azacyclotetradecane)

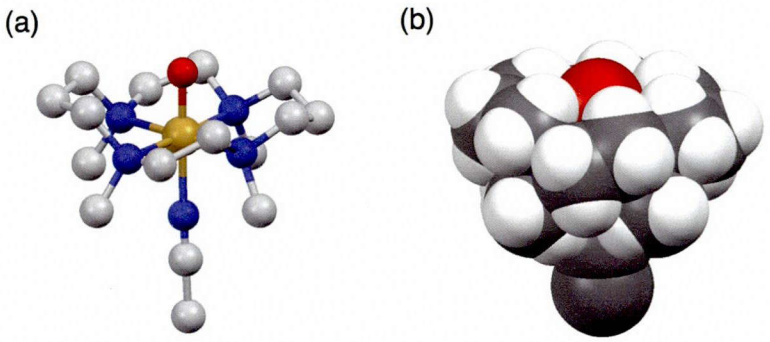

Figure 4. Crystal structure of $[Fe^{IV}(O)(TMC)(NCMe)]^{2+}$ (A: ball and stick; B space fill).

and the solution of its crystal structure (Figure 4) have been a significant breakthrough in nonheme Fe(IV)-oxo chemistry,[45a] allowing the detailed study of the reactivity of oxidation of a variety of substrates mimicking the enzymatic oxidation reactions.[38,42–44] Since the report of the crystal structure of $[Fe^{IV}(O)(TMC)(CH_3CN)]^{2+}$ in 2003, a handful of nonheme iron(IV)-oxo complexes have been synthesized in the past 10 years, using various tetradentate and pentadentate ligand systems, containing pyridine and amine nitrogen donors, and four of them are crystalized successfully.[42b] A nonheme iron(IV)-oxo complex with pentadentate ligand, $[Fe^{IV}(O)(N4Py)]^{2+}$ (N4Py: *N*,*N*-bis(2-pyridylmethyl)-*N*-bis(2-pyridyl)methylamine) is one of them, which have been studied as much as $[Fe^{IV}(O)(TMC)(CH_3CN)]^{2+}$ due to their stability and conciseness to generate iron(IV)-oxo complex under room temperature.[45b] These iron(IV)-oxo complexes are produced by the reactions of corresponding iron(II) complexes with iodosylbenzene (PhIO) in acetonitrile and unreacted redundant oxidant can be separated by simple filtration (Scheme 4).

With those iron(IV)-oxo complex, various types of oxidation reactions have been examined to understand fundamental reaction mechanisms performed by iron(IV)-oxo complex.[44] In parallel the electron-transfer properties of $[Fe^{IV}(O)(TMC)(NCMe)]^{2+}$, $[Fe^{IV}(O)(N4Py)]^{2+}$ and other iron(IV)-oxo complexes have been reported in relation with the hydride transfer reactions with NADH analogs.[46–49] Because electron transfer is the most fundamental chemical process, understanding of the electron-transfer properties of iron(IV)-oxo complexes provide valuable mechanistic insights

Scheme 4. Formations of (a) $[Fe^{IV}(O)(TMC)(NCMe)]^{2+}$ and (b) $[Fe^{IV}(O)(N4Py)]^{2+}$ by the reactions of $[Fe^{II}(TMC)(NCMe)_2]^{2+}$ and $[Fe^{II}(N4Py)(NCMe)]^{2+}$ with PhIO, respectively.

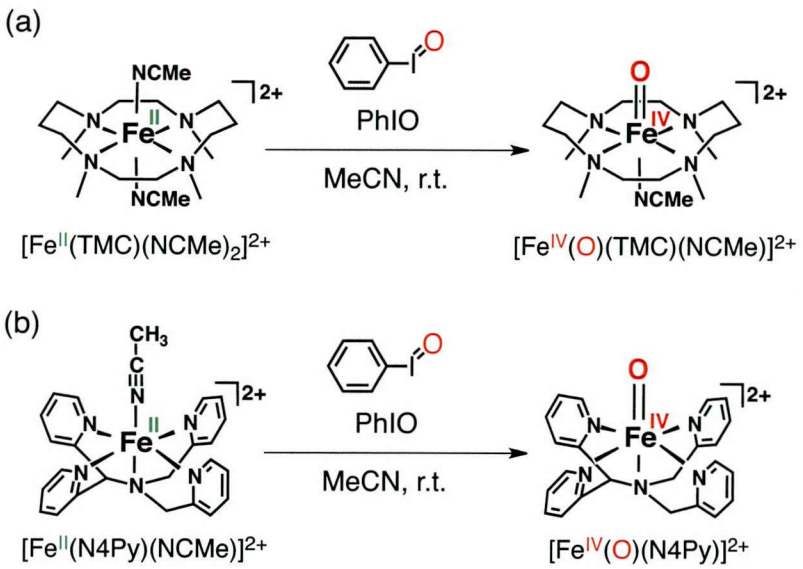

into a variety of oxidation reactions with iron(IV)-oxo complexes.[46,50]

In general, Lewis acid such as proton and metal ions play pivotal roles in controlling biological electron-transfer processes of coenzymes such as dihydronicotinamide adenine dinucleotide (NADH), flavins, quinones, in biological redox processes, particularly in photosynthesis and respiration.[50–59] Binding proton or redox inactive metal ions to electron acceptors results in a positive shift of the one-electron reduction potentials of electron acceptors, because the binding of metal ions to the one-electron reduced species, *i.e.*, the radical anions of electron acceptors, is stronger as compared to the electron acceptors due to stronger electrostatic interaction.[54–59]

Thus, endergonic electron transfer from electron donors (**D**) to electron acceptors (**A**) without metal ions has often been made possbile in the presence of Lewis acids by strong binding of Lewis acids to the radical anions ($\mathbf{A}^{\bullet-}$).[59–63] Such electron transfer involving metal ion binding is defined as proton-coupled electron transfer (PCET) and metal ion-coupled electron transfer (MCET).[55]

There are two types of mechanisms of PCET/MCET; (a) binding of Lewis acids (M^{n+}) to **A** followed by electron transfer from **D** to **A**–M^{n+} (MB/ET), (b) electron transfer from **D** to **A** followed by Lewis acids binding to $\mathbf{A}^{\bullet-}$ (ET/MB), and (c) Lewis acids binding to **A** and electron transfer from **D** to **A** occur in a concerted manner,[55] as shown in Scheme 5a, 5b, and 5c respectively.[50] PCET of high-valent metal-oxo species have been studied well with model complexes, in paticure ruthenium-oxo complex due to their stubility.[50] Watanabe *et al.* reported the effect of acidic amino acid regidues placed on the distal side of heme in HRP to enhance the oxidation power of compound I by the interaction between oxo moiety of compound I and proton (Figure 5a).[50]

Scheme 5. Mechanisms of Proton-Coupled Electron Transfer (PCET) and Metal Ion-Coupled Electron Transfer (MCET); (a) Lewis Acids Binding Followed by Electron Transfer (PT/ET or MB/ET), (b) Electron Transfer Followed by Lewis Acids Binding (ET/PT or ET/MB), and (c) Electron Transfer and Lewis Acids Binding to **A** Occurs in a Concerted Manner (CPET (Concerted Proton Electron Transfer) or CMET (Concerted Metal Ion-Coupled Electron Transfer))

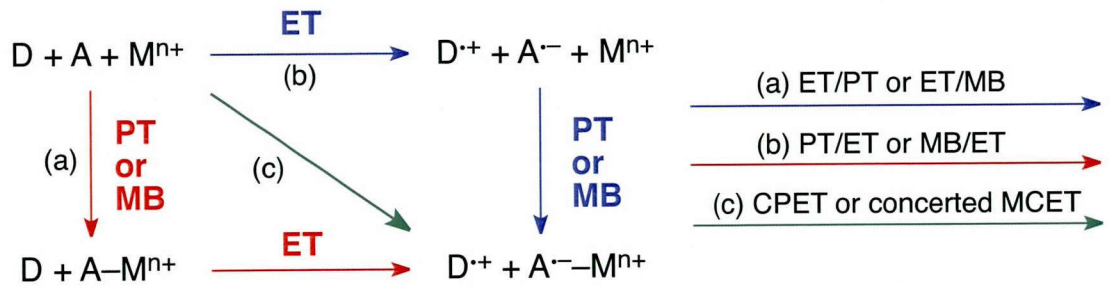

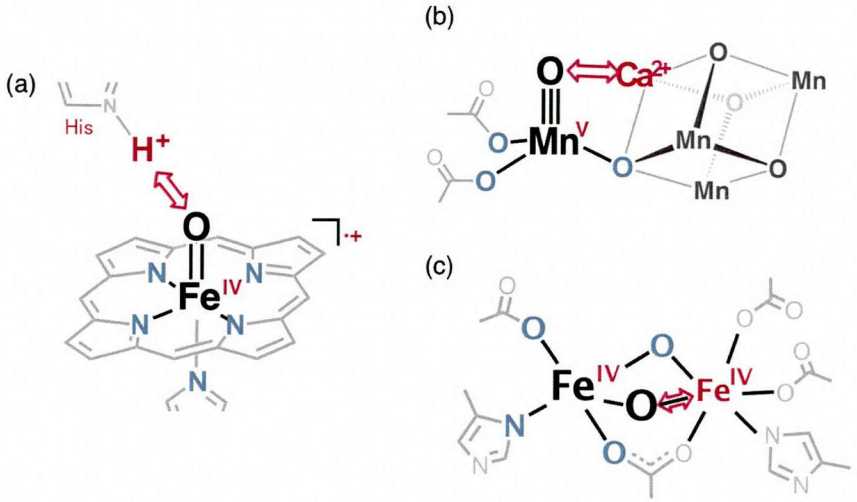

Figure 5. (a) Interaction between proton of histidine and iron(IV)-oxo moiety in compound I of HRP. (b) Interaction between calcium ion and manganese(V)-oxo moiety in S_4 state of OEC. (c) Interaction between iron(IV)-dimer core in **Q** state of MMO.

Despite metal ions enhance electron acceptobility of oxidant by binding as well as proton, however, no work forcused on the effect of metal ions. on the reactivity of high-valent metal-oxo complexes. For instance, effect of Ca^{2+} in the OEC in PS II which plays essencial role (vide supra) or dimerization of iron(IV) interacting each other via μ-oxo blidge that is observed in active species (intermediate **Q**) of soluble methane monooxygenase (sMMO), had yet to be explained clearly ever (Figure 5b, c). Thus, mechanisms of MCET of iron(IV)-oxo complexes in Scheme 3 had remained to be clarified. Another important problem that had yet to be clarified in iron(IV)-oxo chemistry was the mechanisms of formation of iron(IV)-oxo complexes via O_2 activation with two electrons and protons and also via proton-coupled electron transfer with H_2O.

From aforementioned points of view, the author has investigated i) reactivity control of iron(IV)-oxo complex with metal ions and proton via MCET and PCET and ii) environmental benign formation of iron(IV)-oxo complex via reductive activation of O_2 and also via oxidative activation of water (Scheme 5) without using active oxygen species such as PhIO and peracids. Model Compounds of active centers of non-heme iron enzymes employed in this thesis are iron(IV)-oxo complexes with TMC and N4Py as supporting ligands. The contents of this thesis consist of seven chapters (vide infra).

Scheme 5. Formation Pathways of High-Valent Metal-Oxo Complex

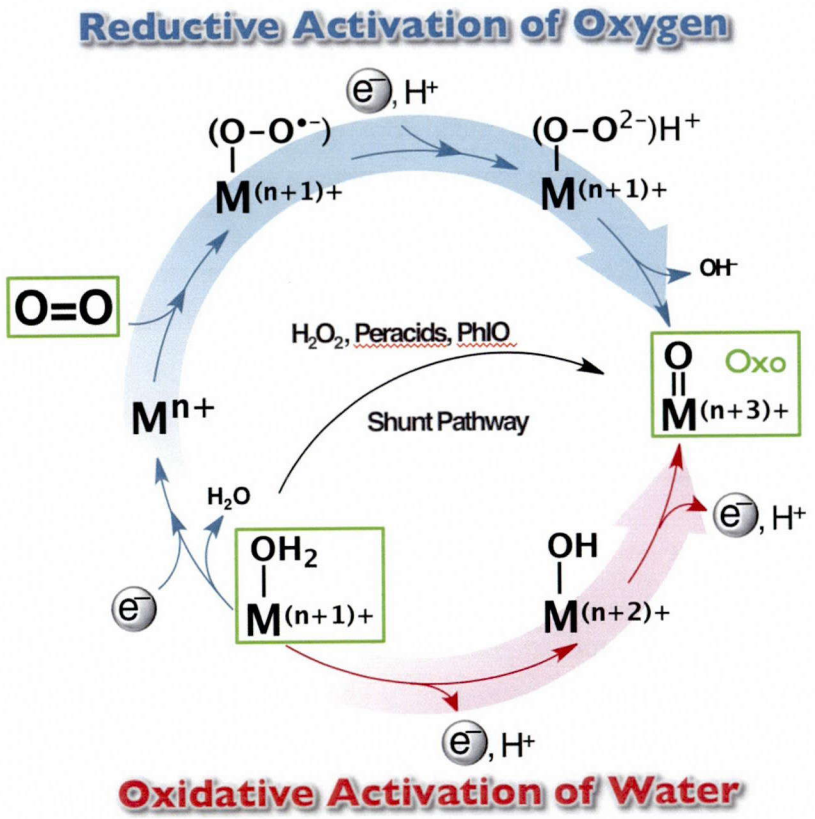

In chapter 1, the change in the redox properties of an iron(IV)-oxo complex by binding of metal ions acting as Lewis acid has been described by focusing on successful determination of the crystal structure of a novel $Fe^{IV}(O)$–Sc^{3+} complex in which the binding of Sc^{3+} resulted in distortion of the coordinating environment of the iron(IV) center.

In chapter 2, it is shown that mechanism of enhancement of electron acceptability of iron(IV)-oxo complex with metal-ion acting as Lewis acid is scrutinized by thermodynamic and kinetic studies. The electron-transfer reduction of iron(IV)-oxo complex is coupled with bond formation between iron(IV)-oxo and metal ions. Details of metal ion-coupled electron transfer (MCET) in high-valent metal-oxo complex chemistry are described in this chapter.

In chapter 3, it is shown that how the change in electron acceptability of the iron(IV)-oxo complex by metal-ions shown in chapter 2 affects the oxidation reactions of substrates including C–H bond dissociation processes. The changes in the reaction pathway and products depending of the oxidation potentials of substrates have been demonstrated to clarify the boundary between hydrogen atom transfer and MCET pathways.

In chapter 4, the author focused on the effects of proton vs metal ions on the electron acceptability of an iron(IV)-oxo complex. Proton-coupled electron transfer (PCET) is ubiquitous event seen in a wide rage of chemistry fields. However, there is no example showing the quantitative comparison between PCET and MCET processes. Here, the acceleration effects of proton or metal ions on the electron-transfer reduction of an iron(IV)-oxo complex are well correlated with a quantitative measure of acidity of metal ions and Brønsted acids.

In chapter 5, the acceleration effect of Brønsted bases on formation reaction of an iron(IV)-oxo complex is shown in contrast to the Brønsted acid effect on the electron-transfer reduction of an iron(IV)-oxo complex in chapter 4. Consecutive oxidation of low-valent metal-aqua/hydroxo complexes discharging proton producing high-valent metal-oxo species may also be accelerated by Brønsted bases in OEC in PS II.

In chapter 6, it is described that hydrogen abstraction from olefin by an iron(III)-superoxo complex is the key reaction in formation reaction of an iron(IV)-oxo complex from an iron(II) and oxygen in the presence of hydrogen donor. This is the first time to demonstrate oxygen activation with a non-heme iron(II) complex in the presence of hydrogen donors to produce iron(IV)-oxo complex.

In chapter 7, it is demonstrated that an iron(IV)-oxo complex is able to start autocatalytic radical chain reactions by abstracting hydrogen from a substrate to produce hydrogen peroxide catalytically in the presence of O_2. The iron(IV)-oxo complex is formed autocatalytically by the reaction between iron(II) complex and hydrogen peroxide produced in the radical chain reactions.

References

(1) Hoff A. J.; Deisenhofer, J. *Phys. Rep.* **1997**, *287*, 1. (b) Blankenship, R. E.; Madigan, M. T.; Bauer, C. E., Eds.; *Anoxygenic Photosynthetic Bacteria*; Kluwer Academic Publishers: Dordrecht, The Netherlands, 1995.

(2) (a) Woodrow, I. R.; Berry, J. A. *Annu. Rev. Plant Physiol. Plant Mol. Biol.* **1988**, *39*, 533. (b) Brugnoli, E.; Farquhar, G. D. *Adv. Photosynth.* **2000**, *9*, 399.

(3) Conlan, B.; Hillier, W.; Wydrzynski, T. *Engineering model proteins for Photosystem II function, Photosynth. Res.* **2007**, *94*, 225.

(4) (a) Barber, J. *Chem. Soc. Rev.* **2009**, *38*, 185. (a) Barber, J.; Murray, J. W. *Coord. Chem. Rev.* **2008**, *252*, 233. (c) Ferreira, K. N.; Iverson, T. M.; Maghlaoui, K.; Barber J.; Iwata, S. *Science* **2004**, *303*, 1831.

(5) (a) Pereira, M. M.; Santana, M.; Teixeira, M. *Biochim. Biophys. Acta* **2001**, *1505*, 185. (b) Winter, M.; Brodd, R. J. *Chem. Rev.* **2004**, *104*, 4245.

(6) (a) Ferguson-Miller, S.; Babcock, G. T. *Chem. Rev.* **1996**, *96*, 2889. (b) Hosler, J. P.; Ferguson-Miller, S.; Mills, D. A. *Annu. Rev. Biochem.* **2006**, *75*, 165. (c) Kaila, V. R. I.; Verkhovsky, M. I.; Wikström, M. *Chem. Rev.* **2010**, *110*, 7062.

(7) (a) von Ballmoos, C.; Lachmann, P.; Gennis, R. B.; Ädelroth, P.; Brzezinski, P. *Biochemistry* **2012**, *51*, 4507. (b) Belevich, I.; Verkhovsky, M. I. *Antioxid. Redox Signal.* **2008**, *10*, 1.

(8) Usharani, D.; Janardanan, D.; Li, C.; Shaik, S. *Acc. Chem. Res.* **2013**, in press.

(9) McAlpina, J. G.; Sticha, T. A.; Caseya, W. H.; Britt, R. D. *Coord. Chem. Rev.* **2012**, *256*, 2445.

(10) Najafpour, M. M.; Moghaddam, A. N.; Allakhverdiev, S. I.; Govindjee, *Biochim. Biophys. Acta* **2012**, *1817*, 1110.

(11) (a) Holm, R. H. *Chem. Rev.* **1987**, *87*, 1401. (b) Shilov, A. E.; Shul'pin, G. B. *Chem. Rev.* **1997**, *97*, 2879. (c) Balcells, D.; Clot, E.; Eisenstein, O. *Chem. Rev.* **2010**, *110*, 749. (d) Gunay, A.; Theopold, K. H. *Chem. Rev.* **2010**, *110*, 1060.

(12) (a) Aromi, G.; Brechin, E. K. *Struct. Bonding* **2006**, *122*, 1. (b) Bagai, R.; Christou, G. *Chem. Soc. Rev.* **2009**, *38*, 1011.

(13) (a) Mullins, C. S.; Pecoraro, V. L. *Coord. Chem. Rev.* **2008**, *252*, 416. (b) Iwata, S.; Barber, J. *Curr. Opin. Struct. Biol.* **2004**, *14*, 447.

(14) (a) Barber, J. *Philos. Trans. R. Soc. B* **2008**, *363*, 2665. (b) Barber, J. *Chem. Soc. Rev.* **2009**, *38*, 185. (c) Renger, G.; Renger. T. *Photosynth. Res.* **2008**, *98*, 53. (d) Nelson, N.; Ben-Shem, A. *Nat. Rev. Mol. Cell. Biol.* **2004**, *5*, 1.

(15) (a) Umena, Y.; Kawakami, K.; Shen, J.-R.; Kamiya, N. *Nature* **2011**, *473*, 55. (b) Kawakami, K.; Umena, Y.; Kamiya, N.; Shen, J.-R. *J. Photochem. Photobiol. B* **2011**, *104*, 9. (c) Kawakami, K.; Umena, Y.; Kamiya, N.; Shen, J.-R. *Proc. Natl. Acad. Sci. U.S.A.* **2009**, *106*, 8567. (d) Kamiya, N; Shen, J.-R. *Proc. Natl. Acad. Sci. U.S.A.* **2003**, *100*, 98. (e) Zouni, A.; Witt H.-T.; Kern J.; Fromme P.; Krauss N.; Saenger W.; Orth P. *Nature* **2001**, *409*, 739. (f) Ferreira, K. N.; Iverson, T. M.; Maghlaoui, K. Barber, J.; Iwata, S. *Science* **2004**, *303*, 1831. (g) Loll, B.; Kern, J.; Saenger, W.; Zouni, A. Biesiadka, J. *Nature* **2005**, *438*, 1040.

(16) (a) Yocum, C. F. *Biochim. Biophys. Acta* **1991**, *1059*, 1. (b) Boussac, A.; Rappaport, F.; Carrier, P.; Verbavatz, J.-M.; Gobin, R.; Kirilovsky, D.; Rutherford, A. W.; Sugiura, M. J. Biol. Chem. **2004**, *279*, 22809. (c) Lohmiller, T.; Cox, N.; Su, J.-H.; Messinger, J.; Lubitz, W. *J. Biol. Chem.* **2012**, *287*, 24721.

(17) (a) Dismukes, G. C.; Brimblecombe, R.; Felton, G. A. N.; Pryadun, R. S.; Sheats, J. E.; Spiccia, L.; Swiegers, G. F. *Acc. Chem. Res.* **2009**, *42*, 1935. (b) Mukherjee, S.;

Stull, J. A.; Yano, J.; Stamatatos, T. C.; Pringouri, K.; Stich, T. A.; Abboud, K. A.; Britt, R. D.; Yachandra, V. K.; Christou G. *Proc. Natl. Acad. Sci. U.S.A.* **2012**, *109*, 2257.

(18) Yagi, M.; Kaneko, M. *Chem. Rev.* **2001**, *101*, 21.

(19) (a) McEvoy, J. P.; Brudvig, G. W. *Chem. Rev.* **2006**, *106*, 4455. (b) Sproviero, E. M.; Gascon, J. A.; McEvoy, J. P.; Brudvig, G. W.; Batista, V. S. *J. Am. Chem. Soc.* **2008**, *130*, 3428. (c) Siegbahn, P. E. M. *Acc. Chem. Res.* **2009**, *42*, 1871. (d) Siegbahn, P. E. M. *Chem.–Eur. J.* **2006**, *12*, 9217. (e) Siegbahn, P. E. M. *Inorg. Chem.* **2008**, *47*, 1779. (f) Siegbahn, P. E. M. *Chem.–Eur. J.* **2008**, *14*, 8290.

(20) (a) Nayak, S.; Nayek, H. P.; Dehnen, S.; Powell, A. K.; Reedijk, J. *Dalton Trans.* **2011**, *40*, 2699. (b) Kotzabasaki, V.; Siczek, M.; Lis, T.; Milios, C. J. *Inorg. Chem. Commun.* **2011**, *14*, 213. (c) Koumousi, E. S.; Mukherjee, S.; Beavers, C. M.; Teat, S. J.; Christou, G.; Stamatatos, T. C. *Chem. Commun.* **2011**, *47*, 11128.

(21) Mukherjee, S.; Stull, J. A.; Yano, J.; Stamatatos, T. C.; Pringouri, K.; Stich, T. A.; Abboud, K. A.; Britt, R. D.; Yachandra, V. K.; Christou, G. *Proc. Natl. Acad. Sci. U.S.A.* **2012**, *109*, 2257.

(22) Lacy, D. C.; Park, Y. J.; Ziller, J. W.; Yano, J. Borovik, A. S. *J. Am. Chem. Soc.* **2012**, *134*, 17526.

(23) Kanady, J. S.; Tsui, E. Y.; Day, M. W.; Agapie, T. *Science* **2011**, *333*, 733.

(24) Halime, Z.; Kotani, H.; Li, Y.; Fukuzumi, S.; Karlin, K. D. *Proc. Natl. Acad. Sci. U.S.A.* **2011**, *108*, 13990.

(25) Groves, J. T. *Models and mechanisms of cytochrome P450 action*, in: Ortiz de Montellano, P. R. Ed.; *Cytochrome P450: Structure, Mechanism, and Biochemistry*; Kluwer Academic/Plenum Publishers: New York, 2005, p. 1.

(26) (a) Penner-Hahn, J. E.; Eble, K. S.; McMurry, T. J.; Renner, M.; Balch, A. L.; Groves, J. T.; Dawson, J. H.; Hodgson, K. O. *J. Am. Chem. Soc.* **1986**, *108*, 7819. (b) Green, M. T.; Dawson, J. H.; Gray, H. B. *Science* **2004**, *304*, 1653. (c) Rittle, J.; Green, M. T. *Science* **2011**, *330*, 933. (d) Dunford, H. B. *Heme Peroxidases*; Wiley-VCH: New York, 1999.

(27) Ortiz de Montellano, P. R., 2nd ed.; *Cytochrome P–450: Structure, Mechanism and Biochemistry*; Plenum Press: New York, 1995.

(28) (a) Schlichting, I.; Berendzen, J.; Chu, K.; Stock, A. M.; Maves, S. A.; Benson, D. E.; Sweet, R. M.; Ringe, D.; Petsko, G. A.; Sligar, S. G. *Science* **2000**, *287*, 1615. (b) Williams, P. A.; Cosme, J.; Ward, A.; Angove, H. C.; Vinkovic, D. M.; Jhoti, H. *Nature* **2003**, *424*, 464. (c) Denisov, L. G.; Makris, T. M.; Sligar, S. G.; Schlichting, L. *Chem. Rev.* **2005**, *105*, 2253.

(29) (a) Meunier, B.; de Visser, S. P.; Shaik, S. *Chem. Rev.* **2004**, *104*, 3947. (b) Shaik,

S.; Kumar, D.; de Visser, S. P.; Altun, A.; Thiel, W. *Chem. Rev.* **2005**, *105*, 2279. (c) Shaik, S.; Lai, W.; Chen, H.; Wang, Y. *Acc. Chem. Res.* **2010**, *43*, 1154. (d) Ortiz de Montellano, P. R. *Chem. Rev.* **2010**, *110*, 932.

(30) (a) Pérez, U.; Dunford, H. B. *Biochemistry* **1990**, *29*, 2757. (b) Pérez, U.; Dunford, H. B. *Biochim. Biophys. Acta* **1990**, *1038*, 98. (c) de Visser, S. P.; Shaik, S. Sharma, P. K. Kumar, D. Thiel, W. *J. Am. Chem. Soc.* **2003**, *125*, 15779.

(31) (a) Groves, J. T.; Han, Y.-Z. In *Cytochrome P–450: Structure, Mechanism and Biochemistry*; Ortiz de Montellano, P. R., 2nd ed.; Plenum Press: New York, 1995; pp 3–48. (b) McLain, J. L.; Lee, J.; Groves, J. T. In *Biomimetic Oxidations Catalyzed by Transition Metal Complexes*; Meunier, B., Ed.; Imperial College Press: London, 2000. pp 91–169. (c) Cooper, H. L. R.; Groves, J. T. *Arc. Biochem. Biophys.* **2010**, *507*, 111.

(32) (a) Mlodnika, T.; James, B. R. In *Metalloporphyrin Catalyzed Oxidations*; Montanari, F., Casella, L., Eds.; Kluwer: Netherland, 1994; p 121. (b) Che, C.-M.; Lo, V. K.-Y.; Zhou, C.-Y.; Huang, J.-S. *Coord. Chem. Rev.* **2011**, *40*, 1950.

(33) (a) Dolphin, D.; Traylor, T. G.; Xie, L.Y. *Acc. Chem. Res.* **1997**, *30*, 251. (b) Traylor, T. G. *Pure Appl. Chem.* **1991**, *63*, 265. (c) Ortiz de Montellano, P. R. *Acc. Chem. Res.* **1987**, *20*, 289. (d) Sono, M.; Roach, M. P.; Counlter, E. D.; Dawson, J. H. *Chem. Rev.* **1996**, *96*, 2841. (e) Bruice, T. C. *Acc. Chem. Res.* **1991**, *24*, 243. (f) Guengerich, F. P.; Macdonald, T. L. *Acc. Chem. Res.* **1984**, *17*, 9. (g) Bukowski, M. R.; Koehntop, K. D.; Stubna, A.; Bominaar, E. L.; Halfen, J. A.; Münck, E.; Nam, W.; Que, L., Jr. *Science* **2005**, *310*, 1000.

(34) (a) Meunier, B. *Chem. Rev.* **1992**, *92*, 1411. (b) Ostovic, D.; Bruice, T. C. *Acc. Chem. Res.* **1992**, *25*, 314. (c) Tabushi, I.; Koga, N. *J. Am. Chem. Soc.* **1979**, *101*, 6456. (d) Labat, G.; Meunier, B. *J. Org. Chem.* **1989**, *54*, 5008. (e) Katsuki, T. *J. Mol. Catal. A.* **1996**, *113*, 87.

(35) (a) Groves, J. T.; Nemo, T. E.; Myers, R. S. *J. Am. Chem. Soc.* **1979**, *101*, 1032. (b) Groves, J. T.; Kruper, W. J.; Haushalter, R. C. *J. Am. Chem. Soc.* **1980**, *102*, 6375. (c) Groves, J. T.; Kruper, W. J. *J. Am. Chem. Soc.* **1979**, *101*, 7613. (d) Groves, J. T.; Haushalter, R. C.; Nakamura, M.; Nemo, T. E.; Evans, B. J. *J. Am. Chem. Soc.* **1981**, *103*, 2884. (e) Groves, J. T.; Quinn, R. *J. Am. Chem. Soc.* **1985**, *107*, 5790.

(36) (a) Groves, J. T.; Watanabe, Y. *J. Am. Chem. Soc.* **1988**, *110*, 8443. (b) Czernuszewicz, R. S.; Su, Y. O.; Stern, M. K.; Macor, K. A.; Kim, D.; Groves, J. T.; Spiro, T. G. *J. Am. Chem. Soc.* **1988**, *110*, 4158. (c) Su, J.; Groves, J. T. *J. Am. Chem. Soc.* **2009**, *131*, 12979.

(37) (a) van Eldik, R. *Chem. Rev.* **2005**, *105*, 1917. (b) Krebs, C.; Fujimori, D. G.; Walsh, C. T.; Bollinger, J. M., Jr. *Acc. Chem. Res.* **2007**, *40*, 484. (c) Jin, Y.; Lipscomb, J. D. *J. Biol. Inorg. Chem.* **2001**, *6*, 717. (d) Nam, W. *Acc. Chem. Res.* **2007**, *40*, 465. (e) Galonić, D. P.; Barr, E. W.; Walsh, C. T.; Bollinger, J. M., Jr.; Krebs, C. *Nat. Chem. Biol.* **2007**, *3*, 113.

(38) McDonald, A. R.; Que, L., Jr., *Coord. Chem. Rev.* **2013**, *257*, 414.

(39) (a) Hegg, E. L.; Que, L., Jr. *Eur. J. Biochem.* **1997**, *250*, 625. (b) Que, L., Jr. *Nat. Struct. Biol.* **2000**, *7*, 182. (c) Koehntop, K. D.; Emerson, J. P.; Que, L., Jr. *J. Biol. Inorg. Chem.* **2005**, *10*, 87.

(40) (a) Solomon, E. I.; Brunold, T. C.; Davis, M. I.; Kemsley, J. N.; Lee, S.-K.; Lehnert, N.; Neese, F.; Skulan, A. J.; Yang, Y.-S.; Zhou, J. *Chem. Rev.* **2000**, *100*, 235. (b) Bruijnincx, P. C. A.; van Koten, G.; Gebbink, R. J. M. K. *Chem. Soc. Rev.* **2008**, *37*, 2716.

(41) (a) Wolfe, M. D.; Lipscomb, J. D. *J. Biol. Chem.* **2003**, *278*, 829. (b) Neibergall, M. B.; Stubna, A.; Mekmouche, Y.; Münck, E.; Lipscomb, J. D. *Biochemistry* **2007**, *46*, 8004.

(42) (a) Costas, M.; Mehn, M. P.; Jensen, M. P.; Que, L., Jr., *Chem. Rev.* **2004**, *104*, 939. (b) Hohenberger, J.; Ray, K.; Meyer, K. *Nat. Commun.* **2012**, *3*, 720.

(43) de Visser, S. P.; Rohde, J.-U.; Lee, Y.-M.; Cho, J.; Nam, W. *Coord. Chem. Rev.* **2013**, *257*, 381.

(44) Cho, J.; Sarangi, R.; Nam, W. *Acc. Chem. Res.* **2012**, *45*, 1321.

(45) (a) Rohde, J.-U.; In, J.-H.; Lim, M. H.; Brennessel, W. W.; Bukowski, M. R.; Stubna, A.; Münck, E.; Nam, W.; Que, L., Jr., *Science* **2003**, *299*, 1037. (b) Klinker, E. J.; Kaizer, J.; Brennessel, W. W.; Woodrum, N. L.; Cramer, C. J.; Que, L., Jr. *Angew. Chem., Int. Ed.* **2005**, *44*, 3690.

(46) Fukuzumi, S. *Coord. Chem. Rev.* **2013**, in press.

(47) Lee, Y.-M.; Kotani, H.; Suenobu, T.; Nam, W.; Fukuzumi, S. *J. Am. Chem. Soc.* **2008**, *130*, 434.

(48) Fukuzumi, S.; Kotani, H.; Suenobu, T.; Hong, S.; Lee, Y.-M.; Nam, W. *Chem.–Eur. J.* **2010**, *16*, 354.

(49) Comba, P; Fukuzumi, S.; Kotani, H.; Wunderlich, S. *Angew. Chem., Int. Ed.* **2010**, *49*, 2622.

(50) Fukuzumi, S.; Ohkubo, K.; Morimoto, Y. *Phys. Chem. Chem. Phys.* **2012**, *14*, 8472.

(51) Kaim, W.; Schwederski, B. *Bioinorganic Chemistry, Inorganic Elements in the Chemistry of Life*; John Wiley & Son: Chichester, 1994.

(52) Lu, Y.; Yeung, N.; Sieracki, N.; Marshall, N. M. *Nature* 2009, **460**, 855.

(53) Zastrow, M. L.; Peacock, A. F. A.; Stuckey, J. A.; Pecoraro, V. L. *Nature Chem.* **2012**, 4, 118.

(54) Fukuzumi, S.; Kojima, T. *J. Biol. Inorg. Chem.* **2008**, *13*, 321.

(55) Yocum, C. F. *Coord. Chem. Rev.* **2008**, *252*, 296.

(56) (a) Fukuzumi, S. *Prog. Inorg. Chem.* **2009**, *56*, 49. (b) Fukuzumi, S. *Bull. Chem. Soc. Jpn.* **1997**, *70*, 1.

(57) (c) Fukuzumi, S.; Ohkubo, K. *Coord. Chem. Rev.* **2010**, *254*, 372. (d) Fukuzumi, S. *Chem. Lett.* **2008**, *37*, 808.

(58) (a) Fukuzumi, S.; Ohtsu, H.; Ohkubo, K.; Itoh, S.; Imahori, H. *Coord. Chem. Rev.* **2002**, *226*, 71. (b) Fukuzumi, S.; Itoh, S. *Antioxid. Redox Signal.* **2001**, *3*, 807.

(59) (a) Fukuzumi, S. *Pure Appl. Chem.* **2003**, *75*, 577. (b) Fukuzumi, S. ; *Electron Transfer in Chemistry*, vol. 4, ed. V. Balzani; Wiley-VCH: Weinheim, Germany, 2001, pp. 3–59.

(60) (a) Fukuzumi, S.; Nishizawa, N.; Tanaka, T. *J. Chem. Soc. Perkin Trans. 2* **1985**, 371. (b) Fukuzumi, S.; Okamoto, T.; Otera, J. *J. Am. Chem. Soc.* **1994**, *116*, 5503.

(61) (a) Fukuzumi, S.; Fujii, Y. Suenobu, T. *J. Am. Chem. Soc.* **2001**, *123*, 10191. (b) Fukuzumi, S.; Ohkubo, K.; Okamoto, T. *J. Am. Chem. Soc.* **2002**, *124*, 14147. (c) Yuasa, J.; Suenobu, T.; Fukuzumi, S. *J. Am. Chem. Soc.* **2003**, *125*, 12090.

(62) (a) Fukuzumi, S.; Kuroda, S.; Tanaka, T. *J. Am. Chem. Soc.* **1985**, *107*, 3020. (b) Fukuzumi, S.; Okamoto, T. *J. Am. Chem. Soc.* **1993**, *115*, 11600.

(63) (a) Wu, H.; Zhanga, D.; Zhu, D. *Tetrahedron Lett.* **2007**, *48*, 8951. (b) Jia, L.; Zhang, G.; Zhang, D.; Xiang, J.; Xu, W.; Zhu, D. *Chem. Commun.* **2011**, *47*, 322. (c) Wu, H.; Zhang, D.; Su, L.; Ohkubo, K.; Zhang, C.; Yin, S.; Mao, L.; Shuai, Z.; Fukuzumi, S.; Zhu, D. *J. Am. Chem. Soc.* **2007**, *129*, 6839. (d) Wu, H.; Zhang, D.; Zhang, G.; Zhu, D. *J. Org. Chem.* **2008**, *73*, 4271.

Chapter 1. *Crystal Structure of a Metal Ion-Bound Oxoiron(IV) Complex and Implications for Biological Electron Transfer*

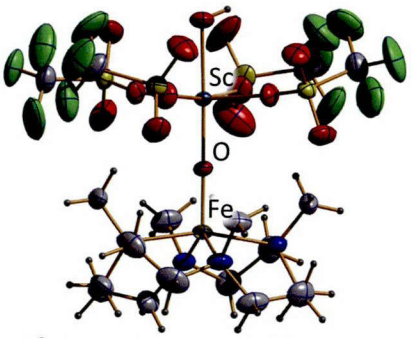

Sc^{3+}-Bound Oxoiron(IV) Complex

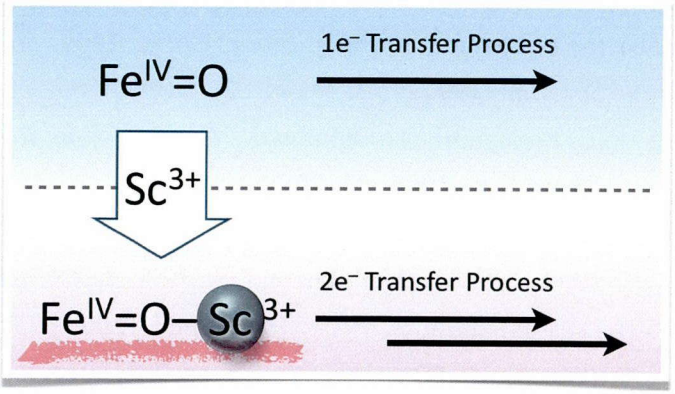

Abstract: Critical biological electron-transfer processes involving high-valent oxometal chemistry occur widely, such as in heme proteins [oxoiron(IV); $Fe^{IV}(O)$] and in photosystem II (PS II). The latter case involves Ca^{2+} together with high-valent oxomanganese cluster species. However, there is no example for an interaction between metal ions and oxoiron(IV) complexes. Here, the author report new findings concerning the binding of the redox-inactive metal ions, Ca^{2+} and Sc^{3+}, to a non-heme oxoiron(IV) complex, $[Fe^{IV}(O)(TMC)]^{2+}$ (TMC = 1,4,8,11-tetramethyl-1,4,8,11-tetraazacyclotetra-decane). As determined by an X-ray diffraction analysis, an oxo-Sc^{3+} interaction leads to a structural distortion of the oxoiron(IV) moiety. More importantly, this interaction facilitates a two-electron reduction by ferrocene, whereas only a one-electron reduction process occurs without the metal ions. This control of redox behavior provides valuable mechanistic insights into oxometal redox chemistry, and suggests a possible key role that an auxiliary Lewis acid metal ion could play in nature, as in PS II.

Introduction

Metal ions play pivotal roles in biological electron-transfer (ET) systems such as photosynthesis and respiration.[1–6] Oxoiron(IV) interactions occur widely in enzymes facilitating oxidative processes using molecular oxygen or hydrogen peroxide.[1–3] Another very important example is the oxygen-evolving complex (OEC) of photosystem II (PS II), where Ca^{2+} acts as an essential cofactor in the manganese-calcium (Mn_4Ca) active site responsible for the earth's molecular oxygen, via oxygen evolution in photosynthesis.[4–11] Although high-valent oxomanganese(V) species are considered as reactive intermediates in the O–O bond formation by the OEC of PS II, the exact functional role of Ca^{2+} remains elusive.[4–11] In biomimetic studies, a number of high-valent oxometal intermediates have been synthesized as chemical models of reactive intermediates that are involved in biological redox reactions.[12–16] However, the possible control of oxo-transfer or redox chemistry of high-valent oxometal intermediates by the binding of redox-inactive metal ions appears not to be known or to have been considered. On the other hand, redox-inactive metal ions such as Ca^{2+} are established to control the redox reactivity of organic electron acceptors by binding to the one-electron reduced species involved, i.e., radical anions of electron acceptors.[17–19]

The author report herein the first example of binding of metal ions, such as Sc^{3+} and Ca^{2+}, to a nonheme oxoiron(IV) complex, $[Fe^{IV}(O)(TMC)]^{2+}$ (TMC = 1,4,8,11-tetramethyl-1,4,8,11-tetra-azacyclotetradecane);[20] the crystal structure of Sc^{3+}-bound $[Fe^{IV}(O)(TMC)]^{2+}$ was determined by X-ray crystallography. The binding of Sc^{3+} to $[Fe^{IV}(O)(TMC)]^{2+}$ results in change in the number of electrons transferred from ferrocene (Fc) to the oxoiron complex: Two-electron reduction of $[Fe^{IV}(O)(TMC)]^{2+}$ by Fc occurs with Sc^{3+} binding, whereas only one-electron reduction of $[Fe^{IV}(O)(TMC)]^{2+}$ by Fc occurs in the absence of Sc^{3+}.[21] Such a change in the number of electrons by binding of metal ion to high-valent oxometal species provides valuable insight into the role of metal ion at the active site of the OEC.

Experimental Section

Materials. All solvents and chemicals were of reagent-grade quality, obtained commercially and used without further purification, unless otherwise noted. Solvents were dried according to published procedures and distilled under Ar prior to the use.[22] Iodosylbenzene (PhIO) was prepared from iodobenzene diacetate according to a literature procedure.[23] Scandium triflate [$Sc(OTf)_3$] (OTf = OSO_2CF_3) was purchased

from Aldrich and used as received. $[Fe^{II}(TMC)(NCMe)_2](OTf)_2$ and its oxoiron(IV) complex, $[Fe^{IV}(O)(TMC)(NCMe)]^{2+}$, were prepared by literature methods.[24]

Spectral Titration. Electron transfer from ferrocene to $[Fe^{IV}(O)(TMC)]^{2+}$ (0.10 mM) was examined from the spectral change in the presence of ferrocene (5.0 mM) with $Sc(OTf)_3$ (0–0.20 mM) at 298 K using a Hewlett Packard 8453 photodiode-array spectrophotometer with a quartz cuvette (path length = 10 mm). Typically, a deaerated MeCN solution of ferrocene (0.10 M) was added by means of a microsyringe to deaerated MeCN solution containing $[Fe^{IV}(O)(TMC)]^{2+}$ and $Sc(OTf)_3$. The concentration of ferrocenium ion (Fc^+) was determined from the absorption band at λ_{max} = 615 nm ($\varepsilon = 5 \times 10^2$ M^{-1} cm^{-1}).[25]

Kinetic Measurements. The kinetic measurements were performed on a Hewlett Packard 8453 photodiode-array spectrophotometer at 298 K. Rates of electron transfer from ferrocene derivatives to $[Fe^{IV}(O)(TMC)]^{2+}$ were monitored by the rise and decay of absorption bands due to ferrocenium ions and $[Fe^{IV}(O)(TMC)]^{2+}$ (λ_{max} = 820 nm). All kinetic measurements were carried out under pseudo-first-order conditions where the concentrations of ferrocene were maintained to be more than 20-folds excess of that of $[Fe^{IV}(O)(TMC)]^{2+}$.

Single Crystal Structure Determination. An MeCN solution of $Sc(OTf)_3$ was added to an MeCN solution of $[Fe^{IV}(O)(TMC)]^{2+}$. Single crystals of the compound were grown by the slow gas-liquid diffusion of pure diethyl ether into the MeCN solution of the complex at −15°C. Pale yellow single crystalline plate (235 × 210 × 55 mm) was cut and separated from a larger aggregate. After the crystallizing solution was soaked out, the crystal was quickly washed with diethyl ether, covered with Paratone-N, scooped with a cryoloop and mounted on the goniometer head. The single crystal X-ray diffraction data were collected with the oscillation method with resolution of up to 2Θ = 52° (truncated to the significant intensities of ≤ 50° later in the refinement) at room temperature, by exposures of 10 s for the lower resolution and 20 s for the higher resolution frames, in ω-scan mode. All data were collected before significant decay of the sample started to become apparent about five hours from the start, presumably as a result of partial desolvation. For the data collection, an APEX2 diffractometer (Bruker AXS) was employed,[26] using MoKa X-rays obtained from a rotating anode source, a confocal multilayer X-ray TXS mirror as monochromator, and a Peltier-cooled CCD as area detector. The integrated and scaled data[26] were empirically corrected for absorption effects with SADABS (m = 0.8 mm^{-1}).[27] The structure was solved by using direct

methods[28] and refined on F_o[27] with the SHELXL program.[29] All non-hydrogen atoms were treated anisotropically and the hydrogen atoms were included as riding bodies. The torsion angle of the hydrogen atom of the apical oxygen was refined freely, but the distance to the respective oxygen was constrained to 0.82 Å. All atoms of the triflate groups were found in the difference Fourier map. All four triflate groups are present as ions, and show the disorder typical for the increased oscillations/rotations usually observed in the structures of this ion (not treated), which necessitated application of three similarity restraints in the anisotropic atomic displacement parameters. The lattice MeCN molecule is approximately 1:1 disordered over two positions at the same site (the occupancy refined to 0.52:0.48), resulting in increased thermal displacement parameters and slight deviation of the three non-H atoms from colinearity. The distances of both solvent positions were constrained to 1.44 Å (C–C) and 1.10 Å (C–N).

Results and Discussion

Lee *et al.* have shown recently that electron transfer from one-electron reductants, such as Fc and its derivatives, to $[Fe^{IV}(O)(TMC)]^{2+}$ occurs in acetonitrile (MeCN), thereby producing ferrocenium cation (Fc^+) and $[Fe^{III}(O)(TMC)]^+$.[21] Interestingly, when the author carried out the electron-transfer reaction in the presence of Scandium triflate $[Sc(OTf)_3]$ (OTf = OSO_2CF_3), the author observed two-electron reduction of $[Fe^{IV}(O)(TMC)]^{2+}$ by Fc to give two equivalents of Fc^+ (see solid red line in Figure 1). The temporal profile of electron transfer from Fc to $[Fe^{IV}(O)(TMC)]^{2+}$ is shown in Figure 2, where one equivalent of Fc^+ is formed. By addition of Sc^{3+} to the resulting solution, the additional electron transfer occurs to produce one more equivalent of Fc^+ (see the arrow in Figure 2). When Sc^{3+} is present from the beginning, two equivalents of Fc^+ are formed as a one-step process in the two-electron reduction of $[Fe^{IV}(O)(TMC)]^{2+}$ by Fc (Figure 2). The two-electron reduction of $[Fe^{IV}(O)(TMC)]^{2+}$ by Fc was also observed in the presence of $Ca(OTf)_2$ and $Mg(ClO_4)_2$ (Figure 3). In this case, however, a large excess Ca^{2+} (4.0 mM) was required to complete the two-electron reduction of $[Fe^{IV}(O)(TMC)]^{2+}$ (0.10 mM), probably due to the lower Lewis acidity of Ca^{2+} relative to Sc^{3+} ion.[30,31]

The rate of formation of Fc^+ in the presence of Sc^{3+} obeys pseudo-first-order kinetics, and the pseudo-first-order rate constant (k_{obs}) increases linearly with increasing concentration of Fc (see Figure 4). The ET rate constant (k_{et}) was determined from the slope of the linear plot. The pseudo-first-order kinetics for the two-electron reduction of $[Fe^{IV}(O)(TMC)]^{2+}$

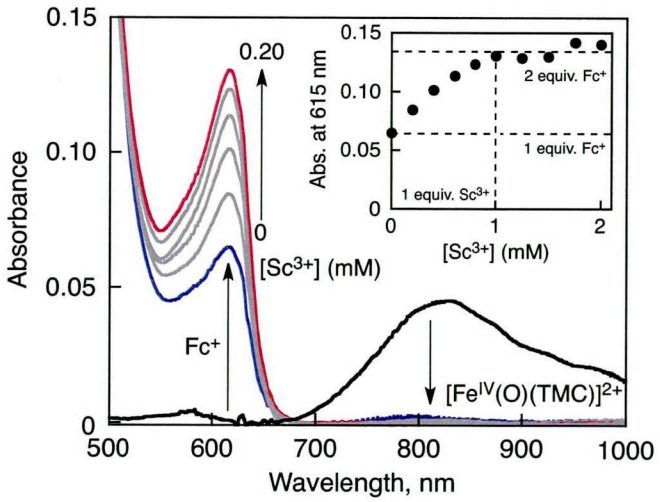

Figure 1. Spectral changes observed in electron transfer from Fc (5.0 mM) to $[Fe^{IV}(O)(TMC)]^{2+}$ (0.10 mM) in the presence of various concentrations of Sc^{3+} (0 mM; blue line, 0.02–0.08 mM; gray lines and 0.2 mM; red line) in MeCN. Inset: The titration curve shows a stoichiometry of $[Fc^{+}]$ with respect to $[Sc^{3+}]$.

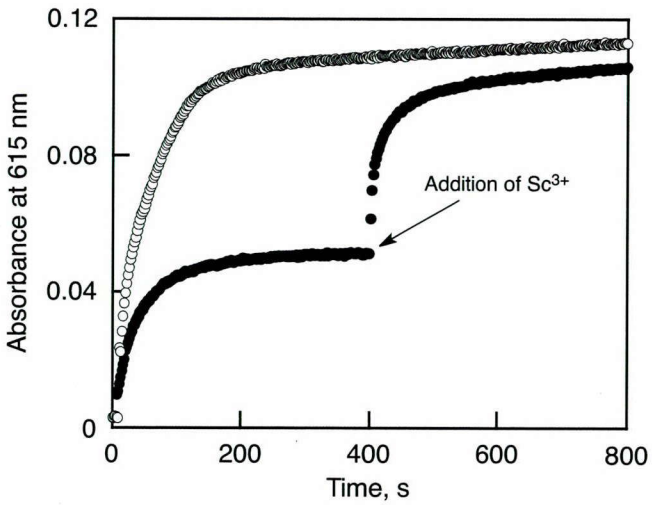

Figure 2. Time profiles of the absorption change at $\lambda = 615$ nm due to Fc^{+} observed in electron transfer from Fc (5.0 mM) to $[Fe^{IV}(O)(TMC)]^{2+}$ (0.10 mM) in a deaerated MeCN at 298 K. Sc^{3+} (0.20 mM) (closed circle) was added after the completion of the one-electron reduction of $[Fe^{IV}(O)(TMC)]^{2+}$ as the arrow indicated. Sc^{3+} (0.10 mM) (open circle) was added from the start of the reaction.

by Fc in the presence of Sc^{3+} indicates that the first electron transfer from Fc to $[Fe^{IV}(O)(TMC)]^{2+}$ is the rate-determining step, followed by the rapid second electron transfer from Fc to the $[Fe^{III}(O)(TMC)]^{+}/Sc^{3+}$ complex to produce one additional equivalent of Fc^{+} and $[Fe^{II}(O)(TMC)]/Sc^{3+}$.

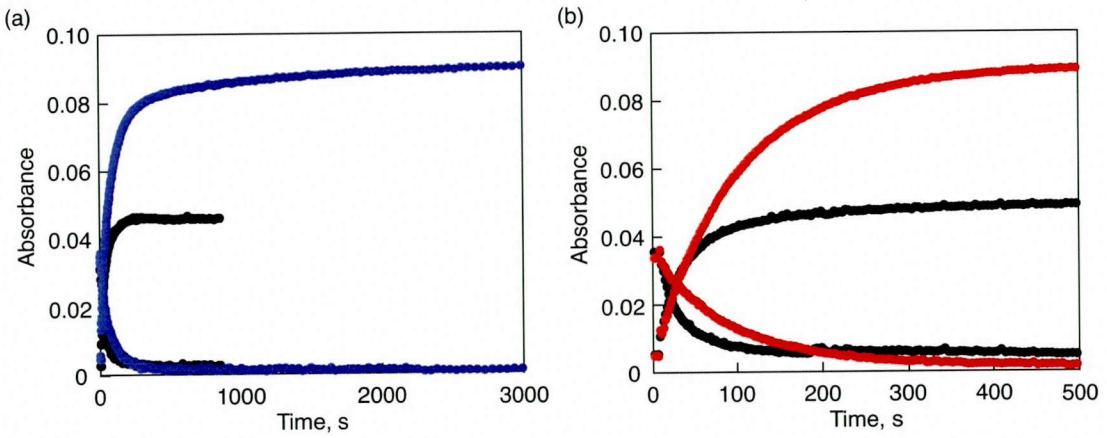

Figure 3. Time course of spectral change in the electron-transfer reaction from Fc (2.0 mM) to $[Fe^{IV}(O)(TMC)]^{2+}$ (0.1 mM) in the absence (black) and presence of (a) $Ca(OTf)_2$ (4.0 mM) (blue) and (b) $Mg(ClO_4)_2$ (20 mM) (red) in deaerated MeCN at 298 K.

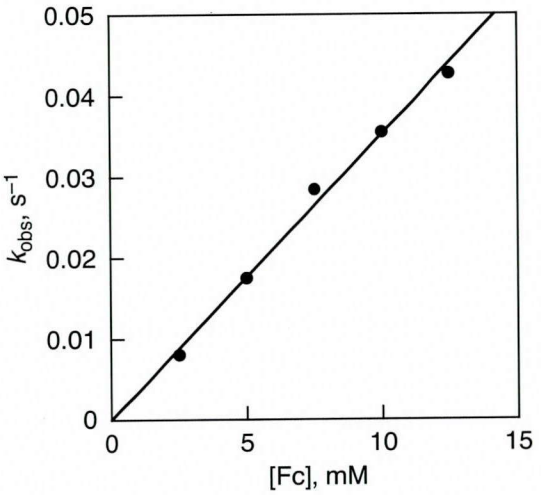

Figure 4. Plot of the pseudo-first-order rate constant (k_{obs}) *vs* [ferrocene] in electron transfer from Fc to $[Fe^{IV}(O)(TMC)]^{2+}$ (0.10 mM) in the presence of Sc^{3+} (0.10 mM) in MeCN at 298 K.

The author also found that the k_{et} value in the presence of Sc^{3+} is smaller than the value in the absence of Sc^{3+}, remaining constant at Sc^{3+} concentrations higher than one equivalent (Figure 5a). This may result from the larger reorganization energy of electron transfer associated with binding of Sc^{3+} to $[Fe^{IV}(O)(TMC)]^{2+}$. This conclusion is confirmed by measurements of the temperature dependence of k_{et} in the absence and presence of Sc^{3+}, which corresponds to activation enthalpies of 57 and 71 kJ mol^{-1}, respectively (Figure 5b).

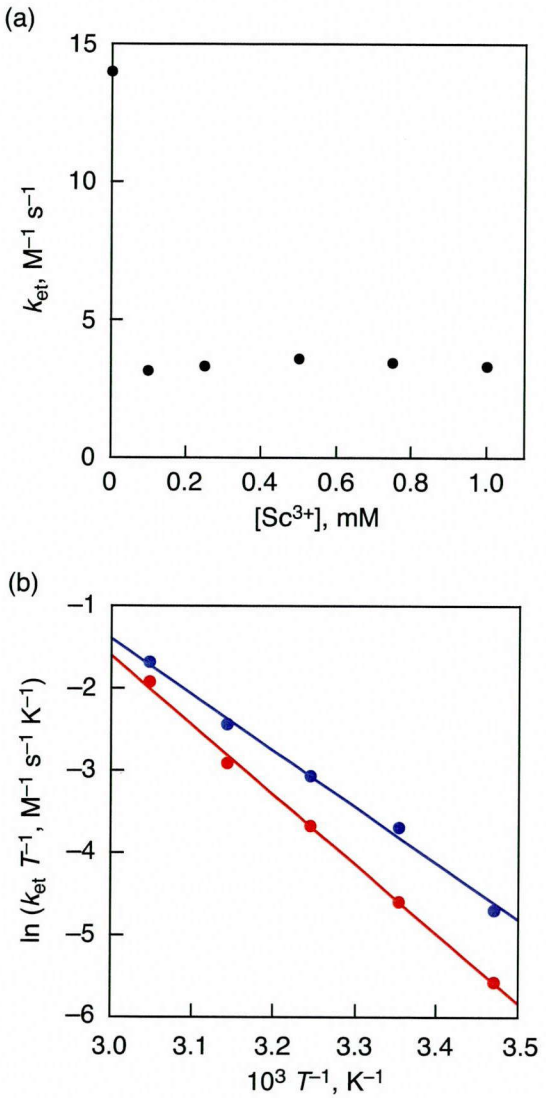

Figure 5. (a) Plot of the pseudo-first-order rate constant (k_{et}) vs concentration of Sc^{3+} in electron transfer from Fc (5.0 mM) to $[Fe^{IV}(O)(TMC)]^{2+}$ (0.10 mM) in the presence of Sc^{3+} in MeCN at 298 K. (b) Eyring plots of the rate constant of electron transfer from Fc (5.0 mM) to $[Fe^{IV}(O)(TMC)]^{2+}$ (0.10 mM) in the absence (blue circle) and presence of Sc^{3+} (red circle) in MeCN at various temperatures.

A question to be answered here is why the two-electron reduction of $[Fe^{IV}(O)(TMC)]^{2+}$ with Fc is made possible by the presence of redox-inactive metal ions. When the $Fe^{IV}(O)$ complex would be reduced to the $Fe^{III}(O)$ complex, the binding of Sc^{3+} to the oxo group is expected to become stronger due to increased electron density on the oxo group. This would facilitate further reduction to an iron(II) complex, accompanied by removal of the oxo group with protons as water (Figure 1).

The author has shown above the 1:1 stoichiometry of Sc^{3+} to $[Fe^{IV}(O)(TMC)]^{2+}$ in the two-electron reduction of $[Fe^{IV}(O)(TMC)]^{2+}$ by Fc in the presence of Sc^{3+} (Figure 1

and Figure 5a) and there is no change in the k_{et} value with increasing Sc^{3+} concentration. Definitive proof for Sc^{3+} binding to the oxo group of $[Fe^{IV}(O)(TMC)]^{2+}$ was obtained from X-ray crystallography. Single crystals of $[Fe^{IV}(O)(TMC)–Sc(OTf)_4(OH)]$ were grown from a MeCN/diethyl ether mixture at –15 °C. The X-ray crystal structure in Figure 6 clearly shows the binding of Sc^{3+} to the oxo moiety of $[Fe^{IV}(O)(TMC)]^{2+}$ (see Supplementary Information for crystallographic data and refinement details (Supplementary Tables 1–4) and also Supplementary Figure 1 for the asymmetric unit of the complex).

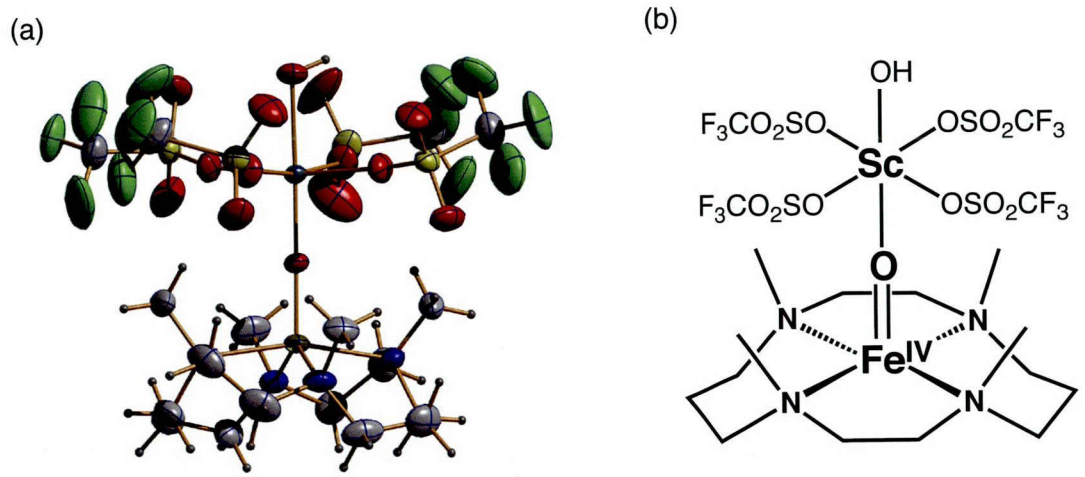

Figure 6. (a) ORTEP-style and (b) chemical structure plots of the Sc^{3+}-bound nonheme oxoiron(IV) complex, $[Fe^{IV}(O)(TMC)–Sc(OTf)_4(OH)]$; *a* (Å) = 12.3656(11), *b* (Å) = 16.4492(13), *c* (Å) = 19.9866(17), β (°) = 94.337(4), V(Å^3) = 4053.7(6), Monoclinic, $P2_1/n$, Z = 4, R_1 = 0.0590, wR_2 = 0.1862, S = 1.030. The displacement ellipsoids are drawn at the 30% probability level.

To the best of our knowledge, this is the first high-valent oxometal species binding a metal ion at the oxometal moiety. The strong binding of Sc^{3+} to the oxo group results in elongation of the Fe–O distance of the $Fe^{IV}(O)–Sc^{3+}$ complex (1.754(3) Å); the Fe–O distances of $[Fe^{IV}(O)(TMC)(NCMe)]^{2+}$, $[Fe^{IV}(O)(TMCS)]^{+}$ (TMCS = 1-mercaptoethyl-4,8,11-trimethyl-1,4,8,11-tetraazacyclotetra-decane), and $[Fe^{IV}(O)(TMC\text{-}py)]^{2+}$ (TMC-py = 1-(2'-pyridylmethyl)-4,8,11-trimethyl-1,4,8,11-tetraazacyclotetradecane) were reported to be 1.643(3) Å by X-ray crystallography, 1.70(2) Å by DFT calculations, and 1.667(3) Å by X-ray crystallography, respectively[20,33,34].

Here, the Sc^{3+}–O (oxo) bond length within the $Fe^{IV}(O)–Sc^{3+}$ moiety is 1.933(3) Å, which is significantly shorter than the Sc^{3+}–OH (hydroxo) distance (2.188(3) Å), a clear indication of stronger binding of Sc^{3+} to the oxo group as compared to the hydroxo group. The Fe–N bonds in the $Fe^{IV}(O)–Sc^{3+}$ complex range from 2.132(3) to 2.210(4) Å

and average 2.175 Å, which is longer than the average value (2.095 Å) of the $Fe^{IV}(O)$ complex without Sc^{3+}. The solution of this complex does not show any signal, where indicate the complex is not iron(III) complex (Figure 7).

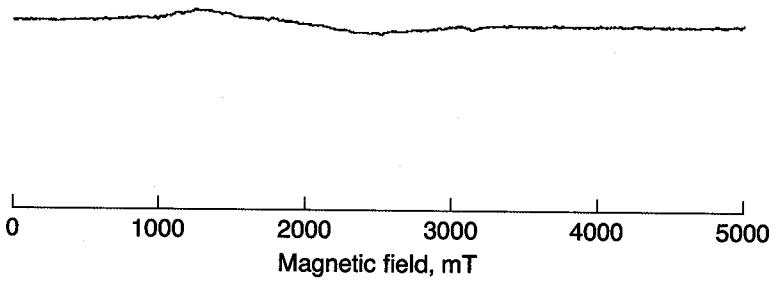

Figure 7. EPR spectrum of the Sc^{3+}-bound nonheme oxoiron(IV) complex, $[Fe^{IV}(O)(TMC)$–$Sc(OTf)_4(OH)]$

By removal of the coordinated MeCN from octahedral six-coordinate $[Fe^{IV}(O)(TMC)(NCMe)]^{2+}$ (Figure 8a)[20] via Sc^{3+} coordination, the iron atom in the $Fe^{IV}(O)$–Sc^{3+} complex adopts a distorted square pyramidal five-coordinated geometry (Figure 8b). All four *N*-methyl groups of the TMC ligand in the $Fe^{IV}(O)$–Sc^{3+} complex point to the same side of the oxo moiety (Figure 6b), whereas those in the $Fe^{IV}(O)$ complex without Sc^{3+} point away from the oxo ligand,

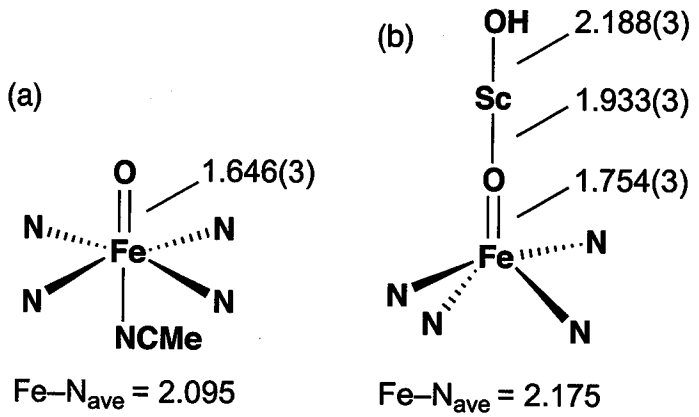

Figure 8. Structures and selected bond lengths (in Ångströms) of (a) $Fe^{IV}(O)(TMC)(NCMe)$ and (b) $[Fe^{IV}(O)(TMC)$–$Sc(OTf)_4(OH)](MeCN)$. The TMC and OTf^- ligands were omitted for clarity.

below the plane defined by the four nitrogens of the TMC ligand and *anti* to the oxo atom[20].Such switching of the four *N*-methyl groups in the binding site of the oxo group from *anti* to *syn* has been recently suggested to occur by treatment of $[Fe^{IV}(O)(TMC)(NCMe)]^{2+}$ with PhIO in the presence of tetrafluoroborate anion, although the X-ray crystal structure has yet to be determined[32].

In the *syn* structure, there is enough space to accommodate the Sc^{3+} complex bound to the oxo moiety, whereas there is no space for the axial binding of MeCN in the trans position to the iron-oxo moiety. At present, the mechanism of the structural change from *anti* to *syn* accompanied by binding of Sc^{3+} and removal of the coordinated MeCN has yet to be clarified.

Conclusion

In conclusion, the author have isolated and determined the crystal structure of the $Fe^{IV}(O)$–Sc^{3+} complex. The strong binding of Sc^{3+} to the oxo group results in significant structural change from an octahedrally hexacoordinated metal center to a pentacoordinated one with square pyramidal coordination, with concomitant switching of the four *N*-methyl groups of the TMC ligand at the binding site of the oxo group from *anti* to *syn* disposition. A dramatic effect on redox properties occurs, wherein the number of electrons transferred from Fc to the $Fe^{IV}(O)$ complex is also changed from one to two, depending on the binding of Sc^{3+} or Ca^{2+} to the oxo group. These findings suggest a likely role for a redox inactive metal ion as a necessary or useful component in chemical or natural systems, for the modulation of redox potential and electron-transfer properties of high-valent oxometal species. Thus, such a role may be considered for discussions of the unveiled role of Ca^{2+} ion found in the vicinity of the active site of the OEC, i.e., its facilitation of the two-electron reduction of an $Mn^{V}{\equiv}O$ group by water/hydroxide.

References

(1) Kovacs, J. A. *Science* **2009**, *299*, 1024.

(2) Ferguson-Miller, S.; Babcock, G. T. *Chem. Rev.* **1996**, *96*, 2889.

(3) Diner, B. A.; Babcock, G. T. *Oxygenic Photosynthesis: The Light Reactions*: Kluwer Academic Publishers: Dordrecht, The Netherlands, 1996.

(4) Yagi, M.; Kaneko, M. *Chem. Rev.* **2001**, *101*, 21.

(5) McEvoy, J. P.; Brudvig, G. W. *Chem. Rev.* **2006**, *106*, 4455.

(6) Zouni, A.; Witt H.-T.; Kern J.; Fromme P.; Krauss N.; Saenger W.; Orth P. *Nature* **2001**, *409*, 739.

(7) (a) Ferreira, K. N.; Iverson, T. M.; Maghlaoui, K. Barber, J.; Iwata, S. *Science* **2004**, *303*, 1831. (b) Loll, B.; Kern, J.; Saenger, W.; Zouni, A. Biesiadka, J. *Nature* **2005**, *438*, 1040.

(8) Yano, J.; Kern, J.; Sauer, K.; Latimer, M. J.; Pushkar, Y.; Biesiadka, J.; Loll, B.; Saenger, W.; Messinger, J. Zouni, A.; Yachandra, V. K. *Science* **2006**, *314*, 821.

(9) Sporoviero, E. M.; Gascón, J. A.; McEvoy, J. P.; Brudvig, G. W.; Batista, V. S. *J. Am. Chem. Soc.* **2008**, *130*, 3428.

(10) Barber, J. *Chem. Soc. Rev.* **2009**, *38*, 185.

(11) Que, L., Jr. *Acc. Chem. Res.* **2007**, *40*, 493.

(12) Nam, W. *Acc. Chem. Res.* **2007**, *40*, 522.

(13) Sono, M.; Roach, M. P.; Coulter, E. D.; Dawson, J. H. *Chem. Rev.* **1996**, *96*, 2841.

(14) *Metal-Oxo and Metal-Peroxo Species in Catalytic Oxidations*; Meunier, B., Ed.; Springer-Verlag: Berlin, 2000.

(15) *Cytochrome P450: Structure, Mechanism, and Biochemistry* Ortiz de Montellano, P. R. Ed.; Kluwer Academic/Plenum Publishers: New York, 2005.

(16) Fukuzumi, S. *Prog. Inorg. Chem.* **2009**, *56*, 49.

(17) Fukuzumi, S. *Bull. Chem. Soc. Jpn.* **1997**, 70, 1.

(18) Fukuzumi, S. *Org. Biomol. Chem.* **2003**, 1, 609.

(19) Rohde, J.-U.; In, J.-H.; Lim, M. H.; Brennessel, W. W.; Bukowski, M. R.; Stubna, A.; Münck, E.; Nam, W.; Que, L., Jr. *Science* **2003**, *299*, 1037.

(20) Lee, Y.-M.; Kotani, H.; Suenobu, T. Nam, W.; Fukuzumi, S. *J. Am. Chem. Soc.* **2008**, *130*, 434.

(21) Armarego, W. L. F.; Perrin, D. D. *Purification of Laboratory Chemicals*, 4th ed.: Pergamon Press: Oxford, 1997.

(22) Saltzman, H.; Sharefkin, J. G. *Organic Syntheses*, Collect. Vol. V: Wiley: New York, 1973, p 658.

(23) Sastri, C. V.; Oh, K.; Lee, Y. J.; Seo, M. S.; Shin, W.; Nam, W. *Angew. Chem., Int. Ed.* **2006**, *45*, 3992.

(24) Yang, E. S.; Chan, M.-S.; Wahl, A. C. *J. Phys. Chem.* **1975**, *79*, 2049.

(25) Bruker AXS Inc., APEX2 (ver. 2.1-4) and SAINT (ver. 7.34A): Madison, Wisconsin, USA, 2007.

(26) Sheldrick, G. M. SADABS, University of Göttingen, Göttingen, Germany, 1996.

(27) Sheldrick, G. M. *Acta Cryst. A* **2008**, *64*, 112.

(28) Sheldrick, G. M. E. *SHELXL-97*: University of Göttingen: Göttingen, Germany, 1997.

(29) Fukuzumi, S. & Ohkubo, K. *Chem.–Eur. J.* **2000**, *6*, 4532.

(30) Fukuzumi, S.; Ohkubo, K.; *J. Am. Chem. Soc.* **2002**, *124*, 10270.

(31) Ray, K.; England, J.; Fiedler, A. T.; Martinho, M.; Münck, E.; Que, L., Jr. *Angew. Chem., Int. Ed.* **2008**, *47*, 8068.

(32) Bukowski, M. R.; Koehntop, K. D.; Stubna, A.; Bominaar, E. L.; Halfen, J. A.; Münck, E.; Nam, W.; Que, L., Jr. *Science* **2005**, *310*, 1000.

(33) Thibon, A.; England, J.; Martinho, M.; Young, Jr., V. G.; Frisch, J. R.; Guillot, R.; Girerd, J.-J.; Münck, E.; Que, L., Jr.; Banse, F. *Angew. Chem., Int. Ed.* **2008**, *47*, 7064.

(34) Ray, K.; England, J.; Fiedler, A. T.; Martinho, M.; Münck, E.; Que, L., Jr. *Angew. Chem., Int. Ed.* **2008**, *47*, 8068.

Supporting Information

for Chapter 1

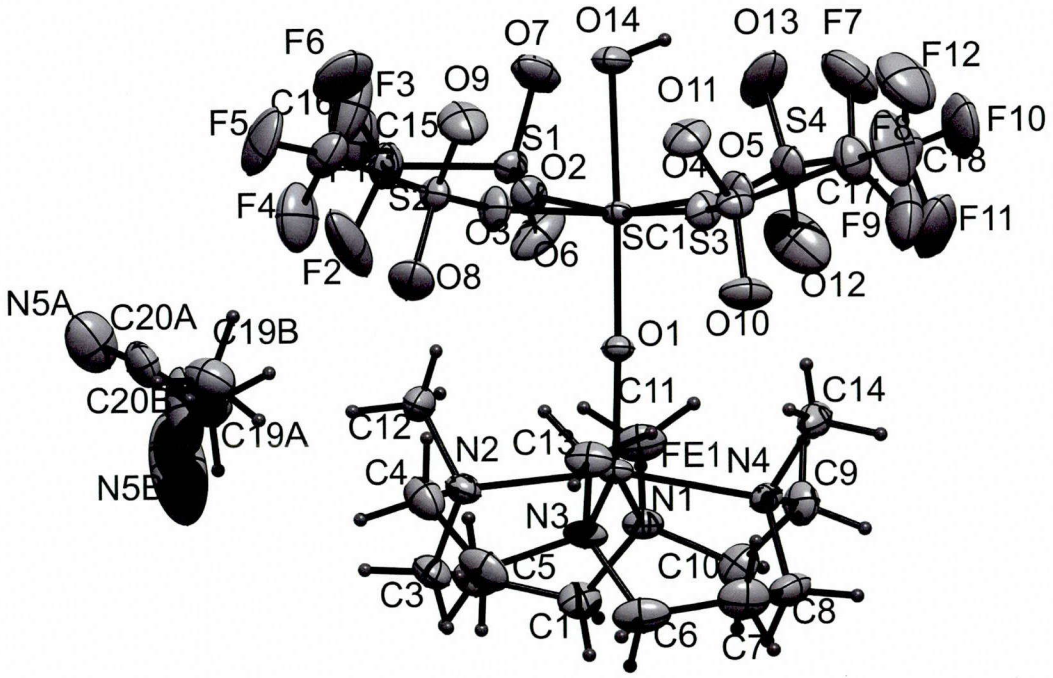

Figure S1. ORTEP-style plot of the asymmetric unit of the complex [Fe^{IV}(O)(TMC)–$Sc(OTf)_4(OH)$], showing the atomic labeling scheme. The displacement ellipsoids are drawn at the 30% probability level.

Table S1. Crystal Data and Structure Refinement Details for [Fe(O)(TMC)–$Sc(OTf)_4(OH)$](MeCN)

Empirical formula	$C_{20}H_{36}F_{12}FeN_5O_{14}S_4Sc$
Formula weight	1027.59
Temperature / K	293
Wavelength / Å	0.71073 A
Crystal system, space group	Monoclinic, $P2_1/n$
Unit cell dimensions	a = 12.3656(11) Å, α = 90 °
	b = 16.4492(13) Å, β = 94.337 °
	c = 19.9866(17) Å, γ = 90 °
Volume /	4053.7(6)
Z, Calculated density	4, 1.684 Mg/m^3
Absorption coefficient / mm^{-1}	0.849
F(000)	2088
Crystal size / μm	235 × 210 × 55
Θ range for data collection / °	2.01 – 25.00
Limiting indices	$-13 \leftarrow h \leftarrow 13, -19 \leftarrow k \leftarrow 19, -17 \leftarrow l \leftarrow 23$
Reflections collected / unique	18985 / 6760 [R_{int} = 0.0534]
Max. and min. transmission	0.9588 / 0.8287
Refinement method	FMLS on F^2
Data / restraints / parameters	6760 / 16 / 544
GoF on F^2	1.030
Final R indices [$I>2\sigma(I)$]	R_1 = 0.0590, wR_2 = 0.1670
R indices (all data)	R_1 = 0.0801, wR_2 = 0.1862
Largest diff. peak / hole	0.661 / –0.474 e·$Å^{-3}$

Table S2. Atomic Coordinates ($\times 10^4$), Equivalent Isotropic Displacement Parameters ($Å^2 \times 10^3$), and U_{eq} Defined as One Third of the Trace of the Orthogonalized U_{ij} tensor.

Atom	x	y	z	U_{eq}
Fe(1)	1484(1)	1529(1)	1809(1)	41(1)
Sc(1)	429(1)	3065(1)	585(1)	35(1)
S(2)	1152(1)	2034(1)	-831(1)	55(1)
S(3)	-1920(1)	1984(1)	99(1)	54(1)
S(1)	2457(1)	4514(1)	870(1)	52(1)
S(4)	-426(1)	4513(1)	1677(1)	74(1)
O(1)	978(2)	2272(2)	1240(1)	46(1)
O(4)	-1054(3)	2485(2)	410(2)	69(1)
O(2)	1857(3)	3788(2)	674(2)	65(1)
O(5)	-319(3)	3799(2)	1272(2)	77(1)
O(3)	1102(3)	2482(2)	-214(2)	73(1)
O(10)	-1919(4)	1191(2)	376(2)	90(1)
O(11)	-2031(4)	2016(3)	-609(2)	90(1)
C(4)	2949(6)	707(5)	922(3)	91(2)
O(14)	-158(3)	3947(2)	-178(2)	73(1)
N(4)	48(3)	1396(2)	2395(2)	56(1)
C(8)	-83(5)	581(4)	2714(3)	83(2)
F(1)	4299(3)	5057(3)	569(2)	119(2)
N(1)	2199(3)	2045(2)	2717(2)	53(1)
O(8)	1461(4)	1222(2)	-702(2)	94(1)
N(2)	3103(3)	1391(3)	1426(2)	61(1)
F(4)	3183(4)	2423(4)	-756(3)	152(2)
O(7)	1985(4)	5234(2)	618(3)	105(2)
N(3)	1249(4)	312(2)	1435(2)	58(1)
F(7)	-3153(5)	3234(4)	165(3)	163(2)
F(11)	-2038(6)	3807(4)	2140(4)	194(3)
F(2)	4194(4)	3786(4)	570(5)	215(4)
F(9)	-3097(4)	2462(5)	1035(3)	160(2)
O(9)	284(4)	2147(4)	-1304(2)	110(2)
F(8)	-3977(4)	2113(4)	145(4)	178(3)

F(6)	2143(6)	3261(3)	-1292(3)	177(3)
O(13)	-321(6)	5250(3)	1342(3)	159(3)
F(5)	2534(5)	2146(4)	-1728(3)	170(2)
C(13)	529(5)	360(3)	811(2)	72(2)
F(10)	-2048(5)	5100(4)	2222(3)	175(3)
O(6)	2831(4)	4512(4)	1549(2)	120(2)
O(12)	126(6)	4432(5)	2319(3)	170(3)
F(3)	3440(5)	4411(5)	-211(3)	175(3)
C(14)	-950(4)	1674(4)	2032(3)	83(2)
C(12)	3409(5)	2094(4)	1029(3)	86(2)
C(6)	872(7)	-296(4)	1899(3)	92(2)
C(7)	-179(6)	-101(4)	2183(4)	93(2)
C(1)	3271(5)	1696(4)	2972(3)	75(2)
C(16)	2327(8)	2496(5)	-1174(4)	96(2)
C(9)	295(5)	1987(4)	2955(3)	80(2)
C(10)	1455(5)	1895(4)	3262(3)	72(2)
C(15)	3668(5)	4426(4)	437(4)	85(2)
C(11)	2298(6)	2937(3)	2607(3)	85(2)
C(17)	-3096(6)	2479(5)	387(4)	97(2)
C(5)	2355(6)	8(4)	1242(4)	94(2)
C(3)	4003(5)	1145(4)	1904(3)	83(2)
C(2)	4149(5)	1734(4)	2498(3)	84(2)
F(12)	-2438(5)	4529(5)	1285(4)	197(3)
C(18)	-1838(8)	4472(5)	1834(5)	107(3)
C(19A)	6270(20)	-143(16)	926(13)	99(7)
C(20A)	5439(17)	-688(11)	1107(13)	99(7)
N(5A)	4754(16)	-1078(12)	1184(12)	152(10)
C(19B)	6601(17)	-52(12)	1214(13)	122(7)
C(20B)	5710(20)	-380(30)	782(17)	196(18)
N(5B)	5140(20)	-330(30)	328(13)	360(40)

Table S3. Bond Lengths [Å] and Angles [°]

Fe(1)-O(1)	1.754(3)	C(8)-C(7)	1.542(9)
Fe(1)-N(1)	2.132(3)	C(8)-H(8A)	0.9700
Fe(1)-N(3)	2.149(4)	C(8)-H(8B)	0.9700
Fe(1)-N(2)	2.208(4)	F(1)-C(15)	1.314(7)
Fe(1)-N(4)	2.210(4)	N(1)-C(11)	1.490(6)
Sc(1)-O(1)	1.933(3)	N(1)-C(1)	1.498(7)
Sc(1)-O(4)	2.072(3)	N(1)-C(10)	1.499(7)
Sc(1)-O(3)	2.088(3)	N(2)-C(12)	1.468(7)
Sc(1)-O(5)	2.095(3)	N(2)-C(3)	1.469(6)
Sc(1)-O(2)	2.125(3)	F(4)-C(16)	1.303(9)
Sc(1)-O(14)	2.188(3)	N(3)-C(6)	1.463(8)
S(2)-O(9)	1.388(4)	N(3)-C(13)	1.478(5)
S(2)-O(8)	1.409(4)	N(3)-C(5)	1.533(8)
S(2)-O(3)	1.443(3)	F(7)-C(17)	1.318(9)
S(2)-C(16)	1.818(8)	F(11)-C(18)	1.286(9)
S(3)-O(11)	1.413(4)	F(2)-C(15)	1.256(8)
S(3)-O(10)	1.417(4)	F(9)-C(17)	1.296(9)
S(3)-O(4)	1.453(3)	F(8)-C(17)	1.304(8)
S(3)-C(17)	1.798(8)	F(6)-C(16)	1.298(9)
S(1)-O(7)	1.397(4)	F(5)-C(16)	1.291(7)
S(1)-O(6)	1.400(4)	C(13)-H(13A)	0.9600
S(1)-O(2)	1.446(3)	C(13)-H(13B)	0.9600
S(1)-C(15)	1.792(7)	C(13)-H(13C)	0.9600
S(4)-O(13)	1.396(5)	F(10)-C(18)	1.329(9)
S(4)-O(12)	1.413(6)	F(3)-C(15)	1.305(8)
S(4)-O(5)	1.439(4)	C(14)-H(14A)	0.9600
S(4)-C(18)	1.799(9)	C(14)-H(14B)	0.9600
C(4)-N(2)	1.513(8)	C(14)-H(14C)	0.9600
C(4)-C(5)	1.529(10)	C(12)-H(12A)	0.9600
C(4)-H(4A)	0.9700	C(12)-H(12B)	0.9600
C(4)-H(4B)	0.9700	C(12)-H(12C)	0.9600
O(14)-H(14)	0.8200	C(6)-C(7)	1.492(10)
N(4)-C(14)	1.457(6)	C(6)-H(6A)	0.9700
N(4)-C(9)	1.496(7)	C(6)-H(6B)	0.9700
N(4)-C(8)	1.498(7)	C(7)-H(7A)	0.9700

C(7)-H(7B)	0.9700
C(1)-C(2)	1.496(9)
C(1)-H(1A)	0.9700
C(1)-H(1B)	0.9700
C(9)-C(10)	1.524(8)
C(9)-H(9A)	0.9700
C(9)-H(9B)	0.9700
C(10)-H(10A)	0.9700
C(10)-H(10B)	0.9700
C(11)-H(11A)	0.9600
C(11)-H(11B)	0.9600
C(11)-H(11C)	0.9600
C(5)-H(5A)	0.9700
C(5)-H(5B)	0.9700
C(3)-C(2)	1.532(8)
C(3)-H(3A)	0.9700
C(3)H(3B)	0.9700
C(2)-H(2A)	0.9700
C(2)-H(2B)	0.9700
F(12)-C(18)	1.279(9)
C(19A)-C(20A)	1.427(18)
C(19A)-H(19A)	0.9600
C(19A)-H(19B)	0.9600
C(19A)-H(19C)	0.9600
C(20A)-N(5A)	1.083(15)
C(19B)-C(20B)	1.449(18)
C(19B)-H(19D)	0.9600
C(19B)-H(19E)	0.9600
C(19B)-H(19F)	0.9600
C(20B)-N(5B)	1.111(18)
N(5B)-N(5B)#	11.72(9)

O(1)-Fe(1)-N(1)	112.29(13)	O(7)-S(1)-O(6)	116.8(4)
O(1)-Fe(1)-N(3)	113.03(14)	O(7)-S(1)-O(2)	114.3(3)
N(1)-Fe(1)-N(3)	134.68(14)	O(6)-S(1)-O(2)	112.7(3)
O(1)-Fe(1)-N(2)	97.74(14)	O(7)-S(1)-C(15)	103.6(3)
N(1)-Fe(1)-N(2)	90.45(16)	O(6)-S(1)-C(15)	103.9(3)
N(3)-Fe(1)-N(2)	83.48(17)	O(2)-S(1)-C(15)	103.4(3)
O(1)-Fe(1)-N(4)	98.67(14)	O(13)-S(4)-O(12)	117.5(5)
N(1)-Fe(1)-N(4)	83.51(15)	O(13)-S(4)-O(5)	115.0(3)
N(3)-Fe(1)-N(4)	89.93(16)	O(12)-S(4)-O(5)	112.1(3)
N(2)-Fe(1)-N(4)	163.58(15)	O(13)-S(4)-C(18)	104.0(4)
O(1)-Sc(1)-O(4)	93.71(14)	O(12)-S(4)-C(18)	104.3(5)
O(1)-Sc(1)-O(3)	93.92(14)	O(5)-S(4)-C(18)	101.5(3)
O(4)-Sc(1)-O(3)	93.37(15)	Fe(1)-O(1)-Sc(1)	177.87(18)
O(1)-Sc(1)-O(5)	95.42(15)	S(3)-O(4)-Sc(1)	161.3(3)
O(4)-Sc(1)-O(5)	86.95(16)	S(1)-O(2)-Sc(1)	153.1(2)
O(3)-Sc(1)-O(5)	170.62(16)	S(4)-O(5)-Sc(1)	154.6(3)
O(1)-Sc(1)-O(2)	94.24(14)	S(2)-O(3)-Sc(1)	159.0(3)
O(4)-Sc(1)-O(2)	172.03(14)	N(2)-C(4)-C(5)	108.8(5)
O(3)-Sc(1)-O(2)	86.79(15)	N(2)-C(4)-H(4A)	109.9
O(5)-Sc(1)-O(2)	91.60(15)	C(5)-C(4)-H(4A)	109.9
O(1)-Sc(1)-O(14)	178.25(14)	N(2)-C(4)-H(4B)	109.9
O(4)-Sc(1)-O(14)	86.84(15)	C(5)-C(4)-H(4B)	109.9
O(3)-Sc(1)-O(14)	84.40(16)	H(4A)-C(4)-H(4B)	108.3
O(5)-Sc(1)-O(14)	86.26(16)	Sc(1)-O(14)-H(14)	109.5
O(2)-Sc(1)-O(14)	85.24(15)	C(14)-N(4)-C(9)	106.5(5)
O(9)-S(2)-O(8)	115.9(3)	C(14)-N(4)-C(8)	112.2(5)
O(9)-S(2)-O(3)	115.7(3)	C(9)-N(4)-C(8)	106.6(4)
O(8)-S(2)-O(3)	110.9(3)	C(14)-N(4)-Fe(1)	113.0(3)
O(9)-S(2)-C(16)	106.7(4)	C(9)-N(4)-Fe(1)	101.8(3)
O(8)-S(2)-C(16)	104.6(3)	C(8)-N(4)-Fe(1)	115.5(4)
O(3)-S(2)-C(16)	101.3(3)	N(4)-C(8)-C(7)	111.3(5)
O(11)-S(3)-O(10)	115.0(3)	N(4)-C(8)-H(8A)	109.4
O(11)-S(3)-O(4)	114.8(3)	C(7)-C(8)-H(8A)	109.4
O(10)-S(3)-O(4)	112.1(2)	N(4)-C(8)-H(8B)	109.4
O(11)-S(3)-C(17)	106.5(3)	C(7)-C(8)-H(8B)	109.4
O(10)-S(3)-C(17)	105.7(4)	H(8A)-C(8)-H(8B)	108.0
O(4)-S(3)-C(17)	101.2(3)	C(11)-N(1)-C(1)	110.2(4)

C(11)-N(1)-C(10)	109.3(4)
C(1)-N(1)-C(10)	105.4(4)
C(11)-N(1)-Fe(1)	107.5(3)
C(1)-N(1)-Fe(1)	115.9(3)
C(10)-N(1)-Fe(1)	108.4(3)
C(12)-N(2)-C(3)	110.8(5)
C(12)-N(2)-C(4)	104.6(5)
C(3)-N(2)-C(4)	106.2(5)
C(12)-N(2)-Fe(1)	112.6(3)
C(3)-N(2)-Fe(1)	117.7(4)
C(4)-N(2)-Fe(1)	103.6(3)
C(6)-N(3)-C(13)	111.8(4)
C(6)-N(3)-C(5)	105.7(5)
C(13)-N(3)-C(5)	107.2(4)
C(6)-N(3)-Fe(1)	117.2(3)
C(13)-N(3)-Fe(1)	107.5(3)
C(5)-N(3)-Fe(1)	106.9(3)
N(3)-C(13)-H(13A)	109.5
N(3)-C(13)-H(13B)	109.5
H(13A)-C(13)-H(13B)	109.5
N(3)-C(13)-H(13C)	109.5
H(13A)-C(13)-H(13C)	109.5
H(13B)-C(13)-H(13C)	109.5
N(4)-C(14)-H(14A)	109.5
N(4)-C(14)-H(14B)	109.5
H(14A)-C(14)-H(14B)	109.5
N(4)-C(14)-H(14C)	109.5
H(14A)-C(14)-H(14C)	109.5
H(14B)-C(14)-H(14C)	109.5
N(2)-C(12)-H(12A)	109.5
N(2)-C(12)-H(12B)	109.5
H(12A)-C(12)-H(12B)	109.5
N(2)-C(12)-H(12C)	109.5
H(12A)-C(12)-H(12C)	109.5
H(12B)-C(12)-H(12C)	109.5
N(3)-C(6)-C(7)	115.0(6)
N(3)-C(6)-H(6A)	108.5
C(7)-C(6)-H(6A)	108.5
N(3)-C(6)-H(6B)	108.5
C(7)-C(6)-H(6B)	108.5
H(6A)-C(6)-H(6B)	107.5
C(6)-C(7)-C(8)	113.1(5)
C(6)-C(7)-H(7A)	108.9
C(8)-C(7)-H(7A)	108.9
C(6)-C(7)-H(7B)	108.9
C(8)-C(7)-H(7B)	108.9
H(7A)-C(7)-H(7B)	107.8
|C(2)-C(1)-N(1)	115.7(5)
C(2)-C(1)-H(1A)	108.4
N(1)-C(1)-H(1A)	108.4
C(2)-C(1)-H(1B)	108.4
N(1)-C(1)-H(1B)	108.4
H(1A)-C(1)-H(1B)	107.4
F(5)-C(16)-F(6)	108.7(7)
F(5)-C(16)-F(4)	107.8(8)
F(6)-C(16)-F(4)	109.2(7)
F(5)-C(16)-S(2)	110.6(6)
F(6)-C(16)-S(2)	109.8(6)
F(4)-C(16)-S(2)	110.7(5)
N(4)-C(9)-C(10)	111.7(5)
N(4)-C(9)-H(9A)	109.3
C(10)-C(9)-H(9A)	109.3
N(4)-C(9)-H(9B)	109.3
C(10)-C(9)-H(9B)	109.3
H(9A)-C(9)-H(9B)	107.9
N(1)-C(10)-C(9)	107.5(4)
N(1)-C(10)-H(10A)	110.2
C(9)-C(10)-H(10A)	110.2
N(1)-C(10)-H(10B)	110.2
C(9)-C(10)-H(10B)	110.2
H(10A)-C(10)-H(10B)	108.5
F(2)-C(15)-F(3)	105.3(7)
F(2)-C(15)-F(1)	109.2(7)
F(3)-C(15)-F(1)	107.1(6)

F(2)-C(15)-S(1)	113.9(5)	N(2)-C(3)-H(3B)	109.3
F(3)-C(15)-S(1)	110.9(5)	C(2)-C(3)-H(3B)	109.3
F(1)-C(15)-S(1)	110.2(5)	H(3A)-C(3)-H(3B)	108.0
N(1)-C(11)-H(11A)	109.5	C(1)-C(2)-C(3)	114.6(5)
N(1)-C(11)-H(11B)	109.5	C(1)-C(2)-H(2A)	108.6
H(11A)-C(11)-H(11B)	109.5	C(3)-C(2)-H(2A)	108.6
N(1)-C(11)-H(11C)	109.5	C(1)-C(2)-H(2B)	108.6
H(11A)-C(11)-H(11C)	109.5	C(3)-C(2)-H(2B)	108.6
H(11B)-C(11)-H(11C)	109.5	H(2A)-C(2)-H(2B)	107.6
F(9)-C(17)-F(8)	107.2(7)	F(12)-C(18)-F(11)	110.5(10)
F(9)-C(17)-F(7)	110.6(7)	F(12)-C(18)-F(10)	108.5(8)
F(8)-C(17)-F(7)	106.8(7)	F(11)-C(18)-F(10)	109.3(7)
F(9)-C(17)-S(3)	111.8(6)	F(12)-C(18)-S(4)	110.8(6)
F(8)-C(17)-S(3)	110.2(6)	F(11)-C(18)-S(4)	109.8(6)
F(7)-C(17)-S(3)	110.0(6)	F(10)-C(18)-S(4)	107.9(7)
C(4)-C(5)-N(3)	109.1(5)	N(5A)-C(20A)-C(19A)	173(3)
C(4)-C(5)-H(5A)	109.9	C(20B)-C(19B)-H(19D)	109.5
N(3)-C(5)-H(5A)	109.9	C(20B)-C(19B)-H(19E)	109.5
C(4)-C(5)-H(5B)	109.9	H(19D)-C(19B)-H(19E)	109.5
N(3)-C(5)-H(5B)	109.9	C(20B)-C(19B)-H(19F)	109.5
H(5A)-C(5)-H(5B)	108.3	H(19D)-C(19B)-H(19F)	109.5
N(2)-C(3)-C(2)	111.6(5)	H(19E)-C(19B)-H(19F)	109.5
N(2)-C(3)-H(3A)	109.3	N(5B)-C(20B)-C(19B)	150(6)
C(2)-C(3)-H(3A)	109.3	C(20B)-N(5B)-N(5B)#1	139(6)

Symmetry transformations used to generate equivalent atoms: #1 $-x+1, -y, -z$

Table S4. Anisotropic Displacement Parameters ($Å^2 \times 10^3$)

	U_{11}	U_{22}	U_{33}	U_{23}	U_{13}	U_{12}
Fe(1)	52(1)	30(1)	38(1)	2(1)	-6(1)	1(1)
Sc(1)	42(1)	28(1)	36(1)	1(1)	1(1)	1(1)
S(2)	66(1)	56(1)	44(1)	-7(1)	6(1)	4(1)
S(3)	52(1)	56(1)	51(1)	5(1)	-9(1)	-6(1)
S(1)	51(1)	45(1)	60(1)	0(1)	4(1)	-11(1)
S(4)	88(1)	49(1)	88(1)	-20(1)	31(1)	2(1)
O(1)	54(2)	39(2)	46(2)	9(1)	1(1)	5(1)
O(4)	54(2)	78(2)	74(2)	3(2)	-8(2)	-20(2)
O(2)	55(2)	50(2)	88(2)	-7(2)	4(2)	-16(2)
O(5)	92(3)	55(2)	87(3)	-26(2)	30(2)	9(2)
O(3)	80(3)	84(3)	56(2)	-23(2)	19(2)	2(2)
O(10)	107(3)	55(2)	104(3)	22(2)	-16(2)	-10(2)
O(11)	100(3)	113(4)	53(2)	3(2)	-17(2)	-5(3)
C(4)	85(5)	105(5)	84(4)	-18(4)	2(3)	25(4)
O(14)	77(3)	64(2)	77(2)	30(2)	0(2)	14(2)
N(4)	64(3)	56(2)	47(2)	11(2)	6(2)	0(2)
C(8)	82(4)	85(4)	79(4)	33(3)	3(3)	-18(3)
F(1)	94(3)	123(3)	145(3)	-17(3)	46(3)	-61(3)
N(1)	67(3)	38(2)	50(2)	-1(2)	-15(2)	-8(2)
O(8)	118(4)	44(2)	121(3)	-3(2)	23(3)	5(2)
N(2)	59(3)	61(3)	62(2)	8(2)	-4(2)	13(2)
F(4)	81(3)	202(6)	178(5)	-36(4)	33(3)	-35(3)
O(7)	82(3)	54(2)	180(5)	34(3)	9(3)	2(2)
N(3)	80(3)	37(2)	52(2)	-3(2)	-17(2)	1(2)
F(7)	153(5)	105(4)	230(6)	-5(4)	11(4)	60(4)
F(11)	212(6)	135(5)	255(7)	39(5)	158(6)	-14(4)
F(2)	88(3)	114(4)	455(13)	35(6)	104(5)	27(3)
F(9)	126(4)	235(7)	127(4)	-31(4)	60(3)	13(4)
O(9)	104(4)	146(5)	75(3)	-2(3)	-25(3)	18(3)
F(8)	50(3)	237(7)	246(7)	-57(5)	4(3)	-22(3)
F(6)	255(7)	77(3)	209(6)	45(3)	94(5)	-17(4)
O(13)	246(8)	51(3)	200(6)	10(3)	145(6)	2(4)

F(5)	223(6)	182(5)	122(4)	-31(3)	121(4)	-20(4)
C(13)	98(4)	59(3)	53(3)	-11(2)	-25(3)	-3(3)
F(10)	187(5)	142(4)	210(6)	-28(4)	118(5)	52(4)
O(6)	126(4)	176(5)	57(2)	6(3)	-12(2)	-75(4)
O(12)	177(6)	173(6)	150(5)	-86(5)	-57(5)	40(5)
F(3)	158(5)	256(8)	121(4)	-64(5)	67(4)	-74(5)
C(14)	51(3)	124(5)	74(4)	34(4)	6(3)	1(3)
C(12)	64(4)	104(5)	95(4)	42(4)	26(3)	16(3)
C(6)	142(7)	51(3)	78(4)	0(3)	-29(4)	-16(4)
C(7)	104(6)	62(4)	110(5)	-1(3)	-14(4)	-26(4)
C(1)	69(4)	85(4)	67(3)	1(3)	-17(3)	-12(3)
C(16)	128(7)	81(5)	84(4)	-8(4)	42(5)	-17(4)
C(9)	88(4)	87(4)	65(3)	-17(3)	15(3)	3(3)
C(10)	88(4)	76(4)	52(3)	-19(3)	2(3)	-15(3)
C(15)	73(4)	83(5)	102(5)	-5(4)	25(4)	-18(4)
C(11)	127(6)	41(3)	82(4)	-8(3)	-18(4)	-20(3)
C(17)	69(5)	104(6)	118(6)	-11(5)	14(4)	-5(4)
C(5)	113(5)	62(4)	103(5)	-34(3)	-16(4)	24(4)
C(3)	65(4)	95(4)	87(4)	12(3)	-3(3)	26(3)
C(2)	83(4)	79(4)	85(4)	2(3)	-19(3)	-7(3)
F(12)	126(5)	237(8)	222(7)	2(6)	-32(5)	51(5)
C(18)	128(7)	89(5)	110(6)	8(4)	57(5)	26(5)
C(20A)	92(18)	96(13)	111(15)	-7(11)	29(11)	37(13)
N(5A)	115(15)	117(14)	220(20)	-21(13)	14(14)	-16(11)
C(19B)	137(18)	107(13)	119(16)	-2(12)	-3(13)	28(12)
C(20B)	100(20)	310(40)	180(30)	-130(30)	40(20)	-10(30)
N(5B)	140(20)	720(100)	210(40)	-230(50)	-30(20)	30(30)

Chapter 2. Metal Ion-Coupled Electron Transfer of a Nonheme Oxoiron(IV) Complex: Remarkable Enhancement of Electron-Transfer Rates by Sc^{3+}

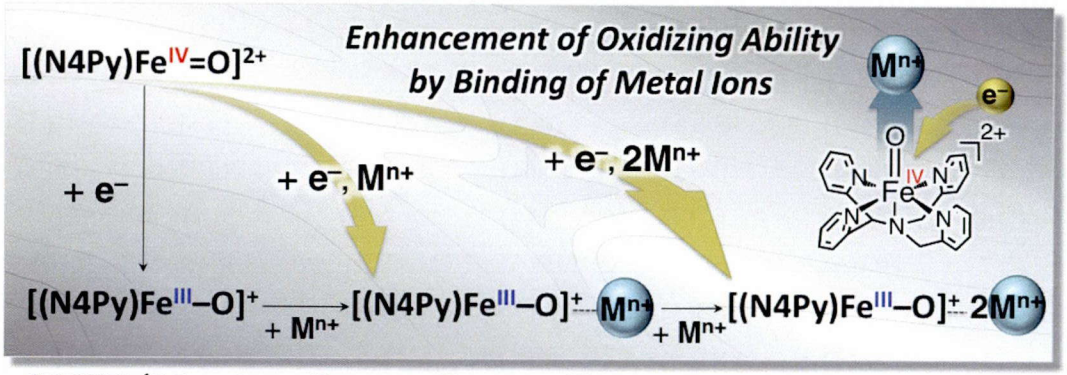

MCET (Metal Ion-Coupled Electron Transfer) of Fe(IV)-Oxo Complex

Abstract: Rates of electron transfer from a series of one-electron reductants to a nonheme oxoiron(IV) complex, $[Fe^{IV}(O)(N4Py)]^{2+}$, are enhanced as much as 10^8-fold by addition of metal ions such as Sc^{3+}, Zn^{2+}, Mg^{2+} and Ca^{2+}; the metal ion effect follows the Lewis acidity of metal ions. The one-electron reduction potential of $[Fe^{IV}(O)(N4Py)]^{2+}$ is shifted to a positive direction by 0.84 V in the presence of Sc^{3+} ion (0.20 M).

Introduction

Electron transfer (ET) is one of the most important elementary steps in biological redox processes, in which high-valent metal-oxo species are often involved as reactive species, e.g., Mn^{V}-oxo species in water oxidation at oxygen-evolving complex (OEC) in photosystem II (PS II) and iron(IV)-oxo species in cyctochrome *c* oxidase and P450, and nonheme iron enzymes.[1–4] In the OEC, Ca^{2+} acts as an essential cofactor in the manganese-calcium (Mn_4Ca) active site responsible for water oxidation in PS II, although the exact functional role of Ca^{2+} has yet to be clarified.[1] ET properties of various high-valent metal-oxo species have merited increasing attention.[5,6] In this context, the author have recently reported the first example of binding of metal ions, such as Sc^{3+} and Ca^{2+}, to a nonheme oxoiron(IV) complex, $[Fe^{IV}(O)(TMC)]^{2+}$ (TMC = 1,4,8,11-tetramethyl-1,4,8,11-tetraazacyclotetradecane), and the crystal structure of the Sc^{3+}-bound $[Fe^{IV}(O)(TMC)]^{2+}$ complex was determined by X-ray crystallography.[7] The binding of Sc^{3+} to $[Fe^{IV}(O)(TMC)]^{2+}$ resulted in change in the number of electrons transferred from ferrocene (Fc) to the oxoiron complex.[7] However, the ET rate from Fc to $[Fe^{IV}(O)(TMC)]^{2+}$ was decelerated by the binding of Sc^{3+} to $[Fe^{IV}(O)(TMC)]^{2+}$ because of an increase in the reorganization energy of ET.[7] Although there are many examples for acceleration of ET rates for reduction of organic electron acceptors by metal ions,[8–10] such acceleration effects of metal ions on the reduction of high-valent metal-oxo species have never been reported previously.

Scheme 1. MCET of $[Fe^{IV}(O)(N4Py)]^{2+}$

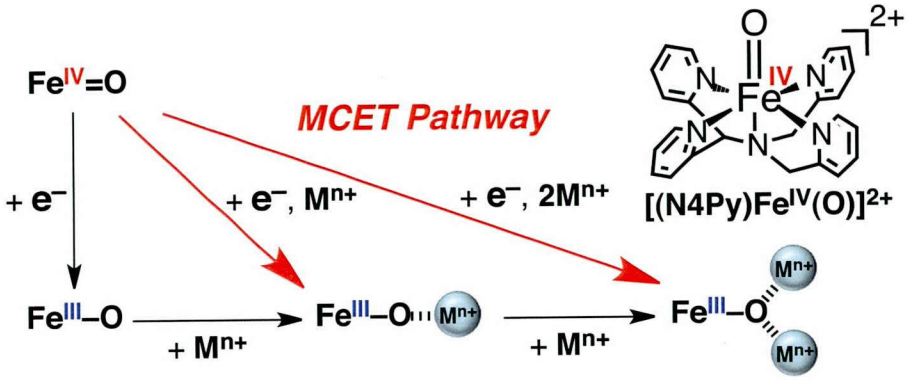

The author report herein for the first time remarkable acceleration effects of metal ions on rates of ET reduction of $[Fe^{IV}(O)(N4Py)]^{2+}$ (N4Py: *N*,*N*-bis(2-pyridylmethyl)-*N*-bis(2-pyridyl)methylamine).[11] Such accelerated ET by metal ions is regarded as metal

ion-coupled electron transfer (MCET)[8] in analogy to proton-coupled electron transfer (PCET),[12,13] as shown in Scheme 1.

The change in the one-electron reduction potential depending on metal ion concentration is determined by the redox titration in the presence of metal ion. The MCET mechanism is discussed based on the thermodynamics, kinetics, and products obtained in the reactions carried out in the presence of metal ion.

Experimental Section

Materials. All solvents and chemicals were of reagent-grade quality, obtained commercially and used without further purification, unless otherwise noted. Acetonitrile (MeCN) was dried according to published procedures and distilled under Ar prior to the use.[14] Scandium triflate [$Sc(OTf)_3$] (OTf = OSO_2CF_3), yttrium triflate [$Y(OTf)_3$], lutetium triflate [$Lu(OTf)_3$], zinc triflate [$Zn(OTf)_2$], magnesium perchlorate [$Mg(ClO_4)_2$], calcium perchlorate [$Ca(ClO_4)_2$] was purchased from Aldrich and used as received. Ferrocene (Fc) was purified by sublimation prior to the use. Octamethylferrocene was purchased from Stream Chemicals, Inc. and used as received. Iodosylbenzene (PhIO) was prepared from iodobenzene diacetate according to a literature procedure.[15] $[Fe^{II}(N4Py)(NCMe)](ClO_4)_2$ and its oxoiron(IV) complex, $[Fe^{IV}(O)(N4Py)]^{2+}$, were prepared by literature methods.[16] $[Ru(bpy)_3](PF_6)_2$ and $[Ru(Me_2\text{-}bpy)_3](PF_6)_2$ were prepared according to published procedures.[17] $[Fe(bpy)_3](PF_6)_2$ were prepared by addition of a stoichiometric amount of the ligand to $Fe(SO_4)\cdot 7H_2O$ solution.

Observation of Spectral Changes. Electron transfer (ET) from $[Fe(bpy)_3]^{2+}$ (1.1×10^{-4} M) to $[Fe^{IV}(O)(N4Py)]^{2+}$ (1.1×10^{-4} M) was examined at 298 K using a Hewlett Packard 8453 photodiode-array spectrophotometer with a quartz cuvette (path length = 1.0 cm). A deaerated MeCN solution of $Sc(OTf)_3$ (1.0×10^{-2} M) was added by means of a microsyringe to a deaerated MeCN solution (2 mL) containing $[Fe(bpy)_3]^{2+}$ and $[Fe^{IV}(O)(N4Py)]^{2+}$.

EPR Measurement. The resulting solution of ET from $[Fe(bpy)_3]^{2+}$ (1.0×10^{-3} M) to $[Fe^{IV}(O)(N4Py)]^{2+}$ (1.0×10^{-3} M) in the presence of Sc^{3+} (5.0×10^{-3} M) in the quartz EPR tube (3.0 mm i.d.) was frozen at 77 K. The EPR spectrum was taken on a JEOL X-band spectrometer (JES-RE1XE) under nonsaturating microwave power conditions (1.0 mW) operating at 9.2025 GHz. The magnitude of the modulation was chosen to optimize the resolution and the signal to noise ratio (S/N) of the observed spectrum

(modulation width, 10 G; modulation frequency, 100 kHz).

Spectral Redox Titration. ET from electron donors ($[Ru^{II}(bpy)_3]^{2+}$ (6.0×10^{-4} M) and $[Ru^{II}(Me_2\text{-}bpy)_3]^{2+}$ (6.0×10^{-4} M)) to $[Fe^{IV}(O)(N4Py)]^{2+}$ was examined from the spectral change in the presence of various concentrations of $[Fe^{IV}(O)(N4Py)]^{2+}$ (0.2×10^{-4}–1.6×10^{-3} M) and Sc^{3+} (5.0×10^{-3}–2×10^{-1} M) at 298 K using a Hewlett Packard 8453 photodiode-array spectrophotometer with a quartz cuvette (path length = 1 mm). Typically, an MeCN solution of $[Fe^{IV}(O)(N4Py)]^{2+}$ (0.2×10^{-4} M) was added by means of a microsyringe to an MeCN solution (200 μL) containing electron donor and Sc^{3+}. The concentration of electron donor was determined from the absorption band due to donor ($[Ru^{II}(bpy)_3]^{2+}$: λ_{max} = 450 nm ($\varepsilon = 1.42 \times 10^4 M^{-1} cm^{-1}$), $[Ru^{II}(Me_2\text{-}bpy)_3]^{2+}$: λ_{max} = 460 nm ($\varepsilon = 1.34 \times 10^4 M^{-1} cm^{-1}$)).

Kinetic Measurements. The kinetic measurements of ET from $[Fe^{II}(bpy)_3]^{2+}$ to $[Fe^{IV}(O)(N4Py)]^{2+}$ were performed on a Hewlett Packard 8453 photodiode-array spectrophotometer at 298 K. Rates of ET from $[Fe^{II}(bpy)_3]^{2+}$ to $[Fe^{IV}(O)(N4Py)]^{2+}$ were monitored by the decay of absorption bands due to $[Fe^{II}(bpy)_3]^{2+}$ (λ_{max} = 520 nm) and $[Fe^{IV}(O)(N4Py)]^{2+}$ (λ_{max} = 695 nm), respectively. All kinetic measurements were carried out under pseudo-second-order conditions where the concentrations of $[Fe^{II}(bpy)_3]^{2+}$ and $[Fe^{IV}(O)(N4Py)]^{2+}$ to be same and of Sc^{3+} were maintained to be more than 20-folds excess of that of $[Fe^{II}(bpy)_3]^{2+}$ and $[Fe^{IV}(O)(N4Py)]^{2+}$. Typically, a deaerated MeCN solution of $Sc(OTf)_3$ (2.0×10^{-3} M) was added by means of a microsyringe to a deaerated MeCN solution (2 mL) containing $[Fe(bpy)_3]^{2+}$ (8.5×10^{-5} M) and $[Fe^{IV}(O)(N4Py)]^{2+}$ (8.5×10^{-5} M).

Rates of ET from Fc to $[Fe^{IV}(O)(N4Py)]^{2+}$ in the presence of metal ions such as Y^{3+}, Lu^{3+}, Zn^{2+}, Mg^{2+}, and Ca^{2+} were performed on a Hewlett Packard 8453 photodiode-array spectrophotometer in MeCN at 298 K. These ET reaction were monitored by the decay and rise of absorption bands due to $[Fe^{IV}(O)(N4Py)]^{2+}$ (λ_{max} = 695 nm) and ferrocenium ion (λ_{max} = 615 nm), respectively. Typically, a deaerated MeCN solution containing $[Fe^{IV}(O)(N4Py)]^{2+}$ (1.0×10^{-4} M) was injected with a microsyringe to a deaerated MeCN solution (2 mL) containing Fc (2.0×10^{-3} M) and metal ion (1.0×10^{-3} M). All kinetic measurements were carried out under pseudo-first-order conditions where the concentrations of Fc and each metal ions were maintained to be more than 10-folds excess of that of $[Fe^{IV}(O)(N4Py)]^{2+}$. Kinetic measurements of the reaction between Fc (2.0×10^{-3} M) and $[Fe^{IV}(O)(N4Py)]^{2+}$ (1.0×10^{-4} M) in the presence of Sc^{3+} (5.0×10^{-4} M–4.0×10^{-3} M) were performed on a UNISOKU RSP-601 stopped-flow spectrometer equipped with a MOS-type highly

sensitive photodiode-array in MeCN at 298 K. Typically, a deaerated MeCN solution of $[Fe^{IV}(O)(N4Py)]^{2+}$ (2.0×10^{-4} M) and a deaerated MeCN solution of Fc (4.0×10^{-3} M) and Sc (2.0×10^{-3} M) were mixed.

Results and Discussion

When $[Fe^{II}(bpy)_3]^{2+}$ (bpy = 2,2'-bipyridine) was employed as an electron donor, no ET from $[Fe^{II}(bpy)_3]^{2+}$ (E_{ox} = 1.06 V vs SCE)[18] to $[Fe^{IV}(O)(N4Py)]^{2+}$ (E_{red} = 0.51 V) occurred in acetonitrile (MeCN), which is in agreement with the highly positive free energy change of ET (ΔG_{et} = 0.55 eV). In the presence of scandium triflate ($Sc(CF_3SO_3)_3$), however, the ET proceeded efficiently as shown in Figure 1. As the reaction proceeds, the absorption band due to $[Fe^{II}(bpy)_3]^{2+}$ (λ_{max} = 520 nm) and $[Fe^{IV}(O)(N4Py)]^{2+}$ (λ_{max} = 695 nm) decreases, accompanied by remaining a weak absorption band due to $[Fe^{III}(bpy)_3]^{3+}$ (λ_{max} = 600 nm) and by showing clean isosbestic points (Figure 1).

Formation of $[Fe^{III}(bpy)_3]^{3+}$ was also confirmed by EPR measurement. The solution containing $[Fe^{IV}(O)(N4Py)]^{2+}$ and $[Fe^{II}(bpy)_3]^{2+}$ exhibited no EPR signal; however, the solution after addition of 5 equiv of Sc^{3+} showed clear EPR signals due to $[Fe^{III}(bpy)_3]^{3+}$ (g = 2.6 and 1.6) (Figure 2a).[19] The EPR signal at g = 4.2 is assigned to a Fe(III) species with an intermediate spin (S = 3/2) by comparison with EPR spectra of Fe(III) complexes with S = 3/2.[20] Alternatively a rhombic S = 5/2 Fe(III) species may also afford an EPR signal at g = 4.2. Further addition of 30 equiv Sc^{3+} resulted in the decrease in the signal at g = 4.2 accompanied by the appearance of a new signal at g = 6.3, which may be assigned to an axial S = 5/2 Fe(III) species by comparison with EPR spectra of high spin Fe(III) complexes (Figure 2b).[21] Similar change in the EPR spectra was observed in ET from octamethylferrocene (E_{ox} = –0.04 V vs SCE) to $[Fe^{IV}(O)(N4Py)]^{2+}$ (see, Figure 3).[6] The identification of the intermediate and high spin Fe(III) products depending on concentration of Sc^{3+} is discussed together with the thermodynamic and kinetic data (vide infra).

When $[Fe^{II}(bpy)_3]^{2+}$ was replaced by $[Ru^{II}(bpy)_3]^{2+}$ (E_{ox} = 1.24 V vs SCE),[22] which is a weaker reductant than $[Fe^{II}(bpy)_3]^{2+}$ (E_{ox} = 1.06 V vs SCE),[18] the ET oxidation by $[Fe^{IV}(O)(N4Py)]^{2+}$ in the presence of Sc^{3+} was in equilibrium; the concentration of remaining $[Ru^{II}(bpy)_3]^{2+}$ decreased with an increase in Sc^{3+} concentration as shown in Figure 4 and 5a for the visible spectral changes in ET from $[Ru^{II}(bpy)_3]^{2+}$ to $[Fe^{IV}(O)(N4Py)]^{2+}$ in the presence of Sc^{3+}. The ET equilibrium constants (K_{et}) in eq 1 were then determined by global fitting of plots in Figure 5a.

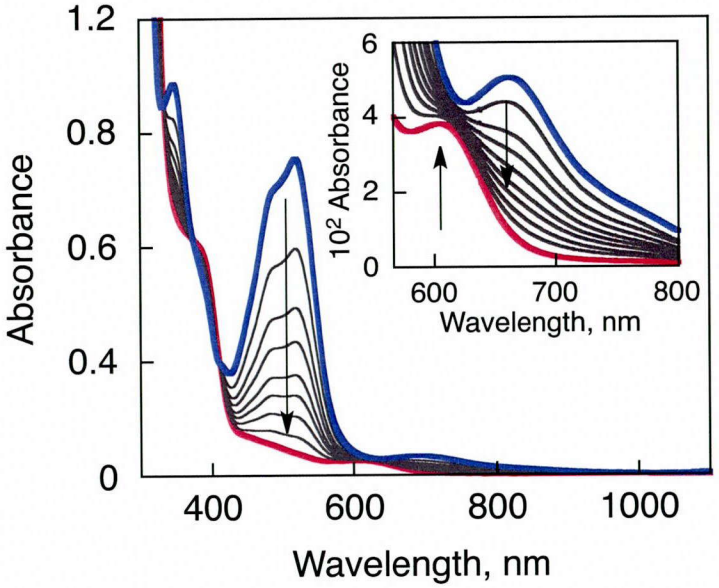

Figure 1. Visible spectral change observed in ET from $[Fe^{II}(bpy)_3]^{2+}$ (1.1×10^{-4} M) to $[Fe^{IV}(O)(N4Py)]^{2+}$ (1.1×10^{-4} M) in the presence of Sc^{3+} (1.0×10^{-2} M) in MeCN at 298 K.

The one-electron reduction potentials of $[Fe^{IV}(O)(N4Py)]^{2+}$ (E_{red}) in the presence of different amounts of Sc^{3+} were also determined from the K_{et} values and the E_{ox} value of $[Ru^{II}(bpy)_3]^{2+}$ using the Nernst equation (eq 2).

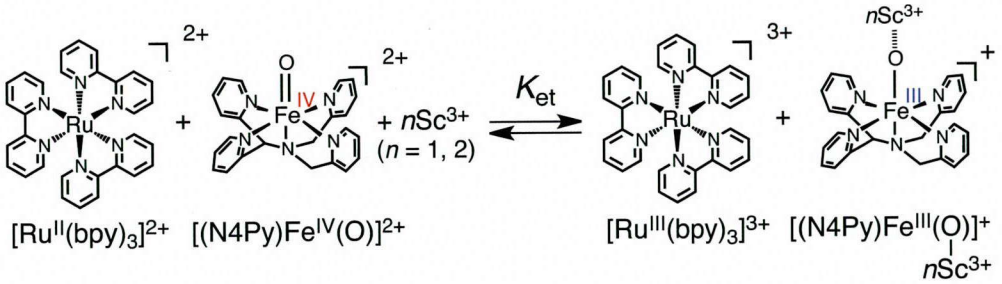

(1)

$$E_{red} = E_{ox} + (RT/F) \ln K_{et} \quad (2)$$

The E_{red} values were also determined from the K_{et} values obtained from the ET equilibrium between $[Ru^{II}(Me_2\text{-bpy})_3]^{2+}$ (Me_2-bpy: 4,4'-dimethyl-2,2'-bipyridine) (E_{ox} = 1.13 V vs SCE)[23] and $[Fe^{IV}(O)(N4Py)]^{2+}$ in the presence of different amounts of Sc^{3+} in MeCN at 298 K (see Figure 6 and Table 1 for the visible spectral changes in ET from $[Ru^{II}(Me_2\text{-bpy})_3]^{2+}$ to $[Fe^{IV}(O)(N4Py)]^{2+}$ and the K_{et} and E_{red} values, respectively).

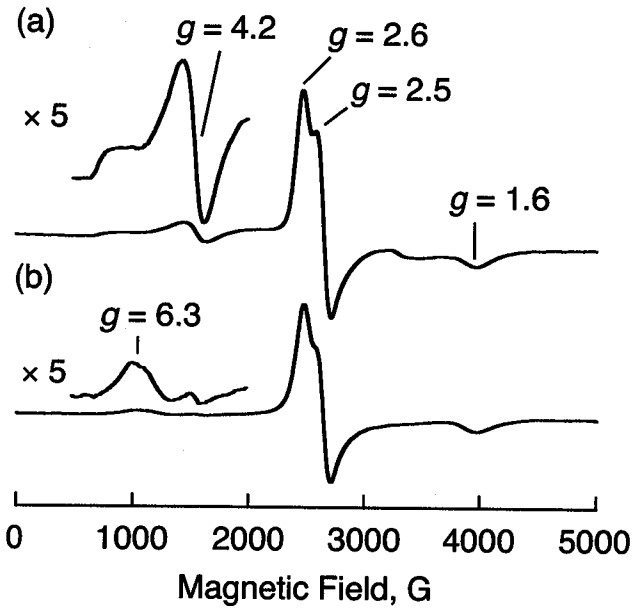

Figure 2. (a) EPR spectrum of an MeCN solution containing $[Fe^{II}(bpy)_3]^{2+}$ (1.0×10^{-3} M), $[Fe^{IV}(O)(N4Py)]^{2+}$ (1.0×10^{-3} M) and 5 equiv of Sc^{3+} (5.0×10^{-3} M) measured at 77 K. (b) EPR spectrum of an MeCN solution containing $[Fe^{II}(bpy)_3]^{2+}$ (1.0×10^{-3} M), $[Fe^{IV}(O)(N4Py)]^{2+}$ (1.0×10^{-3} M) and 30 equiv of Sc^{3+} (3.0×10^{-2} M) measured at 77 K.

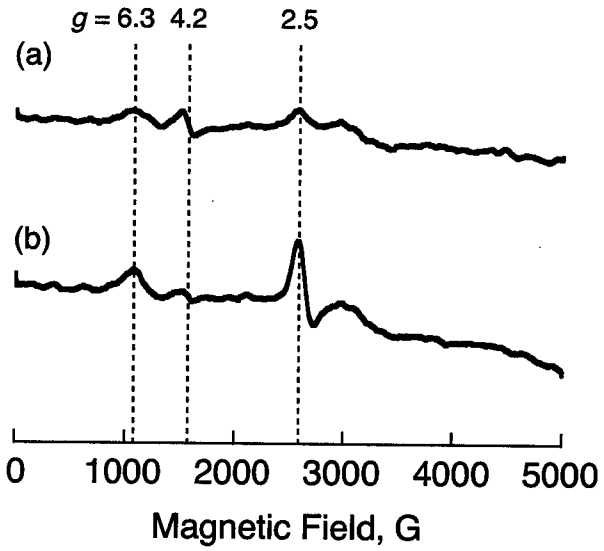

Figure 3. X-band EPR Spectra of $[Fe^{III}(O)(N4Py)]^{+}$ (1.0 mM) produced by addition of 1 equiv of octamethylferrocene in the presence of (a) 5 equiv Sc^{3+} and (b) 30 equiv Sc^{3+} in MeCN and recorded at 77 K.

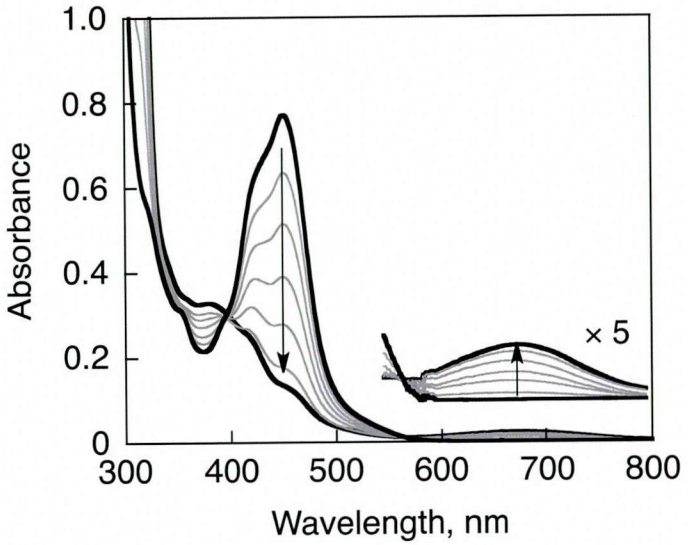

Figure 4. UV–vis spectral changes in ET from $[Ru^{II}(bpy)_3]^{2+}$ (5.7×10^{-4} M) to $[Fe^{IV}(O)(N4Py)]^{2+}$ (from 0 M to 6.8×10^{-4} M) in the presence of Sc^{3+} (2.0×10^{-1} M) in MeCN. Decay of the absorption band at 450 nm is due to $[Ru^{II}(bpy)_3]^{2+}$ and appearance of the absorption band at 680 nm is due to $[Ru^{III}(bpy)_3]^{3+}$.

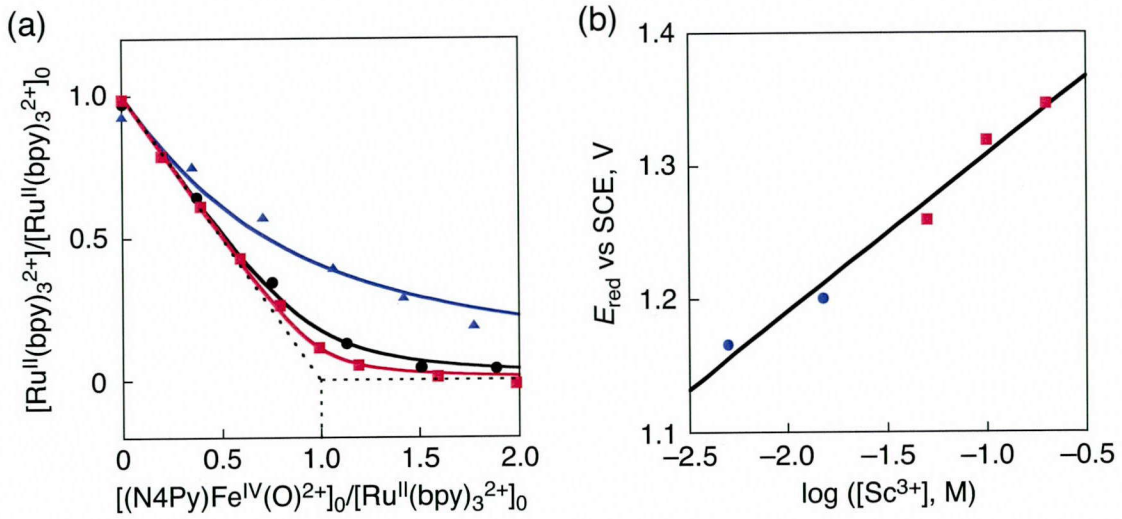

Figure 5. (a) Spectroscopic titration at 450 nm for the disappearance of $[Ru^{II}(bpy)_3]^{2+}$ as a function of equiv of $[Fe^{IV}(O)(N4Py)]^{2+}$ added to a solution of $[Ru^{II}(bpy)_3]^{2+}$ and Sc^{3+} (red square: 200 mM, black circle: 100 mM, blue triangle: 50 mM) in MeCN at 298 K. (b) $[Sc^{3+}]$ dependence of E_{red} of $[Fe^{IV}(O)(N4Py)]^{2+}$ in MeCN at 298 K. E_{red} were derived from equilibrium constants (K_{et}) of the ET from electron donor (blue circle: $[Ru^{II}(Me_2\text{-}bpy)_3]^{2+}$, red square: $[Ru^{II}(bpy)_3]^{2+}$) to $[Fe^{IV}(O)(N4Py)]^{2+}$.

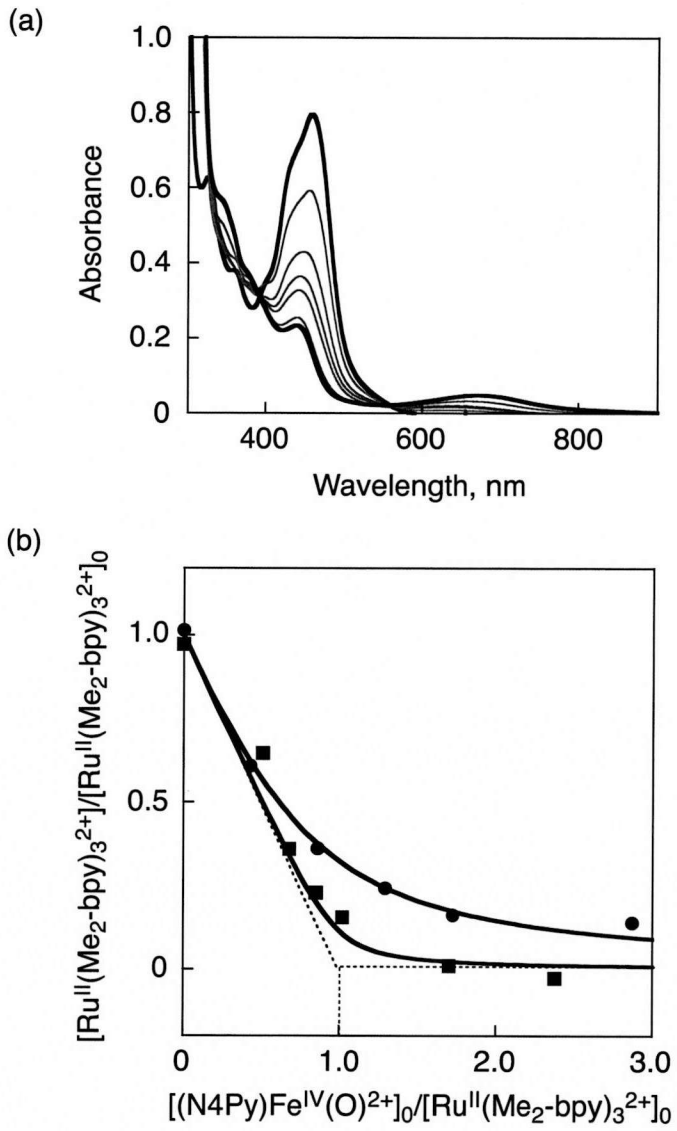

Figure 6. (a) UV–vis spectral changes in ET from $[Ru^{II}(Me_2\text{-bpy})_3]^{2+}$ (5.9×10^{-4} M) to $[Fe^{IV}(O)(N4Py)]^{2+}$ (from 0 to 1.6×10^{-3} M) in the presence of Sc^{3+} (1.5×10^{-2} M) in MeCN. Decay of the absorption band at 460 nm due to $[Ru^{II}(Me_2\text{-bpy})_3]^{2+}$ is accompanied by appearance of the weak absorption band at 650 nm due to $[Ru^{III}(Me_2\text{-bpy})_3]^{3+}$. (b) Spectroscopic titration at 460 nm for the disappearance of $[Ru^{II}(Me_2\text{-bpy})_3]^{2+}$ as a function of equiv of $[Fe^{IV}(O)(N4Py)]^{2+}$ added to a reaction solution containing $[Ru^{II}(Me_2\text{-bpy})_3]^{2+}$ (5.9×10^{-4} M) and Sc^{3+} (square: 15 mM, circle: 5 mM) at 298 K.

A plot of E_{red} vs log ($[Sc^{3+}]$) is shown in Figure 3b, which exhibits a linear correlation with the slope of 118 mV/log ($[Sc^{3+}]$). This indicates that the one-electron reduction of $[Fe^{IV}(O)(N4Py)]^{2+}$ is accompanied by binding of two Sc^{3+} ions to $[Fe^{III}(O)(N4Py)]^{+}$ (n = 2 in eq 1) in accordance with the Nernst equation (eq 3),[24] where E^{o}_{red} is the one-electron reduction potential without Sc^{3+}, and K_1 and K_2 are the

Table 1. One-Electron Oxidation Potentials (E_{ox}) of Electron Donors, Concentrations of Sc^{3+}, Equilibrium Constants (K_{et}) for ET from Electron Donors to $[Fe^{IV}(O)(N4Py)]^{2+}$, and One-Electron Reduction Potentials of $[Fe^{IV}(O)(N4Py)]^{2+}$ (E_{red}) in MeCN at 298 K

electron donor	E_{ox} (V vs SCE)	$[Sc^{3+}]$ (mM)	K_{et}	E_{red} (V vs SCE)
$[Ru^{II}(bpy)_3]^{2+}$	1.24	200	6.4 × 10	1.35
		100	2.2 × 10	1.32
		50	2.2	1.26
$[Ru^{II}(Me_2\text{-}bpy)_3]^{2+}$	1.13	15	5.0 × 10	1.20
		5.0	4.4	1.17

formation constants of 1:1 and 1:2 complexes of $[Fe^{III}(O)(N4Py)]^{+}$ with one Sc^{3+} and two Sc^{3+} ions, respectively.

$$E_{red} = E^{o}_{red} + (2.3RT/F) \log (1 + K_1[Sc^{3+}] + K_1K_2[Sc^{3+}]^2) \quad (3)$$

When $K_1[Sc^{3+}]$ and $K_2[Sc^{3+}] >> 1$, the slope of the plot of E_{red} vs log $[Sc^{3+}]$ is 2 × (2.3*RT*/*F*) that corresponds to 118 mV/log ($[Sc^{3+}]$) at 298 K, which is in agreement with the result in Figure 5b. The E_{red} value in the presence of 0.20 M Sc^{3+} is shifted to 1.35 V vs SCE, which is by 0.84 V higher than the value in its absence.

Since the Nernst plot in Figure 5b indicates that two Sc^{3+} ions bind to $[Fe^{III}(O)(N4Py)]^{+}$ with large excess Sc^{3+}, the Fe^{III} species detected by EPR in Figure 2b may be assigned to a 1:2 complex between $[Fe^{III}(O)(N4Py)]^{+}$ and Sc^{3+} ion, $[Fe^{III}(O)(N4Py)]^{+}$–$(Sc^{3+})_2$.[25] The optimized structure of $[Fe^{III}(O)(N4Py)]^{+}$–$(Sc^{3+})_2$ by the DFT calculation is shown in Figure 7. In such a case, the Fe^{III} species in Figure 2a may be assigned to a 1:1 complex between $[Fe^{III}(O)(N4Py)]^{+}$ and Sc^{3+}, $[Fe^{III}(O)(N4Py)]^{+}$–Sc^{3+}.[25]

Formation of the 1:2 complex, $[Fe^{III}(O)(N4Py)]^{+}$-$(Sc^{3+})_2$, is supported not only by the thermodynamic measurements in Figure 5b but also by the kinetic measurements (vide infra). The ET rate constants from $[Fe^{II}(bpy)_3]^{2+}$ to $[Fe^{IV}(O)(N4Py)]^{2+}$ were determined by monitoring a decrease in absorption peaks at 520 nm and 695 nm due to $[Fe^{II}(bpy)_3]^{2+}$ and $[Fe^{IV}(O)(N4Py)]^{2+}$, respectively. Using the same concentration of $[Fe^{II}(bpy)_3]^{2+}$ and $[Fe^{IV}(O)(N4Py)]^{2+}$ in the presence of a large excess of Sc^{3+}, the rate obeyed second-order kinetics, and the second-order rate constants (k_{obs}) in the presence of various concentrations of Sc^{3+} were determined from the second-order plot (Figure 8).

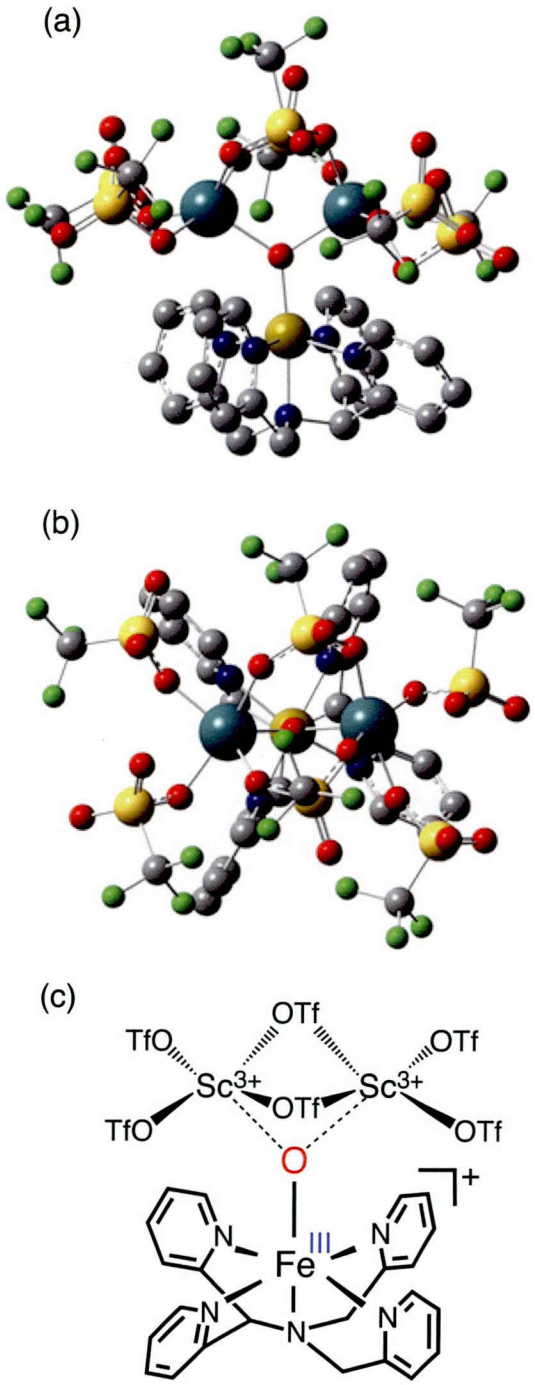

Figure 7. Optimized structure of $[Fe^{III}(O)(N4Py)]^{+}$–$(Sc^{3+})_2$ by DFT calculations (B3LYP, 3-31G*); (a) side view, (b) top view, and (c) chemical structure.

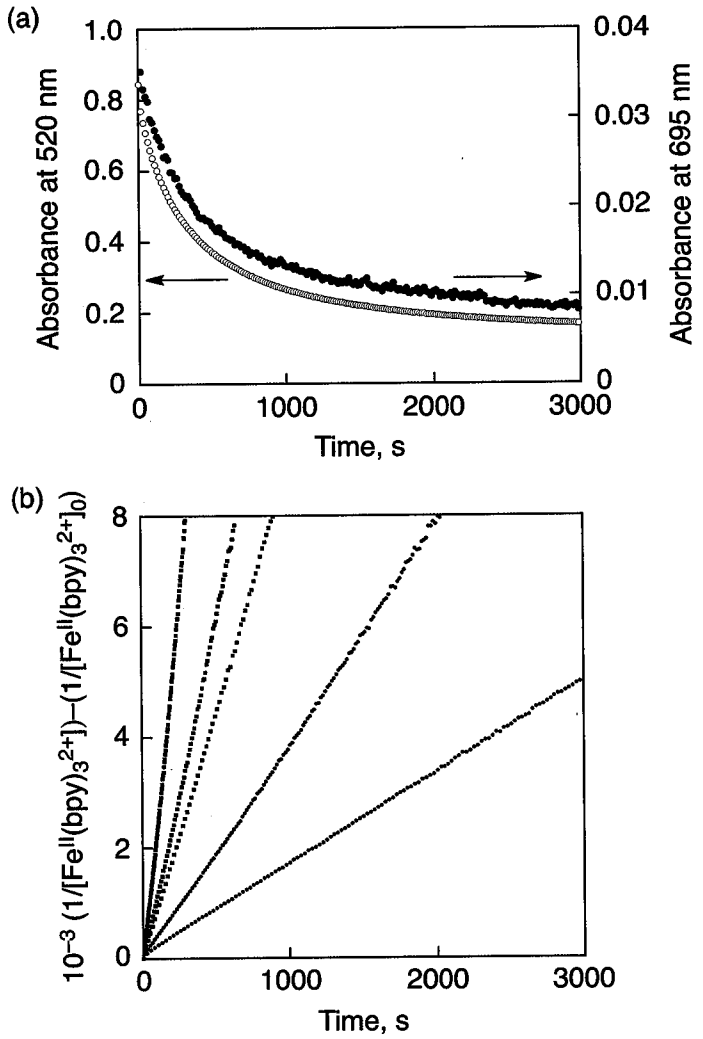

Figure 8. (a) Time profiles of absorption changes at 520 nm and 695 nm due to $[Fe^{II}(bpy)_3]^{2+}$ (open circle) and $[Fe^{IV}(O)(N4Py)]^{2+}$ (closed circle), respectively, in ET from $[Fe^{II}(bpy)_3]^{2+}$ (8.5×10^{-5} M) to $[Fe^{IV}(O)(N4Py)]^{2+}$ (8.5×10^{-5} M) in the presence of Sc^{3+} (4.0×10^{-3} M) in MeCN at 298 K. (b) Second-order plots in ET from $[Fe^{II}(bpy)_3]^{2+}$ (8.5×10^{-5} M) to $[Fe^{IV}(O)(N4Py)]^{2+}$ (8.5×10^{-5} M) in the presence of Sc^{3+} (2.0×10^{-3}–1.2×10^{-2} M) in MeCN at 298 K.

The dependence of k_{obs} on $[Sc^{3+}]$ is shown in Figure 9, where the k_{obs} value increases with exhibiting a first-order dependence on $[Sc^{3+}]$ at low concentrations, changing to a second-order dependence at high concentrations as given by eq 4.[26]

$$k_{obs} = [Sc^{3+}](k_1 + k_2[Sc^{3+}]) \quad (4)$$

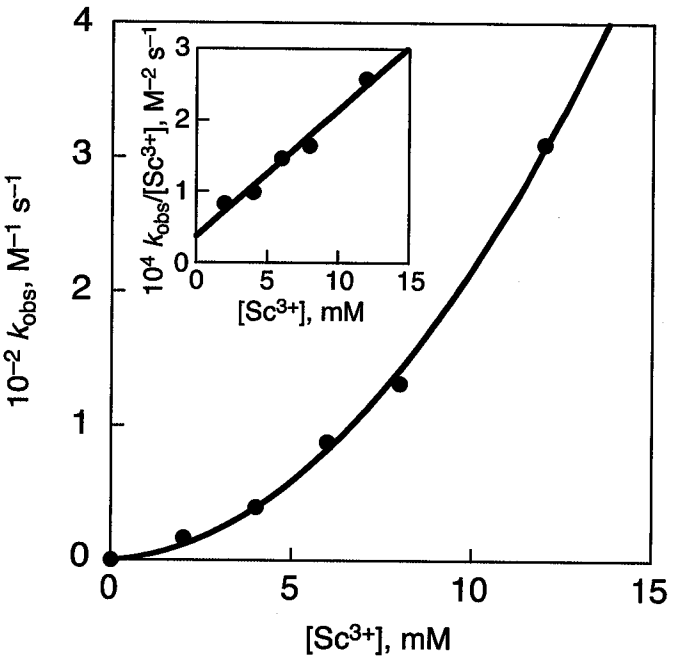

Figure 9. Dependence of k_{obs} on [Sc^{3+}] for the ET from $[Fe^{II}(bpy)_3]^{2+}$ (85 mM) to $[Fe^{IV}(O)(N4Py)]^{2+}$ (85 mM) in the presence of Sc^{3+} (2.0 – 12.5 mM) in MeCN at 298 K. Inset: Plot of k_{obs} /[Sc^{3+}] vs [Sc^{3+}].

The k_1 and the k_1 and k_2 values were determined from the intercept and the slope of the linear plot of k_{obs}/[Sc^{3+}] vs [Sc^{3+}] (inset of Figure 4), respectively. The k_{obs} value in the presence of 12 mM of Sc^{3+} is 2.5×10^2 M^{-1} s^{-1}, which is ca. 10^8-fold larger than the predicted value without Sc^{3+}.[27] When the author employed Fc as an electron donor (E_{ox} = 0.37 V), ET was accelerated by the addition of not only Sc^{3+} but also by other metal ions such as Y^{3+}, Lu^{3+}, Zn^{2+}, Mg^{2+} and Ca^{2+}, which are weaker Lewis acids than Sc^{3+}. Spectral change, time course of the reaction followed with the decay in absorption band due to the iron(IV)-oxo complex, and pseudo-first-order rate constants determined in ET from Fc to $[Fe^{IV}(O)(N4Py)]^{2+}$ in the absence and presence of Sc^{3+} are shown in Figure 10, and 11.

Figure 12 shows pseudo-first-order rate constants of ET from Fc to $[Fe^{IV}(O)(N4Py)]^{2+}$ in the presence of various metal ions. The k_1 and k_2 values for various metal ions were also determined from the dependence of kobs on concentrations of metal ions in Figure 13a using eq 5, where k_0 is the ET rate constant without metal ion.

$$k_{obs} = k_0 + k_1[M^{n+}] + k_2[M^{n+}]_2 \qquad (5)$$

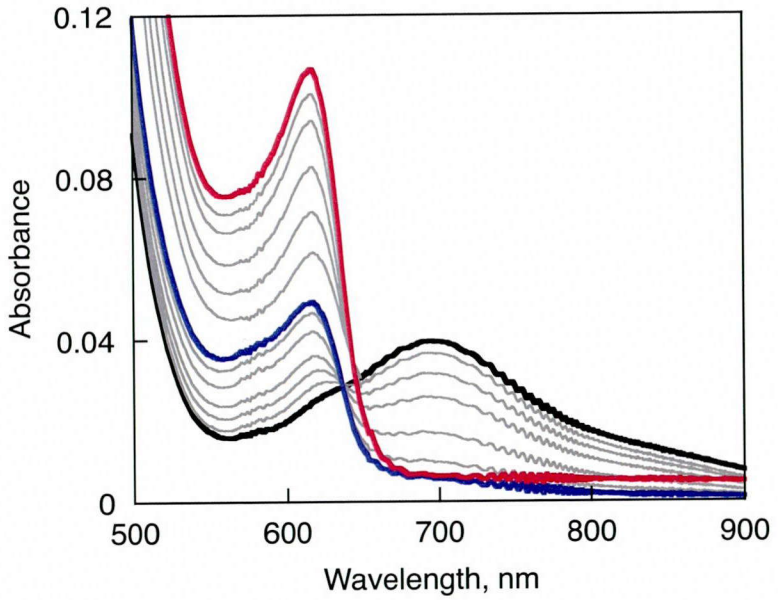

Figure 10. Absorption change in ET from Fc (2.0×10^{-3} M) to $[Fe^{IV}(O)(N4Py)]^{2+}$ (1.0×10^{-4} M) (black to blue: in the absence of Sc^{3+} every 50 seconds) (black to red: in the presence of Sc^{3+} (1.0×10^{-3} M) every 0.5 seconds) in MeCN at 298 K.

K. Ohkubo *et al.* have previously reported that the binding energies (ΔE) of metal ions with $O_2^{\bullet-}$ can be evaluated from the g_{zz} values of the $O^{2\bullet}$–M^{n+} complexes and that the ΔE values are well correlated with logarithm of rate constants of metal ion-coupled electron-transfer (MCET) reduction of *p*-benzoquinone as well as O_2.[9] Plots of log k_1 and log k_2 vs ΔE is shown in Figure 13b, where log k_1 and log k_2 are linearly correlated with ΔE.[28] Thus, the stronger the Lewis acidity of metal ions, the larger become the rate constants (k_1 and k_2) of MCET from Fc to $[Fe^{IV}(O)(N4Py)]^{2+}$.

Conclusion

In summary, the author have demonstrated that metal ions promote ET reduction of $[Fe^{IV}(O)(N4Py)]^{2+}$ markedly. The MCET reactivity increases with increasing the Lewis acidity of metal ions. Among metal ions, Sc^{3+} is the most effective, exhibiting 10^8-fold acceleration of the MCET rate.

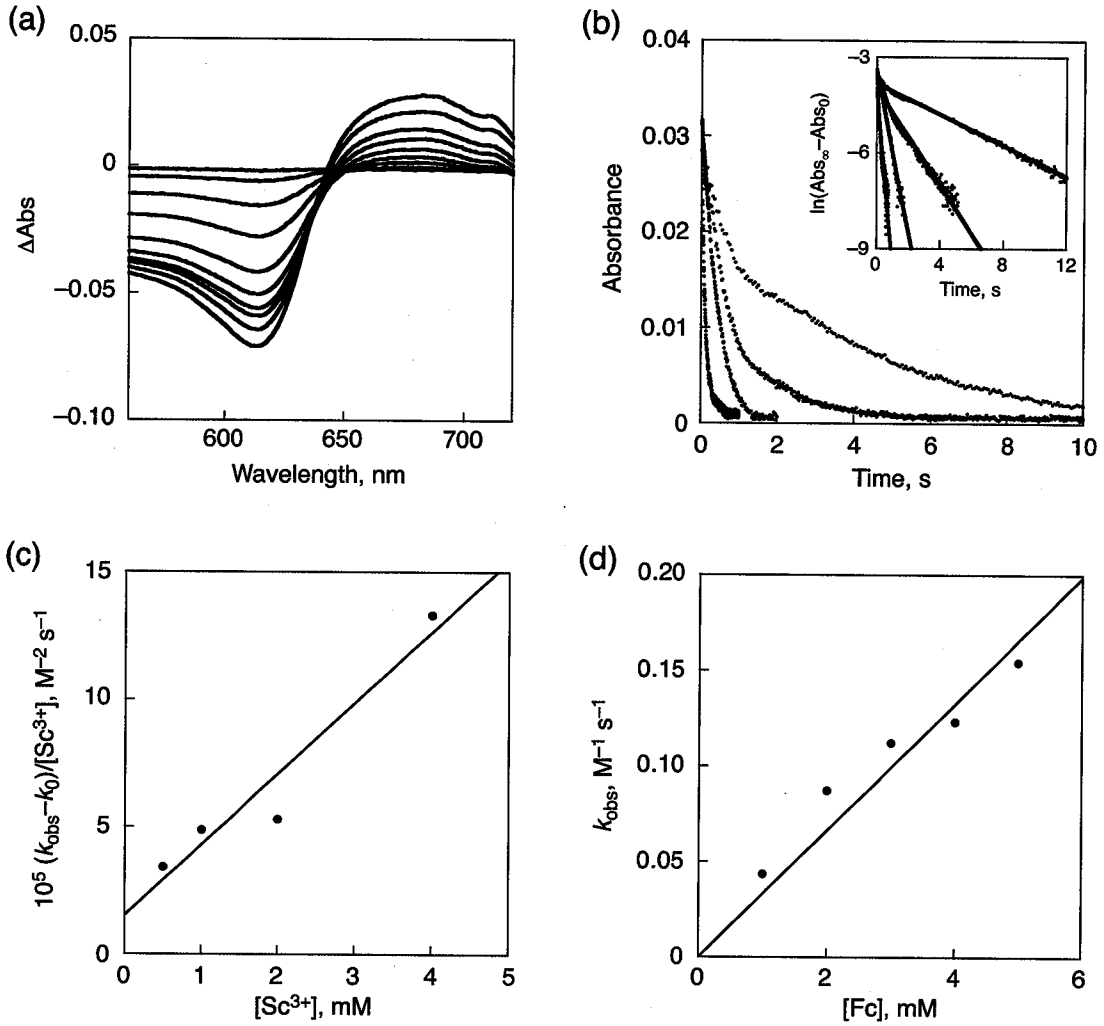

Figure 11. (a) Difference absorption change in ET from Fc (2.0×10^{-3} M) to $[Fe^{IV}(O)(N4Py)]^{2+}$ (1.0×10^{-4} M) in the presence of Sc^{3+} (1.0×10^{-3} M) in MeCN at 298 K. (b) Time profiles of the absorbance at 695 nm due to $[Fe^{IV}(O)(N4Py)]^{2+}$ in ET from Fc (2.0×10^{-3} M) to $[Fe^{IV}(O)(N4Py)]^{2+}$ (1.0×10^{-4} M) in the presence of Sc^{3+} (5.0×10^{-4}–4.0×10^{-3} M) in MeCN at 298 K. Inset shows the first-order plots. (c) Plot of $(k_{obs} - k_0)/[Sc^{3+}]$ vs $[Sc^{3+}]$. (d) Plot of the pseudo-first-order rate constant (k_{obs}) for ET from Fc to $[Fe^{IV}(O)(N4Py)]^{2+}$ (1.0×10^{-4} M) in the presence of Sc^{3+} (2.0×10^{-4} M) vs [Fc] in MeCN at 298 K.

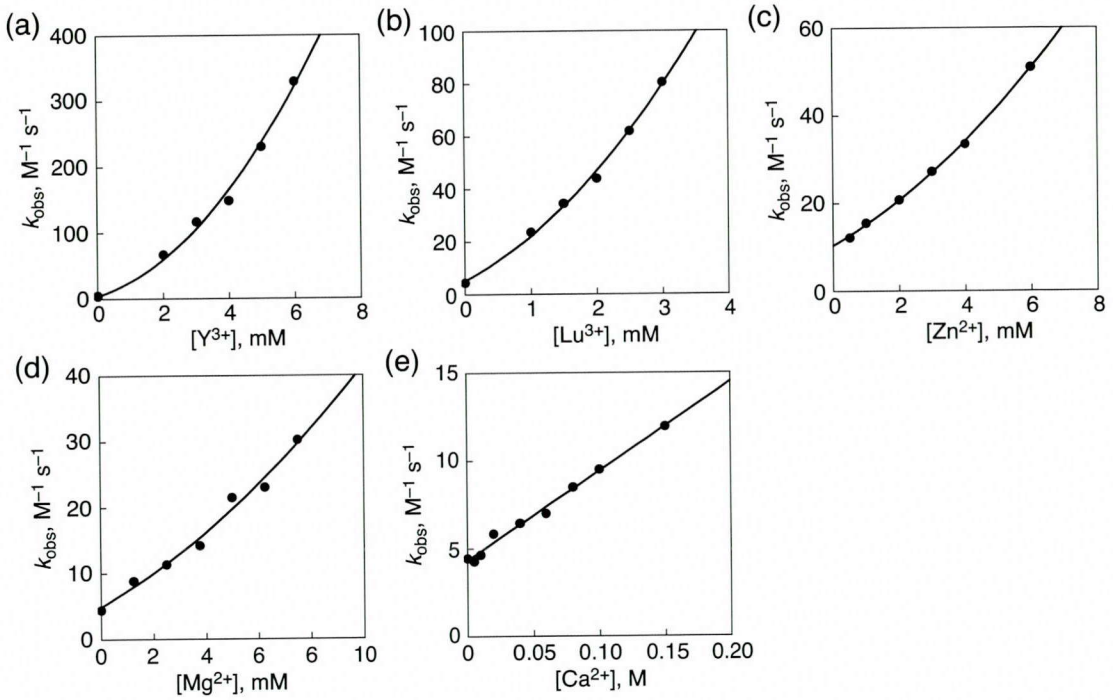

Figure 12. Plots of the rate constant of ET (k_{et}) from Fc (2.0 mM) to $[Fe^{IV}(O)(N4Py)]^{2+}$ (0.10 mM) in the presence of (a) Y^{3+}, (b) Lu^{3+}, (c) Zn^{2+}, (d) Mg^{2+}, and (e) Ca^{2+} in MeCN at 298 K vs metal ion concentrations.

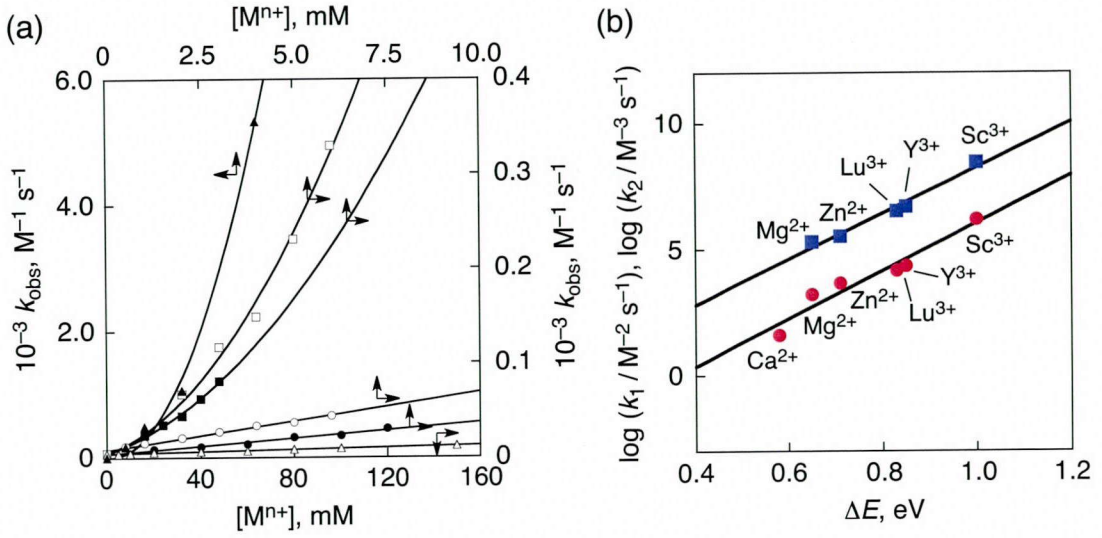

Figure 13. (a) Dependence of k_{obs} of ET from Fc (2.0×10^{-3} M) to $[Fe^{IV}(O)(N4Py)]^{2+}$ (1.0×10^{-4} M) on metal ion concentrations (closed triangle: Sc^{3+}, open square: Y^{3+}, closed square: Lu^{3+}, open circle: Zn^{2+}, closed circle: Mg^{2+}, open triangle: Ca^{2+}) in MeCN at 298 K. (b) Plots of log k_1 (red circle) and log k_2 (blue square) vs DE (quantitative measure of Lewis acidity of metal ions).

References

(1) (a) Ferreira, K. N.; Iverson, T. M.; Maghlaoui, K.; Barber, J.; Iwata S. *Science* **2004**, *303*, 1831. (b) Loll, B.; Kern, J.; Saenger, W.; Zouni, A.; Biesiadka, J. *Nature* **2005**, *438*, 1040. (c) McEvoy, J. P.; Brudvig, G. W. *Chem. Rev.* **2006**, *106*, 4455. (d) Sproviero, E. M.; Gascón, J. A.; McEvoy, J. P.; Brudvig, G. W.; Batista V. S. *J. Am. Chem. Soc.* **2008**, *130*, 3428. (e) Barber, J. *Chem. Soc. Rev.* **2009**, *38*, 185.

(2) Ferguson-Miller, S.; Babcock, G. T. *Chem. Rev.* **1996**, *96*, 2889.

(3) Sono, M.; Roach, M. P.; Coulter, E. D.; Dawson, J. H. *Chem. Rev.* **1996**, *96*, 2841.

(4) Yin, G. *Coord. Chem. Rev.* **2010**, *254*, 1826.

(5) (a) Pestovsky, O; Bakac, A. *J. Am. Chem. Soc.* **2003**, *125*, 14714. (b) Comba, P.; Fukuzumi, S.; Kotani, H.; Wunderlich, S. *Angew. Chem., Int. Ed.* **2010**, *49*, 2622. (c) Hirai, Y.; Kojima, T.; Mizutani, Y.; Shiota, Y.; Yoshizawa, K.; Fukuzumi, S. *Angew. Chem., Int. Ed.* **2008**, *47*, 5772.

(6) (a) Lee, Y.-M.; Kotani, H.; Suenobu, T.; Nam, W.; Fukuzumi, S. *J. Am. Chem. Soc.* **2008**, *130*, 434. (b) Fukuzumi, S.; Kotani, H.; Suenobu, T.; Hong, S.; Lee, Y.-M.; Nam, W. *Chem.–Eur. J.* **2010**, *16*, 354.

(7) (a) Fukuzumi, S.; Morimoto, Y.; Kotani, H.; Naumov, P.; Lee, Y.-M.; Nam, W. *Nature Chem.* **2010**, *2*, 756. (b) Karlin, K. D. *Nature Chem.* **2010**, *2*, 711.

(8) (a) Fukuzumi, S. *Prog. Inorg. Chem.* **2009**, *56*, 49. (b) Fukuzumi, S. *Bull. Chem. Soc. Jpn.* **1997**, *70*, 1. (c) Fukuzumi, S.; Ohkubo, K. *Coord. Chem. Rev.* **2010**, *254*, 372.

(9) Fukuzumi, S.; Ohkubo, K. *Chem.–Eur. J.* **2000**, *6*, 4532.

(10) For the effect of Lewis acid metal ions on the catalytic oxidation of alkanes by peroxides, see: Yiu, S.-M.; Man, W.-L.; Lau, T.-C. *J. Am. Chem. Soc.* **2008**, *130*, 10821.

(11) (a) Lubben, M.; Meetsma, A.; Wilkinson, E. C.; Feringa, B.; Que, L., Jr. *Angew. Chem., Int. Ed.* **1995**, *34*, 1512. (b) Kaizer, J.; Klinker, E. J.; Oh, N. Y.; Rohde, J.–U.; Song, W. J.; Stubna, A.; Kim, J.; Münck, E.; Nam, W.; Que, L., Jr. *J. Am. Chem. Soc.* **2004**, *126*, 472.

(12) (a) Cukier, R. I.; Nocera, D. G. *Annu. Rev. Phys. Chem.* **1998**, *49*, 337. (b) Mayer, J. M. *Annu. Rev. Phys. Chem.* **2004**, *55*, 363.

(13) (a) Moyer, B. A.; Meyer, T. J. *Inorg. Chem.* **1981**, *20*, 436. (b) Huynh, M. H. V.; Meyer, T. J. *Chem. Rev.* **2007**, *107*, 5004. (c) Concepcion, J. J.; Jurss, J. W.; Brennaman, M. K.; Hoertz, P. G.; Patrocinio, A. O. T.; Iha, N. Y. M.; Templeton, J. L.; Meyer, T. J. *Acc. Chem. Res.* **2009**, *42*, 1954.

(14) Armarego, W. L. F.; Chai, C. L. L. *Purification of Laboratory Chemicals*, 6th ed; Pergamon Press: Oxford, 2009.

(15) Saltzman, H.; Sharefkin, J. G. *Organic Syntheses*; Collect. Vol. V; Wiley: New York, 1973, p 658.

(16) (a) Sastri, C. V.; Oh, K.; Lee, Y. J.; Seo, M. S.; Shin, W.; Nam, W. *Angew. Chem., Int. Ed.* **2006**, *45*, 3992. (b) Kaizer, J.; Klinker, E. J.; Oh, N. Y.; Rohde, J.–U.; Song, W. J.; Stubna, A.; Kim, J.; Münck, E.; Nam, W.; Que, L., Jr. *J. Am. Chem. Soc.* **2004**, *126*, 472.

(17) (a) Lin, C-T.; Bottcher, W.; Chou, M.; Creutz, C.; Sutin, N. *J. Am. Chem. Soc.* **1976**, *98*, 6536. (b) Fussa-Rydel, O.; Zhang, H. T.; Hupp, J. T.; Leidnert C. R. *Inorg. Chem.* **1989**, *28*, 1533.

(18) Fukuzumi, S.; Yoshida, Y.; Urano, T.; Suenobu, T.; Imahori, H. *J. Am. Chem. Soc.* **2001**, *123*, 11331.

(19) For the EPR spectrum due to $[Fe^{III}(bpy)_3]^{3+}$, see: DeSimone, R. E.; Drago, R. S. *J. Am. Chem. Soc.* **1970**, *92*, 2343.

(20) (a) Sakai, T.; Ohgo, Y.; Ikeue, T.; Takahashi, M.; Takeda, M.; Nakamura, M. *J. Am. Chem. Soc.* **2003**, *125*, 13028. (b) Kostka, K. L.; Fox, B. G.; Hendrich, M. P.; Collins, T. J.; Rickard, C. E. F.; Wright, L. J.; Münck, E. *J. Am. Chem. Soc.* **1993**, *115*, 6746.

(21) (a) Hijazi, I.; Roisnel, T.; Even-Hernandez, P.; Geneste, F.; Cador, O.; Guizouarn, T.; Boitrel, B. *Inorg. Chem.* **2010**, *49*, 7536. (b) Rath, S. P.; Olmstead, M. M.; Balch, A. L. *Inorg. Chem.* **2006**, *45*, 6083. (c) Annaraj, J.; Suh, Y.; Seo, M. S.; Kim, S. O.; Nam, W. *Chem. Commun.* **2005**, 4529.

(22) Fukuzumi, S.; Nakanishi, I.; Tanaka, K.; Suenobu, T.; Tabard, A.; Guilard, R.; Caemelbecke, E. V.; Kadish, K. M. *J. Am. Chem. Soc.* **1999**, *121*, 785.

(23) Vögtle, F.; Plevoets, M.; Nieger, M.; Azzellini, G. C.; Credi, A.; Cola, L. D.; Marchis, V. D.; Venturi, M.; Balzani, V. *J. Am. Chem. Soc.* **1999**, *121*, 6290.

(24) For similar Nernst analyses, see: (a) Yuasa, J.; Suenobu, T.; Fukuzumi, S. *J. Am. Chem. Soc.* **2003**, *125*, 12090. (b) Okamoto, K.; Imahori, H.; Fukuzumi, S. *J. Am. Chem. Soc.* **2003**, *125*, 7014.

(25) The detection of complexes between $[Fe^{III}(O)(N4Py)]^{+}$ and Sc^{3+} with ESI-MS has yet to be successful.

(26) Judging from the dependence of k_{obs} on $[Sc^{3+}]$ in Figure 4, there should be a weak pre-equilibrium binding of Sc^{3+} to $[Fe^{IV}(O)(N4Py)]^{2+}$ prior to electron transfer.

(27) Although no ET from $[Fe^{II}(bpy)_3]^{2+}$ to $[Fe^{IV}(O)(N4Py)]^{2+}$ occurs without Sc^{3+} due to the highly positive free energy change of ET (ΔG_{et}), the rate constant of ET is

predicted based on the Marcus theory of ET using the λ value of 2.74 eV and ΔG_{et} value of 0.55 eV; see ref 6a.

(28) The k_2 value for Ca^{2+} was too small to be determined accurately.

Chapter 3: Mechanistic Borderline of One-Step Hydrogen Atom Transfer versus Stepwise Sc^{3+}-Coupled Electron Transfer from Benzyl Alcohol Derivatives to a Non-Heme Iron(IV)-Oxo Complex

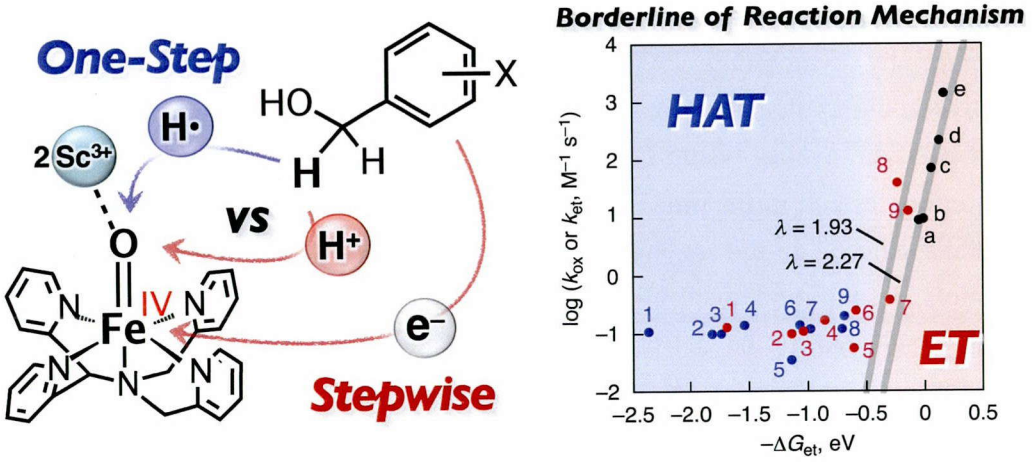

Abstract: The rate of oxidation of 2,5-dimethoxybenzyl alcohol (2,5-$(MeO)_2C_6H_3CH_2OH$) by $[Fe^{IV}(O)(N4Py)]^{2+}$ (N4Py = *N*,*N*-bis(2-pyridylmethyl)-*N*-bis(2-pyridyl)methylamine) was enhanced significantly in the presence of $Sc(OTf)_3$ (OTf^- = trifluoromethanesulfonate) in acetonitrile (e.g., 120 folds acceleration in the presence of Sc^{3+}). Such a remarkable enhancement of the reactivity of $[Fe^{IV}(O)(N4Py)]^{2+}$ in the presence of Sc^{3+} was accompanied by the disappearance of a kinetic deuterium isotope effect. The radical cation of 2,5-$(MeO)_2C_6H_3CH_2OH$ was detected in the course of the reaction in the presence of Sc^{3+}. The dimerized alcohol and aldehyde were also produced in addition to the monomer aldehyde in the presence of Sc^{3+}. These results indicate that the reaction mechanism is changed from one-step hydrogen atom transfer (HAT) from 2,5-$(MeO)_2C_6H_3CH_2OH$ to $[Fe^{IV}(O)(N4Py)]^{2+}$ in the absence of Sc^{3+} to stepwise Sc^{3+}-coupled electron transfer, followed by proton transfer in the presence of Sc^{3+}. In contrast, neither acceleration of the rate nor the disappearance of the kinetic deuterium isotope effect was observed in the oxidation of benzyl alcohol ($C_6H_5CH_2OH$) by $[Fe^{IV}(O)(N4Py)]^{2+}$ in the presence of $Sc(OTf)_3$. Moreover, the rate constants determined in the oxidation of various benzyl alcohol derivatives by $[Fe^{IV}(O)(N4Py)]^{2+}$ in the presence of $Sc(OTf)_3$ (10 mM) were compared with those of Sc^{3+}-coupled electron transfer from one-electron reductants to $[Fe^{IV}(O)(N4Py)]^{2+}$ at the same driving force of electron transfer. This comparison revealed that the borderline of the change in the mechanism from HAT to stepwise Sc^{3+}-coupled electron transfer and proton transfer is dependent on the one-electron oxidation potential of benzyl alcohol derivatives (ca. 1.7 V vs SCE).

Introduction

Homolytic C–H bond cleavage of organic compounds is one of the fundamental reaction steps in various types of oxidation processes both in synthetic and biological chemistry.[1] Laboratory-scale syntheses and industrial oxidation processes have utilized metal-oxo reagents (e.g., $KMnO_4$) and metal oxide surface for the oxidation of organic substrates.[2,3] In the oxidative enzymes, heme and non-heme iron oxygenases represented by cytochrome P450 and taurine/α-ketoglutarate dioxygenase (TauD), respectively, high-valent iron-oxo species have been regarded as reactive intermediates in their catalytic cycles, where C–H bond is cleaved by oxometal species (M=O) and O–H bond is formed in the process of hydrogen atom transfer (HAT) from substrate to oxometal species.[4-6] In the enzymatic oxidation reactions, e.g., hydroxylation, oxidation of alcohols, desaturation, cyclization, and chlorination, the initial step of those processes is widely believed to be activation of C–H bonds via HAT from a substrate to high-valent iron-oxo species.[4-10]

In general, there are three possible reaction pathways in HAT reactions of iron-oxo species (Fe^{IV}=O), as shown in Scheme 1. Since hydrogen atom consists of an electron and a proton, the proposed mechanisms are (1) stepwise proton transfer followed by electron transfer (PT/ET), (2) stepwise electron transfer followed by proton transfer (ET/PT), and (3) one-step HAT, in which an electron and a proton are transferred in a concerted manner. In the case of iron-oxo species, one-step HAT can be generally regarded as concerted proton-electron transfer (CPET),

Scheme 1. Three Possible Reaction Pathways in HAT Reactions of Iron-Oxo Species

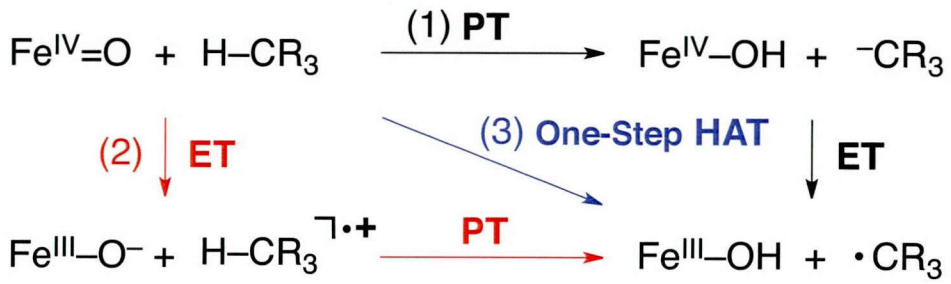

because an electron and a proton are transferred simultaneously to the metal center and the oxo moiety, respectively.[11] Tremendous efforts have so far been devoted to elucidate the mechanism of HAT reactions of iron-oxo species by employing model complexes bearing heme and non-heme ligands in the field of bioinorganic chemistry, where the transfer of an electron and a proton proceeds in a concerted maner.[11-19] There

are some cases where C–H bond activation by iron-oxo species undergoes via an ET/PT pathway when electron-rich substrates such as *N,N*-dimethylaniline derivatives are used as substrates.[20] In the case of HAT reactions from substrates to triplet excited states of photosensitizers, the mechanistic borderline of one-step HAT vs ET/PT pathways has been clarified by changing electron donor ability of hydrogen donors as well as electron acceptor ability of hydrogen acceptors.[21] The borderline of one-step hydride-transfer vs ET/PT pathways has also been discussed for Sc^{3+}-promoted hydride transfer from an NADH analog to a *p*-benzoquinone derivative.[22,23] There are also studies on the mechanistic change from one-step HAT to ET/PT with metal-centered oxidants.[24,25] However, the mechanistic borderline of one-step HAT vs ET/PT pathways in C–H bond cleavage by iron-oxo species has yet to be clarified due to the lack of systematic studies.

We report herein one example of the switch of the reaction pathway from a one-step HAT pathway in C–H bond activation of benzyl alcohol derivatives (X-$C_6H_4CH_2OH$) with a non-heme iron(IV)-oxo complex, $[Fe^{IV}(O)(N4Py)]^{2+}$ (N4Py = *N,N*-bis(2-pyridylmethyl)-*N*-bis(2-pyridyl)methylamine),[15,16] to a stepwise ET/PT pathway by addition of Sc^{3+}. We have recently reported that one-electron reduction of $[Fe^{IV}(O)(N4Py)]^{2+}$ is accelerated by the addition of Lewis acids such as Ca^{2+}, Mg^{2+} and Zn^{2+}, etc.[26,27] Electron-acceptability of $[Fe^{IV}(O)(N4Py)]$ is enhanced by the much stronger binding of Sc^{3+} to $[Fe^{III}(O)(N4Py)]$ than $[Fe^{IV}(O)(N4Py)]$. We have chosen Sc^{3+} in this work, because Sc^{3+} has the largest acceleration effect among examined metal ions. In the presence of 10 mM of Sc^{3+}, the reduction potential of the iron(IV)-oxo complex (E_{red}) was shifted from 0.51 V vs SCE to the positive direction up to 1.19 V.[26-30] Such a change in the E_{red} value of $[Fe^{IV}(O)(N4Py)]^{2+}$ by the presence of Sc^{3+} and well-determined reduction potential provides an excellent opportunity to scrutinize the borderline of one-step HAT vs ET followed by subsequent PT steps in C–H bond activation by metal-oxo species in a systematic manner.

Experimental Section

Materials. benzyl alcohol ($C_6H_5CH_2OH$), pentamethylbenzyl alcohol ($Me_5C_6CH_2OH$), 2,5-dimethoxybenzyl alcohol (2,5-$(MeO)_2C_6H_3CH_2OH$), 2,5-dimethoxybenzoic acid and scandium(III) trifluoromethanesulfonate ($Sc(OTf)_3$) were purchased from Aldrich Chemicals Co. *p*-chlorobenzyl alcohol (*p*-$ClC_6H_4CH_2OH$), *p*-methylbenzyl alcohol (*p*-$MeC_6H_4CH_2OH$), 3,5-dimethoxybenzyl alcohol (3,5-$(MeO)_2C_6H_3CH_2OH$), 3,4,5-trimethoxybenzyl alcohol (3,4,5-$(MeO)_3C_6H_2CH_2OH$) and benzoic acid were obtained from Tokyo Chemical Industry Co., Ltd. *p*-nitrobenzyl alcohol (*p*-$NO_2C_6H_4CH_2OH$) and *p*-methoxybenzyl alcohol (*p*-$MeOC_6H_4CH_2OH$) were

obtained from Wako Pure Chemical Industries, Ltd. and lithium aluminum deuteride ($LiAlD_4$) was purchased from CIL, Inc. The commercially available compounds used in this study were the best available purity and used without further purification unless otherwise noted. Acetonitrile (MeCN) was dried according to the literature procedures and distilled under Ar prior to use.[31] Iodosylbenzene (PhIO) was prepared by a literature method.[32] Non-heme iron(II) complex, $[Fe^{II}(N4Py)](ClO_4)_2$ (N4Py = *N*,*N*-bis(2-pyridyl-methyl)-*N*-bis(2-pyridyl)methylamine), and its iron(IV)-oxo complex, $[Fe^{IV}(O)(N4Py)]^{2+}$, were prepared according to the literature methods.[15,16] For example, $[Fe^{IV}(O)(N4Py)]^{2+}$ was prepared by reacting $[Fe^{II}(N4Py)](ClO_4)_2$ (5.0 mM) with 1.2 equiv of PhIO (6.0 mM) in MeCN at ambient temperature. The deuterated compounds, phenyl [$^2H_2$]methanol ($C_6H_5CD_2OH$) and 2,5-dimethoxyphenyl [$^2H_2$]methanol ($2,5\text{-}(MeO)_2C_6H_3CD_2OH$), were prepared by reduction of benzoic acid and 2,5-dimethoxybenzoic acid ($2,5\text{-}(MeO)_2C_6H_3COOH$) with $LiAlD_4$ in ether.[33]

Spectral and Kinetic Measurements. Reactions of benzyl alcohol and its derivatives with $[Fe^{IV}(O)(N4Py)]^{2+}$ (1.0×10^{-4} M) were examined by monitoring spectral changes in the presence of various concentrations of benzyl alcohol or its derivatives (1.0×10^{-3}–2.0×10^{-1} M) in the absence and presence of $Sc(OTf)_3$ in deaerated MeCN at 298 K using a Hewlett Packard 8453 photodiode-array spectrophotometer and a quartz cuvette (path length = 10 mm). Kinetic measurements for $2,5\text{-}(MeO)_2C_6H_3CH_2OH$ in the presence of Sc^{3+} were performed on a UNISOKU RSP-601 stopped-flow spectrometer equipped with a MOS-type highly sensitive photodiode array or a Hewlett Packard 8453 photodiode array spectrophotometer at 298 K. Rates of reactions of benzyl alcohol and its derivatives with $[Fe^{IV}(O)(N4Py)]^{2+}$ were monitored by a decrease in the absorption band due to $[Fe^{IV}(O)(N4Py)]^{2+}$ (λ_{max} = 695 nm) in the absence and presence of $Sc(OTf)_3$ in MeCN. The concentration of benzyl alcohol or its derivatives was maintained to be more than 10-folds excess of $[Fe^{IV}(O)(N4Py)]^{2+}$ to keep pseudo-first-order conditions. Pseudo-first-order rate constants were determined by a least-squares fit of the first-order plot of time course of spectral change. Reactions of $3,4,5\text{-}(MeO)_3C_6H_2CH_2OH$ with $[Fe^{IV}(O)(N4Py)]^{2+}$ in the presence of Sc^{3+} were performed in the presence of 0.10 mM of $[Fe^{IV}(O)(N4Py)]^{2+}$, 0.050 mM of $3,4,5\text{-}(MeO)_3C_6H_2CH_2OH$, and excess amount of Sc^{3+} (5.0–20 mM).

Electrochemical Measurements. Measurements of cyclic voltammetry (CV) and second harmonic AC voltammetry (SHACV) were performed at 298 K using a BAS 630B electrochemical analyzer in deaerated MeCN containing 0.10 M $TBAPF_6$ as a supporting electrolyte at 298 K. A conventional three-electrode cell was used with a

platinum working electrode and a platinum wire as a counter electrode. The measured potentials were recorded with respect to $Ag/AgNO_3$ (1.0×10^{-2} M). The one-electron oxidation potential values (E_{ox}) (vs $Ag/AgNO_3$) were converted to those vs SCE by adding 0.29 V.[34] All electrochemical measurements were carried out under an Ar atmosphere.

EPR Measurements. EPR detection of iron(III) complexes and radical cation of 2,5-$(MeO)_2C_6H_3CH_2OH$ was performed as follows: Typically, a MeCN solution of $[Fe^{IV}(O)(N4Py)]^{2+}$ (1.0×10^{-3} M) in the absence and presence of $Sc(OTf)_3$ (1.0×10^{-2} M) in an EPR cell (3.0 mm i.d.) was purged with N_2 for 5 min. Then, deaerated benzyl alcohol or 2,5-$(MeO)_2C_6H_3CH_2OH$ solution (5.0×10^{-2} M) was added to the solution. The EPR spectra of the radical cation of 2,5-$(MeO)_2C_6H_3CH_2OH$ and iron(III) complexes were recorded on a JEOL JES-RE1XE spectrometer at 243 K and 77 K, respectively. The magnitude of modulation was chosen to optimize the resolution and signal-to-noise (S/N) ratio of the observed spectra under nonsaturating microwave power conditions. The g value was calibrated using an Mn^{2+} marker (g = 2.034, 1.981). Computer simulation of the EPR spectra was carried out by using Calleo EPR version 1.2 (Calleo Scientific Publisher) on a personal computer.

NMR Measurements. ^1H NMR spectra were recorded on a JEOL JMN-AL-300 NMR spectrometer at room temperature. To obtain clear NMR signal by removing inorganic products, reaction solutions with Sc^{3+} were treated with alumina column before measurement. The yields of the oxidation products were determined based on the peak of iodobenzene (between 7.0 and 8.0 ppm), which is a product of the reaction of $[Fe^{II}(N4Py)]^{2+}$ with iodosylbenzene to form $[Fe^{IV}(O)(N4Py)]^{2+}$.

Calculations. Density functional theory (DFT) calculations on the properties of molecules were performed with the UB3LYP density-functional and the 6-311G++(d,p) basis set.[35] All calculations were performed using Gaussian 09, revision A.02.[36] Graphical outputs of the computational results were generated with the Gauss View software program (ver. 3.09) developed by Semichem, Inc.[37]

Results and Discussion

Oxidation of Benzyl Alcohol by $[Fe^{IV}(O)(N4Py)]^{2+}$. Oxidation of benzyl alcohol by the iron(IV)-oxo complex was examined both in the absence and presence of Sc^{3+} at 298 K in MeCN. Addition of excess amount of benzyl alcohol (50 mM) to the solution of $[Fe^{IV}(O)(N4Py)]^{2+}$ (0.10 mM) caused the spectral change with a clean isosbestic point both in the absence and presence of Sc^{3+} (20 mM) as shown in Figures 1a and 1b, respectively. The decay of the characteristic absorption band due to $[Fe^{IV}(O)(N4Py)]^{2+}$ (695 nm) was accelerated with increase in concentration of benzyl alcohol in both the absence and presence of Sc^{3+} (Figures 2a and 2b), obeying pseudo-first-order kinetics. The pseudo-first-order rate constants (k_{obs}) increased proportionally with an increase in concentration of benzyl alcohol, and the second-order rate constant (k_{ox}) was determined from the linear correlation to be 9.9×10^{-2} M^{-1} s^{-1} in the absence of Sc^{3+},

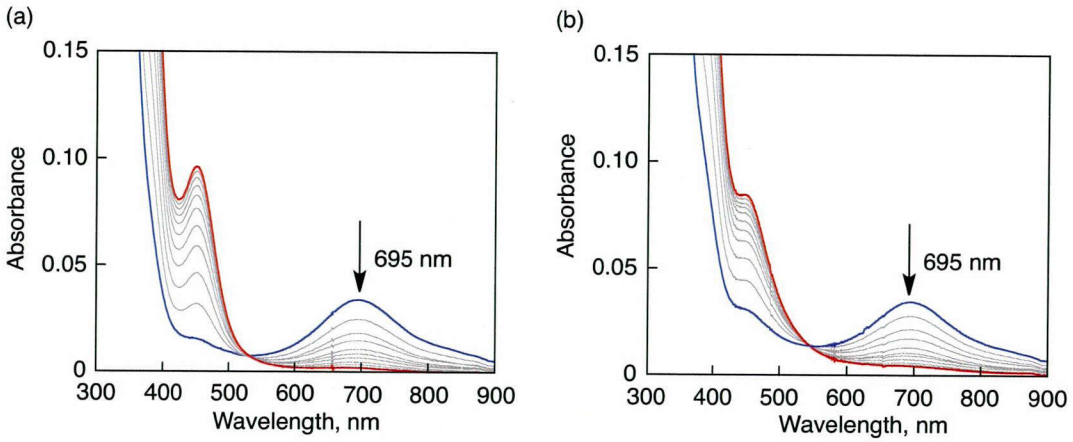

Figure 1. Spectral changes observed in the oxidation of benzyl alcohol (50 mM) by $[Fe^{IV}(O)(N4Py)]^{2+}$ (0.1 mM) in MeCN at 298 K in the absence (a) and presence (b) of Sc^{3+} (20 mM).

which was nearly the same as the value (1.1×10^{-1} M^{-1} s^{-1}) determined in the presence of Sc^{3+} (20 mM) as shown in Figures 2c and 2d in SI, respectively. In addition, the k_{obs} values were constant irrespective of the change in concentration of Sc^{3+} (Figure 3).

Product analysis of the oxidation of benzyl alcohol (1.0 mM) by $[Fe^{IV}(O)(N4Py)]^{2+}$ (1.0 mM) revealed the formation of benzaldehyde with 50% yield as a sole product both in the absence and presence of Sc^{3+} (10 mM) (Figures 4a and 4b). The electrospray ionization mass (ESI-MS) spectrum of the reaction solution performed in the absence of Sc^{3+} shows peaks at *m/z* 539.1 and 629.0, whose mass and isotope distribution indicate formation of $[Fe^{III}(OH)(N4Py)]^{2+}$ and $[Fe^{III}(OCH_2Ph)(N4Py)]^{2+}$,

respectively (Figures 5a and 5b). The formation of the iron(III) species was supported by taking EPR spectra of the reaction solution (Figure 6a).[38] In the presence of Sc^{3+}, the ESI-MS spectrum of the resulting solution of the reaction shows peak at *m/z* 572.4, which indicates formation of $[Fe^{II}(N4Py)(OTf)]^+$ (*calcd. m/z* = 572.4) (Figure 5c).

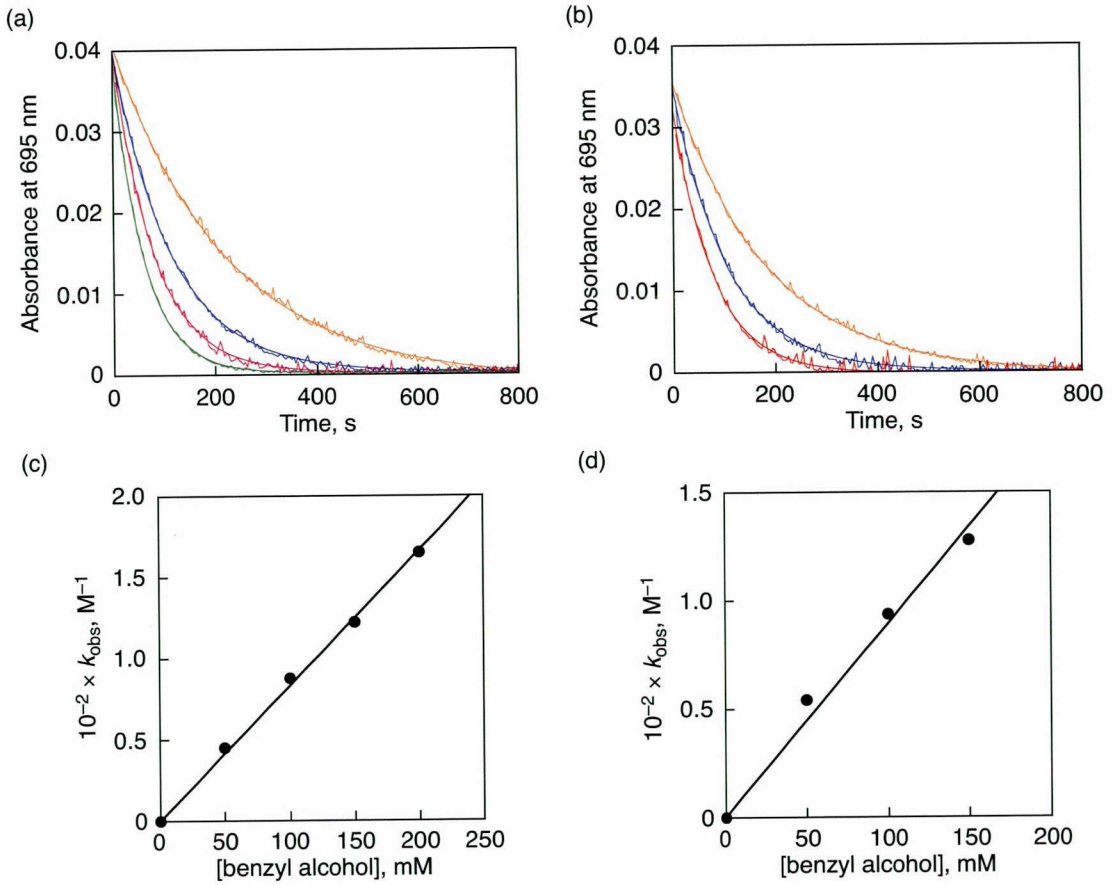

Figure 2. Time profiles of absorbance at 695 nm due $[Fe^{IV}(O)(N4Py)]^{2+}$ in the oxidation of benzyl alcohol (orange: 50 mM, blue: 100 mM, red: 150 mM, green: 200 mM) by $[Fe^{IV}(O)(N4Py)]^{2+}$ (0.10 mM) in the absence (a) and presence (b) of Sc^{3+} (20 mM) in MeCN at 298 K. Plots of pseudo-first-order rate constants for the oxidation of benzyl alcohol by $[Fe^{IV}(O)(N4Py)]^{2+}$ (k_{obs}) vs concentration of benzyl alcohol in the absence (c) and presence (d) of Sc^{3+} (20 mM) in MeCN at 298 K.

The EPR spectrum, however, indicates that the major product of the reaction is not iron(II) but iron(III) species, $[Fe^{III}(N4Py)(NCMe)]^{3+}$ with orthogonal signals around g = 2.5 and 1.7 (Figures 6b and 6c). The iron(III) complex might not be detected by ESI-MS probably due to the high one-electron-reduction potential of $[Fe^{III}(N4Py)(NCMe)]^{3+}$ (E_{red} = 1.0 V vs SCE) and the occurrence of the one-electron reduction from the Fe(III) to Fe(II) species under the ESI-MS condition.[39] In order to

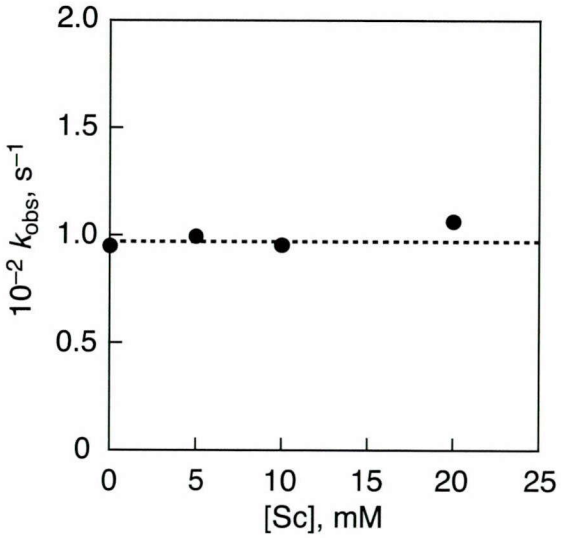

Figure 3. Dependence of the pseudo-first-order rate constant (k_{obs}) determined in the oxidation of $PhCH_2OH$ (1.0×10^2 mM) by $[Fe^{IV}(O)(N4Py)]^{2+}$ (0.10 mM) on concentration of Sc^{3+}.

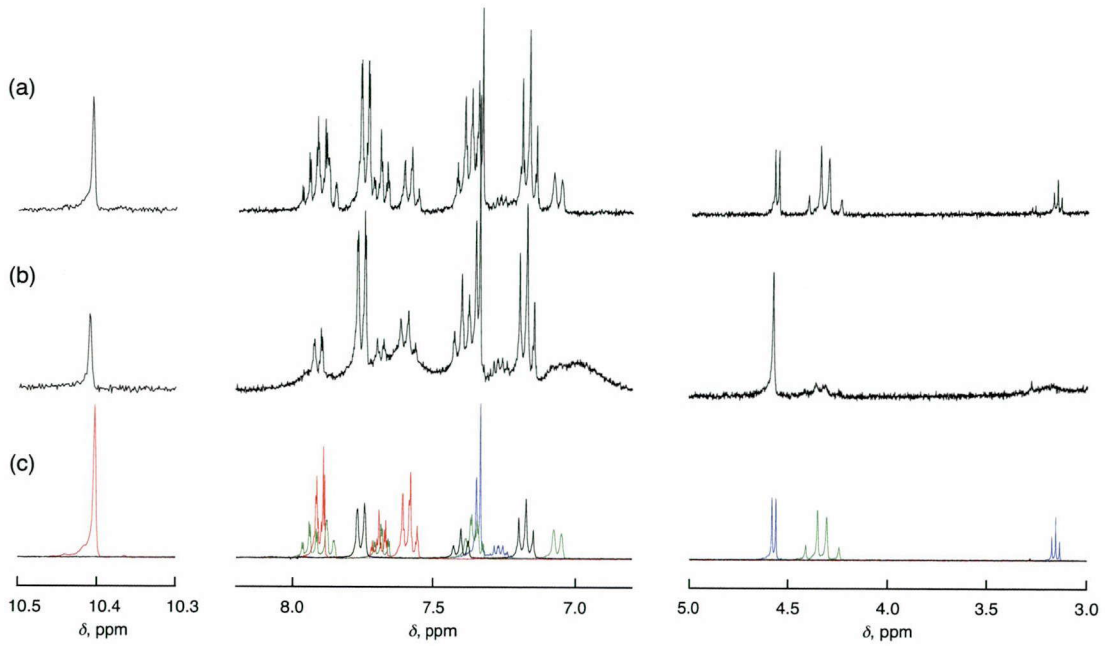

Figure 4. ^{1}H-NMR spectra of benzaldehyde produced in the oxidation of benzyl alcohol (1.0 mM) by $[Fe^{IV}(O)(N4Py)]^{2+}$ (1.0 mM) in the absence (a) and presence (b) of Sc^{3+} (10 mM) in MeCN-d_3 at 298 K. (c) ^{1}H-NMR spectra of authentic compounds, benzyl alcohol (blue), benzaldehyde (red), $[Fe^{II}(N4Py)(NCMe)]^{2+}$ (green) and iodobenzene (black) produced in the formation of $[Fe^{IV}(O)(N4Py)]^{2+}$ with iodosylbenzene.

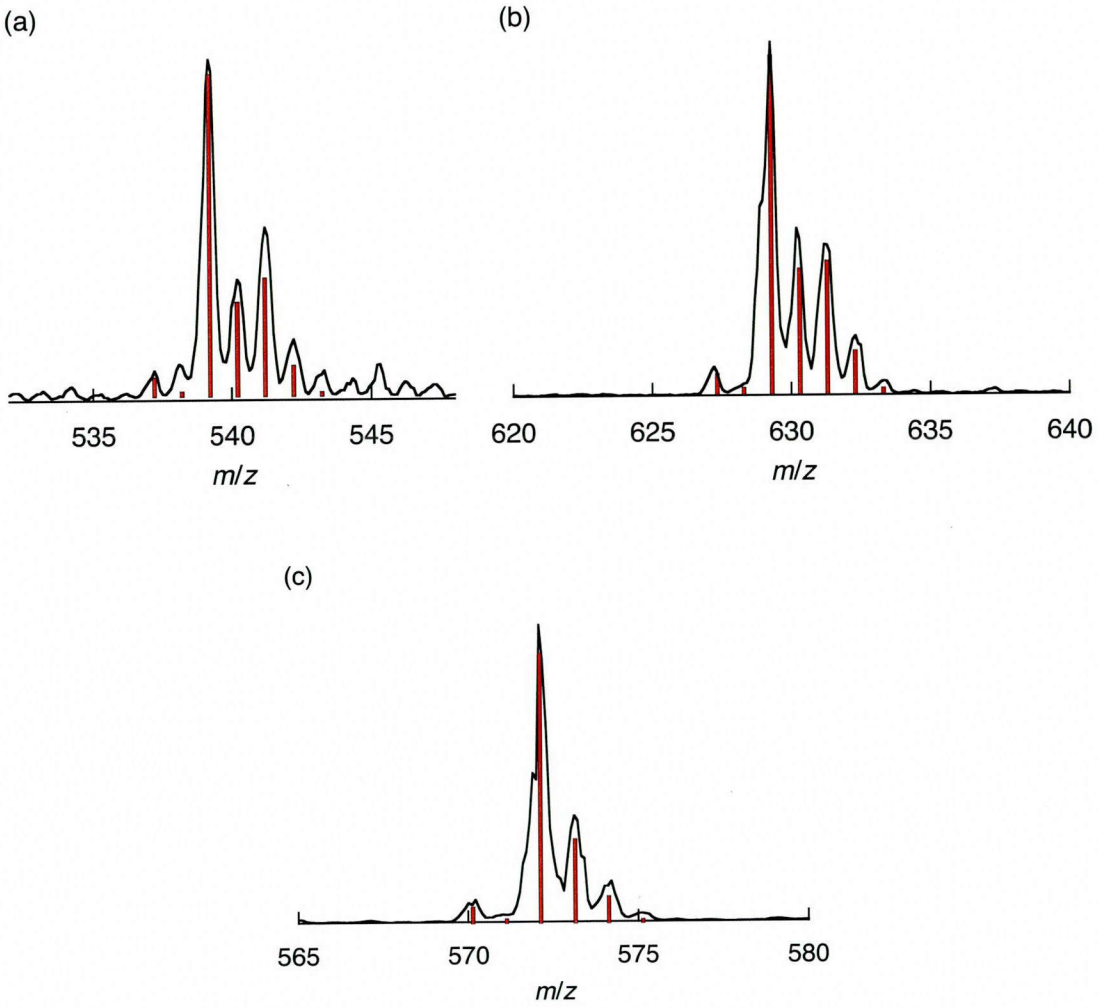

Figure 5. ESI-MS spectra (black line) of resulting solution of reaction between $[Fe^{IV}(O)(N4Py)]^{2+}$ (1.0 mM) and benzyl alcohol (10 mM) in the absence (a and b) and presence (c) of Sc^{3+} (10 mM). Red bars show the simulated mass and isotope distribution patterns of $[Fe^{III}(OH)(N4Py)(ClO_4)]^+$ (*calcd. m/z* = 539.1) (a), $[Fe^{III}(OCH_2Ph)(N4Py)(ClO_4)]^+$ (*calcd. m/z* = 629.0) (b) and $[Fe^{II}(N4Py)(OTf)]^+$ (*calcd. m/z* = 572.4) (c).

confirm the oxidation state of the iron complex in the resulting solution both in the absence and presence of Sc^{3+}, a one-electron donor, ferrocene (Fc) was added into the solutions and one equiv of ferrocenium ion (Fc^+) to $[Fe^{IV}(O)(N4Py)]^{2+}$ was produced with the concurrent formation of $[Fe^{II}(N4Py)(NCMe)]$ in both cases (Figures 7a and 7b). This indicates that $[Fe^{IV}(O)(N4Py)]^{2+}$ acts as a one-electron oxidant rather than

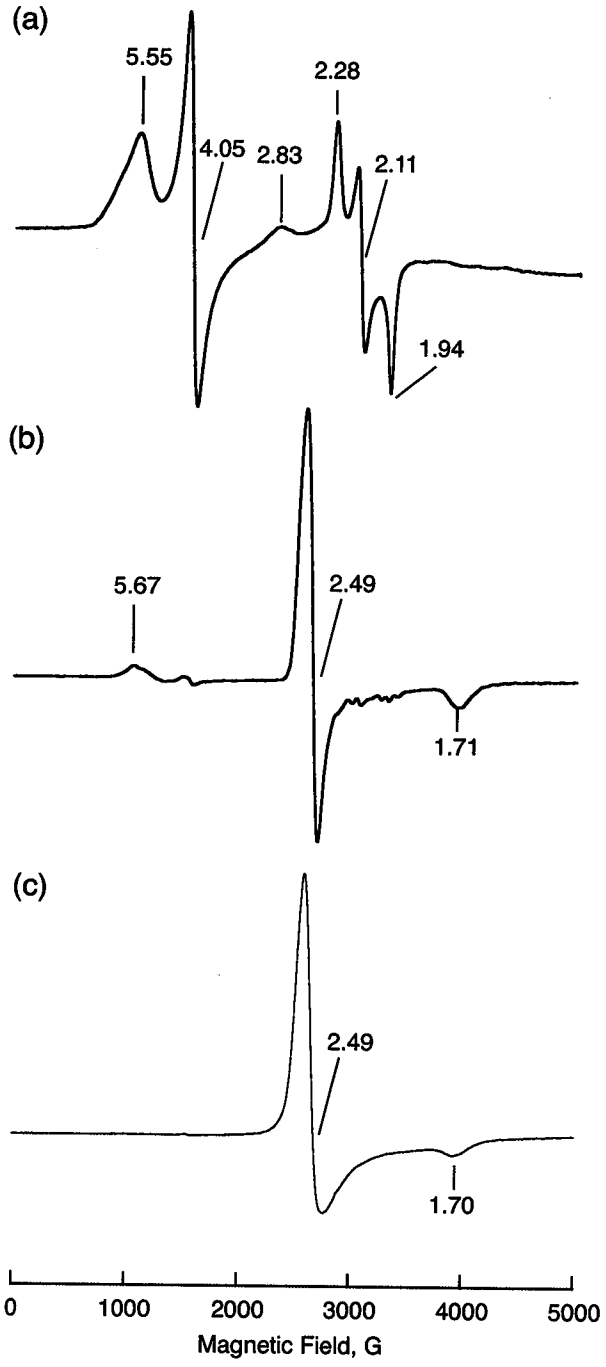

Figure 6. X-band EPR spectra of the reaction products obtained in the reaction between $[Fe^{IV}(O)(N4Py)]^{2+}$ (1.0 mM) and benzyl alcohol (50 mM) in the absence (a) and presence (b) of Sc^{3+} (10 mM) in MeCN recorded at 77 K. (c) Reference EPR spectrum of $[Fe^{III}(OH)(N4Py)]^{2+}$, which is produced by the one-electron oxidation of $[Fe^{II}(N4Py)(NCMe)]^{2+}$ by CAN, recorded in frozen MeCN at 77 K.

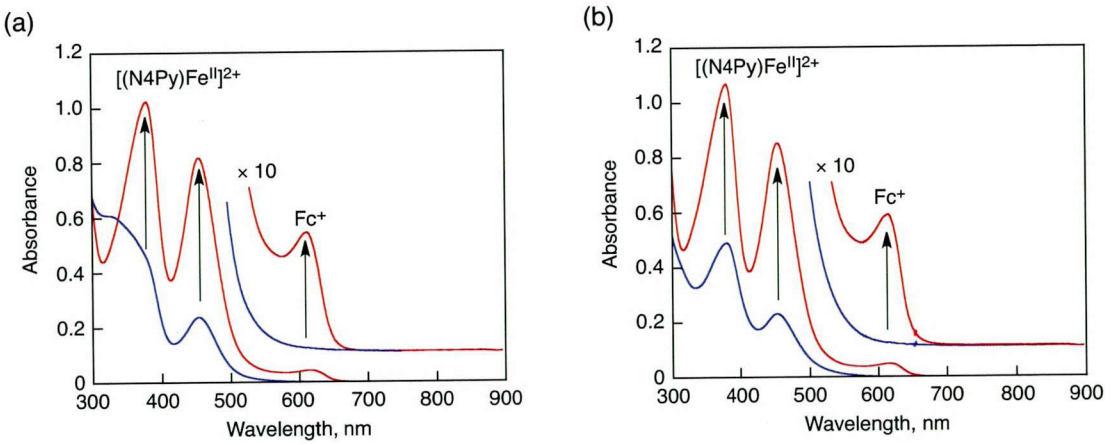

Figure 7. (a) UV–vis spectra of the resulted solution in the oxidation reaction of benzyl alcohol (50 mM) by $[Fe^{IV}(O)(N4Py)]^{2+}$ (0.10 mM) (blue line) and after titration with 2.5 equiv of Fc in the presence of HOTf (10 mM; red line). (b) UV–vis spectra of the resulted solution in the oxidation reaction of benzyl alcohol (50 mM) by $[Fe^{IV}(O)(N4Py)]^{2+}$ (0.10 mM) in the presence of Sc^{3+} (10 mM; blue line) and after titration with 2.5 equiv of Fc (red line).

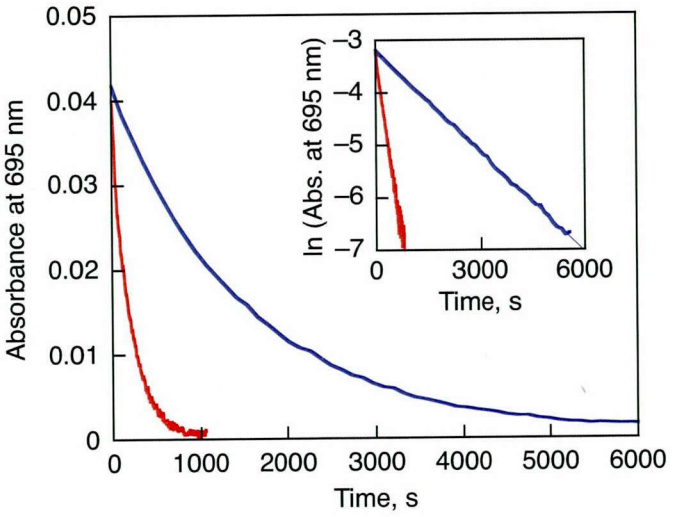

Figure 8. Time profiles of decay at 695 nm due to $[Fe^{IV}(O)(N4Py)]^{2+}$ (1.0 mM) in the oxidation of $PhCH_2OH$ (2.4×10^2 mM) (red) and $PhCD_2OH$ (2.4×10^2 mM) (blue) in the presence of Sc^{3+} (20 mM) in MeCN at 298 K. Inset shows the first-order plots of the spectral changes.

a two-electron oxidant. It should be noted that the $[Fe^{III}(OH)(N4Py)]^{2+}$ produced during the reaction is not so reactive to oxidize $C_6H_5CHOH^{\bullet}$.

The rate of the oxidation of $PhCD_2OH$ in the presence of Sc^{3+} (20 mM) in MeCN is significantly slower than that of $PhCH_2OH$ as shown in Figure 3, giving a deuterium kinetic isotope effect (KIE) of 7.2 at 298 K.[40] As reported previously in the oxidation of benzyl alcohol by $[Fe^{IV}(O)(N4Py)]^{2+}$ in the absence of Sc^{3+},[17] such a large KIE value clearly indicates that the rate-determining step (r.d.s.) of the reaction is HAT from benzyl alcohol to $[Fe^{IV}(O)(N4Py)]^{2+}$ both in the absence and presence of Sc^{3+}. The subsequent HAT from $C_6H_5CHOH^{\bullet}$ to $[Fe^{IV}(O)(N4Py)]^{2+}$ to yield C_6H_5CHO and $[Fe^{III}(OH)(N4Py)]^{2+}$ occurs with a much faster rate than the initial HAT because of the weaker C–H bond in the radical species.[41] This reaction mechanism is summarized in Scheme 2. In the presence of benzyl alcohol, $[Fe^{III}(OH)(N4Py)]^{2+}$ is converted to $[Fe^{III}(OCH_2C_6H_5)(N4Py)]^{2+}$ and H_2O. No acceleration of the initial HAT was observed in the presence of Sc^{3+}.

Oxidation of $2,5\text{-}(MeO)_2C_6H_3CH_2OH$ with $[Fe^{IV}(O)(N4Py)]^{2+}$. Different from the benzyl alcohol oxidation shown in Scheme 2, the rate of the oxidation of $2,5\text{-}(MeO)_2C_6H_3CH_2OH$ by $[Fe^{IV}(O)(N4Py)]^{2+}$ was significantly accelerated by the presence of Sc^{3+} (Figure 9b), as compared to the rate determined in the absence of Sc^{3+} (Figure 9a). In the presence of Sc^{3+}, an intermediate with two absorption maxima at 430 nm and 455 nm appeared although it is not observed in the absence of Sc^{3+} (vide infra). The decay of the absorption band at 695 nm due to $[Fe^{IV}(O)(N4Py)]^{2+}$ both in the absence and presence of Sc^{3+} obeyed first-order kinetics (Figures 10a and 10c).[16]

Scheme 2. Proposed Mechanism of Benzyl Alcohol Oxidation by $[Fe^{IV}(O)(N4Py)]^{2+}$

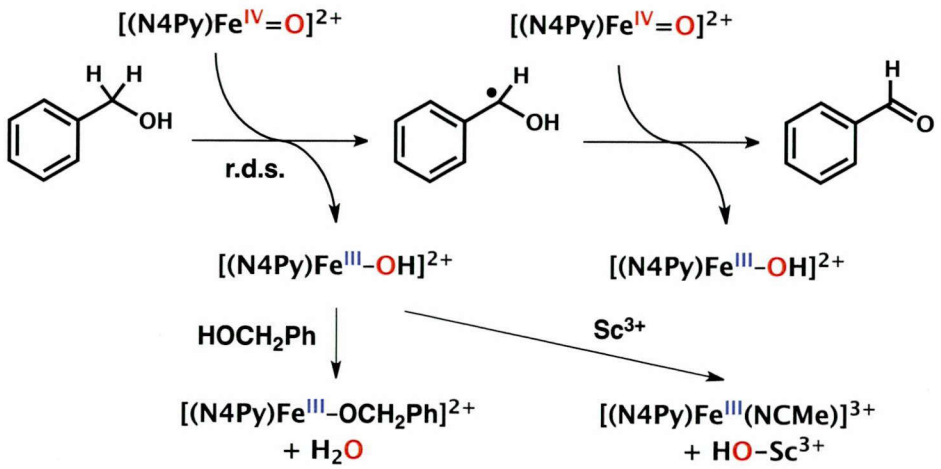

The pseudo-first order rate constant (k_{obs}) increased linearly with increasing concentration of 2,5-$(MeO)_2C_6H_3CH_2OH$, and the second-order rate constant (k_{ox}) was determined by plotting k_{obs} vs [2,5-$(MeO)_2C_6H_3CH_2OH$]. The dependence of k_{ox} on [Sc^{3+}] is shown in Figure 11 (red circles), where k_{obs} values increased with increasing concentration of Sc^{3+}, exhibiting both a first-order dependence and a second-order dependence on [Sc^{3+}] as given by eq 1, where k_0 is the rate constant in the absence of Sc^{3+}, k_1 and k_2 are the rate constants exhibiting the first-order and second-order dependences on [Sc^{3+}]. The first-order and second-order dependence of k_{ox} on [Sc^{3+}] is shown by a linear plot of $(k_{ox} - k_0)/[Sc^{3+}]$ vs [Sc^{3+}] as shown in Figure 12, where the intercept and the slope correspond to the contribution of the first-order and second-order dependence,

$$k_{ox} = k_0 + k_1[Sc^{3+}] + k_2[Sc^{3+}]^2 \quad (1)$$

respectively. Such a dependence of electron-transfer rate constants on [Sc^{3+}] was reported previously for metal ion-coupled electron transfer from one-electron reductant to $[Fe^{IV}(O)(N4Py)]^{2+}$.[27] For instance, the dependence of second-order rate constant of electron transfer (k_{et}) from $[Fe^{II}(bpy)_3]^{2+}$ to $[Fe^{IV}(O)(N4Py)]^{2+}$ on [Sc^{3+}] is shown in Figure 11 (black squares).

In order to determine KIE value, the oxidation rate of a deuterated substrate (2,5-$(MeO)_2C_6H_3CD_2OH$) by $[Fe^{IV}(O)(N4Py)]^{2+}$ was also examined both in the absence and presence of Sc^{3+}. In the absence of Sc^{3+}, the oxidation rate of 2,5-$(MeO)_2C_6H_3CD_2OH$ (1.0×10^2 mM) by $[Fe^{IV}(O)(N4Py)]^{2+}$ (0.060 mM) was significantly slower than that of 2,5-$(MeO)_2C_6H_3CH_2OH$ by $[Fe^{IV}(O)(N4Py)]^{2+}$ under the same conditions as employed in the oxidation of benzyl alcohol (Figure 13a). Second-order rate constants (k_H and k_D) were determined from the slopes of the plots of pseudo-first order rate constants of 2,5-$(MeO)_2C_6H_3CH_2OH$ ($k_{H,obs}$) and (2,5-$(MeO)_2C_6H_3CD_2OH$ ($k_{D,obs}$) vs [2,5-$(MeO)_2C_6H_3CH_2OH$] and [2,5-$(MeO)_2C_6H_3CD_2OH$], respectively (red and blue circles in Figure 13c), respectively. The KIE value was determined to be 14 for the reaction performed at 298 K. This clearly indicates that HAT is the rate-determining step as the case of oxidation of benzyl alcohol by $[Fe^{IV}(O)(N4Py)]^{2+}$ in Scheme 2.[12b,16,42-45] In sharp contrast to the case of the absence of Sc^{3+}, no KIE was observed in the presence of Sc^{3+} (Figures 13b and 13c). The disappearance of KIE by the presence of Sc^{3+} indicates a mechanistic change from HAT to a process in which C–H bond cleavage is not involved in the rate-determining step, which is most likely to be electron transfer (vide infra). Indeed, new transient absorption bands around 430 and 455 nm, which were not observed in the

absence of Sc^{3+} in Figure 9a, were detected in the presence of Sc^{3+} (Figure 9b). These absorption bands agree with those observed in the one-electron oxidation of 2,5-$(MeO)_2C_6H_3CH_2OH$ by a strong one-electron oxidant such as CAN, as shown in Figure 9b (green line).[46] This indicates the occurrence of electron transfer from 2,5-$(MeO)_2C_6H_3CH_2OH$ to $[Fe^{IV}(O)(N4Py)]^{2+}$ to produce a radical cation of 2,5-$(MeO)_2C_6H_3CH_2OH$ (i.e., 2,5-$(MeO)_2$-$C_6H_3CH_2OH^{\bullet+}$). The formation of the radical cation was confirmed by EPR measurements. Figure 14a shows an EPR spectrum of 2,5-$(MeO)_2C_6H_3CH_2OH^{\bullet+}$ produced in the oxidation of 2,5-$(MeO)_2C_6H_3CH_2OH$ by $[Fe^{IV}(O)(N4Py)]^{2+}$ in the presence of Sc^{3+}.

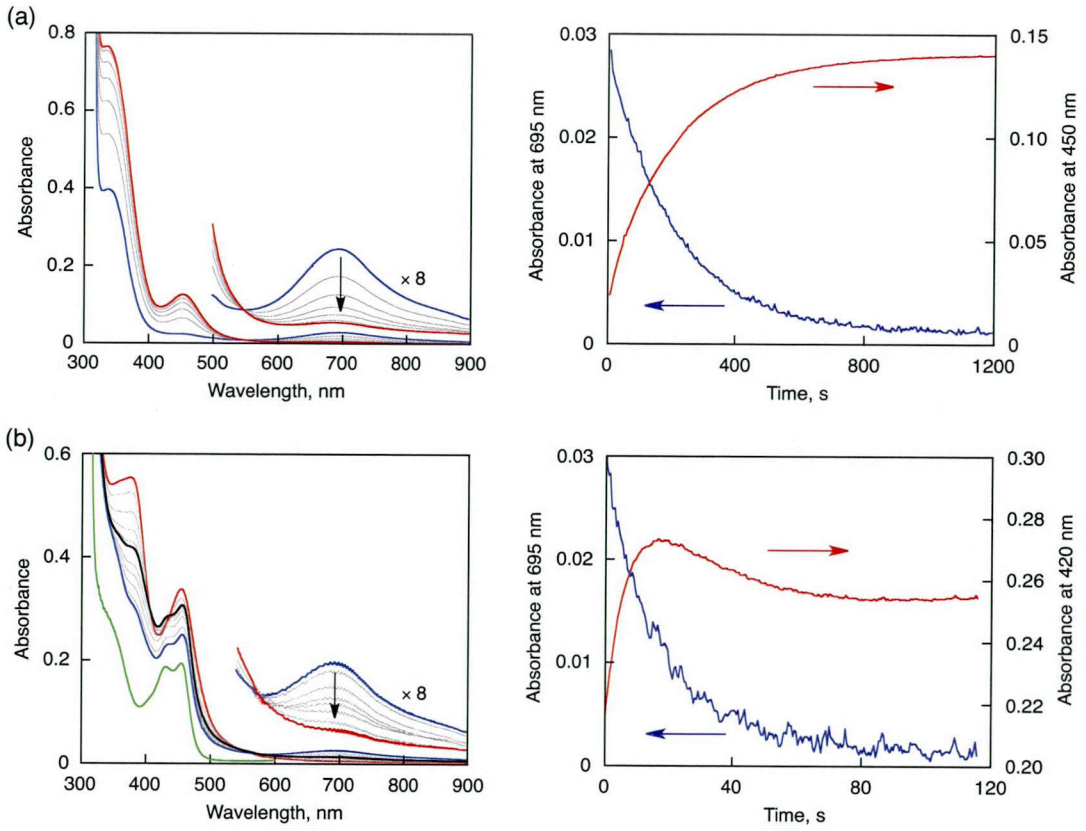

Figure 9. (a) Spectral changes observed in the oxidation of 2,5-$(MeO)_2C_6H_3CH_2OH$ (20 mM) by $[Fe^{IV}(O)(N4Py)]^{2+}$ (0.060 mM) in the absence of Sc^{3+} in deaerated MeCN. Right panel shows time courses monitored at 695 nm (blue) and 450 nm (red). (b) Spectral changes observed in the oxidation of 2,5-$(MeO)_2C_6H_3CH_2OH$ (2.5 mM) by $[Fe^{IV}(O)(N4Py)]^{2+}$ (0.060 mM) in the presence of Sc^{3+} (10 mM) (left panel; 4 s (blue), 30 s (black), and 120 s (red) after mixing) in deaerated MeCN. Green line indicates the reference spectrum of 2,5-$(MeO)_2C_6H_3CH_2OH$ radical cation produced by oxidizing 2,5-$(MeO)_2C_6H_3CH_2OH$ with $(NH_3)_2[Ce^{IV}(NO_3)_6]$ (CAN). Right panel shows time courses monitored at 695 nm (blue) and 420 nm due to 2,5-$(MeO)_2C_6H_3CH_2OH$ radical cation (red).

The hyperfine coupling constants obtained in the computer similation spectrum (Figure 14b) are in a reasonable agreement with those calcurated by the DFT method (Figure 14c). The same EPR signal was observed in the one-electron oxidation of 2,5-$(MeO)_2C_6H_3CH_2OH$ by $[Ru^{III}(bpy)_3]^{3+}$ (Figure 15a).

The decay of the EPR signal of 2,5-$(MeO)_2C_6H_3CH_2OH^{\bullet+}$ produced in the oxidation of 2,5-$(MeO)_2C_6H_3CH_2OH$ by $[Fe^{IV}(O)(N4Py)]^{2+}$ in the presence of Sc^{3+} obeyed second-order kinetics (Figure 16a).[47] The second-order rate constant was determined to be 2.3×10^3 M^{-1} s^{-1} from the linear

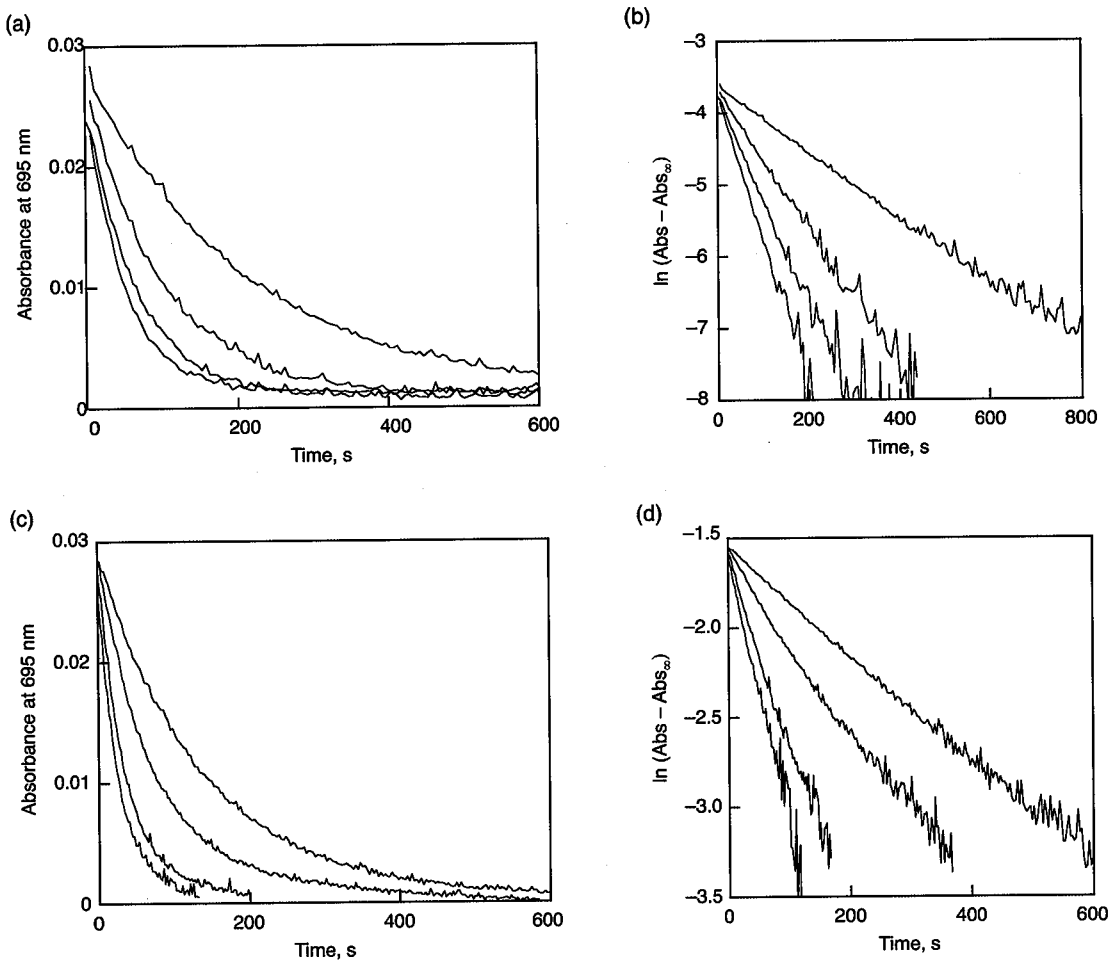

Figure 10. (a) Time courses monitored at 695 nm due $[Fe^{IV}(O)(N4Py)]^{2+}$ in the reaction of $[Fe^{IV}(O)(N4Py)]^{2+}$ (0.060 mM) and 2,5-$MeO_2C_6H_3CH_2OH$ (2.5×10–1.0×10^2 mM) in the absence of Sc^{3+} in MeCN at 298 K. (b) First-order plots of the absorption changes shown in Figure 10a. (c) Time courses monitored at 695 nm due to $[Fe^{IV}(O)(N4Py)]^{2+}$ in the reaction of $[Fe^{IV}(O)(N4Py)]^{2+}$ (0.060 mM) and 2,5-$MeO_2C_6H_3CH_2OH$ (2.0–8.0 mM) in the presence of Sc^{3+} (2.5 mM) in MeCN at 298 K. (d) First order plots of the absorption changes shown in Figure 10c.

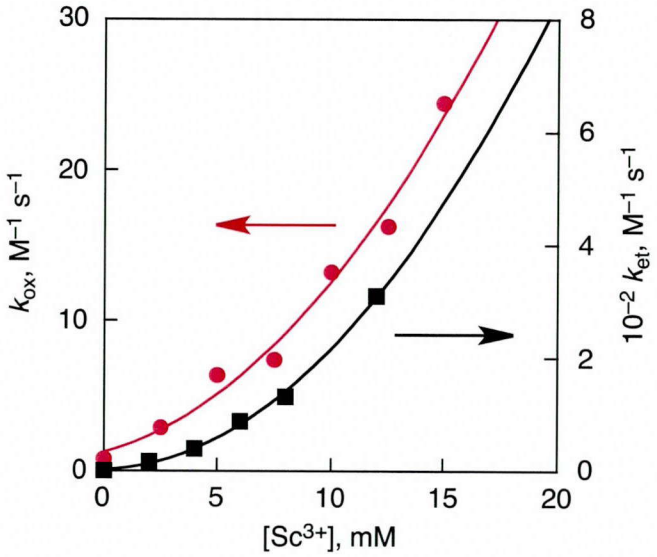

Figure 11. Plots of the second-order rate constant (k_{ox}) vs Sc^{3+} concentration in the oxidaiton of 2,5-$(MeO)_2C_6H_3CH_2OH$ by $[Fe^{IV}(O)(N4Py)]^{2+}$ (red circles) and the second-order rate constant (k_{et}) vs Sc^{3+} concentration in the Sc^{3+}-coupled ET from $[Fe(bpy)_3]^{2+}$ to $[Fe^{IV}(O)(N4Py)]^{2+}$ (black squares) in deaerated MeCN at 298 K.

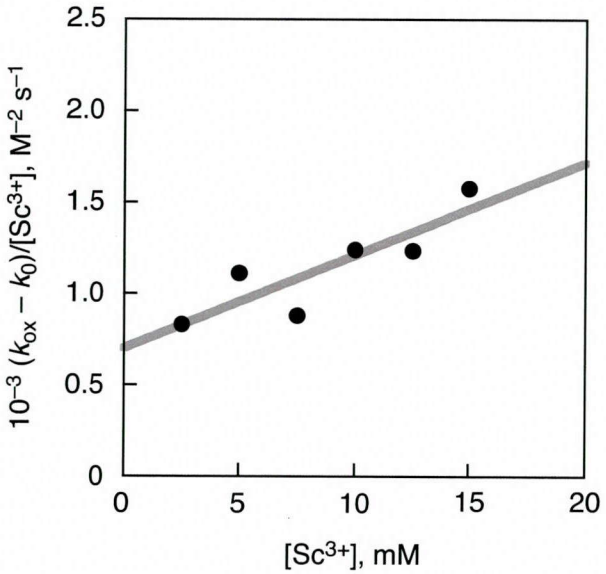

Figure 12. Plot of $(k_{ox} - k_0)/[Sc^{3+}]$ vs $[Sc^{3+}]$.

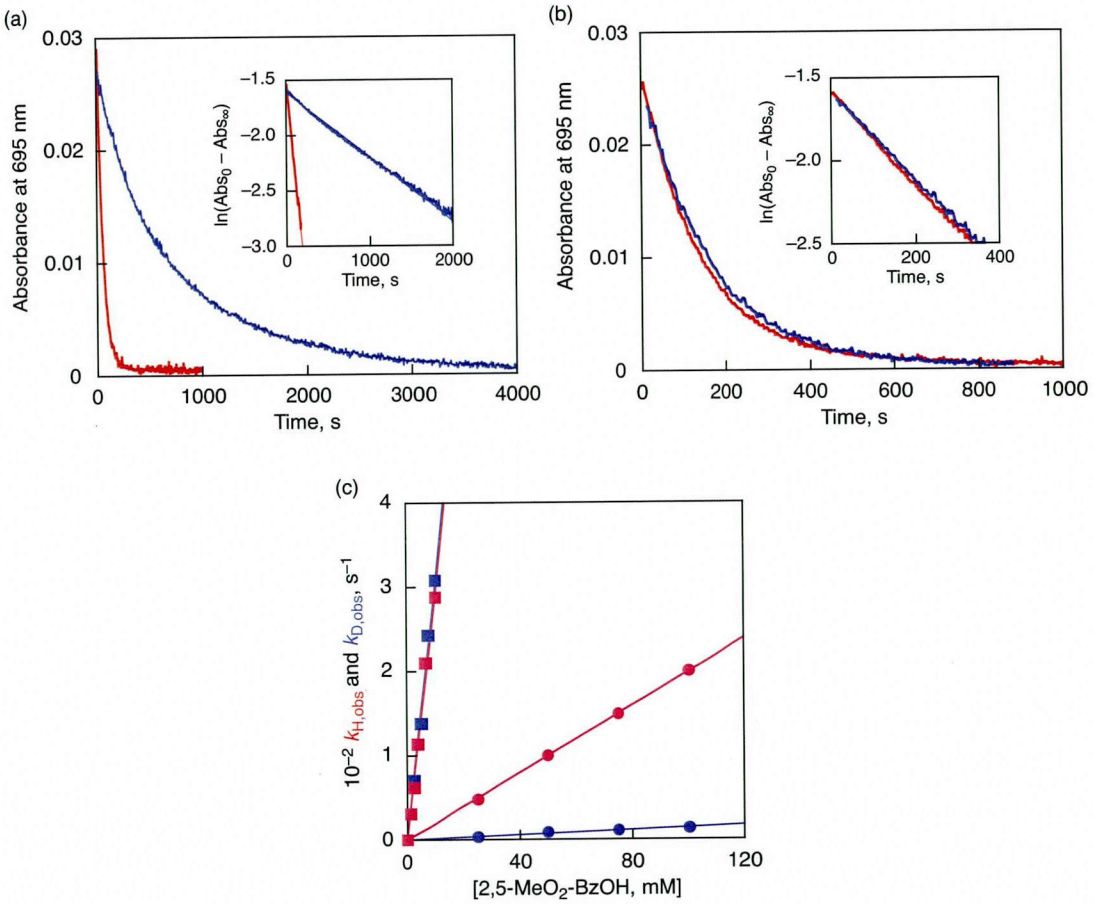

Figure 13. (a) Time courses of the absorption spectral changes obserbed at 695 nm due to $[Fe^{IV}(O)(N4Py)]^{2+}$ (0.060 mM) in the oxidation of 2,5-$(MeO)_2C_6H_3CH_2OH$ (1.0×10^2 mM) (red) and 2,5-$(MeO)_2C_6H_3CD_2OH$ (1.0×10^2 mM) (blue) in the absence of Sc^{3+}. Inset shows first-order plots of the absorption change at 695 nm. (b) Time courses of the absorption spectral changes obserbed at 695 nm due to $[Fe^{IV}(O)(N4Py)]^{2+}$ (0.060 mM) in the oxidation of 2,5-$(MeO)_2C_6H_3CH_2OH$ (2.5 mM) (red) and 2,5-$(MeO)_2C_6H_3CD_2OH$ (2.5 mM) (blue) in the presence of Sc^{3+} (2.5 mM). Inset shows first-order plots of the absorption change at 695 nm. (c) Plots of $k_{H,obs}$ (red) and $k_{D,obs}$ (blue) vs [2,5-$(MeO)_2C_6H_3CH_2OH$] and [2,5-$(MeO)_2C_6H_3CD_2OH$] in the absence (circles) and presence (squares) of Sc^{3+} (2.5 mM), respectively.

second-order plot (Figure 16b) and the initial concentration of 2,5-$(MeO)_2C_6H_3CH_2OH$, which was determined by the double integration of the EPR spectrum by comparing with an authentic radical sample of 2,2-diphenyl-2-picrylhydrazyl (DPPH). The decay of the EPR signal of 2,5-$(MeO)_2C_6H_3CH_2OH^{\bullet+}$ produced in the one-electron oxidation of 2,5-$(MeO)_2C_6H_3CH_2OH$ by $[Ru^{III}(bpy)_3]^{3+}$ also obeyed second-order kinetics (Figure 15b), indicating that bimolecular reactions of 2,5-$(MeO)_2C_6H_3CH_2OH^{\bullet+}$ are responsible for the decay of 2,5-$(MeO)_2C_6H_3CH_2OH^{\bullet+}$.

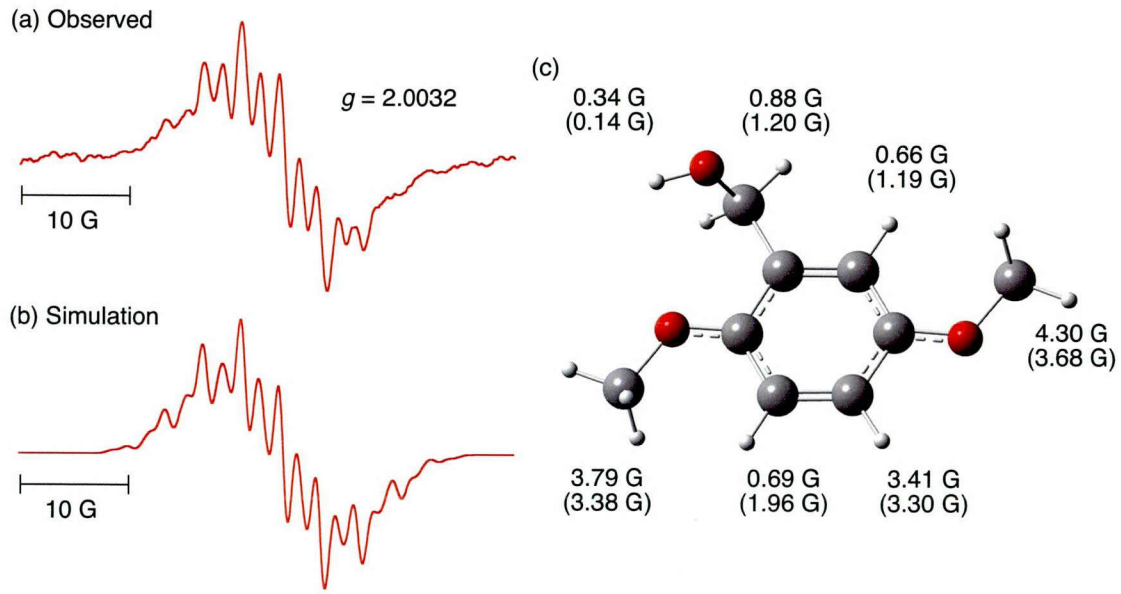

Figure 14. (a) X-band EPR spectrum of 2,5-$(MeO)_2C_6H_3CH_2OH^{\bullet+}$ produced by electron-transfer oxidation of 2,5-$(MeO)_2C_6H_3CH_2OH$ (1.0 mM) by $[Fe^{IV}(O)(N4Py)]^{2+}$ (1.0 mM) in the presence of Sc^{3+} (10 mM) in deaerated MeCN at 298 K. (b) The computer simulation spectrum. (c) DFT optimized structure of 2,5-$(MeO)_2C_6H_3CH_2OH^{\bullet+}$ with hyperfine coupling constants together with the calculated values given in parentheses.

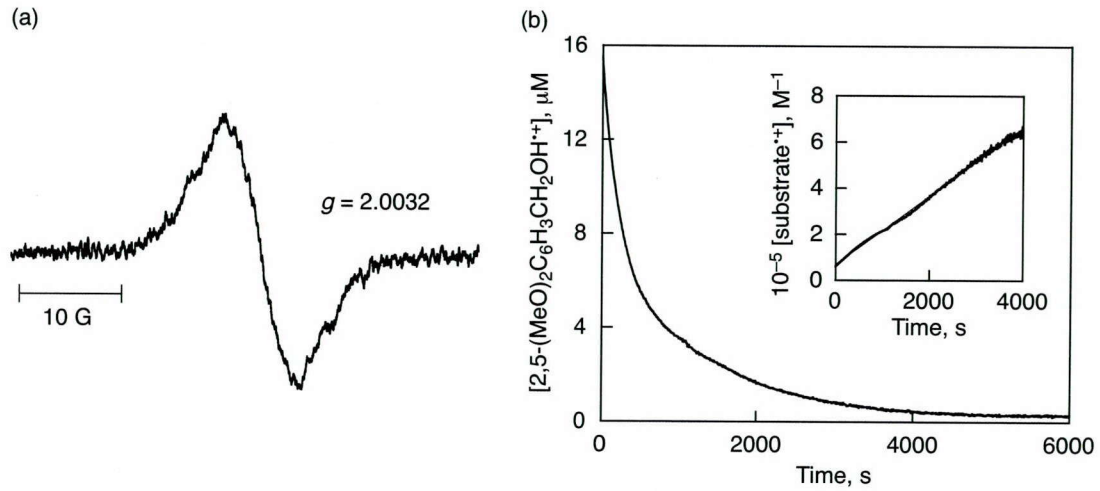

Figure 15. (a) X-band EPR spectrum of 2,5-$(MeO)_2C_6H_3CH_2OH^{\bullet+}$ produced in the electron-transfer oxidation of 2,5-$(MeO)_2C_6H_3CH_2OH$ (1.0 mM) by $[Ru^{III}(bpy)_3]^{3+}$ (1.0 mM) in the presence of Sc^{3+} (10 mM) in deaerated MeCN at 298 K. (b) Decay time profile of 2,5-$(MeO)_2C_6H_3CH_2OH^{\bullet+}$, the concentrations of which were determined by double integration in comparion with that of authentic sample ($DPPH^{\bullet}$). Inset shows second-order plot of the decay of 2,5-$(MeO)_2C_6H_3CH_2OH^{\bullet+}$.

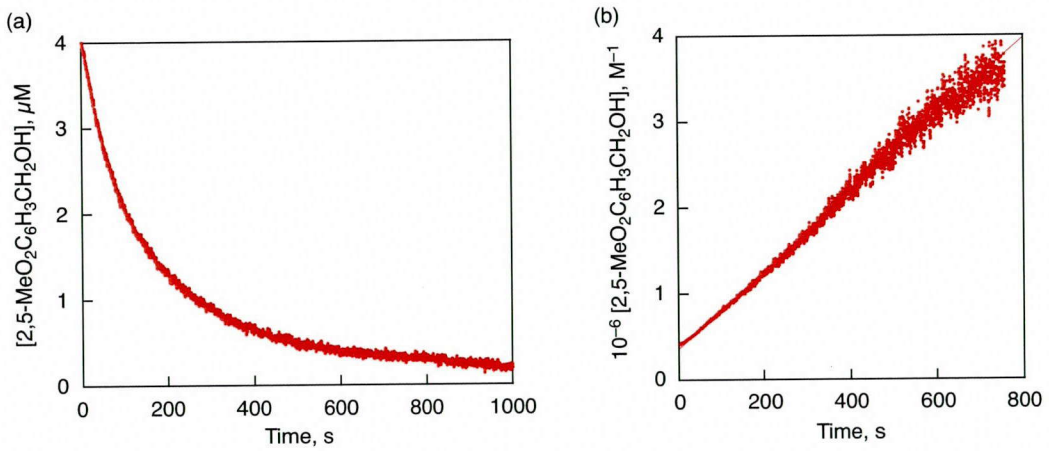

Figure 16. (a) Time course of decay of $[2,5\text{-}(MeO)_2C_6H_3CH_2OH^{\bullet+}]$ observed by EPR measured at 243 K in deaerated MeCN. (b) Second-order plot of the time course of decay in EPR signal of $2,5\text{-}(MeO)_2C_6H_3CH_2OH^{\bullet+}$.

Product analyses of the oxidation of $2,5\text{-}(MeO)_2C_6H_3CH_2OH$ by $[Fe^{IV}(O)(N4Py)]^{2+}$ in the absence and presence of Sc^{3+} were performed by the same method for the benzyl alcohol oxidation. ^{1}H-NMR spectra of the reaction products obtained in the oxidation of $2,5\text{-}(MeO)_2C_6H_3CH_2OH$ (1.0 mM) by one equiv of $[Fe^{IV}(O)(N4Py)]^{2+}$ (1.0 mM) in the absence of Sc^{3+} in CD_3CN revealed that $2,5\text{-}(MeO)_2C_6H_3CH_2OH$ was converted to the corresponding aldehyde, $2,5\text{-}(MeO)_2C_6H_3CHO$, with 50% yield as the case of benzyl alcohol oxidation (Figure 17).[48] The major inorganic products were determined to be $[Fe^{III}(OH)(N4Py)]^{2+}$ and $[Fe^{III}(OCH_2C_6H_5(OMe)_2)(N4Py)]^{2+}$ by ESI-MS and EPR spectroscopy (Figures 18 and 19). Titration of the resulting solution by Fc resulted in formation of Fc^+ with the same concentration as the initial concentration of $[Fe^{IV}(O)(N4Py)]^{2+}$ to produce $[Fe^{II}(N4Py)(NCMe)]^{2+}$ (Figure 20). This indicates that $[Fe^{IV}(O)(N4Py)]^{2+}$ acts as a one-electron oxidant rather than two-electron oxidant in the oxidation of $2,5\text{-}(MeO)_2C_6H_3CH_2OH$ as the case of $PhCH_2OH$ oxidation.

In the presence of Sc^{3+} (10 mM), however, the oxidation of $2,5\text{-}(MeO)_2C_6H_3CH_2OH$ by $[Fe^{IV}(O)(N4Py)]^{2+}$ (1.0 mM) resulted in the oxidative coupling to yield 2,2',5,5'-tetramethoxybiphenylyl-4,4'-dimethanol as a major product (31% yield, 0.31 mM) together with the further oxidized product 2,2',5,5'-tetramethoxybiphenylyl-4,4'-dicarbaldehyde (1.0% yield, 0.010 mM) as well as the corresponding aldehyde ($2,5\text{-}(MeO)_2C_6H_3CHO$) only in 10% yield (0.10 mM) as shown in Scheme 3 with each products' yield and the oxidation equivalent (see Figure 15b).[48] ESI-MS and EPR spectrum of the resulting solution and titration of the resulting solution by Fc indicate that the inorganic products are Fe(III) species and

$[Fe^{IV}(O)(N4Py)]^{2+}$ acts as a one-electron oxidant in the presence of Sc^{3+} as the case in the absence of Sc^{3+} (Figures 18 and 19).[49] The overall oxidation efficiency was determined to be 88% by counting number of electrons oxidized by $[Fe^{IV}(O)(N4Py)]^{2+}$ ($31 \times 2 + 10 \times 2 + 1 \times 6 = 88$). Because oxidative coupling products was obtained by the oxidation of $2,5\text{-}(MeO)_2C_6H_3CH_2OH$ with one-electron oxidant CAN,[50–52]

Scheme 3. Proposed Oxidation Pathways for Oxidation of $2,5\text{-}(MeO)_2C_6H_3CH_2OH$ by $[Fe^{IV}(O)(N4Py)]^{2+}$ in the Presence of Sc^{3+}

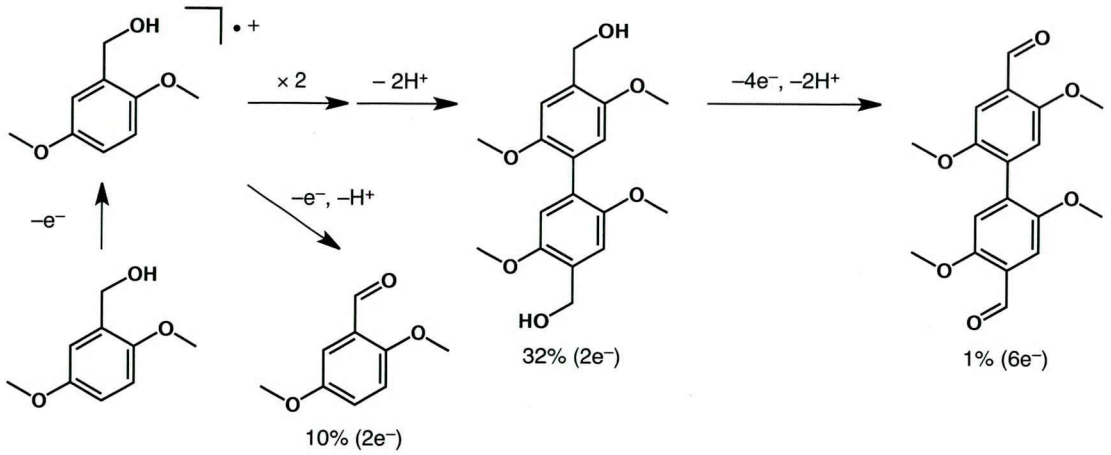

Scheme 4. Reaction Pathway for Oxidation of $2,5\text{-}(MeO)_2C_6H_3CH_2OH$ by $[Fe^{IV}(O)(N4Py)]^{2+}$ in the Absence and Presence of Sc^{3+}

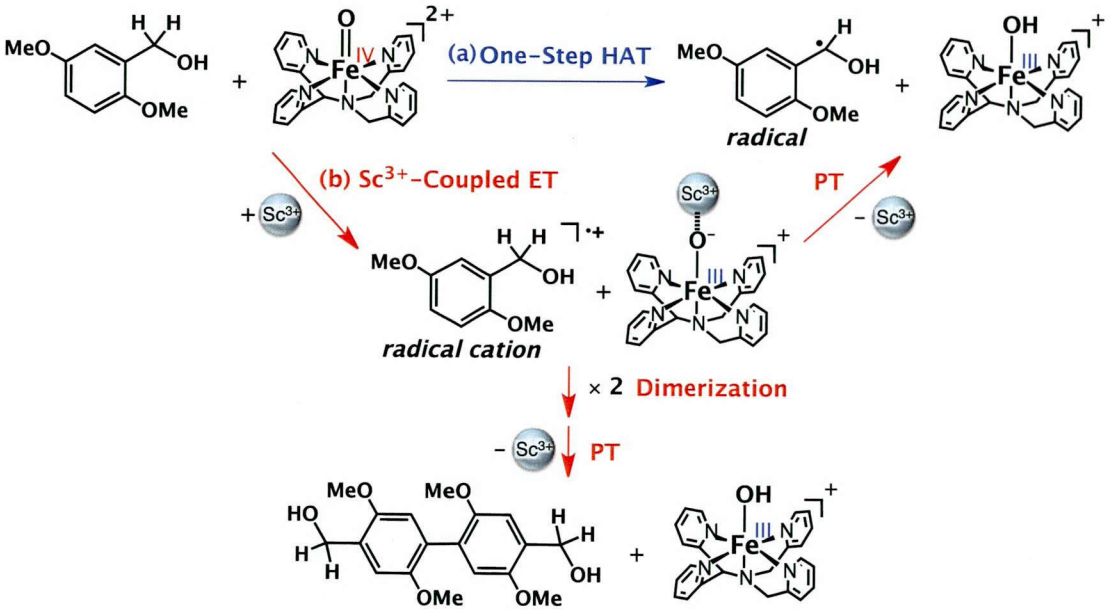

formation of the dimer products, together with the detection of the radical cation intermediate by absorption and EPR spectra in the oxidation of 2,5-$(MeO)_2C_6H_3CH_2OH$ by $[Fe^{IV}(O)(N4Py)]^{2+}$ in the presence of Sc^{3+} indicates the change of the reaction pathway from the one-step HAT in the absence of Sc^{3+} (step a shown in Scheme 4) to the Sc^{3+}-coupled ET pathway in the presence of Sc^{3+} (step b shown in Scheme 4).[53,54] Figure 16. The Sc^{3+}-coupled electron-transfer pathway is further confirmed by the first-order and second-order dependence of k_{ox} of the oxidation of 2,5-$(MeO)_2C_6H_3CH_2OH$ by $[Fe^{IV}(O)(N4Py)]^{2+}$ in the presence of Sc^{3+} on $[Sc^{3+}]$, which is quite similar to that observed Sc^{3+}-coupled ET from $[Fe(bpy)_3]^{2+}$ (one-electron reductant) to $[Fe^{IV}(O)(N4Py)]^{2+}$ on $[Sc^{3+}]$ (Figure 11) and the absence of KIE. This is consistent with the bimolecular decay kinetics of 2,5-$(MeO)_2C_6H_3CH_2OH^{\bullet+}$ in

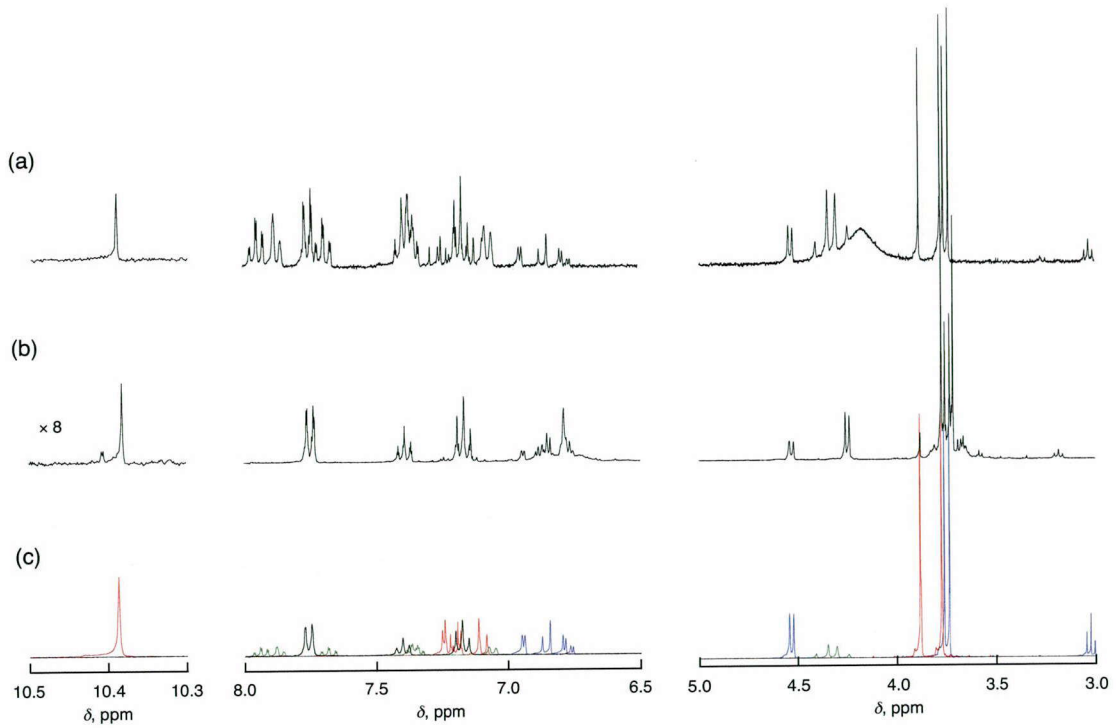

Figure 17. ^{1}H-NMR spectra of the reaction products obtained in the oxidation of 2,5-$(MeO)_2C_6H_3CH_2OH$ by $[Fe^{IV}(N4Py)(O)]^{2+}$ in the absence (a) and presence (b) of Sc^{3+} (10 mM) in CD_3CN. (c) ^{1}H-NMR spectra of authentic samples, 2,5-$(MeO)_2C_6H_3CH_2OH$ (blue), 2,5-$(MeO)_2C_6H_3CHO$ (red), $[Fe^{II}(N4Py)(NCMe)]^{2+}$ (green), and iodobenzene (black) produced in the formation reaction of $[Fe^{IV}(N4Py)(O)]^{2+}$ with iodosylbenzene.

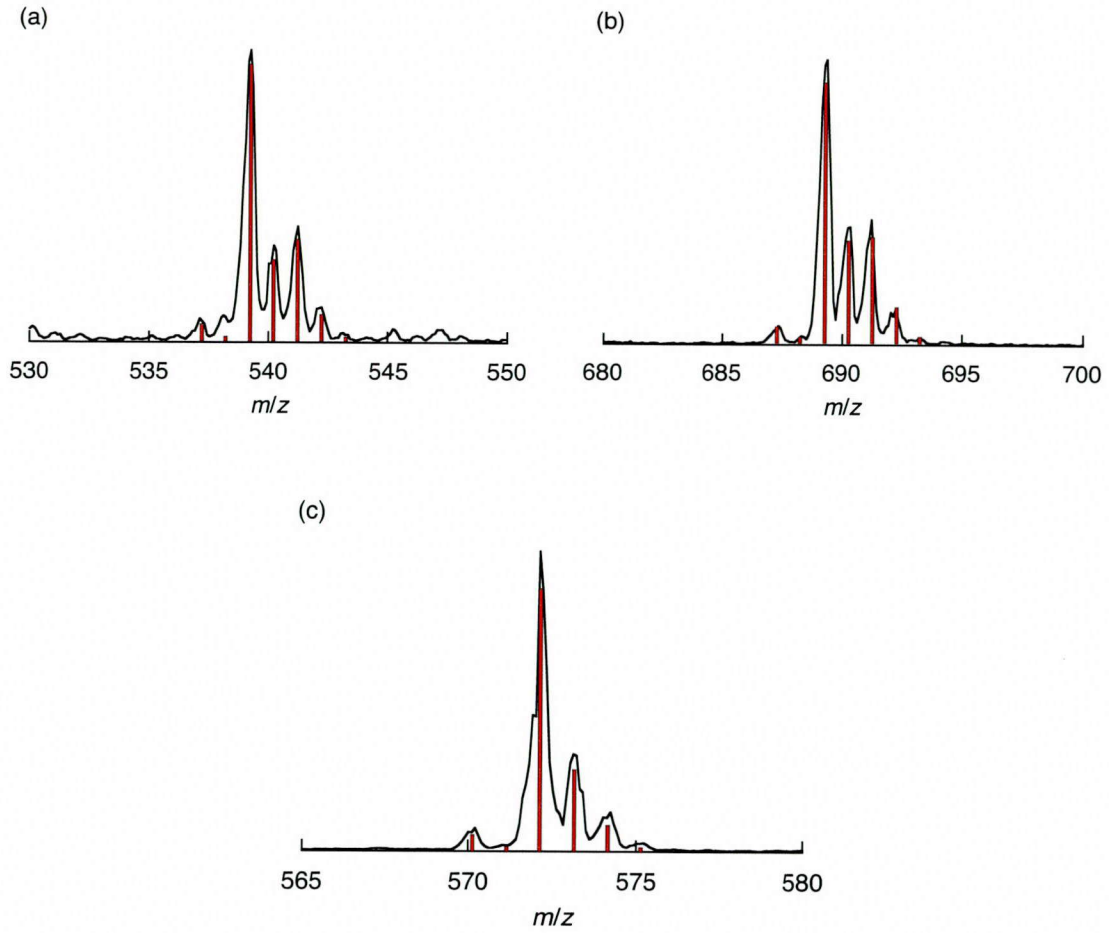

Figure 18. ESI-MS spectra (black line) of the reaction products obtained in the reaction between $[Fe^{IV}(O)(N4Py)]^{2+}$ (1.0 mM) and 2,5-$(MeO)_2C_6H_3CH_2OH$ (10 mM) in the absence (a and b) and presence (c) of Sc^{3+} (10 mM). Red bars show the simulated mass and isotope distribution patterns of $[Fe^{III}(N4Py)(OH)(ClO_4)]^+$ (m/z = 539.1) (a) and $[Fe^{III}(N4Py)(OCH_2CH_3(MeO)_2)(ClO_4)]^+$ (m/z = 689.1) (b) and $[Fe^{II}(N4Py)(OTf)]^+$ (m/z = 572.4) (c).

Effect of Sc^{3+} on the Oxidation Rate of Benzyl Alcohol Derivatives by $[Fe^{IV}(O)(N4Py)]^{2+}$. The change in the reaction pathway from one-step HAT to Sc^{3+}-coupled ET may be determined by the one-electron oxidation potentials (E_{ox}) of benzyl alcohol derivatives (see Table 1 for the E_{ox} values of benzyl alcohol derivatives). In order to explore the borderline between one-step HAT and Sc^{3+}-coupled ET pathways, we investigated the dependence of the second-order rate constants for the

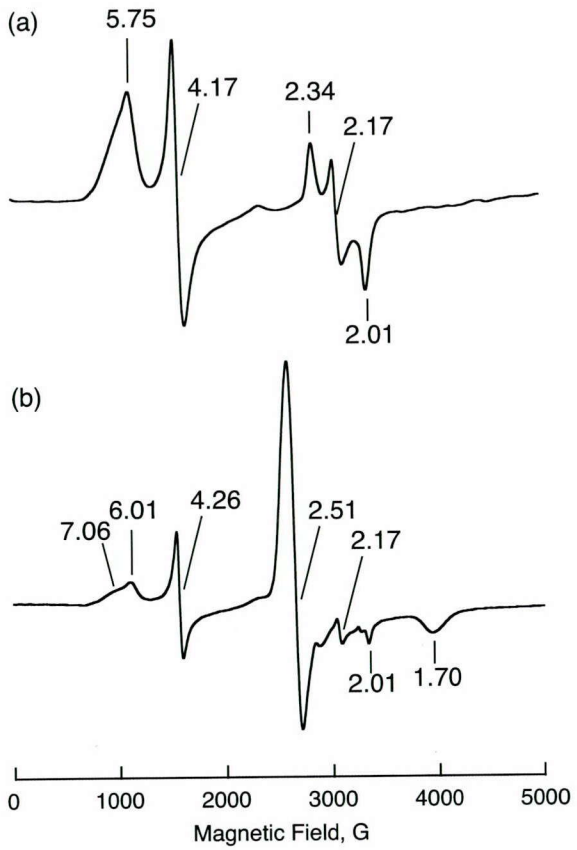

Figure 19. X-band EPR spectra of the reaction products obtained in the reaction between $[Fe^{IV}(O)(N4Py)]^{2+}$ (1.0 mM) and 2,5-$(MeO)_2C_6H_3CH_2OH$ (10 mM) in the absence (a) and presence (b) of Sc^{3+} (10 mM) in MeCN recorded at 77 K.

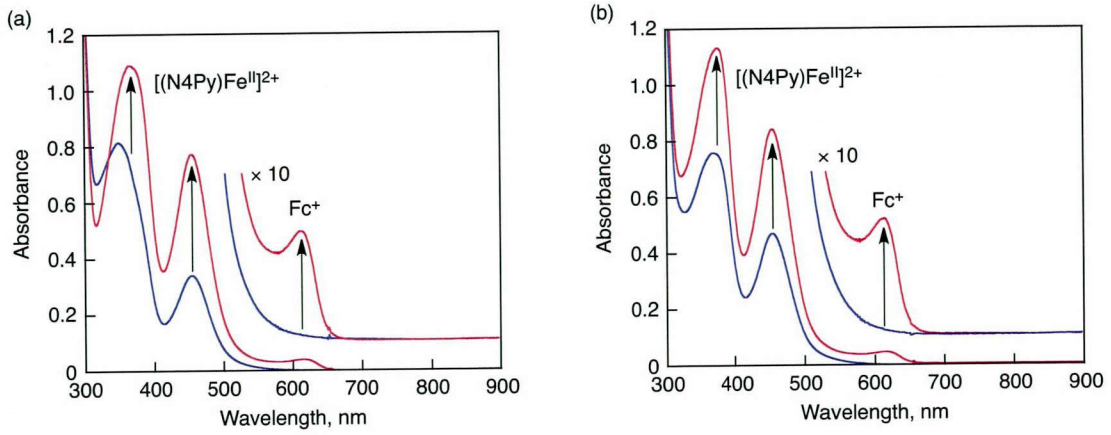

Figure 20. (a) UV–vis spectra of the resulted solution in the oxidation reaction of 2,5-$(MeO)_2C_6H_3CH_2OH$ (5.0 mM) by $[Fe^{IV}(O)(N4Py)]^{2+}$ (0.10 mM) (blue line) and after titration with 2.5 equiv of Fc in the presence of HOTf (10 mM; red line). (b) UV–vis spectra of the resulted solution in the oxidation reaction of 2,5-$(MeO)_2C_6H_3CH_2OH$ (5.0 mM) by $[Fe^{IV}(O)(N4Py)]^{2+}$ (0.10 mM) in the presence of Sc^{3+} (10 mM; blue line) and after titration with 2.5 equiv of Fc (red line).

oxidation of a series of benzyl alcohol derivatives on [Sc^{3+}]. The results are shown in Figures 21a–21g. The k_{ox} values for the oxidation of benzyl alcohol derivatives with relatively high E_{ox} values, *p*-$NO_2C_6H_4CH_2OH$, $C_6H_5CH_2OH$ and *p*-$ClC_6H_4CH_2OH$, were the same as those in the absence of Sc^{3+} with increasing concentration of Sc^{3+} (Figures 21a–21c), whereas the k_{ox} values for the oxidation of benzyl alcohol derivatives with lower oxidation potentials, *p*-$MeC_6H_4CH_2OH$, *p*-$MeOC_6H_4CH_2OH$, $Me_5C_6CH_2OH$, 3,5-$(MeO)_2C_6H_3CH_2OH$, 3,4,5-$(MeO)_3C_6H_2CH_2OH$ and 2,5-$(MeO)_2C_6H_3CH_2OH$, increased with increasing concentration of Sc^{3+} (Figures 21d–21g) as is the case for the oxidation of 2,5-$(MeO)_2C_6H_3CH_2OH$ (Figure 11). Although no radical cation intermediates were observed in the oxidation of *p*-$MeOC_6H_4CH_2OH$, $Me_5C_6CH_2OH$, 3,5-$(MeO)_2C_6H_3CH_2OH$ and 3,4,5-$(MeO)_3$-$C_6H_2CH_2OH$ in the presence of Sc^{3+} (10 mM), the acceleration may be attributed to Sc^{3+}-coupled ET. The $-\Delta G_{et}$ and k_{ox} values of the oxidation of a series of benzyl alcohol derivatives by $[Fe^{IV}(O)(N4Py)]^{2+}$ in the absence and presence of Sc^{3+} (10 mM) are summarized in Table 2. The $-\Delta G_{et}$ values (in eV) were determined from the E_{ox} values of benzyl alcohol derivatives for the one-electron oxidation to give the corresponding radical cations and the E_{red} values of $[Fe^{IV}(O)(N4Py)]^{2+}$ in the absence and presence of Sc^{3+} (10 mM) by eq 2, where *e* is the elementary charge.[55]

$$-\Delta G_{et} = e(E_{red} - E_{ox}) \tag{2}$$

Table 1. One-Electron Oxidation Potentials of Substituted Benzyl Alcohol Derivatives (E_{ox}) in the Absence and Presence of Sc^{3+} (10 mM)

entry	substituent	E_{ox} vs SCE, V	
		without Sc^{3+}	with Sc^{3+} (10 mM)
1	*p*-NO_2	2.88	2.88
2	*p*-H	2.33	2.33
3	*p*-Cl	2.25	2.23
4	*p*-Me	2.05	2.05
5	Me_5	1.65	1.80
6	*p*-MeO	1.58	1.78
7	3,5-$(MeO)_2$	1.49	1.49
8	3,4,5-$(MeO)_3$	1.22	1.42
9	2,5-$(MeO)_2$	1.20	1.33

Figure 22 shows plots of log k_{ox} of oxidation of benzyl alcohols by $[Fe^{IV}(O)(N4Py)]^{2+}$ in the absence and presence of Sc^{3+} (10 mM) and log k_{et} of electron transfer from one-electron reductants to $[Fe^{IV}(O)(N4Py)]^{2+}$ in the presence of Sc^{3+} (10 mM) vs driving force of ET ($-\Delta G_{et}$). In the absence of Sc^{3+}, the $-\Delta G_{et}$ values are largely negative (endergonic) and the log k_{ox} values are rather independent of the $-\Delta G_{et}$ values (blue points in Figure 22). The log k_{ox} values in the absence of Sc^{3+} are much larger than those predicted by the extrapolated line of electron transfer, indicating that the oxidation of benzyl alcohol derivatives by $[Fe^{IV}(O)(N4Py)]^{2+}$ undergoes via one-step HAT rather than via electron transfer. This is also supported by the KIE observed in the oxidations of $C_6H_5CD_2OH$ and 2,5-$(MeO)_2C_6H_3CD_2OH$ in the absence of Sc^{3+} (Figure 8).

In sharp contrast to the case in the absence of Sc^{3+}, log k_{ox} values of benzyl alcohol derivatives, which are accelerated by the presence of Sc^{3+} (10 mM) (entries 7–9), show similar driving force dependence to that of log k_{et} of electron transfer from a series of one-electron reductants to $[Fe^{IV}(O)(N4Py)]^{2+}$ in the presence Sc^{3+} (10 mM).[56] Both log k_{ox} and log k_{et} values increase with increasing the ET driving force ($-\Delta G_{et}$ values). The ET drivingforce dependence of k_{et} and k_{ox} is well fitted by the Marcus equation of outer-sphere electron transfer (eq 3), where Z is the frequency factor (1×10^{11} M^{-1} s^{-1}) and λ is the reorganization energy of electron transfer.[57,58] The dependence of log k_{ox} on $-\Delta G_{et}$ clearly indicates the occurrence of Sc^{3+}-coupled ET from benzyl alcohol derivatives to $[Fe^{IV}(O)(N4Py)]^{2+}$. Although the $-\Delta G_{et}$ values for entry 7–9 are negative (endergonic),

Table 2. Driving Force for ET ($-\Delta G_{et}$) and Second-Order Rate Constants (k_{ox}) for Oxidation of Benzyl Alcohol Derivatives with $[Fe^{IV}(O)(N4Py)]^{2+}$ in the Absence and Presence of Sc^{3+} (10 mM) in MeCN at 298 K

entry	substituent	$-\Delta G_{et}$, eV		k_{ox}, M^{-1} s^{-1}	
		Sc^{3+} (0 mM)	Sc^{3+} (10 mM)	Sc^{3+} (0 mM)	Sc^{3+} (10 mM)
1	*p*-NO_2	–2.37	–1.69	1.1×10^{-1}	1.3×10^{-1}
2	*p*-H	–1.82	–1.14	9.9×10^{-2}	9.9×10^{-2}
3	*p*-Cl	–1.74	–1.04	1.0×10^{-1}	1.1×10^{-1}
4	*p*-Me	–1.54	–0.86	1.4×10^{-1}	1.7×10^{-1}
5	Me_5	–1.14	–0.61	3.5×10^{-2}	5.6×10^{-2}
6	*p*-MeO	–1.07	–0.59	1.4×10^{-1}	2.5×10^{-1}
7	3,5-$(MeO)_2$	–0.98	–0.30	1.2×10^{-1}	3.8×10^{-1}
8	3,4,5-$(MeO)_3$	–0.71	–0.23	1.5×10^{-1}	4.0×10
9	2,5-$(MeO)_2$	–0.69	–0.14	2.0×10^{-1}	1.3×10

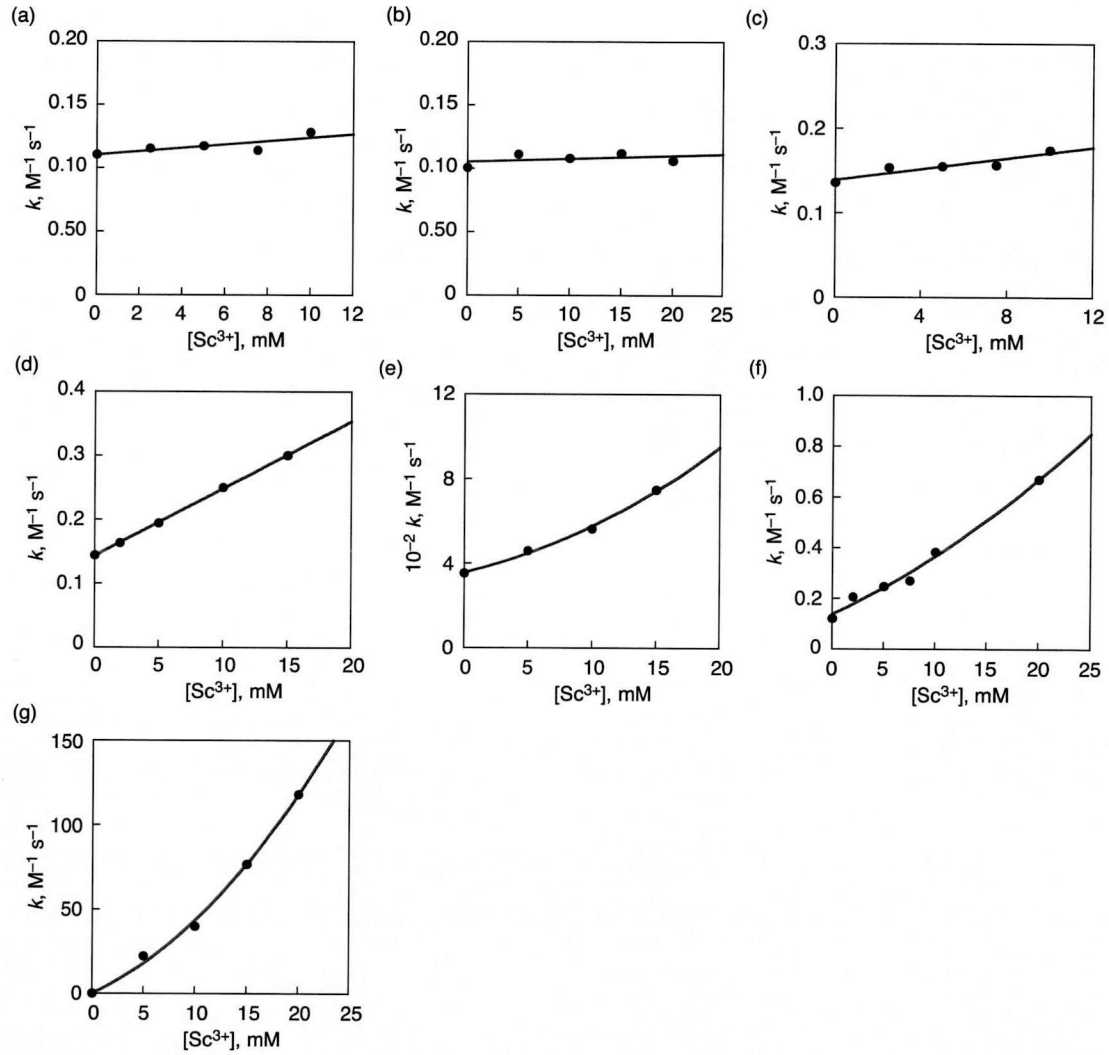

Figure 21. Plots of k_{ox} vs $[Sc^{3+}]$ in the reaction of $[Fe^{IV}(O)(N4Py)]^{2+}$ (0.10 mM) and benzyl alcohol derivatives in the presence of Sc^{3+} in deareted MeCN at 298 K: (a) *p*-$NO_2C_6H_4CH_2OH$ (25 mM), (b) *p*-$ClC_6H_4CH_2OH$ (50 mM), (c) *p*-$MeC_6H_4CH_2OH$ (25 mM), (d) *p*-$MeOC_6H_4CH_2OH$ (50 mM), (e) $Me_5C_6CH_2OH$ (25 mM), (f) 3,5-$(MeO)_2C_6H_3CH_2OH$ (10 mM) and (g) 3,4,5-$(MeO)_3C_6H_2CH_2OH$ (0.050 mM).

the Sc^{3+}-coupled ET may be followed by fast subsequent reaction (pathway b in Scheme 4). The λ values for electron transfer from one-electron reductants and benzyl alcohol derivatives to $[Fe^{IV}(O)(N4Py)]^{2+}$ in the presence of 10 mM of Sc^{3+} are determined to be 2.27 and 1.93 eV by fitting plots of entries a–e and 7–9 in red in Figure 22 with eq 3, respectively.

$$\log k_{ox} = \log Z - \lambda(1 + \Delta G_{et}/\lambda)^2/(2.3 \times 4k_B T) \qquad (3)$$

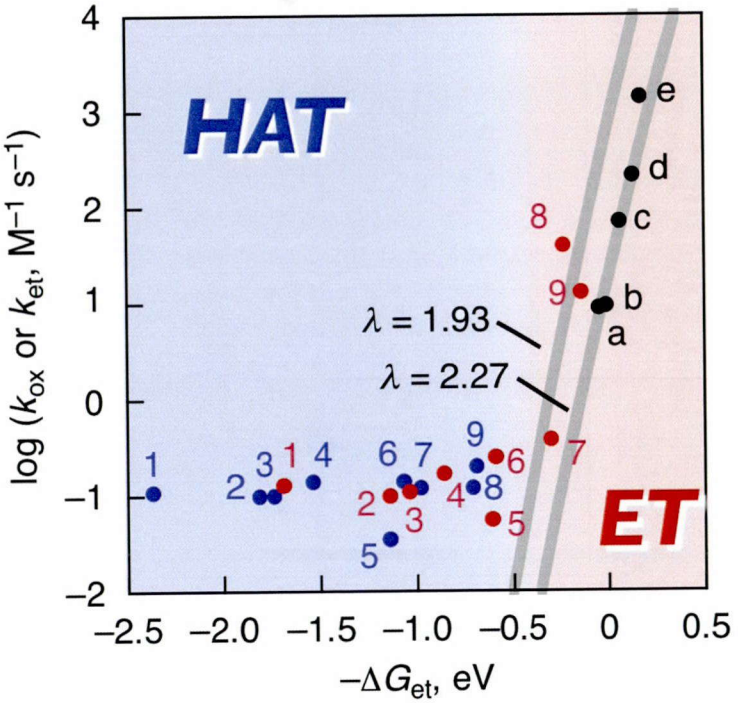

Figure 22. Plots of log k_{ox} for oxidation of benzyl alcohol derivatives (numbers refer to compounds in Table 1) by $[Fe^{IV}(O)(N4Py)]^{2+}$ in MeCN at 298 K vs $-\Delta G_{et}$ for electron transfer from benzyl alcohol derivatives to $[Fe^{IV}(O)(N4Py)]^{2+}$ in the absence (blue) of Sc^{3+} and presence (red) of Sc^{3+} (10 mM). Black points are plots of log k_{et} of electron transfer from one-electron reductants (a: $[Ru^{II}(bpy)_3]^{2+}$, b: $[Fe^{II}(Clphen)_3]^{2+}$, c: $[Ru^{II}(Me_2bpy)_3]^{2+}$, d: $[Fe^{II}(bpy)_3]^{2+}$, e: $[Fe^{II}(Ph_2phen)_3]^{2+}$) to $[Fe^{IV}(N4Py)(O)]^{2+}$ in the presence of 10 mM of Sc^{3+} in MeCN at 298 K vs $-\Delta G_{et}$. The blue and red parts correspond to HAT and ET pathways, respectively. The solid lines are drawn using eq 4 with l values of 1.93 and 2.27 eV.

On the other hand, the k_{ox} values of benzyl alcohol derivatives are independent of the ET deriving force even in the presence of Sc^{3+} (10 mM) when $-\Delta G_{et}$ is smaller than –0.5 eV (entries 1–4 in Table 2). This indicates that the oxidation of those benzyl alcohol derivatives proceeds via one-step HAT, which is an energetically much more favorable pathway than the highly endergonic Sc^{3+}-coupled ET. The rates of oxidation of benzyl alcohol derivatives (entries 5 and 6 in Table 2) are slightly accelerated by the presence of Sc^{3+} (10 mM) (1.8 and 1.6 times respectively), and the log k_{ox} values are on the borderline of the mechanism change between one-step HAT and Sc^{3+}-coupled ET.[59] No clear correlation between log k_{ox} values and bond dissociation energies ($BDE_{(C–H)}$) of C–H bonds at the benzyl position of a series of benzyl alcohol derivatives calculated with DFT excludes the possibility that reaction pathway is controlled by $BDE_{(C–H)}$ (Figure 23).

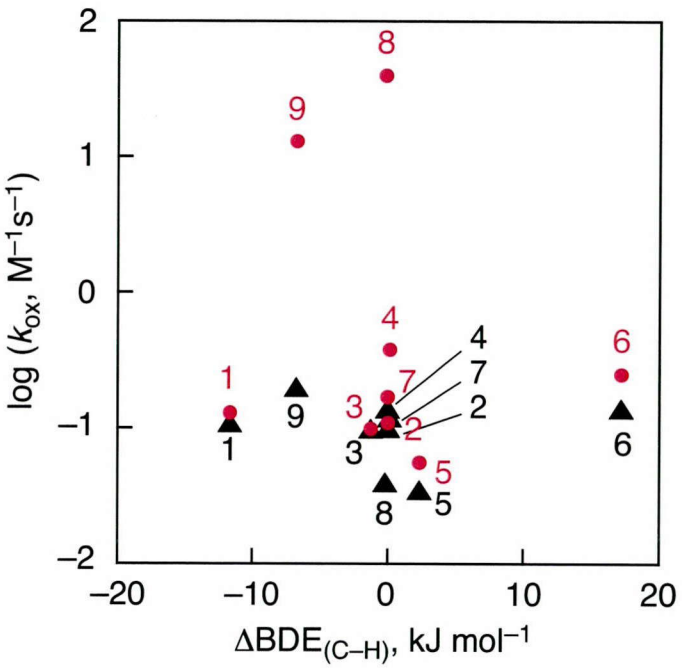

Figure 23. Plots of log k_{ox} for in the absence and presence of Sc^{3+} (10 mM) vs bond-dissociation energies ($\Delta BDE_{(C-H)}$) of C–H bond at the benzyl position of benzyl alcohol derivatives relative to that of benzyl alcohol, which is taken as zero (numbers refer to compounds in Table 1).

The comparison of the driving force dependence of k_{ox} and k_{et} in Figure 22 has provided a clear view with regard to the borderline of the mechanism change between one-step HAT and Sc^{3+}-coupled ET. The results at a different concentration of Sc^{3+} (1.0 mM) are presented in Figure 24. Although the best fit λ value (2.33 eV) for the driving force dependence of log k_{et} with 1.0 mM Sc^{3+} becomes larger than the value with 10 mM Sc^{3+} (2.27 eV) and therefore the plot looks somewhat different, the conclusion on the mechanism change between one-step HAT and Sc^{3+}-coupled ET remains virtually the same.

It should be noted that it is rather unusual to apply the Marcus theory to conditional rate constants that depend on the concentration of Sc^{3+}. Nevertheless we can explain the dependence of the rate constant on the concentration of Sc^{3+} using the Marcus theory as follows.[58] Under the conditions such that $\lambda << -\Delta G_{et}$ in Figure 22, the k_{et} value is estimated by the Marcus cross relationship as shown in eq 4,[57] where k_{Dex}, k_{Aex} and K_{et} are the rate constant of electron exchange

$$k_{et} = (k_{Dex}k_{Aex}K_{et})^{1/2} \qquad (4)$$

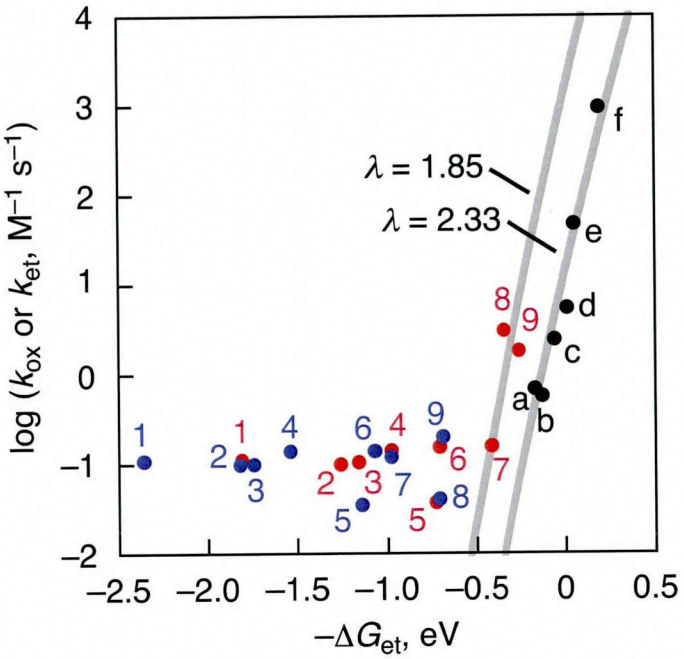

Figure 24. Plots of log k_{ox} for oxidation of benzyl alcohol derivatives (numbers refer to compounds in Table 1) by $[Fe^{IV}(O)(N4Py)]^{2+}$ in MeCN at 298 K vs $-\Delta G_{et}$ for electron transfer from benzyl alcohol derivatives to $[Fe^{IV}(O)(N4Py)]^{2+}$ in the absence (blue) of Sc^{3+} and presence (red) of Sc^{3+} (1 mM). The $-\Delta G_{et}$ values were determined from the E_{red} of $[Fe^{IV}(O)(N4Py)]^{2+}$ in the presence of 1 mM of Sc^{3+} determined by extrapolation of relationship between E_{red} and $[Sc^{3+}]$ previously reported in ref 27a and the E_{ox} values of benzyl alcohol derivatives in the presence of 10 mM of Sc^{3+} shown in Table S1. Black points are plots of log k_{et} of electron transfer from one-electron reductants (a: $[Ru^{II}(bpy)_3]^{2+}$, b: $[Fe^{II}(Clphen)_3]^{2+}$, c: $[Ru^{II}(Me_2bpy)_3]^{2+}$, d: $[Fe^{II}(bpy)_3]^{2+}$, e: $[Fe^{II}(Ph_2phen)_3]^{2+}$, f: $[Fe^{II}(Me_2bpy)_3]^{2+}$) to $[Fe^{IV}(N4Py)(O)]^{2+}$ in the presence of 10 mM of Sc^{3+} in MeCN at 298 K vs $-\Delta G_{et}$. The solid lines are drawn using eq 4 with λ values of 1.85 and 2.33 eV.

between electron donor (D) and the radical cation, the rate constant of electron exchange between electron acceptor (A) and the one-electron reduced species, and the equilibrium constants of the electron transfer from D to A. The k_{Dex} value is constant independent of concentration of Sc^{3+}, whereas k_{Aex} and K_{et} are expected to increase in proportion to $[Sc^{3+}]^2$ at high concentrations of Sc^{3+} as given by eqs 5 and 6, respectively, where k_{Aex0} and K_{et0} are the proportional constants. In such a case, the dependence of k_{et}

$$k_{Aex} = k_{Aex0}[Sc^{3+}]^2 \tag{5}$$

$$K_{et} = K_{et0}[Sc^{3+}]^2 \tag{6}$$

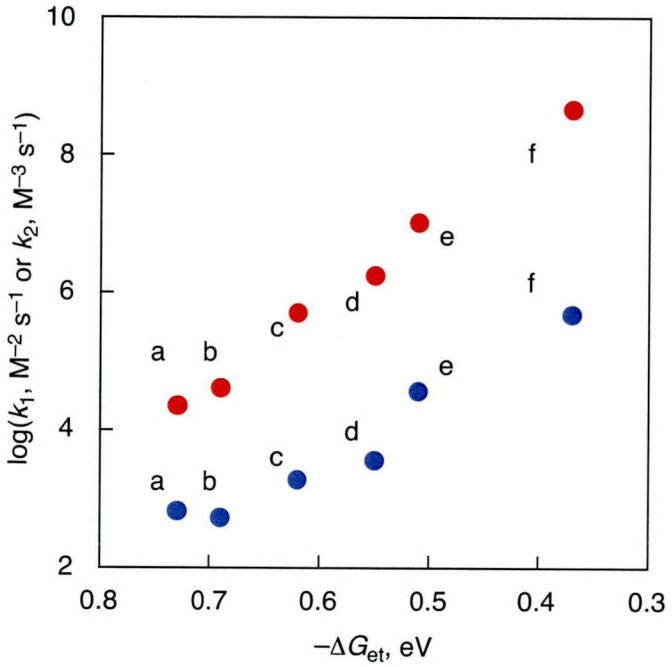

Figure 25. Plots of log k_1 (blue circle) and k_2 (red circle) (eq 1) for Sc^{3+} ion-coupled ET from electgron donors with various one-electron oxidation potentials (numbers refer to compounds in Figure S14) to $[Fe^{IV}(O)(N4Py)]^{2+}$ in MeCN at 298 K vs $-\Delta G_{et}$ for electron transfer from those compounds to $[Fe^{IV}(O)(N4Py)]^{2+}$ in the absence of Sc^{3+}.

on $[Sc^{3+}]$ is given by eq 7, which agrees with the results in Figure 5.

$$k_{et} = (k_{Dex}k_{Aex0}K_{et0})^{1/2}[Sc^{3+}]^2 \quad (7)$$

The dependence of log k_1 and log k_2 of Sc^{3+}-coupled ET on $-\Delta G_{et}$ in the absence of Sc^{3+} is shown in Figure 25, where a roughly parallel relationship between k_1 and k_2 is observed. This plot for benzyl alcohol derivatives is not shown because the k_1 and k_2 values of benzyl alcohol derivatives close to the region of one-step HAT could not be obtained accurately due to the large contribution of k_0.

Conclusion

In this study, we have demonstrated the change of the rate-determining step in the oxidation of benzyl alcohol derivatives by $[Fe^{IV}(O)(N4Py)]^{2+}$ from one-step HAT to Sc^{3+}-coupled ET depending on the one-electron oxidation potentials of benzyl alcohol derivatives. The change in the reaction mechanism is initiated by acceleration of ET by

Sc^{3+} while HAT is not accelerated by Sc^{3+} at all.[60] Such a change in the reaction pathways by the presence of Sc^{3+} has been clearly shown by the disappearance of KIE in the presence of Sc^{3+} in contrast to a large KIE value observed in the absence of Sc^{3+}, when formation of the radical cation of a benzyl alcohol derivative was detected as the initial product of Sc^{3+}-coupled ET from the substrate to $[Fe^{IV}(O)(N4Py)]^{2+}$, leading to the dimerized product as a major product in contrast to the corresponding aldehyde obtained as the sole product in the absence of Sc^{3+}. The mechanistic borderline between one-step HAT and Sc^{3+}-coupled ET has been found to be determined by the ET driving force from the substrate to $[Fe^{IV}(O)(N4Py)]^{2+}$ with the borderline of $-\Delta G_{et} \approx -0.5$ eV. The C–H bond is cleaved via HAT when $-\Delta G_{et}$ is more negative than –0.5 eV, whereas Sc^{3+}-coupled ET becomes a predominant pathway when $-\Delta G_{et}$ is more positive than –0.5 eV. In other words, Sc^{3+}-coupled ET occurs when E_{ox} of substrate is more negative than 1.7 V. This study provides the first example for the change in the mechanism of oxidation of substrates by a high-valent metal-oxo complex from one-step HAT to ET that is accelerated by Sc^{3+} depending on the ET driving force. The oxidation reaction takes place even when $-\Delta G_{et}$ is negative, i.e., ET is endergonic, indicating the ET process is coupled with the following proton transfer. It is of interest to note that the borderline between one-step HAT and Sc^{3+}–coupled ET is at the ET driving force (ΔG_{et}) of ca. –0.5 eV, which is similar to that reported previously for the borderline between one-step oxygen atom transfer and Sc^{3+}–coupled ET.[57] This type of switching in reaction pathway from HAT to ET depending on the $-\Delta G_{et}$ value would generally appear in the reaction systems where high-valent oxometal species are employed as an oxidant such as Compound I or MnO_4^-, especially in oxidation of substrates with relatively low oxidation potential or in the presence of acids which shift one-electron reduction potential of metal-oxo species positively.

References

(1) (a) Kochi, J. K., Ed. *Free Radicals*; Wiley: New York, 1973. (b) Olah, G. A.; Molnár, Á. *Hydrocarbon Chemistry*; Wiley: New York, 1995. (c) Larock, R. C. *Comprehensive Organic: A Guide to Functional Group Preparations*; Wiley-VCH: New York, 1999. (d) Halliwell, B.; Gutteridge, J. M. C. *Free Radicals in Biology and Medicine*; Oxford University Press: Oxford, U.K., 2007. (e) Hynes, J. T.; Klinman, J. P.; Limbach, H.-H.; Schowen, R. L., Ed. *Hydrogen-Transfer Reactions: Biological Aspects I-II, Volume 3.*; Wiley-VCH: Weinheim, 2007.

(2) (a) Stewart, R. *Oxidation Mechanisms*; Benjamin: New York, 1964. (b) Mijs, W. J.; De Jonge, C. R. H. I. *Organic Synthesis by Oxidation with Metal Compounds;* Plenum: New York, 1986.

(3) (a) Roithová, J.; Schröder, D. *Chem. Rev.* **2010**, *110*, 1170. (b) Chiesa, M.; Giamello, E.; Che, M. *Chem. Rev.* **2010**, *110*, 1320. (c) Ding, X.-L.; Wu, X.-N.; Zhao, Y.-X.; He, S.-G. *Acc. Chem. Res.* **2012**, *45*, 382. (d) Dietl, N.; Schlangen, M.; Schwarz, H. *Angew. Chem., Int. Ed.* **2012**, *51*, 2.

(4) (a) Penner-Hahn, J. E.; Eble, K. S.; McMurry, T. J.; Renner, M.; Balch, A. L.; Groves, J. T.; Dawson, J. H.; Hodgson, K. O. *J. Am. Chem. Soc.* **1986**, *108*, 7819. (b) Schlichting, I.; Berendzen, J.; Chu, K.; Stock, A. M.; Maves, S. A.; Benson, D. E.; Sweet, R. M.; Ringe, D.; Petsko, G. A.; Sligar, S. G. *Science* **2000**, *287*, 1615. (c) Green, M. T.; Dawson, J. H.; Gray, H. B. *Science* **2004**, *304*, 1653. (d) Rittle, J.; Green, M. T. *Science* **2011**, *330*, 933. (e) Dunford, H. B. *Heme Peroxidases*; Wiley-VCH: New York, 1999. (f) Ortiz de Montellano, P. R. *Cytochrome P450: Structure, Mechanism, and Biochemistry*, 3rd ed.; Kluwer Academic/Plenum Publishers, New York, 2005.

(5) (a) Sono, M.; Roach, M. P.; Coulter, E. D.; Dawson, J. H. *Chem. Rev.* **1996**, *96*, 2841. (b) Harris, D. L.; Loew, G. H. *J. Am. Chem. Soc.* **1998**, *120*, 8941. (c) Newcomb, M; Shen, R.; Choi, S.-Y.; Toy, P. H.; Hollenberg, P. F.; Vaz, A. D. N.; Coon, M. J. *J. Am. Chem. Soc.* **2000**, *122*, 2677. (d) Ortiz de Montellano, P. R. *Chem. Rev.* **2010**, *110*, 932.

(6) (a) Elkins, J. M.; Ryle, M. J.; Clifton, I. J.; Hotopp, J. C. D.; Lloyd, J. S.; Burzlaff, N. I.; Baldwin, J. E.; Hausinger, R. P.; Roach, P. L. *Biochemistry* **2002**, *41*, 5185. (b) Price, J. C.; Barr, E. W.; Glass, T. E.; Krebs, C.; Bollinger, J. M., Jr. *J. Am. Chem. Soc.* **2003**, *125*, 13008. (c) Price, J. C.; Barr, E. W.; Tirupati, B.; Krebs, C.; Bollinger, J. M., Jr. *Biochemistry* **2003**, *42*, 7497. (d) Proshlyakov, D. A.; Henshaw, T. F.; Monterosso, G. R.; Ryle, M. J.; Hausinger, R. P. *J. Am. Chem. Soc.* **2004**, *126*, 1022. (e) Price, J. C.; Barr, E. W.; Hoffart, L. M.; Krebs, C.; Bollinger, J. M., Jr. *Biochemistry* **2005**, *44*, 8138.

(7) (a) Ekstrom, G.; Norsten, C.; Cronholm, T.; Ingelman-Sundberg, M. *Biochemistry* **1987**, *26*, 7348. (b) Vaz, A. D. N.; Coon, M. J. *Biochemistry* **1994**, *33*, 6442. (c) Guengerich, F. P. *Chem. Res. Toxicol.* **2001**, *14*, 611. (d) Kroutil, W.; Mang, H.; Edegger, K.; Faber, K. *Adv. Synth. Catal.* **2004**, *346*, 125.

(8) (a) Rettie, A. E.; Rettenmeier, A. W.; Howald, W. N.; Baillie, T. A. *Science* **1987**, *235*, 890. (b) Rettie, A. E.; Boberg, M.; Rettenmeier, A. W.; Baillie, T. A. *J. Biol. Chem.* **1988**, *263*, 13733. (c) Giner, J. L.; Silva, C. J.; Djerassi, C. *J. Am. Chem. Soc.* **1990**, *112*, 9626. (d) Collins, J. R.; Camper, D. L.; Loew, G. H. *J. Am. Chem.*

Soc. **1991**, *113*, 2736. (e) Buist, P. H.; Marecak, D. M. *J. Am. Chem. Soc.* **1992**, *114*, 5073.

(9) (a) Baldwin, J. E.; Schofield, C. *Chemistry of β-Lactams*; Blackie: Glasgow, 1992. (b) Roach, P. L.; Clifton, I. J.; Hensgens, C. M. H.; Shibata, N.; Schofield, C. J.; Hajdu, J.; Baldwin, J. E. *Nature* **1997**, *387*, 827. (c) Brown, C. D.; Neidig, M. L.; Neibergall, M. B.; Lipscomb, J. D.; Solomon, E. I. *J. Am. Chem. Soc.* **2007**, *129*, 7427.

(10) (a) Krebs, C.; Fujimori, D. G.; Walsh, C. T.; Bollinger, J. M., Jr. *Acc. Chem. Res.* **2007**, *40*, 484. (b) Galonić, D. P.; Barr, E. W.; Walsh, C. T.; Bollinger, J. M. Jr.; Krebs, C. *Nat. Chem. Biol.* **2007**, *3*, 113.

(11) Warren, J. J.; Tronic, T. A.; Mayer, J. M. *Chem. Rev.* **2010**, *110*, 6961.

(12) (a) Balcells, D.; Clot, E.; Eisenstein, O. *Chem. Rev.* **2010**, *110*, 749. (b) Gunay, A.; Theopold, K. H. *Chem. Rev.* **2010**, *110*, 1060.

(13) (a) MacBeth, C. E.; Golombek, A. P.; Young, V. G., Jr.; Yang, C.; Kuczera, K.; Hendrich, M. P.; Borovik, A. S. *Science* **2000**, *289*, 938. (b) Rohde, J.-U.; In, J.-H.; Lim, M. H.; Brennessel, W. W.; Bukowski, M. R.; Stubna, A.; Münck, E.; Nam, W.; Que, L., Jr. *Science* **2003**, *299*, 1037. (c) Que, L., Jr.; Ho, R. Y. N. *Chem. Rev.* **1996**, *96*, 2607. (d) Solomon, E. S.; Brunold, T. C.; Davis, M. I.; Kemsley, J. N.; Lee, S.-K.; Lehnert, N.; Neese, F.; Skulan, A. J.; Yang, Y.-S.; Zhou, J. *Chem. Rev.* **2000**, *100*, 235. (e) Que, L., Jr. *Acc. Chem. Res.* **2007**, *40*, 493. (f) Nam, W. *Acc. Chem. Res.* **2007**, *40*, 522. (g) Hohenberger, J.; Ray, K.; Meyer, K. *Nat. Commun.* **2012**, *3*, 720. (h) de Visser, S. P.; Rohde, J.-U.; Lee, Y.-M.; Cho, J.; Nam, W. *Coord. Chem. Rev.* **2012**, ASAP.

(14) (a) Groves, J. T.; Haushalter, R. C.; Nakamura, M.; Nemo, T. E.; Evans, B. J. *J. Am. Chem. Soc.* **1981**, *103*, 2884. (b) Meunier, B. *Chem. Rev.* **1992**, *92*, 1411. (c) Sheldon, R. A. *Metalloprophyrins in Catalytic Oxidations*; Marcel Dekker: New York, 1994. (d) Meunier, B., Ed. *Metal-Oxo and Metal-Peroxo Species in Catalytic Oxidations*; Springer-Verlag: Berlin, 2000. (e) Shaik, S.; Cohen, S.; Wang, Y.; Chen, H.; Kumar, D.; Thiel, W. *Chem. Rev.* **2010**, *110*, 949.

(15) Lubben, M.; Meetsma, A.; Wilkinson, E. C.; Feringa, B.; Que, L., Jr. *Angew. Chem., Int. Ed.* **1995**, *34*, 1512.

(16) (a) Kaizer, J.; Klinker, E. J.; Oh, N. Y.; Rohde, J.-U.; Song, W. J.; Stubna, A.; Kim, J.; Münck, E.; Nam, W.; Que, L., Jr. *J. Am. Chem. Soc.* **2004**, *126*, 472. (b) Kumar, D.; Hirao, H.; Que, L., Jr.; Shaik, S. *J. Am. Chem. Soc.* **2005**, *127*, 8026. (c) Wang, D.; Zhang, M.; Bühlmann, P. B.; Que, L., Jr. *J. Am. Chem. Soc.* **2010**, *132*, 7638.

(17) Oh, N. Y.; Suh, Y.; Park, M. J.; Seo, M. S.; Kim, J.; Nam, W. *Angew. Chem., Int. Ed.* **2005**, *44*, 4235.

(18) (a) Gupta R.; Borovik, A. S. *J. Am. Chem. Soc.* **2003**, *125*, 13234. (b) Pestovsky, O.; Bakac, A. *J. Am. Chem. Soc.* **2004**, *126*, 13757. (c) Lam, W. W. Y.; Man, W.-L.; Lau, T,-C. *Coord. Chem. Rev.* **2007**, *251*, 2238. (d) de Visser, S. P. *J. Am. Chem. Soc.* **2010**, *132*, 1087. (e) Prokop, K. A.; de Visser, S. P.; Goldberg, D. P. *Angew. Chem., Int. Ed.* **2010**, *49*, 5091. (f) Kojima, T.; Nakayama, K.; Ikemura, K.; Ogura, T.; Fukuzumi, S. *J. Am. Chem. Soc.* **2011**, *133*, 11692.

(19) (a) Mayer, J. M. *Acc. Chem. Res.* **1998**, *31*, 441. (b) Cukier, R. I.; Nocera, D. G. *Annu. Rev. Phys. Chem.* **1998**. *49*, 337. (c) Mayer, J. M. *Annu. Rev. Phys. Chem.* **2004**. *55*, 363. (d) Huynh, M. H. V.; Meyer, T. J. *Chem. Rev.* **2007**, *107*, 5004. (e) Mayer, J. M. *Acc. Chem. Res.* **2011**, *44*, 36.

(20) (a) Goto, Y.; Watanabe, Y.; Fukuzumi, S.; Jones, J. P.; Dinnocenzo, J. P. *J. Am. Chem. Soc.* **1998**, *120*, 10762. (b) Goto, Y.; Matsui, T.; Ozaki, S.; Watanabe, Y.; Fukuzumi, S. *J. Am. Chem. Soc.* **1999**, *121*, 9497. (c) Nehru, K.; Seo, M. S.; Kim, J.; Nam, W. *Inorg. Chem.* **2007**, *46*, 293.

(21) Yuasa, J.; Fukuzumi, S. *J. Am. Chem. Soc.* **2006**, *128*, 14281.

(22) Yuasa, J.; Yamada, S.; Fukuzumi, S. *J. Am. Chem. Soc.* **2006**, *128*, 14938.

(23) For other metal ion-promoted reactions, see: (a) Fukuzumi, S.; Ohkubo, K.; Morimoto, Y. *Phys. Chem. Chem. Phys.* **2012**, *14*, 8472. (b) Fukuzumi, S.: Ohkubo, K.; Okamoto, T. *J. Am. Chem. Soc.* **2002**, *124*, 14147. (c) Fukuzumi, S.; Fujii, Y.; Suenobu, T. *J. Am. Chem. Soc.* **2001**, *123*, 10191. (d) Fukuzumi, S. *Bull. Chem. Soc. Jpn.* **1997**, *70*, 1. (e) Fukuzumi, S.; Okamoto, T. *J. Am. Chem. Soc.* **1993**, *115*, 11600. (f) Fukuzumi, S.; Koumitsu, S.; Hironaka, K.; Tanaka, T. *J. Am. Chem. Soc.* **1987**, *109*, 305. (g) Fukuzumi, S.; Nishizawa, N.; Tanaka, T. *J. Chem. Soc., Perkin Trans. 2* **1985**, 371. (h) Fukuzumi, S.; Kuroda, S.; Tanaka, T. *J. Am. Chem. Soc.* **1985**, *107*, 3020.

(24) (a) Abu-Omar, M. M. *J. Am. Chem. Soc.* **2007**, *129*, 11505. (b) Shearer, J.; Zhang, C. X.; Hatcher, L. Q.; Karlin, K. D. *J. Am. Chem. Soc.* **2003**, *125*, 12670.

(25) There has been no example of C–H bond cleavage that proceeds via a PT/ET pathway, however that of O–H bond cleavage via a PT/ET pathway has been reported. See: Litwinienko, G.; Ingold, K. U. *Acc. Chem. Res.* **2007**, *40*, 222.

(26) (a) Lee, Y.-M.; Kotani, H.; Suenobu, T.; Nam, W.; Fukuzumi, S. *J. Am. Chem. Soc.* **2008**, *130*, 434. (b) Fukuzumi, S.; Kotani, H.; Suenobu, T.; Hong, S.; Lee, Y.-M.; Nam, W. *Chem.–Eur. J.* **2010**, *16*, 354.

(27) (a) Morimoto, M.; Kotani, H.; Park, J.; Lee, Y.-M.; Nam, W.; Fukuzumi, S. *J. Am. Chem. Soc.* **2011**, *133*, 403. (b) Fukuzumi, S. *Prog. Inorg. Chem.* **2009**, *56*, 49.

(28) For the crystal structure of a Sc^{3+}-bound Fe(IV)-oxo complex, see: Fukuzumi, S.; Morimoto, Y.; Kotani, H.; Naumov, P.; Lee, Y.-M.; Nam, W. *Nature Chem.* **2010**, *2*, 756.

(29) Sc^{3+} ion is known to be the most effective for metal ion-coupled electron transfer. See: (a) Fukuzumi, S.; Ohkubo, K. *Chem.–Eur. J.* **2000**, *6*, 4532. (b) Fukuzumi, S.; Ohkubo, K. *J. Am. Chem. Soc.* **2002**, *124*, 10270.

(30) For the effect of Brønsted acid on the reactivity of the Fe(IV)-oxo complex, see: Park, J.; Morimoto, Y.; Lee, Y.-M.; Nam. W.; Fukuzumi, S. *J. Am. Chem. Soc.* **2012**, *134*, 3903.

(31) Armarego, W. L. F.; Chai, C. L. L. *Purification of Laboratory Chemicals*, 6th ed.; Pergamon Press: Oxford, 2009.

(32) Saltzman, H.; Sharefkin, J. G., Eds. *Organic Syntheses,* vol. V; Wiley: New York, 1973; p 658.

(33) Tsai, S.-C.; Klinman, J. P. *Biochemistry* **2001**, *40*, 2303.

(34) Mann, C. K.; Barnes, K. K. *Electrochemical Reactions in Non-aqueous Systems*; Mercel Dekker: New York, 1970.

(35) Becke, A. D. *J. Chem. Phys.* **1993**, *98*, 5648.

(36) Gaussian 09, Revision A.02, Gaussian, Inc.: Wallingford CT, 2004.

(37) Dennington II, R.; Keith, T.; Millam, J.; Eppinnett, K.; Hovell, W. L.; Gilliland, R. *Gaussview Version 4.1*; Semichem, Inc.,: Shawnee Mission, KS,. 2003.

(38) The EPR signals assigned as an alkoxo complex are similar to $[Fe(OMe)(N4Py)]^{2+}$. See: Roelfes, G.; Lubben, M.; Chen, K.; Ho, R. Y. N.; Meetsma, A.; Genseberger, S.; Hermant, R. M.; Hage, R.; Mandal, S. K.; Young, V. G.; Zang, Y.; Kooijman, H.; Spek, A. L.; Que, L., Jr.; Feringa, B. L. *Inorg. Chem.* **1999**, *38*, 1929.

(39) Hong, S.; Lee, Y.-M.; Shin, W.; Fukuzumi, S.; Nam, W. *J. Am. Chem. Soc.* **2009**, *131*, 13910.

(40) The KIE value for this reaction performed at 298 K in the absence of Sc^{3+} is determined to be 13.

(41) There is another possibility that $[Fe^{III}(OH)(N4Py)]^{2+}$ oxidizes 2,5-$(MeO)_2C_6H_3CHOH^{\bullet}$ to yield $[Fe^{II}(N4Py)]^{2+}$, H_2O and 2,5-$(MeO)_2C_6H_3CHO$. Then, $[Fe^{II}(N4Py)]^{2+}$ is oxidized by $[Fe^{IV}(O)(N4Py)]^{2+}$ to yield 2,5-$(MeO)_2C_6H_3CHO$ and $[Fe^{III}(OH)(N4Py)]^{2+}$. However, a control experiment shows that $[Fe^{IV}(O)(N4Py)]^{2+}$ does not oxidize $[Fe^{II}(N4Py)]^{2+}$ in the presence of 2,5-$(MeO)_2C_6H_3CH_2OH$ in MeCN. Thus, the proportionation of the iron(IV) and iron(II) complexes as a reason why $[Fe^{IV}(O)(N4Py)]^{2+}$ acts as a one-electron

oxidant rather than a two-electron oxidant is unlikely under the present reaction conditions.

(42) (a) Atkinson, J. K.; Hollenberg, P. F.; Ingold, K. U.; Johnson, C. C.; Le Tadic, M.-H.; Newcomb, M.; Putt, D. A. *Biochemistry* **1994**, *33*, 10630. (b) Matsuo, T.; Mayer, J. M. *Inorg. Chem.* **2005**, *44*, 2150.

(43) Melander, L.; Saunders, W. H. Jr. *Reaction Rates of Isotopic Molecules*; Wiley Interscience: New York, 1980, pp 29–36.

(44) Klinker, E. J.; Shaik. S.; Hirao, H.; Que, L., Jr. *Angew. Chem., Int. Ed.* **2009**, *48*, 1291.

(45) (a) Lehnert, N.; Solomon, E. I. *J. Biol. Inorg. Chem.* **2003**, *8*, 294. (b) Hatcher, E.; Soudackov, A. V.; Hammes-Schiffer, S. *J. Am. Chem. Soc.* **2004**, *126*, 5763. (c) Meyer, M. P.; Klinman, J. P. *J. Am. Chem. Soc.* **2011**, *133*, 430.

(46) For $2,5\text{-}(MeO)_2C_6H_3OH^{\bullet+}$ produced by photochemical methods, see: (a) Branchi, B.; Bietti, M; Ercolani, G.; Izquierdo, M. A.; Miranda, M. A.; Stella, L. *J. Org. Chem.* **2004**, *69*, 8874. (b) Baciocchi, E.; Bietti, M.; Gerini, M. F.; Manduchi, L. Salamone, M. Steenken, S. *Chem.–Eur. J.* **2001**, *7*, 1408.

(47) The extrapolation of the second-order plot to the time when the reaction was started by mixing two reactant solutions, which is about 5 min before starting EPR measurements, suggests that the radical cation is produced quantitatively.

(48) Yield = $[Product]/[2,5\text{-}(MeO)_2C_6H_3CH_2OH]_0 \times 100$ where $[2,5\text{-}(MeO)_2C_6H_3CH_2OH]_0$ is the initial concentration of $2,5\text{-}(MeO)_2C_6H_3CH_2OH$.

(49) We could not observe the Sc^{3+}-bound complexes by ESI-mass except for $[Fe^{III}(N4Py)(NCMe)]^{3+}$ may be due to weak Fe–O bond of the Sc^{3+}-bound complex. However, the EPR spectrum of resulting solution shown in Figure S11b agreed with the spectrum of the Sc^{3+}-bound complex reported in our previous study.[27a]

(50) Love, B. E.; Bonner-Stewart, J.; Forrest, L. A. *Synlett* **2009**, *5*, 813.

(51) The major product in the oxidation of $2,5\text{-}(MeO)_2C_6H_3CH_2OH$ by CAN is not a dimer of aldehyde but diquinone, 4,4'-dimethoxy-[bi-1,4-cyclohexadien-1-yl]-3,3',6,6'-tetrone.[50]

(52) In the oxidation of benzyl alcohol by $[Fe(O)(N4Py)]^{2+}$ both in the presence and absence of Sc^{3+}, we cannot detect dimerized products as shown in Figure 4. This may be because the hydrogen-abstracted radicals by $[Fe(O)(N4Py)]^{2+}$ can not produce dimerized products not like radical cations of substrates.

(53) In the oxidation of $2,5\text{-}(MeO)_2C_6H_3CH_2OH$ by $[Ru^{III}(bpy)_3]^{2+}$, no aldehyde formation was observed as a product. This indicates that $[Fe^{III}(O)(N4Py)]^{2+}$–Sc^{3+}

works as a base to accept proton released from $2,5\text{-}(MeO)_2C_6H_3CH_2OH^{\bullet+}$ to produce $2,5\text{-}(MeO)_2C_6H_3CHO$.

(54) The pseudo-first-order rate constants were proportional to concentrations of substrates without exhibiting no intercepts as shown in Figure 6. This indicates that the rate-determining step is the Sc^{3+}-coupled electron transfer followed by subsequent reactions which are faster than the back electron-transfer reaction.

(55) Some of benzyl alcohol derivatives interact with Sc^{3+}. This interaction resulted in the positive shifts of the one-electron oxidation potentials (Table S1 in SI).

(56) The observed rate constant (k_{ox}) consists of three rate constants, i.e., k_0, k_1 and k_2 (eq 1). Under the conditions in Figure 5 ($[Sc^{3+}]$ = 10 mM), k_2 is the main component. Thus, k_{ox} in Figure 10 virtually corresponds to the rate constant for elementary step electron transfer to $[Fe^{IV}(O)(N4Py)]^{2+}$–$(Sc^{3+})_2$.[27a]

(57) (a) Marcus, R. A. *Annu. Rev. Phys. Chem.* **1964**, *15*, 155. (b) Marcus, R. A. *Angew. Chem., Int. Ed.* **1993**, *32*, 1111.

(58) The Marcus equation can be applied at different concentrations of Sc^{3+}, when the driving force and reorganization energy of electron transfer are changed as discussed previously on metal ion-coupled electron transfer; see: Okamoto, K.; Imahori, H.; Fukuzumi, S. *J. Am. Chem. Soc.* **2003**, *125*, 7014.

(59) For the use of the Marcus plot to clarify the reaction mechanisms of $[Fe^{IV}(O)(N4Py)]^{2+}$, see: (a) Park, J.; Morimoto, Y.; Lee, Y.-M.; Nam, W.; Fukuzumi, S. *J. Am. Chem. Soc.* **2011**, *133*, 5236. (b) Park, J.; Morimoto, Y.; Lee, Y.-M.; You, Y.; Nam, W.; Fukuzumi, S. *Inorg. Chem.* **2011**, *50*, 11612.

(60) The binding of Sc^{3+} to $[Fe^{IV}(O)(N4Py)]^{2+}$ may increase the oxidizing ability. However, the direct hydrogen atom transfer reaction may be prohibited by the steric effect of Sc^{3+}. In contrast to this, electron transfer is generally insensitive to the steric effect because outer-sphere electron transfer requires little interaction between electron donor and acceptor molecules. This is the reason why ET is accelerated whereas no acceleration of HAT occurs by the addition of Sc^{3+}.

Chapter 4: Proton-coupled electron transfer vs. metal ion-coupled electron transfer in electron-transfer reduction of an iron(IV)-oxo complex

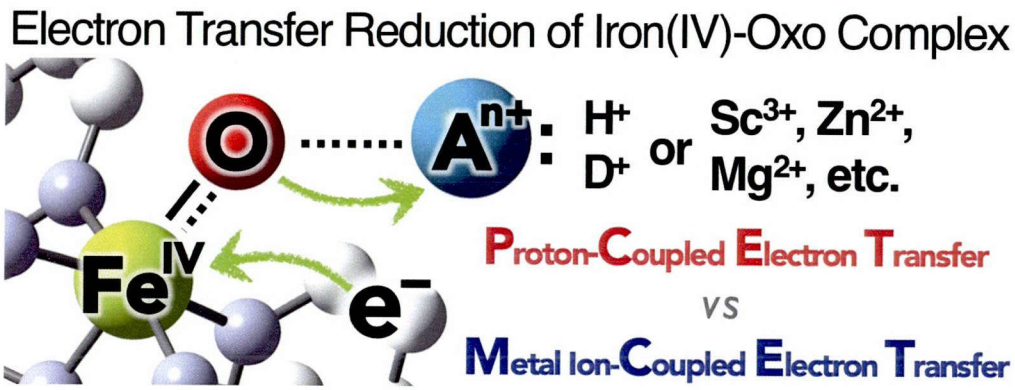

Abstract: The reactivity of the proton-coupled electron transfer (PCET) *vs.* metal ion-coupled electron (MCET) transer in reduction of a non-heme iron(IV)-oxo complex was found to be well correlated with a quantitive measure of acididy of triflic acid and variuos metal triflates. An inverse kinetic isotope effect (KIE = 0.56) was observed in the PCET with CH_3COOH vs CH_3COOD, suggesting the couple of ET and protonation of the iron complex.

Introduction

Electron acceptability of dioxygen (O=O) and carbonyl compounds containing carbon-oxygen double bonds (C=O) is known to be enhanced by proton-coupled electron transfer (PCET) with proton and also by metal ion-coupled electron transfer (MCET) with metal ions acting as Lewis acids.[1–10] We use PCET and MCET herein as abbreviations for reactions in which electron transfer (ET) is coupled with binding of proton and metal ions, respectively.[9,10] Proton is known to play pivotal roles to control ET of such molecules in biological systems including high-valent metal-oxo species containing metal-oxygen double bonds (M=O).[11] For instance, ET of Compound I in peroxidase is known to be affected by acidic amino acid residues placed on the distal side of heme.[12] In model systems, ET reduction of high-valent metal-oxo complexes is also accelerated by not only by PCET with one and two protons (Scheme 1a) but also by MCET with one and two metal ions (Scheme 1b).[10,13–16] The acceleration effects of metal ions on the MCET reactions of *p*-benzoquinone and an iron(IV)-oxo complex are well correlated with quantitative measure of Lewis acidity of metal ions, which was evaluated based on *g*-values of EPR signals of $O_2^{\bullet-}$–metal ion complexes[8] and also fluorescence maxima of *N*-methylacridone–metal ion complexes.[17] However, there has

Scheme 1. (a) PCET and (b) MCET Pathway of an $Fe^{IV}(O)$ Complex

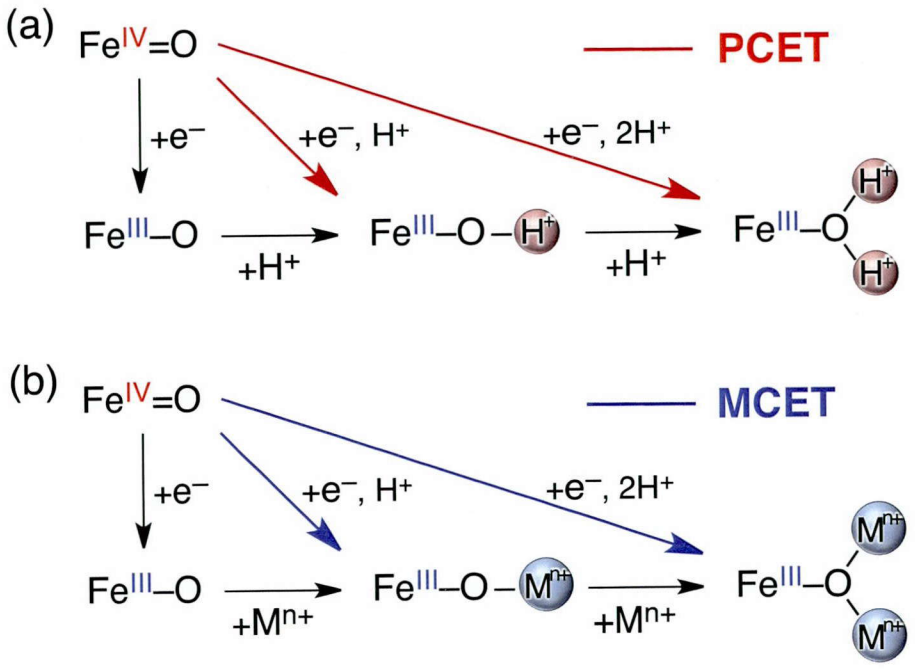

been no quantitative comparison of acidity of proton *vs.* metal ions. There has been no example of comparison of the PCET *vs.* MCET reactivity, either. In addition, the question whether the protonation and ET occur concomitantly or not has yet to be clarified.

We report herein comparison of the PCET *vs.* MCET reactivity in the ET reduction of an iron(IV)-oxo complex, $[Fe^{IV}(O)(N4Py)]^{2+}$ [N4Py = *N*,*N*-bis(2-pyridylmethyl)-*N*-bis(2-pyridyl)methylamine],[18] by ferrocene with triflic acid (HOTf) and metal triflates ($M^{n+}(OTf)_n$) in acetonitrile (MeCN). It has been found that the PCET *vs.* MCET reactivity is well correlated with a quantitative measure of acidity of HOTf and $M^{n+}(OTf)_n$, which was obtained by fluorescence maxima of *N*-methylacridone with HOTf and $M^{n+}(OTf)_n$.[19] Whether the protonation and ET occur concomitantly or not has been clarified by examining the deuterium kinetic isotope effect in the PCET reaction of $[Fe^{IV}(O)(N4Py)]^{2+}$.

Experimental Section

Materials. All solvents and chemicals were of reagent-grade quality, obtained commercially and used without further purification, unless otherwise noted. Acetonitrile (MeCN) was dried according to published procedures and distilled under Ar prior to use.[20] Scandium triflate [$Sc(OTf)_3$] ($OTf^- = {}^-OSO_2CF_3$), yttrium triflate [$Y(OTf)_3$], trifluoromethanesulfonic acid [HOTf], trifluoroacetic acid [HTFA] ($TFA^- = {}^-OCOCF_3$), acetic acid [HOAc] ($OAc^- = {}^-OCOCH_3$), Ferrocene (Fc), and *N*-methylacridone (AcrCO) were purchased from Sigma-Aldrich Co. Ferrocene (Fc) was purified by sublimation prior to the use. Iodosylbenzene (PhIO) was prepared from iodobenzene diacetate according to a literature procedure.[21] $[Fe^{II}(N4Py)(NCMe)](ClO_4)_2$ and its Fe(IV)-oxo complex, $[Fe^{IV}(O)(N4Py)]^{2+}$, were prepared by literature methods.[18]

Kinetic Measurements. Rates of ET from Fc to $[Fe^{IV}(O)(N4Py)]^{2+}$ in the presence of Brønsted acids, such as HOTf, HTFA and HOAc, were performed on a UNISOKU RSP-601 stopped-flow spectrometer equipped with a MOS-type highly sensitive photodiode-array in MeCN at 298 K. These ET reactions were monitored by the decay of absorption band at 695 nm due to $[Fe^{IV}(O)(N4Py)]^{2+}$ (λ_{max} = 695 nm) and formation of absorption band at 615 nm due to ferrocenium ion (λ_{max} = 615 nm), respectively. Typically, the deaerated MeCN solution of $[Fe^{IV}(O)(N4Py)]^{2+}$ (2.0×10^{-4} M) and deaerated MeCN solution of Fc (4.0×10^{-3} M) and Brønsted acid (2.0×10^{-3} M) were mixed. All kinetic measurements were carried out under pseudo-first-order conditions where the concentrations of Fc and each Brønsted acid were maintained to be more than

10-folds excess of that of $[Fe^{IV}(O)(N4Py)]^{2+}$.

Observation of Absorption Spectral Changes of AcrCO. Absorption spectral change of AcrCO upon the addition of HOTf, $Sc(OTf)_3$ and $Y(OTf)_3$ was examined at 298 K using a Hewlett Packard 8453 photodiode-array spectrophotometer with a square quartz cuvette (path length = 1.0 cm). The deaerated MeCN solutions of HOTf (2.5 mM), $Sc(OTf)_3$ (2.5 mM) and $Y(OTf)_3$ (2.5 mM) were added by means of a microsyringe to a deaerated MeCN solution (2.0 mL) containing AcrCO (3.3 mM).

Observation of Fluorescence Spectral Changes of AcrCO. Fluorescence spectral change of AcrCO upon addition of HOTf, $Sc(OTf)_3$ and $Y(OTf)_3$ was investigated at room temperature after observation of absorption spectral change noted above with a Shimadzu RF-5300PC fluorescence spectrophotometer.

Results and Discussion

ET from ferrocene (Fc) to $[Fe^{IV}(O)(N4Py)]^{2+}$ occurs in MeCN at 298 K as reported previously.[22] The rate of ET increased proportionally with increasing concentrations of Fc and $[Fe^{IV}(O)(N4Py)]^{2+}$. The observed second-order rate constant of ET (k_{et}) increased with increasing concentration of HOTf as shown in Figure 1, where k_{et} exhibits both first-order dependence and second-order dependence on [HOTf]. The dependence of k_{et} on [HOTf] is given by eq 1, where k_1 and k_2 are the third-order and fourth-order rate constants for ET from Fc to the iron(IV)-oxo complex coupled with one- and two-proton-binding (Scheme 1a), and k_0 is the second-order rate constant for the ET in the absence of acid (Scheme 1). Eq 1 is rewritten by eq 2, which affords a linear plot of $(k_{et} - k_0)$/[HOTf] *vs.* [HOTf] as shown in inset of Figure 1. The k_1 and k_2

$$k_{et} = k_0 + k_1[HOTf] + k_2[HOTf]^2 \quad (1)$$

$$(k_{et} - k_0)/[HOTf] = k_1 + k_2[HOTf] \quad (2)$$

values were determined from the intercept and slope of a plot of $(k_{et} - k_0)$/[HOTf] *vs.* [HOTf], respectively.

Similarly, the k_{et} value increased with increasing concentrations of metal triflates.[14] The most reactive metal triflate to accelerate the MCET reactions was $Sc(OTf)_3$. The comparison of the k_{et} value with HOTf *vs.* $Sc(OTf)_3$ is also shown in Figure 1. The k_{et} values with HOTf are always larger than those with $Sc(OTf)_3$. The k_1 and k_2 values with

various metal triflates were determined previously from the intercepts and slopes of plots of $(k_{et} - k_0)/[M^{n+}(OTf)_n]$ *vs.* $[M^{n+}(OTf)_n]$, respectively.[14] The k_1 and k_2 values of HOTf and various metal triflates are listed in Table 1.

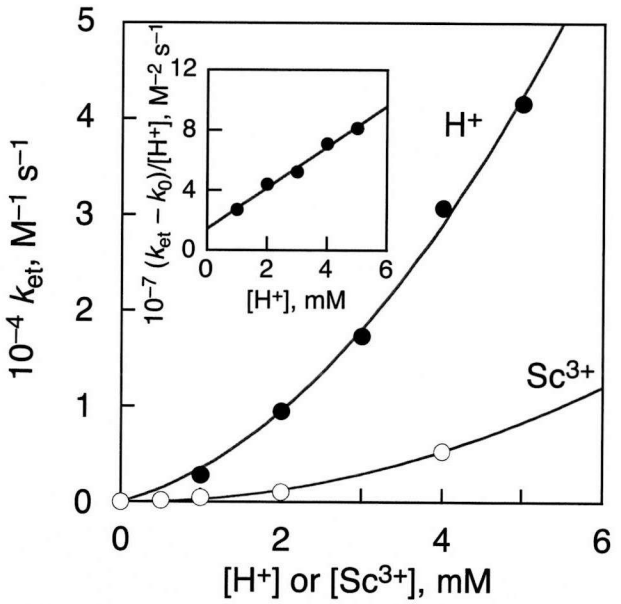

Figure 1. Plots of k_{et} *vs.* [HOTf] and [$Sc(OTf)_3$] for PCET and MCET from Fc to $[Fe^{IV}(O)(N4Py)]^{2+}$ in the presence of HOTf and $Sc(OTf)_3$ in MeCN at 298 K, respectively. Inset shows plot of $(k_{et} - k_0)/[HOTf]$ *vs.* [HOTf].

In order to compare the PCET *vs.* MCET reactivity, we have measured the absorption and fluorescence spectra of *N*-methylacridone (AcrCO) in the presence of HOTf and various metal triflates. When HOTf and metal triflates were added to an MeCN solution of AcrCO, the absorption and fluorescence spectra are shifted due to binding of HTOF and metal triflates (Scheme 2) as shown in Figure 2a and 2b, respectively (see also Scheme 2). The red shifts of the fluorescence emission energies (ΔE) due to binding of metal triflates from that in the absence of metal triflate have been reported to be well correlated with the MCET reactivity of $[Fe^{IV}(O)(N4Py)]^{2+}$.[14]

Figure 3 shows plots of log k_1 and log k_2 *vs.* ΔE for both PCET and MCET reactions of $[Fe^{IV}(O)(N4Py)]^{2+}$. Good linear correlations are obtained for both PCET and MCET reactions of $[Fe^{IV}(O)(N4Py)]^{2+}$, indicating the ΔE values determined from the fluorescence shift due to binding of HOTf and metal triflates can be used as quantitative measure of acidity of both proton and metal ions. The stronger is the acidity, the stronger becomes the binding of acids to $[Fe^{IV}(O)(N4Py)]^{2+}$ as well as the excited state of AcrCO.

Table 1. Lewis Acidity of Lewis Acids (ΔE) and, Third- and Forth-Order Rate constants (k_1 and k_2) for ET from Fc to $[Fe^{IV}(O)(N4Py)]^{2+}$ in MeCN at 298 K.

Lewis acid	ΔE (eV)	k_1 (M^{-2} s^{-1})	log (k_1)	k_2 (M^{-3} s^{-1})	log (k_2)
HOTf	0.26	1.5×10^6	6.2	1.4×10^9	9.1
$Sc(OTf)_3$	0.25	1.5×10^6	6.2	2.8×10^8	8.4
$Y(OTf)_3$	0.17	2.2×10^4	4.3	5.0×10^6	6.7
$Lu(OTf)_3$	0.18	1.4×10^4	4.2	3.3×10^6	6.5
$Zn(OTf)_2$	0.15	6.8×10^3	3.8	3.3×10^5	5.5
$Mg(OTf)_2$	0.12	3.3×10^3	3.5	2.0×10^5	5.3

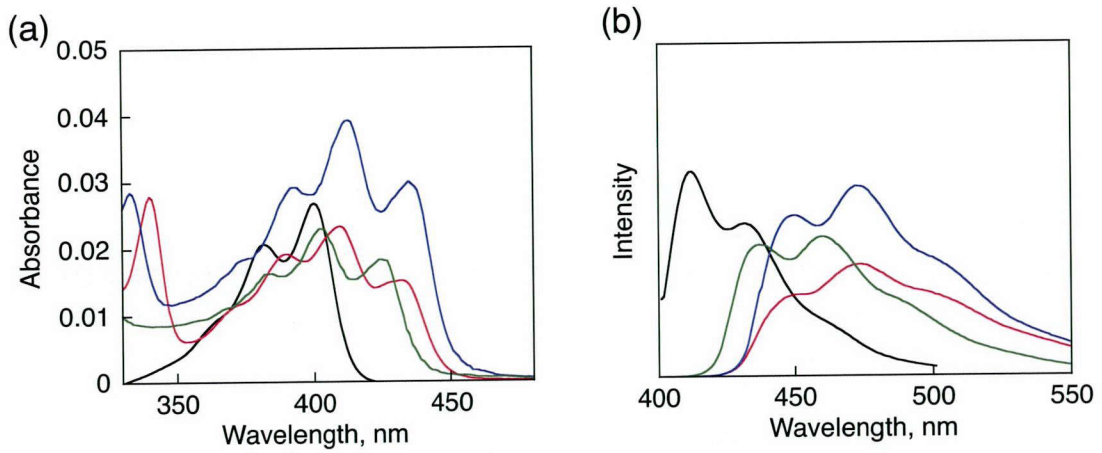

Figure 2. Absorption spectra (a) and fluorescence spectra (b) of *N*-methylacridone (3.3 μM) in the absence (black) and presence of HOTf (red, 2.5 mM), $Sc(OTf)_3$ (blue, 2.5 mM) and $Y(OTf)_3$ (green, 2.5 mM) in deaerated MeCN at 298 K.

Scheme 2. Binding of Lewis Acid (A^{n+}: H^+ and M^{n+}) to AcrCO

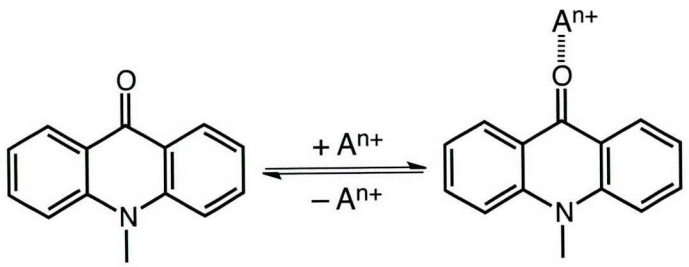

This is the reason why there are good linear correlations between log k_1 and log k_2 *vs.* the ΔE values, which were determined from the fluorescence emission energies of AcrCO with HOTf and metal triflates.

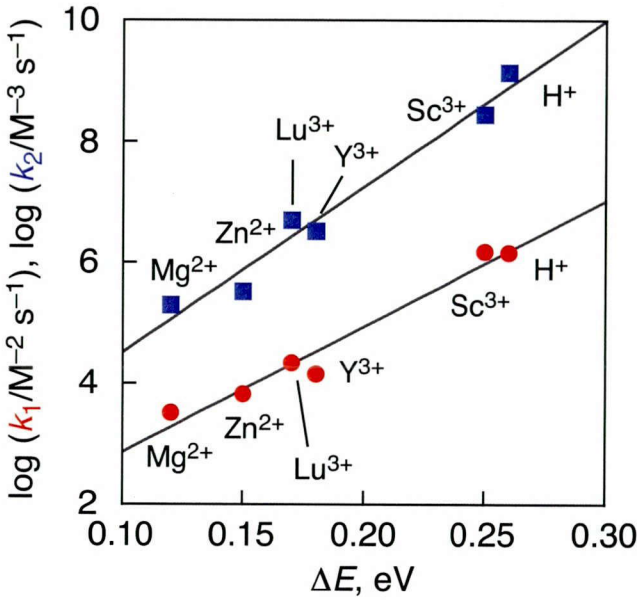

Figure 3. Plots of log k_1 (red) and log k_2 (blue) *vs.* ΔE for PCET and MCET from Fc to $[Fe^{IV}(O)(N4Py)]^{2+}$ in the presence of HOTf and metal triflates in MeCN at 298 K. The ΔE values were determined from the fluorescence emission energies of AcrCO in the presence of HOTf and metal triflates relative to the energy in their absence.

As shown in Figure 3, HOTf acts as a stronger acid than $Sc(OTf)_3$, which is the strongest Lewis acid among metal triflates. When HOTf was replaced by other weaker Brønsted acids of trifluoroacetic acid (HTFA) and acetic acid (HOAc), the k_1 value becomes smaller with acid dissociation constant of Brønsted acids ($k_1 = 8.7 \times 10^6$ M^{-2} s^{-1} and $k_2 = 1.4 \times 10^9$ M^{-3} s^{-1} for HOTf (pK_a = 0.7),[23a] $k_1 = 3.0 \times 10^4$ M^{-2} s^{-1} for HTFA (pK_a = 12.9),[23b] $k_1 = 8.7 \times 10$ M^{-2} s^{-1} for HOAc (pK_a = 23.5)).[23c,] The plots of k_{et} *vs.* [HOAc] and [HTFA] for PCET from Fc to $[Fe^{IV}(O)(N4Py)]^{2+}$ in MeCN at 298 K to determine the k_1 value is shown in Figure 4 and Figure 5, respectively. In the case of HOAc and HTFA, ET from ferrocene to the iron(IV)-oxo complexes occurs, exhibiting the first-order dependence of k_{et} on [HOAc] and [HTFA] with an intercept, which corresponds to k_0. However, no contribution of the second-order dependence of k_{et} on [HOAc] and [HTFA] was observed because of the low acidity of HOAc and HTFA.

When HOAc was replaced by the deuterated acid (DOAc), the k_1 value of PCET from Fc to the $Fe^{IV}(O)$ coupled with transfer of deuterium from DOAc to the complex in MeCN becomes larger than that with HOAc as shown in Figure 4.

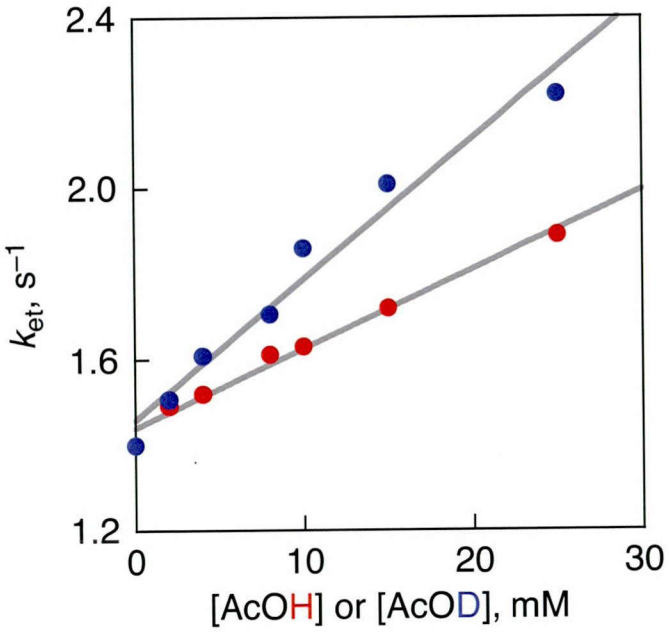

Figure 4. Plots of k_{et}/[HOAc] *vs.* [HOAc] (red circle) and k_{et}/[DOAc] *vs.* [DOAc] (blue circle) for PCET form Fc to $[Fe^{IV}(O)(N4Py)]^{2+}$ in the presence of HOAc and DOAc in MeCN at 298 K, respectively.

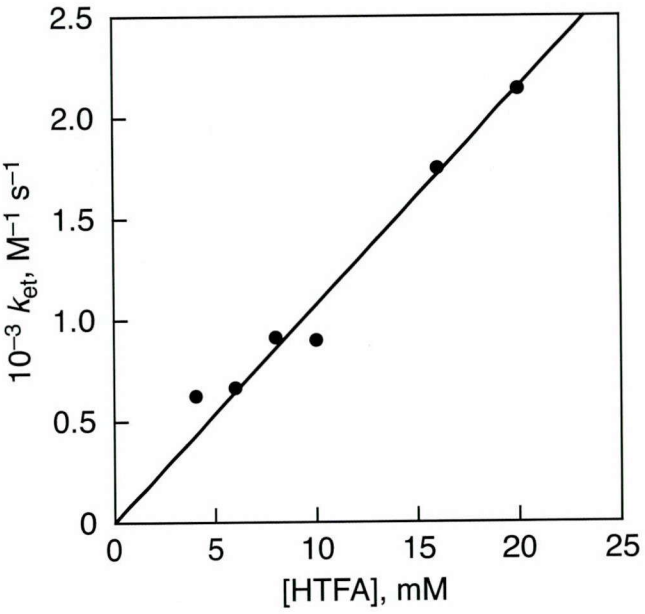

Figure 5. Plot of second-order rate constant (k_{et}) for PCET from Fc to $[Fe^{IV}(O)(N4Py)]^{2+}$ in the presence of various concentrations of HTFA (4.0–20 mM) in deaerated MeCN at 298 K.

The kinetic isotope effect (KIE) value at 298 K was determined to be 0.56 for k_1. Such an inversed KIE indicates that the protonation to form the O–H (or O–D) bond in the $Fe^{IV}(O)$ complex is involved in the rate-determining step of the PCET from Fc to $[Fe^{IV}(O)(N4Py)]^{2+}$, because an inverse KIE results from a larger zero-point energy difference in the transition state relative to the ground state.[24–25] Thus, protonation of $[Fe^{IV}(O)(N4Py)]^{2+}$ occurs concomitantly with ET.

Conclusion

In summary, the rate constants of PCET and MCET reactions of $[Fe^{IV}(O)(N4Py)]^{2+}$ are well correlated with quantitative measure of Lewis acidity of HOTf and metal triflates, which was determined from the fluorescence emission energies of AcrCO in the presence of HOTf and metal triflates as shown in Figure 3. The PCET reactivity decreased with increasing pK_a of Brønsted acids and an inverse kinetic isotope effect in Figure 4 clearly indicate that protonation and ET occur concomitantly in the rate-determining step of the PCET reaction. This study provides quantitative basis to predict the PCET and MCET reactivities.

References

(1) (a) Fukuzumi, S. *Bull. Chem. Soc. Jpn.* **1997**, *70*, 1. (b) Fukuzumi, S.; Itoh, S. *Antioxid. Redox Sign.* **2001**, *3*, 807. (c) Fukuzumi, S. *Pure Appl. Chem.* **2003**, *75*, 577. (*d*) Fukuzumi, S.; *Prog. Inorg. Chem.* **2009**, *56*, 49. (e) Fukuzumi, S. *Chem. Lett.* **2008**, *37*, 808. (f) Fukuzumi, S.; Ohkubo, K. *Coord. Chem. Rev.* **2010**, *254*, 372.

(2) Rosenthal, J.; Hodgkiss, J. M.; Young, E. R.; Nocera, D. G. *J. Am. Chem. Soc.* **2006**, *128*, 10474.

(3) (a) Rosenthal, J.; Nocera, D. G. *Acc. Chem. Res.* **2007**, *40*, 543. (b) Chang, C. J.; Loh, Z.-H.; Shi, C.; Anson, F. C.; Nocera, D. G. *J. Am. Chem. Soc.* **2004**, *126*, 10013. (c) Fukuzumi, S.; Okamoto, K.; Gros, C. P.; Guilard, R. *J. Am. Chem. Soc.* **2004**, *126*, 10441. (d) Halime, Z.; Kotani, H.; Fukuzumi, S.; Karlin, K. D. *Proc. Natl. Acad, Sci. USA*, **2011**, *108*, 13990.

(4) Park, Y. J.; Ziller, J. W.; Borovik, A. S. *J. Am. Chem. Soc.* **2011**, *133*, 9258.

(5) Fukuzumi, S.; Kotani, H. In *Proton-Coupled Electron Transfer*; Formoshinho, S. and Barroso, M., Ed.; RSC Publishing: Cambridge, 2012, p 89

(6) (a) Tan, L.; Zhang, G.; Zhang, D.; Zhu, D. *J. Org. Chem.* **2011**, *76*, 9046. (b) Zeng,

Y.; Zhang, G.; Zhang, D.; Zhu, D. *J. Org. Chem.* **2009**, *74*, 4375. (c) Yang, G.; Zhang, G.; Sheng, P.; Sun, F.; Xu, W.; Zhang, D. *J. Mater. Chem.* **2012**, *22*, 4391. (d) Wu, H.; Zhang, D.; Su, L.; Ohkubo, K.; Zhang, C.; Yin, S.; Mao, L.; Shuai, Z.; Fukuzumi, S.; Zhu, D. *J. Am. Chem. Soc.* **2007**, *129*, 6839.

(7) (a) Fukuzumi, S.; Okamoto, K.; Yoshida, Y.; Imahori, H.; Araki, Y.; Ito, O. *J. Am. Chem. Soc.* **2003**, *125*, 1007. (b) Okamoto, K.; Imahori, H.; Fukuzumi, S. *J. Am. Chem. Soc.* **2003**, *125*, 7014.

(8) (a) Fukuzumi, S.; Ohkubo, K. *Chem.–Eur. J.* **2000**, *6*, 4532. (b) Ohkubo, K.; Menon, S. C.; Orita, A.; Otera, J.; Fukuzumi, S. *J. Org. Chem.* **2003**, *68*, 4720.

(9) For definition and acronyms of PCET see: (a) Costentin, C.; Robert, M.; Savéant, J.-M. *Chem. Rev.* **2010**, *110*, PR1. (b) Hammes-Schiffer, S.; Stuchebrukhov, A. A. *Chem. Rev.* **2010**, *110*, 6369. (c) Cuckier, R. I.; Nocera, D. G. *Annu. Rev. Phys. Chem.* **1998**, *49*, 337. (d) Warren, J. J.; Tronic, T. A.; Mayer, J. M. *Chem. Rev.* **2010**, *110*, 6961. (e) Weinberg, D. R.; Gagliardi, C. J.; Hull, J. F.; Murphy, C. F.; Kent, C. A.; Westlake, B. C.; Paul, A.; Ess, D. H.; McCafferty, D. G.; Meyer, T. J. *Chem. Rev.* **2012**, *112*, 4016.

(10) (a) Fukuzumi, S.; Ohkubo, K.; Morimoto, Y. *Phys. Chem. Chem. Phys.* **2012**, *14*, 8472. (b) Fukuzumi, S. *Coord. Chem. Rev.* DOI: 10.1016/j.ccr.2012.07.021.

(11) (a) *The Photosynthetic Reaction Center*, ed. Deisenhofer, J.; Norris, J. R. Academic Press, San Diego, 1993. (b) *Anoxygenic Photosynthetic Bacteria*, ed. Blankenship, R. E.; Madigan, M. T.; Bauer, C. E. Kluwer Academic Publishing, Dordrecht, 1995. (c) Armstrong, F. A.; Kaim, W.; Schwederski, B. *Bioinorganic Chemistry: Inorganic Chemistry in the Chemistry of Life*, Oxford University, U.K., 1995. (d) Ferguson-Miller, S.; Babcock, G. T. *Chem. Rev.* **1996**, *96*, 2889.

(12) (a) Nagano, S.; Tanaka, M.; Ishimori, K.; Watanabe, Y.; Morishima, I. *Biochemistry* **1996**, *35*, 14251. (b) Mukai, M.; Nagano, S.; Tanaka, M.; Ishimori, K.; Morishima, I.; Ogura, T.; Watanabe. Y.; Kitagawa, T. *J. Am. Chem. Soc.* **1997**, *119*, 1758.

(13) (a) Fukuzumi, S.; Kotani, H.; Lee, Y.-M.; Nam, W. *J. Am. Chem. Soc.* **2008**, *130*, 15134. (b) Fukuzumi, S.; Kotani, H.; Suenobu, T.; Hong, S.; Lee, Y.-M.; Nam, W. *Chem.–Eur. J.* **2010**, *16*, 354. (c) Fukuzumi, S.; Kotani, H.; Prokop, K. A.; Goldberg, D. P. *J. Am. Chem. Soc.* **2011**, *133*, 1859.

(14) Morimoto, Y.; Kotani, H.; Park, J.; Lee, Y.-M.; Nam, W.; Fukuzumi, S. *J. Am. Chem. Soc.* **2011**, *133*, 403.

(15) (a) Fukuzumi, S.; Morimoto, Y.; Kotani, H.; Naumov, P.; Lee, Y.-M.; Nam, W. *Nature Chem.* **2010**, *2*, 756. (b) Park, J.; Morimoto, Y.; Lee, Y.-M.; Nam, W.; Fukuzumi, S. *J. Am. Chem. Soc.* **2011**, *133*, 5236. (c) Park, J.; Morimoto, Y.; Lee,

Y.-M.; Nam, W.; Fukuzumi, S. *Inorg. Chem.* **2011**, *50*, 11612. (d) Park, J.; Morimoto, Y.; Lee, Y.-M.; Nam, W.; Fukuzumi, S. *J. Am. Chem. Soc.* **2012**, *134*, 3903. (e) Morimoto, Y.; Park, J.; Suenobu, T.; Lee, Y.-M.; Nam, W.; Fukuzumi, S. *Inorg. Chem.* **2012**, *51*, 10025.

(16) (a) Wang, D.; Zhang, M.; Bühlmann, P.; Que, L., Jr. *J. Am. Chem. Soc.* **2010**, *132*, 7638. (b) Ohzu, S.; Ishizuka, T.; Hirai, Y.; Jiang, H.; Sakaguchi, M.; Ogura, T.; Fukuzumi, S.; Kojima, T. *Chem. Sci.* **2012**, *3*, 3241.

(17) Fukuzumi, S.; Ohkubo, K. *J. Am. Chem. Soc.* **2002**, *124*, 10270.

(18) Kaizer, J.; Klinker, E. J.; Oh, N. Y.; Rohde, J.-U.; Song, W. J.; Stubna, A.; Kim, J.; Münck, E.; Nam, W.; Que, L., Jr. *J. Am. Chem. Soc.* **2004**, *126*, 472.

(19) $Mg(ClO_4)_2$ was employed instead of $Mg(OTf)_2$ due to the low solubility of triflate salt in MeCN.

(20) Armarego, W. L. F.; Chai, C. L. L. *Purification of Laboratory Chemicals*, 6th ed; Pergamon Press: Oxford, 2009.

(21) Saltzman, H.; Sharefkin, J. G. Ed.; *Organic Syntheses*; Wiley: New York, 1973, Collect. Vol. V, pp. 658.

(22) Lee, Y.-M.; Kotani, H.; Suenobu, T.; Nam, W.; Fukuzumi, S. *J. Am. Chem. Soc.* **2008**, *130*, 434.

(23) (a) Kütt, A.; Rodima, T.; Saame, J.; Raamat, E.; Mäemets, V.; Kaljurand, I.; Koppel, I. A.; Garlyauskayte, R. Y.; Yagupolskii, Y. L.; Yagupolskii, L. M.; Bernhardt, E.; Willner, H.; Leito, I. *J. Org. Chem.* **2011**, *76*, 391. (b) Anne, A.; Morioux, J.; Savéant, J. M. *J. Am. Chem. Soc.* **1993**, *115*, 10224. (c) Kütt, A.; Leito, I.; Kajurand, I.; Sooväli, L.; Vlasov, V. M.; Yagupolskii, L. M.; Koppel, I. A. *J. Org. Chem.* **2006**, *71*, 2829.

(24) (a) Wolfsberg, M. *Acc. Chem. Res.* **1972**, *5*, 225. (b) Parkin, G. *Acc. Chem. Res.* **2009**, *42*, 315.

(25) (a) Tanner, M. J.; Brookhart, M.; DeSimone, J. M. *J. Am. Chem. Soc.* **1997**, *119*, 7617. (b) Kotani, H.; Hanazaki, R.; Ohkubo, K.; Yamada, Y.; Fukuzumi, S. *Chem.–Eur. J.* **2011**, *17*, 2777.

Chapter 5: Effects of Proton Acceptors on Formation of a Non-Heme Iron(IV)-Oxo Complex via Proton-Coupled Electron Transfer

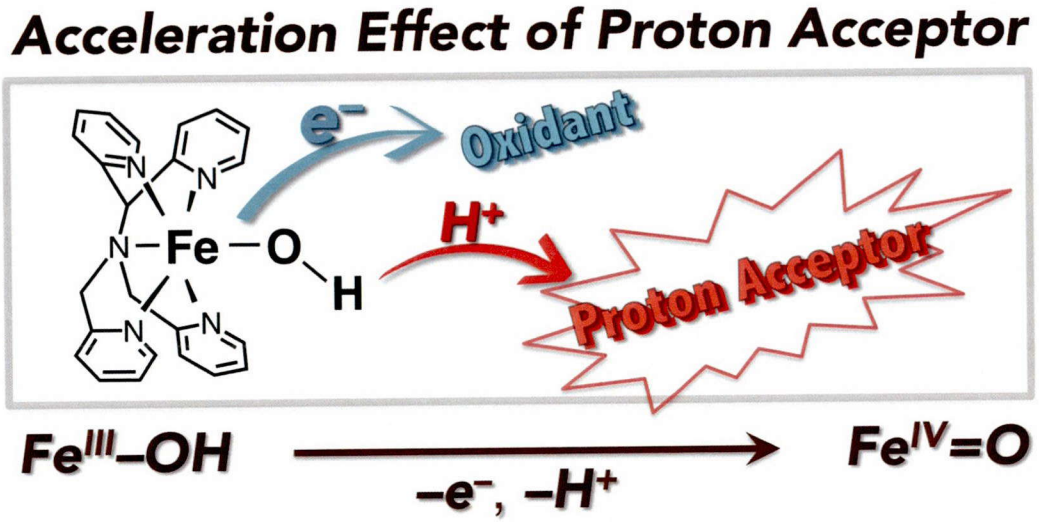

Abstract: The rates of formation of a non-heme iron(IV)-oxo complex, $[Fe^{IV}(O)(N4Py)]^{2+}$ (N4Py = *N*,*N*-bis(2-pyridylmethyl)-*N*-bis(2-pyridyl)methylamine) via the electron-transfer oxidation of $[Fe^{III}(OH)(N4Py)]^{2+}$ in acetonitrile (MeCN) containing H_2O (0.56 M) were accelerated as much as 390-fold by addition of proton acceptors such as CF_3COO^-, TsO^- (p-$MeC_6H_4SO_3^-$), NsO^- (o-$NO_2C_6H_4SO_3^-$), $DNsO^-$ (2,4-$(NO_2)_2C_6H_3SO_3^-$) and TfO^- ($CF_3SO_3^-$). The acceleration effect of proton acceptors increases with increasing basicity of the proton acceptors. The one-electron oxidation potential of $[Fe^{III}(OH)(N4Py)]^{2+}$ was shifted from 1.24 V vs SCE to 0.96 V vs SCE in the presence of TsO^- (10 mM). The electron-transfer oxidation of Fe^{III}–OH complex was coupled with the deprotonation process by proton acceptors in which deuterium kinetic isotope effects were observed when H_2O was replaced by D_2O.

Introduction

High-valent metal-oxo species ($M^{(n+2)+}$=O) have been investigated intensively because of their importance as common reactive species in various kinds of oxidation reactions in chemical and biological redox processes, i.e. hydroxylations, chlorinations and desaturations of aliphatic C–H bonds, epoxidation, sulfoxidation and water oxidation.[1–4] In parallel with studies on the reactivity, the formation processes of $M^{(n+2)+}$=O have also merited special attention.[2–7] Metalloenzymes are known to generate $M^{(n+2)+}$=O under mild conditions. In oxidation by enzymes represented by Cytochrome P450 and taurine/*a*-ketoglutarate dioxygenase (TauD), dioxygen (O_2) is employed as a terminal oxidant as well as an oxygen source, where O_2 is activated through a two-electron reduction and protonations (eq 1):[2,5,6]

$$Fe^{n+} + O_2 + 2e^- + 2H^+ \rightarrow Fe^{(n+2)+}{=}O + H_2O \qquad (1)$$

In contrast to the reductive activation of O_2, the oxygen evolving complex (OEC), consisting of manganese and calcium ions in photosystem II (PSII), employs a different method to produce the manganese(V)-oxo ($Mn^V{\equiv}O$) complex (Scheme 1), which is regarded as the oxidative activation of water responsible for the earth's oxygen and solar energy storage.[7–9]

Scheme 1. Hypothetical Representation of Conversion from the *S3 State to the S4 State in OEC

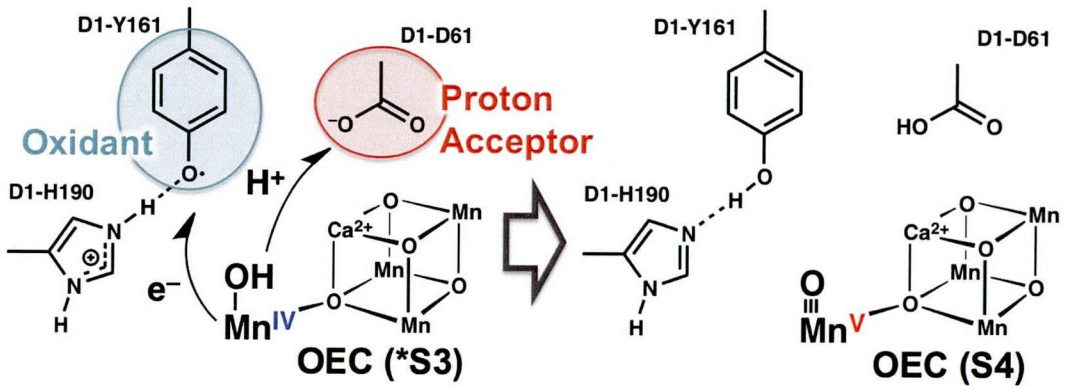

In the OEC, the $Mn^V{\equiv}O$ complex is produced by stepwise one-electron oxidations of the manganese-aqua (Mn^{III}–OH_2) complex (eqs 2 and 3), which are key mechanistic steps prior to O_2 evolution.[7]

Formation of $M^{(n+2)+}$=O through stepwise oxidations of the corresponding low-valent metal-hydroxo or -aqua complex has attracted increasing attention associated with

increasing demand for water-oxidation catalyst.[10] This is also important in the development of environmentally benign oxidation processes.[11–16]

$$Mn^{III}–OH_2 \; - \; e^- \; - \; H^+ \; \rightarrow \; Mn^{IV}–OH \qquad (2)$$

$$Mn^{IV}–OH \; - \; e^- \; - \; H^+ \; \rightarrow \; Mn^{V}\equiv O \qquad (3)$$

With regard to the thermodynamics of formation of $M^{(n+2)+}$=O, the redox potentials between $M^{(n+1)+}$–OH and $M^{(n+2)+}$=O have been shown to be dependent on the pH value of solution.[17] The kinetics as well as the thermodynamics of formation of $M^{(n+2)+}$=O via proton-coupled electron transfer (PCET) may also be affected by the presence of proton acceptors (PA) as seen in PSII, where a conjugate base of asparagine acid helps deprotonation of OEC (Scheme 1).[9] However, to the best of our knowledge, the effects of PA on the kinetics of formation of $M^{(n+2)+}$=O via PCET have yet to be clarified.[18,19]

We report herein remarkable acceleration effects of PA on the rates of formation of a non-heme iron(IV)-oxo complex, $[Fe^{IV}(O)(N4Py)]^{2+}$ (N4Py = *N*,*N*-bis(2-pyridylmethyl)-*N*-bis(2-pyridyl)methylamine) via PCET oxidation of the corresponding iron(III)-hydroxo complex, $[Fe^{III}(OH)(N4Py)]^{2+}$.[20] The detailed study on the kinetics and thermodynamics provides valuable insights into the PCET mechanism.

Results and Discussion

When one equivalent of $[Ru^{III}(bpy)_3]^{3+}$ was added into an MeCN solution of $[Fe^{II}(NCMe)(N4Py)]^{2+}$ (0.50 mM), electron transfer from $[Fe^{II}(NCMe)(N4Py)]^{2+}$ to $[Ru^{III}(bpy)_3]^{3+}$ occurred to produce $[Fe^{III}(NCMe)(N4Py)]^{3+}$ and $[Ru^{II}(bpy)_3]^{2+}$. Then, one volume percent of H_2O (0.56 M) and TsO^- (p-$MeC_6H_4SO_3^-$; 10 mM) were added into the resulting solution. Formation of Fe^{III} species were confirmed by EPR and the signals around g = 4.2 and g = 2.40, 2.17, 1.92 are assigned to $[Fe^{III}(OH)(N4Py)]^{2+}$ (Figure 1).[21] Further addition of another equiv of $[Ru^{III}(bpy)_3]^{3+}$ into the solution gave $[Fe^{IV}(O)(N4Py)]^{2+}$ (86% yields) (Scheme 2) as shown in Figure 2a. In the reaction of $[Fe^{III}(OH)(N4Py)]^{2+}$ with $[Ru^{III}(bpy)_3]^{3+}$, the decay of the absorption band due to $[Ru^{III}(bpy)_3]^{3+}$ coincides with the rise of the absorption band due to $[Fe^{IV}(O)(N4Py)]^{2+}$ (Figure 2b). The formation of the iron(IV)-oxo complex was also confirmed by NMR spectroscopic method (Figure 3). The rise of absorbance at 875 nm due to $[Fe^{IV}(O)(N4Py)]^{2+}$ in the reaction of $[Fe^{III}(OH)(N4Py)]^{2+}$ (0.50 mM) with one equiv of $[Ru^{III}(bpy)_3]^{3+}$ in the presence of large excess of TsO^- (5–20 mM) (Figure 4) obeyed second-order kinetics (see the second-order plot in the inset).

Scheme 2. Formation of $[Fe^{IV}(O)(N4Py)]^{2+}$ via Stepwise Oxidation of $[Fe^{II}(NCMe)(N4Py)]^{2+}$ in the Presence of Water

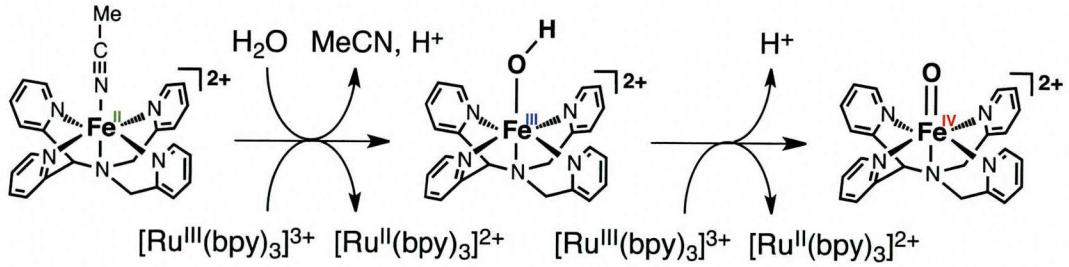

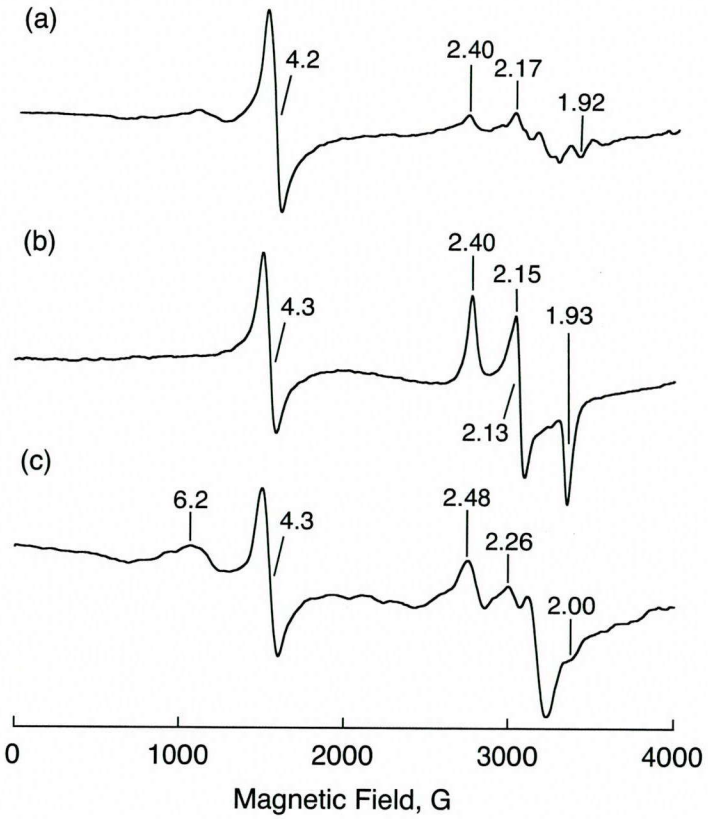

Figure 1. (a) X-band EPR spectrum of a resulting solution of an oxidation of $[Fe^{II}(N4Py)]^{2+}$ (1.0×10^{-3} M) by $[Ru^{III}(bpy)_3]^{3+}$ (1.0×10^{-3} M) in the presence of TsO^- (1.0×10^{-2} M) and H_2O (0.56 M). (b) X-band EPR spectrum of $[Fe^{III}(OH)(N4Py)]^{2+}$ produced by the oxidation of $[Fe^{II}(N4Py)]^{2+}$ (1.25×10^{-3} M) by H_2O_2 (0.62×10^{-3} M) in MeCN at 298 K. (c) X-band EPR spectrum of a resulting solution of an oxidation of $[Fe^{II}(N4Py)]^{2+}$ (1.0×10^{-3} M) by $[Ru^{III}(bpy)_3]^{3+}$ (1.0×10^{-3} M) in the presence of CF_3COO^- (1.0×10^{-2} M) and H_2O (0.56 M) in MeCN at 298 K. Spectra were recorded at 77 K.

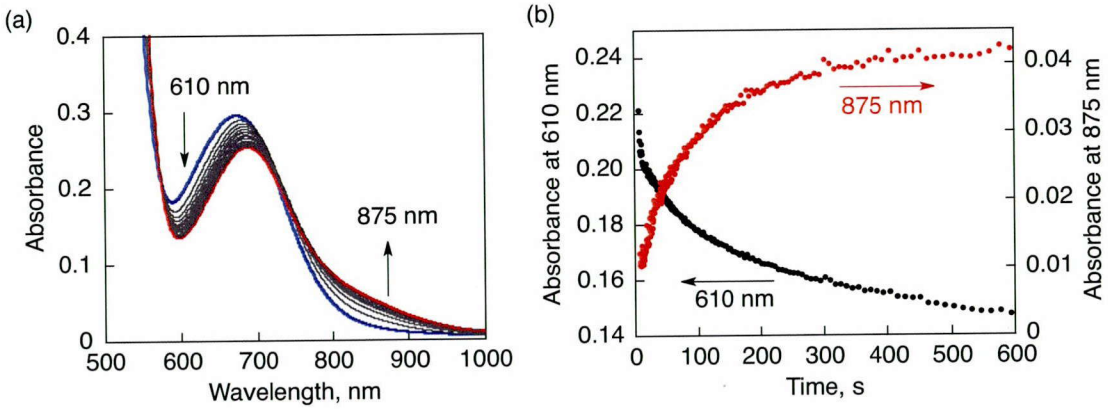

Figure 2. (a) Spectral change observed in PCET oxidation of $[Fe^{III}(OH)(N4Py)]^{2+}$ (0.50 mM) with $[Ru^{III}(bpy)_3]^{3+}$ (0.50 mM) in the presence of TsO^- (p-$MeC_6H_4SO_3^-$) (10 mM) and one volume percent of H_2O (0.56 M) in MeCN at 298 K. (b) Time courses of the spectral changes monitored at 610 nm (black) and 875 nm (red) due to decay of $[Ru^{III}(bpy)_3]^{3+}$ and formation of $[Fe^{IV}(O)(N4Py)]^{2+}$, respectively.

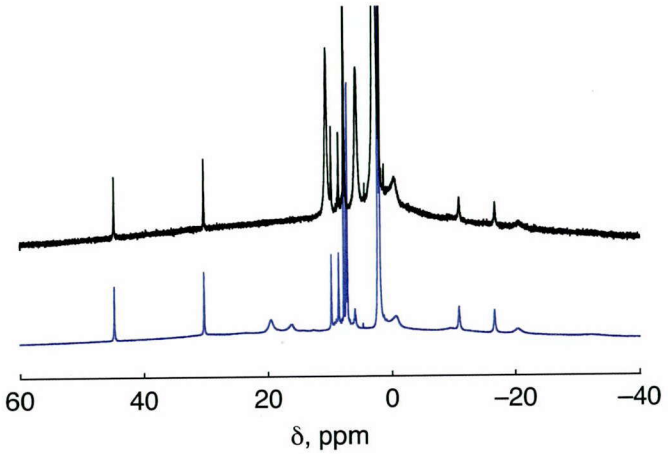

Figure 3. ^{1}H-NMR spectra of $[Fe^{IV}(O)(N4Py)]^{2+}$ produced by PCET oxidation of $[Fe^{III}(OH)(N4Py)]^{2+}$ with $[Ru^{III}(bpy)_3]^{3+}$ in MeCN containing 0.56 M of H_2O and 1.0 × 10^2 mM of TfO^- (black) and the oxidation of $[Fe^{II}(NCMe)(N4Py)]^{2+}$ by 1.2 equiv of PhIO (blue) at 298 K.

The observed second-order rate constant (k_{obs}) increased linearly with increasing concentration of TsO^- (Figure 4b). The kinetic formulation was also confirmed under pseudo-first order conditions of $[Fe^{III}(OH)(N4Py)]^{2+}$ with large excess of $[Ru^{III}(bpy)]^{3+}$ and TsO^- (Figure 5). The k_{obs} value also increased linearly with increasing concentration of H_2O in the absence of an additional PA (Figure 6 and Table 1). This indicates that H_2O acts as not only an oxygen source but also a PA in the formation of $[Fe^{IV}(O)(N4Py)]^{2+}$. Thus, the rate of PCET formation of $[Fe^{IV}(O)(N4Py)]^{2+}$ is given by

eq 4, where $k_{obs} = k_{H2O}[H_2O] + k_{PA}[TsO^-]$; k_{H2O} is the rate constant without proton acceptors (PA) and k_{PA} is the rate constant with PA.

$$d[Fe^{IV}(O)]/dt = (k_{H2O}[H_2O] + k_{PA}[TsO^-])[Fe^{III}(OH)][Ru^{III}] \quad (4)$$

The PCET formation of $[Fe^{IV}(O)(N4Py)]^{2+}$ was also accelerated by other PA [CF_3COO^-, NsO^- (o-O_2N-$C_6H_4SO_3^-$), $DNsO^-$ (2,4-$(O_2N)_2$-$C_6H_3SO_3^-$) and TfO^- ($CF_3SO_3^-$)] (Figures 7 and 8).[22–24] The k_{PA} values were determined for other PA and the results are listed in Table 1 together with the basicity values of the PA employed (K_b).[25]

When H_2O was replaced by D_2O in the PCET formation of $[Fe^{IV}(O)(N4Py)]^{2+}$ in the presence of TsO^-, a deuterium kinetic isotope effect (KIE) was observed as shown in Figure 4b and Figure 9. The reactions in the presence of other PA were also deterred by the replacement of H_2O by D_2O. The KIE values were determined from the comparison of the slope of k_{obs} or pseudo-first-order rate constant (k'_{obs}) dependence on concentration of PA (k_{PA} and $k_{PA,D}$) in the presence of 0.56 M of H_2O and D_2O.

In the presence of 50 mM of CF_3COO^-, which has the largest K_b value among PA examined in this study, the k_{obs} value is 390-fold larger than the value in the absence of CF_3COO^-.[26] In the case of CF_3COO^-, however, plot of k'_{obs} vs $[CF_3COO^-]$ exhibits a saturation behavior (Figure 7).

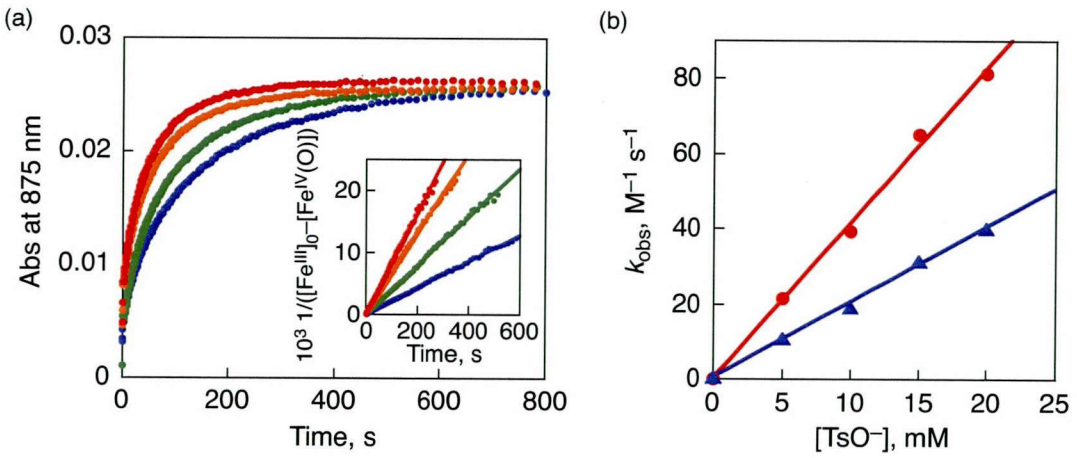

Figure 4. (a) Time profiles of absorption change at 875 nm due to the rise of $[Fe^{IV}(O)(N4Py)]^{2+}$ in ET from $[Fe^{III}(OH)(N4Py)]^{2+}$ (0.50 mM) to $[Ru^{III}(bpy)_3]^{3+}$ (0.50 mM) in the presence of TsO^- (blue: 5 mM, green: 10 mM, orange: 15 mM, red: 20 mM) and 1 volume percent of H_2O (0.56 M) in MeCN at 298 K. Inset: Second-order plots of the time profiles. (b) Plots of pseudo-second order rate constants (k_{obs}) for the reaction of $[Fe^{III}(OH)(N4Py)]^{2+}$ with $[Ru^{III}(bpy)_3]^{3+}$ vs $[TsO^-]$ in the presence of H_2O (0.56 M) (red) or D_2O (0.56 M) (blue).

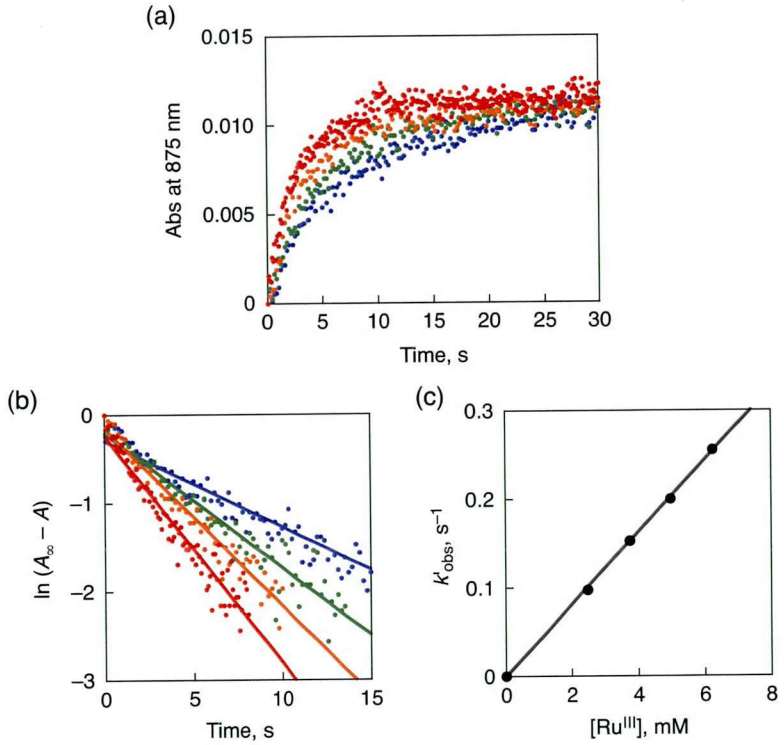

Figure 5. (a) Time courses of spectral changes observed at 875 nm due to formation of $[Fe^{IV}(O)(N4Py)]^{2+}$ by PCET oxidation of $[Fe^{III}(OH)(N4Py)]^{2+}$ (0.25 mM) with $[Ru^{III}(bpy)_3]^{3+}$ (2.5–6.3 mM) in the presence of TsO^- (10 mM) in MeCN containing 0.56 M of H_2O at 298 K. (b) The first-order plots for the absorbance changes. A and A_∞ represent absorbance at 875 nm during the reactions and final absorbance at 875 nm, respectively. (c) Plot of the pseudo-first-order rate constants (k'_{obs}) vs concentration of $[Ru^{III}(bpy)_3]^{3+}$ ($[Ru^{III}]$) (2.5–6.3 mM).

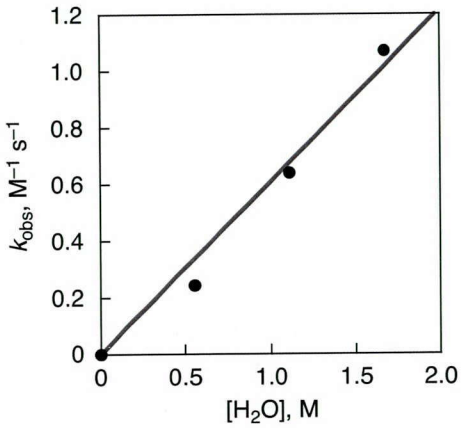

Figure 6. Plot of the pseudo-second-order rate constant (k_{obs}) for formation of $[Fe^{IV}(O)(N4Py)]^{2+}$ by PCET oxidation of $[Fe^{III}(OH)(N4Py)]^{2+}$ (0.50 mM) with $[Ru^{III}(bpy)_3]^{3+}$ (0.50 mM) in the presence of H_2O (0.56–1.68 M) in MeCN at 298 K vs concentration of H_2O.

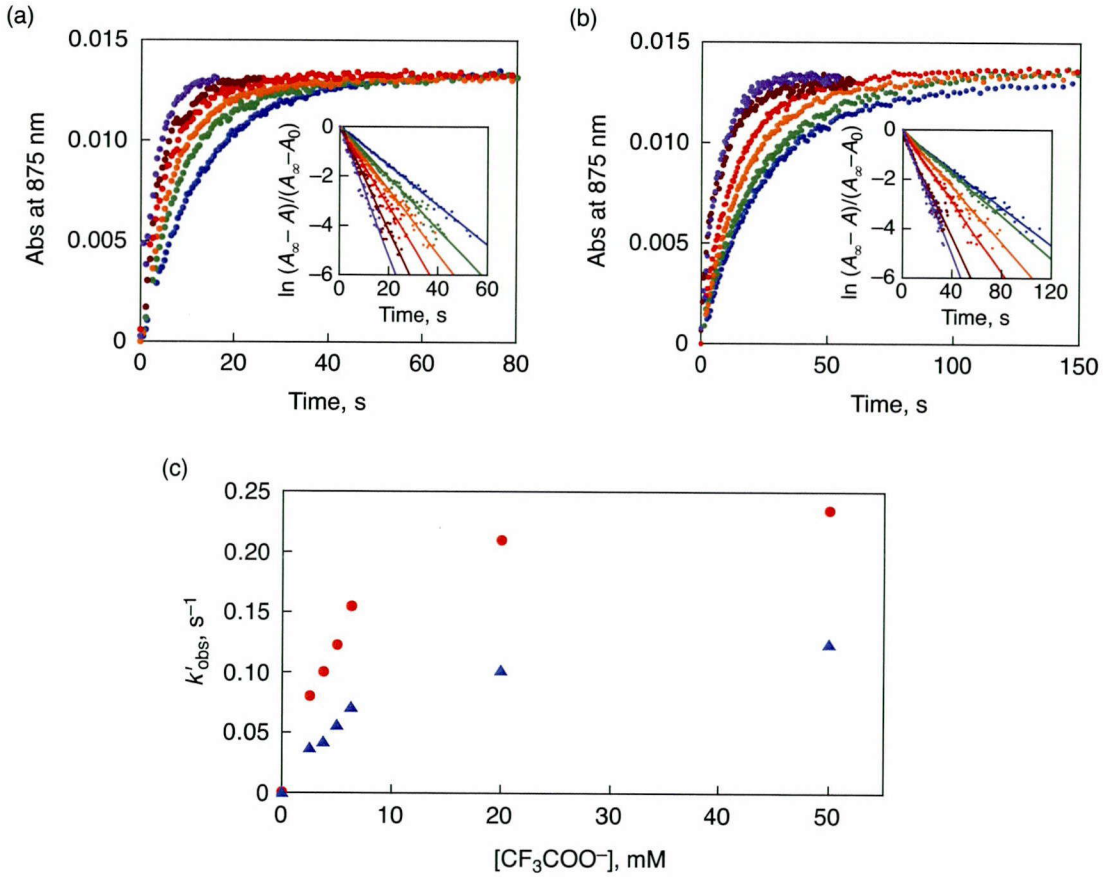

Figure 7. Time courses of absorbance changes at 875 nm due to $[Fe^{IV}(O)(N4Py)]^{2+}$ produced by PCET oxidation of $[Fe^{III}(OH)(N4Py)]^{2+}$ (0.25 mM) with $[Ru^{III}(bpy)_3]^{3+}$ (2.5 mM) in MeCN containing 0.56 M of (a) H_2O and (b) D_2O in the presence of CF_3COO^- (blue, 2.5 mM; green, 3.8 mM; orange, 5.0 mM; red, 6.3 mM; brown, 20 mM; purple, 50 mM) at 298 K, respectively. Insets show the pseudo-first-order plots of the spectral changes in the reaction observed at 875 nm. A_0, A_∞ and A represent initial and final absorbance at 875 nm, and absorbance at 875 nm during the reactions, respectively. (c) Plot of the pseudo-first-order rate constant (k'_{obs}) vs $[CF_3COO^-]$ for the reactions in MeCN containing 0.56 M H_2O (red) and D_2O (blue), respectively.

Such a saturation behavior in Figure 7c may be explained by a change in the rate-determining step from proton transfer from $[Fe^{III}(OH)(N4Py)]^{2+}$ to CF_3COO^- to electron transfer from $[Fe^{III}(O)(N4Py)]^+$, which is produced by deprotonation with a strong base (CF_3COO^-), to $[Ru(bpy)_3]^{3+}$. Alternatively the rate-determining step may be changed to electron transfer from $[Fe^{III}(OH)(N4Py)]^{2+}$ to $[Ru(bpy)_3]^{3+}$, followed by fast depotonation of $[Fe^{IV}(OH)(N4Py)]^{3+}$ with CF_3COO^- at large concentrations. In both cases, the KIE value would be changed to unity at the saturated stage. However, the KIE value remains constant even at the saturated stage in Figure 7c.

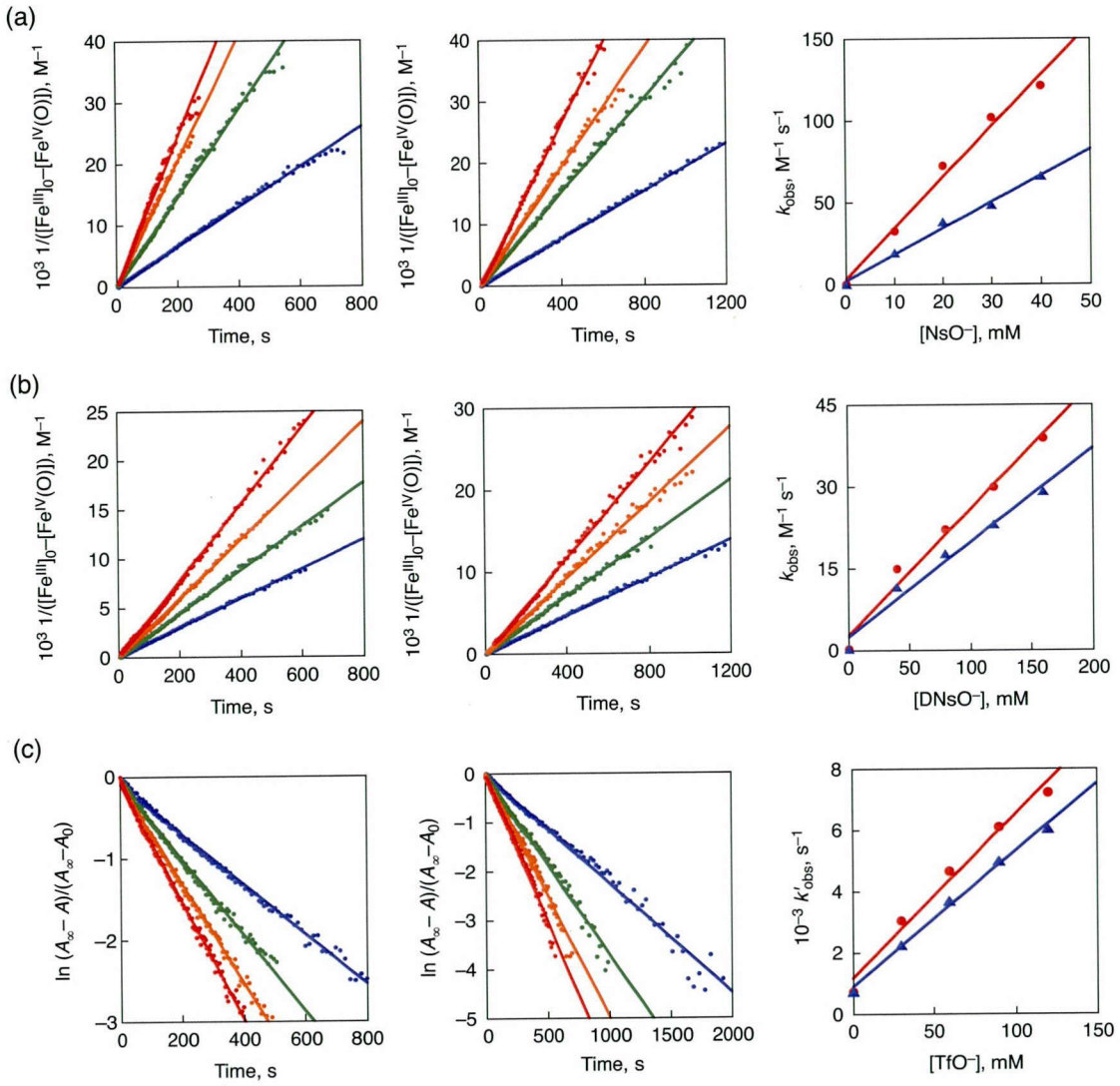

Figure 8. Left and middle panels: second-order plots of time traces of absorption band at 875 nm due to $[Fe^{IV}(O)(N4Py)]^{2+}$ observed in PCET oxidation of $[Fe^{III}(OH)(N4Py)]^{2+}$ (0.25 mM) with $[Ru^{III}(bpy)_3]^{3+}$ (0.25 mM) in the presence of (a) NsO^- (10–40 mM), (b) $DNsO^-$ (40–160 mM); (c) first-order plots of the time traces in PCET oxidation of $[Fe^{III}(OH)(N4Py)]^{2+}$ (0.25 mM) with $[Ru^{III}(bpy)_3]^{3+}$ (2.5 mM) in the presence of TfO^- (30–120 mM) in MeCN containing 0.56 M H_2O (left panels) and D_2O (middle panels) in MeCN at 298 K, respectively. Right panels: dependence of pseudo-second-order rate constant (k_{obs}) for the reactions on (a) [NsO^-] and (b) [$DNsO^-$]; (c) dependence of pseudo-first-order rate constant (k'_{obs}) on [TfO^-] in MeCN containing 0.56 M of H_2O (red) and D_2O (blue).

Thus, the saturation behavior in Figure 7c may result from the binding of CF_3COO^- to the iron(III) species, where the rate-determining step of the reaction is changed to the dissociation of CF_3COO^-.

Table 1. Rate Constants for the PCET Oxidations of $[Fe^{III}(OH)(N4Py)]^{2+}$ by $[Ru^{III}(bpy)_3]^{3+}$ with Various PA

proton acceptor	K_b	k_{PA}, M^{-2} s^{-1}	$k_{PA,D}$, M^{-2} s^{-1}	KIE
CF_3COO^- [a]	7.9×10^{12}	9.6×10^3	4.4×10^3	2.2
TsO^- [b]	4.0×10^8	4.1×10^3	2.0×10^3	2.1
NsO^- [b]	6.3×10^6	3.1×10^3	1.6×10^3	1.9
$DNsO^-$ [c]	1.0×10^3	2.3×10^2	1.7×10^2	1.3
TfO^- [c]	5.0	2.1×10	1.7×10	1.2
H_2O	n.d. [d]	6.1×10^{-1} [e]	n.d. [d]	n.d. [d]

[a,b,c] K_b values in MeCN are taken from refs 22, 23 and 24, respectively. [d] n.d.: Not determined. [e] k_{H2O}.

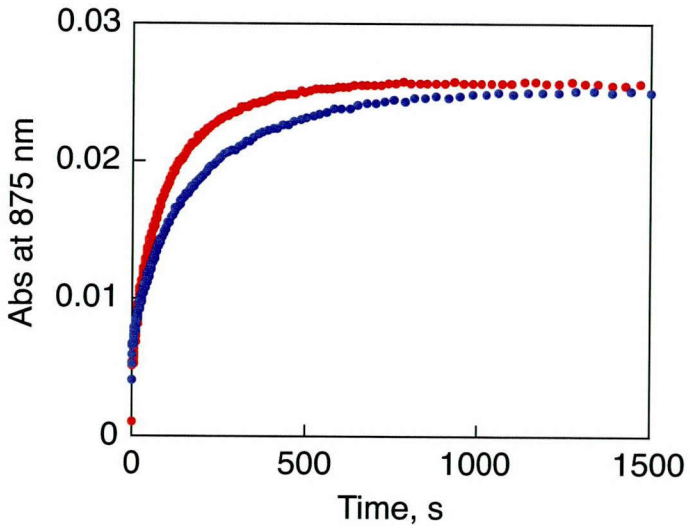

Figure 9. Time profiles of absorption changes observed at 875 nm due to $[Fe^{IV}(O)(N4Py)]^{2+}$ in PCET oxidation of $[Fe^{III}(OH)(N4Py)]^{2+}$ (0.50 mM) with $[Ru^{III}(bpy)_3]^{3+}$ (0.50 mM) in the presence of TsO^- (10 mM) in MeCN containing 0.56 M of H_2O (red) and D_2O (blue) at 298 K.

In fact, the EPR spectrum of the iron(III) complex in the presence of 10 mM of CF_3COO^- showed a different signal from that in the absence of CF_3COO^- (see Figure 1). Because the concentration of $[Fe^{III}(OH)(N4Py)]^{2+}$ ($[Fe^{III}(OH)]$) is equal to $[Fe^{III}(OH)]_0/(1 + K[CF_3COO^-]$, where $[Fe^{III}(OH)]_0$ is the concentration without CF_3COO^- and K is the equilibrium constant of formation of $[Fe^{III}(CF_3COO^-)]$, k'_{obs} is given by eq 5, which agrees with the

$$k'_{obs} = k_{PA}[CF_3COO^-][Ru^{III}]/(1 + K[CF_3COO^-]) \quad (5)$$

experimental observation in Figure 7c. In this case, the k_{PA} value was determined from the slope of plot of k'_{obs} vs [CF_3COO^-] in the range of 0–6 mM, where a linear correlation was maintained.

The k_{PA} value increases with increasing K_b value of the proton acceptors to approach a constant value as shown in Figure 10a, where log k_{PA} values are plotted against log K_b values. The KIE value also increased with an increase in log K_b (Figure 10b).[27] The observation of KIE suggests that the O–H bond cleavage of $[Fe^{III}(OH)(N4Py)]^{2+}$ is involved in the rate-determining step of PCET formation of $[Fe^{IV}(O)(N4Py)]^{2+}$.

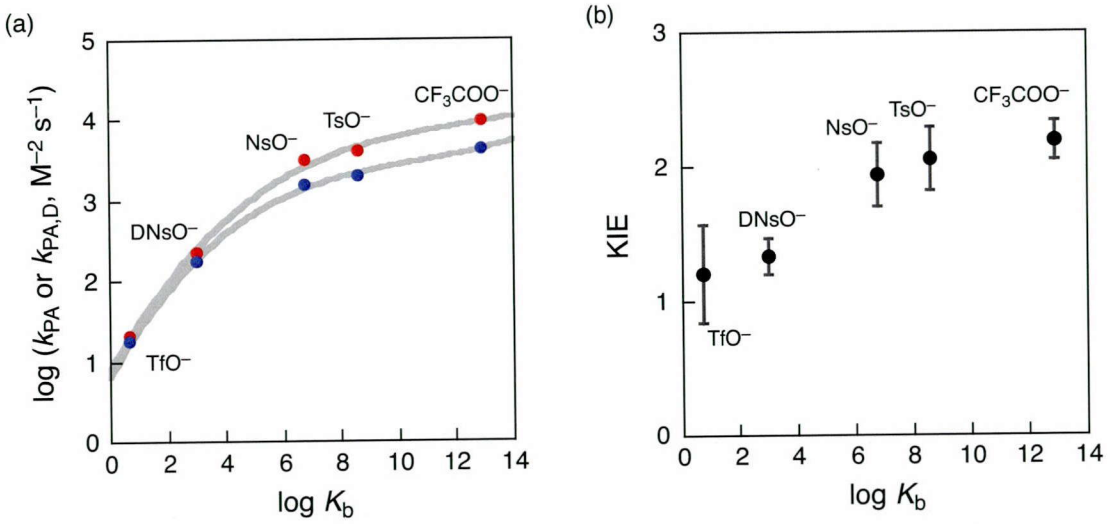

Figure 10. (a) Plot of log k_{PA} and $k_{PA,D}$ for the reaction between $[Fe^{III}(OH)(N4Py)]^{2+}$ and $[Ru^{III}(bpy)_3]^{3+}$ vs log K_b performed in the presence of PA and 0.56 M H_2O (red points) and D_2O (blue points) in MeCN at 298 K. (b) Plots of KIE vs log K_b. The KIE values are determined by dividing k_{PA} by $k_{PA,D}$.

Remarkable acceleration effects of PA on PCET formation of $[Fe^{IV}(O)(N4Py)]^{2+}$ may result from the change in the one-electron oxidation potential (E_{ox}) of $[Fe^{III}(OH)(N4Py)]^{2+}$ in the presence of PA. Thus, we have determined the E_{ox} values of $[Fe^{III}(OH)(N4Py)]^{2+}$ in the absence and presence of TsO^- by spectropotentiometic titration. Figure 11a shows the differential absorption change of $[Fe^{III}(OH)(N4Py)]^{2+}$ solution observed by changing the applied potential. The E_{ox} values in the absence and presence of TsO^- (10 mM) in MeCN containing 0.56 M of H_2O have been determined by fitting the plots of absorbance change at 695 nm (Figure 11b) using the Nernst equation.[28,29]

The best fits of the plots (solid gray lines in Figure 11b) afford the E_{ox} values of 1.24 and 0.96 V vs SCE in the absence and presence of TsO^-, respectively. The E_{ox} value of

$[Fe^{IV}(O)(N4Py)]^{2+}$ in MeCN containing H_2O (0.56 M) without an additional PA is comparable to the reported value by Collins and co-workers in MeCN containing H_2O (1.0 M).[30] The negative shift of 0.28 V in the presence of TsO^- is attributed to stabilization of proton released in the oxidation of $[Fe^{III}(OH)(N4Py)]^{2+}$ by the proton acceptor. The E_{ox} value of $[Fe^{III}(OH)(N4Py)]^{2+}$ (0.96 V vs SCE) in the presence of TsO^- (10 mM) is still more positive than the one-electron reduction potential of $[Fe^{IV}(O)(N4Py)]^{2+}$ in the absence of proton source (E_{red} = 0.51 V vs SCE)[27] because of the protonation of $[Fe^{III}(O)(N4Py)]^{+}$ by TsOH.[31] Such shift of the redox potential by assisting protonation/deprotonation by changing pH values of aqueous solutions have been reported in other systems.[12,16a,17] The PCET formation of $[Fe^{IV}(O)(N4Py)]^{2+}$ becomes thermodynamically more favorable by 0.28 eV in the presence of TsO^- (10 mM), resulting in 160-fold acceleration of the PCET rate.[32]

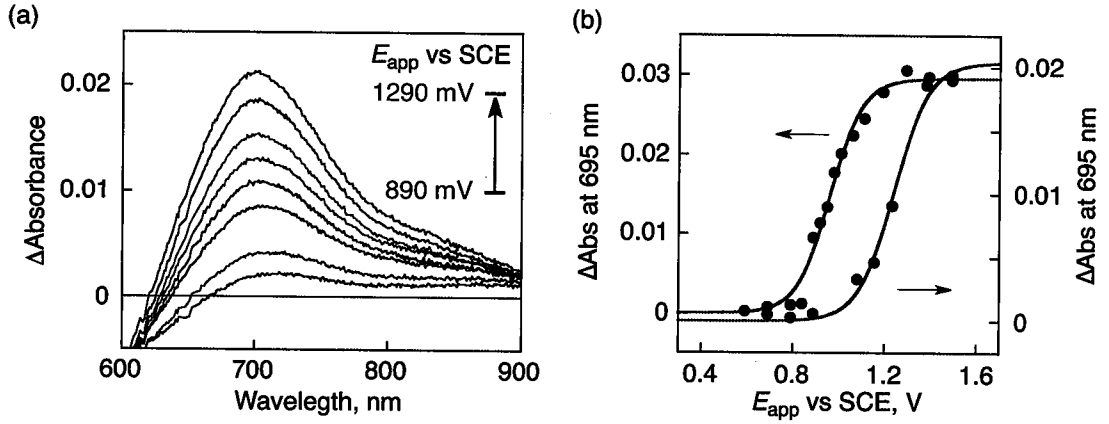

Figure 11. (a) Differential spectral changes of $[Fe^{III}(OH)(N4Py)]^{2+}$ solution (0.20 mM) on applying electric potential (E_{app}) (0.89–1.29 V vs SCE) in the presence of H_2O (0.56 M) and TsO^- (10 mM) in MeCN at 298 K. (b) Plots of differential absorption change vs applied potential in the absence (blue) and presence of TsO^- (red) (10 mM).

The kinetic results obtained in this study provide valuable insights into the mechanism of proton acceptor-enhanced PCET oxidation of $[Fe^{III}(OH)(N4Py)]^{2+}$ with $[Ru^{III}(bpy)_3]^{3+}$ to produce $[Fe^{IV}(O)(N4Py)]^{2+}$ (vide infra). The PCET pathways are generally divided into three cases: (1) an electron transfer followed by a proton transfer (ET/PT), (2) a proton transfer followed by an electron transfer (PT/ET) or (3) a concerted proton-electron transfer (CPET, where the proton moves to the proton acceptor and the electron moves from the iron(III) complex to the ruthenium(III) complex in a single kinetic step) as shown in Scheme 3.[33] If proton transfer from $[Fe^{III}(OH)(N4Py)]^{2+}$ to PA occurred first in the rate-determining step, and that was

followed by fast electron transfer from $[Fe^{III}(O)(N4Py)]^{+}$ to $[Ru^{III}(bpy)_3]^{3+}$ (PT/ET in Scheme 3), the rate of formation $[Fe^{IV}(O)(N4Py)]^{2+}$ would be independent of the concentration of $[Ru^{III}(bpy)_3]^{3+}$. Alternatively if electron transfer from $[Fe^{III}(OH)(N4Py)]^{2+}$ to $[Ru^{III}(bpy)_3]^{3+}$ occurred first in the rate-determining step, and that was followed by fast proton transfer from $[Fe^{IV}(OH)(N4Py)]^{3+}$ to PA (ET/PT in Scheme 3), the rate of formation $[Fe^{IV}(O)(N4Py)]^{2+}$ would be independent of the concentration of PA. Neither case agrees with the experimental observation in eq 4, where the rate is proportional to concentrations of both PA and $[Ru^{III}(bpy)_3]^{3+}$.

The first-order dependences of the rate on concentrations of both $[Ru^{III}(bpy)_3]^{3+}$ and PA together with the observation of KIE's (Figure 10) indicate that both electron transfer and proton transfer are involved in the rate-determining step or the equilibrium. If the initial electron transfer from $[Fe^{III}(OH)(N4Py)]^{2+}$ to $[Ru^{III}(bpy)_3]^{3+}$ is in an uphill equilibrium, followed by deprotonation of $[Fe^{IV}(OH)(N4Py)]^{3+}$, the rate of formation of $[Fe^{IV}(O)(N4Py)]^{2+}$ is given by eq 6,

$$d[Fe^{IV}(O)]/dt = k_{pt1}K_{et}[Fe^{III}(OH)][PA] \quad (6)$$

where k_{pt1} is the rate constant of proton transfer from $[Fe^{IV}(OH)(N4Py)]^{3+}$ to PA and K_{et} is the electron-transfer equilibrium constant between $[Fe^{III}(OH)(N4Py)]^{2+}$ and $[Ru^{III}(bpy)_3]^{3+}$ ($K_{et} = k_{et1}/k_{et-1}$). In such a case, the observed KIE in Figure 10b results from the proton transfer step from $[Fe^{IV}(OH)(N4Py)]^{3+}$ to PA, which must be exergonic to yield $[Fe^{IV}(O)(N4Py)]^{2+}$. Because the KIE of proton-transfer reactions is known to decrease with increasing the driving force in the exergonic region,[34,35] the increasing KIE with increasing log K_b in Figure 10b suggests that the proton-transfer is not the rate-determining step.

Alternatively, if the proton transfer from $[Fe^{III}(OH)(N4Py)]^{2+}$ to PA is an uphill equilibrium, followed by the rate-determining electron transfer from $[Fe^{III}(O)(N4Py)]^{+}$ to $[Ru^{III}(bpy)_3]^{3+}$, the rate of formation of $[Fe^{IV}(O)(N4Py)]^{2+}$ is given by eq 7,

$$d[Fe^{IV}(O)]/dt = k_{et2}K_{pt}[Fe^{III}(OH)][PA] \quad (7)$$

where k_{et2} is the rate constant of electron transfer from $[Fe^{III}(O)(N4Py)]^{+}$ to $[Ru^{III}(bpy)_3]^{3+}$ and K_{pt} is the proton-transfer equilibrium constant between $[Fe^{III}(OH)(N4Py)]^{2+}$ and PA ($K_{pt} = k_{pt2}/k_{pt-2}$). In such a case, the observed KIE in Figure 10b results from the equilibrium deuterium isotope effect in K_{pt}. Typical deuterium isotope effects on the ionization constants of an acid (H^{+}–PA) at 298 K, DpK_a = $pK_a(D^{+}\text{–PA}) - pK_a(H^{+}\text{–PA})$, have been reported to range from $0.2 < DpK_a < 0.7$.[35] This

corresponds to the isotope effects of 1.4–5.0. The observed KIE values in Figure 10b are within this range. The concerted proton and electron transfer (CPET) pathway can also explain the kinetic results in eq 4. In such a case, however, the KIE value would decrease with increasing the driving force of proton transfer in the exergonic region.[36,37] Thus, the uphill proton-transfer equilibrium of $[Fe^{III}(OH)(N4Py)]^{2+}$ and PA followed by the rate-determining electron transfer from $[Fe^{III}(O)(N4Py)]^{+}$ to $[Ru^{III}(bpy)_3]^{3+}$ may be the most likely pathway for the PCET formation of $[Fe^{IV}(O)(N4Py)]^{2+}$ with proton acceptors. In order to clarify the reason of a saturation behavior of log k_{PA} vs log K_b in Figure 10a as well as KIE vs log K_b in Figure 10b, we need to examine and compare the PCET reactions of different Fe^{III}–OH complexes with various one-electron oxidants, which we plan to do in the next step.

Scheme 3. Mechanisms of Formation of $[Fe^{IV}(O)(N4Py)]^{2+}$ via PCET Oxidation of $[Fe^{III}(OH)(N4Py)]^{2+}$

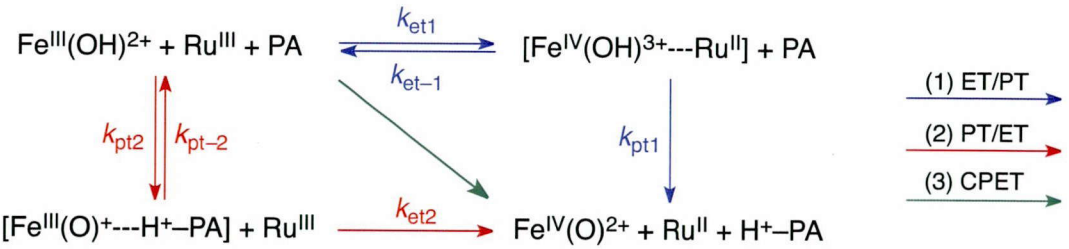

Conclusion

In conclusion, the rate of PCET oxidation of $[Fe^{III}(OH)(N4Py)]^{2+}$ by $[Ru^{III}(bpy)_3]^{3+}$ in MeCN containing water to produce $[Fe^{IV}(O)(N4Py)]^{2+}$ was remarkably accelerated by proton acceptors (PA). The acceleration rate increased with increasing the basicity of PA although the basicity of PA employed in this study is limited because of the instability of the one-electron oxidant, $[Ru^{III}(bpy)_3]^{3+}$ in the presence of a strong base. This study provides new and valuable insights into PCET formation of $M^{(n+2)+}=O$.[38]

Experimental Section

Materials. All solvents and chemicals were of reagent-grade quality, obtained commercially and used without further purification, unless otherwise noted. Acetonitrile (MeCN) was dried according to published procedures and distilled under Ar prior to the use.[39] Tetramethylammonium hydroxide (TMAOH), trifluoroacetic acid (TFA), *p*-toluenesulfonic acid (TsOH), 3-nitrobenzenesulfonic acid (NsOH),

2,4-dinitrobenzenesulfonic acid (DNsOH), and trifluoromethanesulfonic acid (TfOH) were purchased from Tokyo Chemical Industry Co., Ltd. D_2O (99.9% D) was purchased from Cambridge Isotope Laboratories. Hydrogen peroxide (35%) was purchased from KISHIDA CHEMICAL Co., Ltd. They were used without further purification. All PA were prepared by neutralizing above acids with TMAOH in methanol at room temperature. The salts were purified by recrystallization by slow vapor diffusion of diethyl ether into methanol solutions of the salts. $[Fe^{II}(N4Py)(NCMe)](ClO_4)_2$, $[Fe^{III}(OH)(N4Py)]^{2+}$ and $[Fe^{IV}(O)(N4Py)]^{2+}$ were prepared by literature methods.[20,21,41] Iodosylbenzene (PhIO), $[Ru^{II}(bpy)_3](PF_6)_2$ and $[Ru^{III}(bpy)_3](PF_6)_3$ were prepared according to published procedures.[41,42]

Kinetic Measurements. Electron transfer (ET) from $[Fe^{III}(OH)(N4Py)]^{2+}$ to $[Ru^{III}(bpy)_3]^{3+}$ was examined at 298 K using a Hewlett Packard 8453 photodiode-array spectrometer with a quartz cuvette (path length = 1.0 cm) or a UNISOKU RSP-601 stopped-flow spectrometer equipped with a MOS-type highly sensitive photodiode-array. Generally, in the experiments to determine the pseudo-second-order rate constant, $[Fe^{III}(NCMe)(N4Py)]^{2+}$ was produced first by the one-electron oxidation of $[Fe^{II}(NCMe)(N4Py)]^{2+}$ with 1 equiv of $[Ru^{III}(bpy)_3]^{3+}$ in dry MeCN. H_2O (0.56 M) and large excess of PA (TsO^-, NsO^- or $DNsO^-$) were added into the solution to form $[Fe^{III}(OH)(N4Py)]^{2+}$. Then another equiv of $[Ru^{III}(bpy)_3]^{3+}$ added into the solution to start the kinetic measurements. The pseudo-second-order rate constants (k_{obs}) for the ET were determined by the second-order plots of the absorption changes observed at 875 nm due to $[Fe^{IV}(O)(N4Py)]^{2+}$ and the extinction coefficient of the complex at 875 nm (60 M^{-1} cm^{-1}). Kinetic measurements to obtain pseudo-first-order rate constants (k'_{obs}) for the ET reaction were started by the addition of $[Fe^{II}(NCMe)(N4Py)]^{2+}$ into the MeCN solution of 11 equiv of $[Ru^{III}(bpy)_3]^{3+}$ and excess amount of PA and 0.56 M of H_2O. Because the formation of $[Fe^{III}(OH)(N4Py)]^{2+}$ was finished immediately (< 1.0 s), the ET from $[Fe^{III}(OH)(N4Py)]^{2+}$ to $[Ru^{III}(bpy)_3]^{3+}$ proceeded under simple pseudo-first-order reaction conditions. The k'_{obs} values in the absence of PA and in the presence of CF_3COO^-, TsO^- or TfO^- at 298 K were determined by the first-order plots of the spectral changes observed at 875 nm.

EPR Measurements. The resulting solutions of ET from $[Fe^{II}(NCMe)(N4Py)]^{2+}$ (1.0×10^{-3} M) to $[Ru(bpy)_3]^{3+}$ (1.0×10^{-3} M) in the presence of TsO^- (1.0×10^{-2} M), CF_3COO^- (1.0×10^{-2} M) or the oxidation of $[Fe^{II}(NCMe)(N4Py)]^{2+}$ (1.25×10^{-3} M) by half equivs of H_2O_2 in MeCN in quartz EPR tubes (3.0 mm i.d.) were frozen at 77 K after deaeration. The EPR spectra were taken on a JEOL X-band spectrometer

(JES-RE1XE) under nonsaturating microwave power conditions (1.00 mW) operating at 9.2025 GHz. The magnitude of the modulation was chosen to optimize the resolution and the signal to noise ratio (S/N) of the observed spectra (modulation width, 10 G; modulation frequency, 100 kHz). The *g* values were calibrated using an Mn^{2+} marker.

Spectroelectrochemical Experiments. UV–vis spectroelectrochemical experiments were performed with an ALS630B electrochemical analyzer and a Hewlett Packard 8453 photodiode-array spectrometer in MeCN containing 0.10 M Bu_4NPF_6 as a supporting electrolyte at 298 K in a cuvette (path length of 10 mm). A working electrode was 100 ppi porous reticulated vitreous carbon (BAS Inc.) cut to 10 mm × 9 mm × 20 mm so as to fit into the cuvette with electrical contact by means of a Pt wire.[31] Another Pt wire was used as a counter electrode. Potential was applied with respect to an $Ag/AgNO_3$ (10.0 mM) reference electrode. All potentials (vs Ag/Ag^+) were converted to values vs SCE by adding 0.29 V.[43]

^{1}H-NMR Measurement. ^{1}H-NMR spectra were measured after ET oxidation of $[Fe^{III}(OH)(N4Py)]^{2+}$ by $[Ru^{III}(bpy)_3]^{3+}$ in MeCN-d_3 containing D_2O (0.56 M) and of TfO^- (1.0×10^2 mM), or the oxidation of $[Fe^{II}(NCMe)(N4Py)]^{2+}$ by 1.2 equiv of PhIO in MeCN-d_3 (blue) in NMR tubes at 298 K with a JEOL JNM-AL300 (300 MHz) NMR spectrometer.

References

(1) (a) Stewart, R. *Oxidation Mechanisms*; Benjamin: New York, 1964. (b) Mijs, W. J.; De Jonge, C. R. H. I. *Organic Synthesis by Oxidation with Metal Compounds*; Plenum: New York, 1986. (c) Sheldon, R. A.; Kochi, J. K. *Metal-Catalyzed Oxidations of Organic Compounds*; Academic Press: New York, 1981. (d) Nugent, W. A.; Mayer, J. M. *Metal–Ligand Multiple Bonds*; Wiley: New York, 1988. (e) Meunier, B. *Biomimetic Oxidations Catalyzed by Transition Metal Complexes*; Imperial College Press: London, 1998. (f) Punniyamurthy, T.; Velusamy, S.; Iqbal, J. *Chem. Rev.* **2005**, *105*, 2329.

(2) (a) Sono, M.; Roach, M. P.; Coulter, E. D.; Dawson, J. H. *Chem. Rev.* **1996**, *96*, 2841. (b) Harris, D. L.; Loew, G. H. *J. Am. Chem. Soc.* **1998**, *120*, 8941. (c) P. R. Ortiz de Montellano, *Cytochrome P450: Structure, Mechanism, and Biochemistry*, 3rd ed.; Kluwer Academic/Plenum: New York, 2004. (d) Meunier, B.; de Visser, S. P.; Shaik, S. *Chem. Rev.* **2004**, *104*, 3947. (e) Denisov, I. G.; Makris, T. M.; Sligar, S. G.; Schlichting, I. *Chem. Rev.* **2005**, *105*, 2253.

(3) (a) Holm, R. H. *Chem. Rev.* **1987**, *87*, 1401. (b) Shilov, A. E.; Shul'pin, G. B. *Chem. Rev.* **1997**, *97*, 2879. (c) Balcells, D.; Clot, E.; Eisenstein, O. *Chem. Rev.* **2010**, *110*, 749. (d) Gunay, A.; Theopold, K. H. *Chem. Rev.* **2010**, *110*, 1060.

(4) Meunier, B., Ed. *Metal-Oxo and Metal-Peroxo Species in Catalytic Oxidations*; Springer-Verlag: Berlin, 2000.

(5) J. A. Kovacs, *Science* **2009**, *299*, 1024.

(6) (a) Krebs, C.; Fujimori, D. G.; Walsh, C. T.; Bollinger, J. M., Jr. *Acc. Chem. Res.* **2007**, *40*, 484. (b) Kovaleva, E. G.; Lipscomb, J. D. *Nat. Chem. Biol.* **2008**, *3*, 186.

(7) McEvoy, J. P.; Brudvig, G. W. *Chem. Rev.* **2006**, *106*, 4455.

(8) OEC Architecture of the Photosynthetic Oxygen-Evolving Center; see: (a) Ferreira, K. N.; Iverson, T. M.; Maghlaoui, K.; Barber, J.; Iwata, S. *Science* **2004**, *303*, 1831. (b) Loll, B.; Kern, J.; Saenger, W.; Zouni, A.; Biesiadka. J. *Nature* **2005**, *438*, 1040. (c) Umena, Y.; Kawakami, K.; Shen, J.-R.; Kamiya, N. *Nature* **2011**, *473*, 55.

(9) For recent study to assign the primal proton acceptor in a bucket-brigade-type mechanism of proton transfer from OEC to outside of lumen as carboxylate anion form of D1-Asp-61, see: Siegbahn, P. E. M. *Phys. Chem. Chem. Phys.* **2012**, *14*, 4849.

(10) Lewis, N. S.; Nocera, D. G. *Prog. Natl. Acad. Sci. U.S.A.* **2006**, *103*, 15729.

(11) Fukuzumi, S.; Kishi, T.; Kotani, H.; Lee, Y.-M.; Nam, W. *Nature Chem.* **2011**, *3*, 38.

(12) Ohzu, S.; Ishizuka, T.; Hirai, Y.; Jiang, H.; Sakaguchi, M; Ogura, T.; Fukuzumi S.; Kojima, T. *Chem. Sci.* **2012**, *3*, 3241.

(13) Che, C.-M.; Yam, V. W.-W.; Mak, T. C. W. *J. Am. Chem. Soc.* **1990**, *112*, 2284.

(14) Low, D. W.; Winkler, J. R.; Gray, H. B. *J. Am. Chem. Soc.* **1996**, *118*, 117.

(15) Kotani, H; Suenobu, T.; Lee, Y.-M.; Nam, W.; Fukuzumi, S. *J. Am. Chem. Soc.* **2011**, *133*, 3249.

(16) (a) Hirai, Y.; Kojima, T.; Mizutani, Y.; Shiota, Y.; Yoshizawa, K.; Fukuzumi, S. *Angew. Chem., Int. Ed.* **2008**, *47*, 5772. (b) Lee, Y.-M.; Dhuri, S. N.; Sawant, S. C.; Cho, J.; Kubo, M.; Ogura, T.; Fukuzumi, S.; Nam, W. *Angew. Chem., Int. Ed.* **2009**, *48*, 1803.

(17) Huynh, M. H. V.; Meyer, T. J. *Chem. Rev.* **2007**, *107*, 5004.

(18) For detailed kinetic analysis of PCET of phenol derivatives or a cobalt cluster; see: (a) Sjödin, M.; Styring, S.; Wolpher, H.; Xu, Y.; Sun, L.; Hammarström, L. *J. Am. Chem. Soc.* **2005**, *127*, 3855. (b) Markle, T. F.; Rhile, I. J.; Mayer, J. M. *J.*

Am. Chem. Soc. **2011**, *133*, 17341. (c) Symes, M. D.; Surendranath, Y.; Lutterman, D. A.; Nocera, D. G. *J. Am. Chem. Soc.* **2011**, *133*, 5174.

(19) PCET formation of $[Fe^{IV}(O)(N4Py)]^{2+}$ in a mixed solvent of acetonitrile and acetate buffer solution (pH 5.0) was previously reported in ref 15.

(20) Kaizer, J.; Klinker, E. J.; Oh, N. Y.; Rohde, J.-U.; Song, W. J.; Stubna, A.; Kim, J.; Münck, E.; Nam, W.; Que, L., Jr. *J. Am. Chem. Soc.* **2004**, *126,* 472.

(21) Roelfes, G.; Lubben, M.; Chen, K.; Ho, R. Y. N.; Meetsma, A.; Genseberger, S.; Hermant, R. M.; Hage, R.; Mandal, S. K.; Young, V. G.; Zang, Y.; Kooijman, H.; Spek, A. L.; Que, L., Jr.; Feringa, B. L. *Inorg. Chem.* **1999**, *38*, 1929.

(22) p*K*a for CF_3COOH; see: Anne, A.; Morioux, J.; Savéant, J. M. *J. Am. Chem. Soc.* **1993**, *115*, 10224.

(23) p*K*a for TsOH and NsOH; see: Kütt, A.; Leito, I.; Kajurand, I.; Sooväli, L.; Vlasov, V. M.; Yagupolskii, L. M.; Koppel, I. A. *J. Org. Chem.* **2006**, *71*, 2829.

(24) p*K*a for DNsOH and TfOH; see: Kütt, A.; Rodima, T.; Saame, J.; Raamat, E.; Mäemets, V.; Kaljurand, I.; Koppel, A.; Garlyauskayte, R. Y.; Yagupolskii, Y. L.; Yagupolskii, L. M.; Bernhardt, E.; Willner, H.; Leito, I. *J. Org. Chem.* **2011**, *76*, 391.

(25) $[Ru^{III}(bpy)]^{3+}$ was not stable in the presence of stronger base than CF_3COO^-, e.g., CH_3COO^-.

(26) The reliable acidity of Brønsted acids in MeCN has been reported in refs 22–24. Because we used anions of relatively strong acids, the effect of water molecules is expected to be much smaller as compared with anions of weak acids. Thus, the reported K_b (or K_a) values in MeCN are accurate enough to discuss the dependence of k_{PA} on K_b of different anions of strong acids.

(27) For the dependence of KIE value on pK_b value of proton acceptor; see: Dixon, J. E.; Bruice, T. C. *J. Am. Chem. Soc.* **1970**, *92*, 905.

(28) Lee, Y.-M.; Kotani, H.; Suenobu, T.; Nam, W.; Fukuzumi, S. *J. Am. Chem. Soc.* **2008**, *130*, 434.

(29) Because the spectral change observed in Figure 6a was not completely reversible, the $E_{1/2}$ values in Figure 6b should be regarded as the apparent E_{ox} values under the present electrochemical oxidation conditions.

(30) Collins, M. J.; Ray, K.; Que, L., Jr. *Inorg. Chem.* **2006**, *45*, 8009.

(31) Wang, D.; Zang, M.; Bühlmann, P.; Que, L., Jr. *J. Am. Chem. Soc.* **2010**, *132*, 7638.

(32) In this case, about 46% of the free energy change is reflected in the activation free energy, because 160-fold acceleration of the PCET rate corresponds to 0.13 eV in terms of activation free energy.

(33) Warren, J. J.; Tronic, T. A.; Mayer, J. M. *Chem. Rev.* **2010**, *110*, 6961.

(34) Fukuzumi, S.; Koumitsu, S.; Hironaka, K.; Tanaka, T. *J. Am. Chem. Soc.* **1987**, *109*, 305.

(35) Cohen, A. O.; Marcus, R. A. *J. Phys. Chem.* **1968**, *72*, 4249.

(36) (a) Erickson, K. M.; Arcis, H.; Raffa, D.; Zimmerman, G. H.; Tremaine, P. R. *J. Phys. Chem. B* **2011**, *115*, 3038. (b) Jancso, G.; Van Hook, W. A. *Chem. Rev.* **1974**, *74*, 689.

(37) (a) Pryor, W. A.; Kneipp, K. G. *J. Am. Chem. Soc.* **1971**, *93*, 5584. (b) Ishikawa, M.; Fukuzumi, S. *J. Chem. Soc., Faraday Trans.* **1990**, *86*, 3531.

(38) For oxidation of Mn^{IV}–OH to form $Mn^{V}\equiv O$ in OEC, which is thought to proceed via PT/ET, see: Haumann, M.; Liebisch, P.; Müller, C.; Barra, M.; Grabolle, M.; Dau, H. *Science* **2005**, *310*, 1019.

(39) Armarego, W. L. F.; Chai, C. L. L. *Purification of Laboratory Chemicals,* 6th ed.; Pergamon Press: Oxford, 2009.

(40) Lubben, M.; Meetsma, A.; Wilkinson, E. C.; Feringa, B.; Que, L., Jr. *Angew. Chem., Int. Ed. Engl.* **1995**, *34*, 1512.

(41) DeSimone, R. E.; Drago, R. S. *J. Am. Chem. Soc.* **1970**, *92*, 2343.

(42) Saltzman, H.; Sharefkin, J. G. *Organic Syntheses*; Collect. Vol. V; Wiley: New York, 1973, p 658.

(43) Mann, C. K.; Barnes, K. K. *Electrochemical Reactions in Non-aqueous Systems*; Mercel Dekker: New York, 1970.

Chapter 6: Dioxygen Activation by a Non-Heme Iron(II) Complex: Formation of an Iron(IV)–Oxo Complex via C–H Activation by a Putative Iron(III)–Superoxo Species

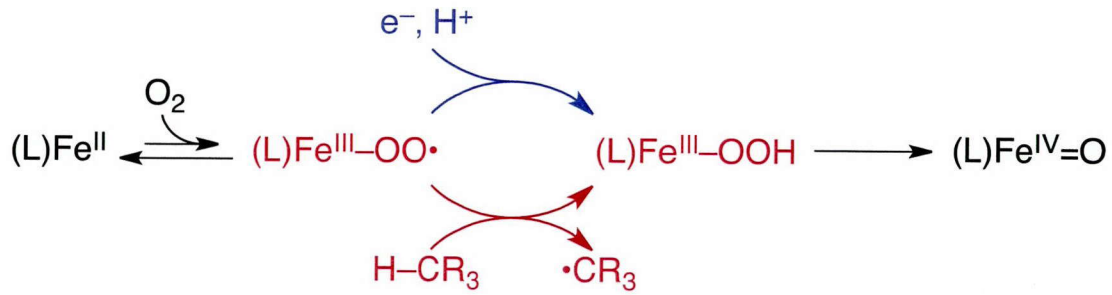

Abstract: Iron(III)-superoxo intermediates are believed to play key roles in oxygenation reactions by non-heme iron enzymes. We now report that a non-heme iron(II) complex activates O_2 and generates its corresponding iron(IV)-oxo complex in the presence of substrates with weak C–H bonds (e.g., olefins and alkylaromatic compounds). We propose that a putative iron(III)-superoxo intermediate initiates the O_2-activation chemistry by abstracting a H atom from the substrate, with subsequent generation of a high-valent iron(IV)-oxo intermediate from the resulting iron(III)-hydroperoxo species.

Introduction

The nature of metal-oxygen intermediates involved in the catalytic cycles of dioxygen activation by oxygenase enzymes has been intensively investigated over the past several decades.[1] Among the metal-oxygen intermediates, such as metal-superoxo, -peroxo, -hydroperoxo, and -oxo, metal-superoxo species have attracted much attention recently, as iron(III)- and cupper(II)-superoxo intermediates have been invoked as active oxidants in H-atom abstraction reactions by non-heme iron and copper enzymes, respectively.[2,3] In biomimetic models, synthetic Cu(II)-superoxo complexes have shown reactivities in the oxidation of ligand C–H bonds and weak O–H bonds of substrates,[4] but iron(III)-superoxo species have rarely been explored in H-atom abstraction reactions.[5]

In non-heme iron models, the formation of iron(III)-hydroperoxo and iron(IV)-oxo species has recently been demonstrated in the reactions of iron(II) complexes and O_2 in the presence of electron and proton donors (Scheme 1, pathway A).[6] In accord with the cytochrome P450 paradigm,[7] the electron and proton donors, respectively, were proposed to reduce an iron(III)-superoxo species to an iron(III)-peroxo intermediate and subsequently generate an iron(III)-hydroperoxo species by the protonation of the iron(III)-peroxo intermediate.[6] In another case, the reaction of $[Fe^{II}(TMC)]^{2+}$ (**1**) (TMC = 1,4,8,11-tetramethyl-1,4,8,11-tetraazacyclotetradecane) with O_2 generated $[Fe^{IV}(O)(TMC)]^{2+}$ (**2**) in MeCN/alcohol or MeCN/ether solvent mixtures,[8] but the reaction mechanism was not well established. Herein, we report that **1** activates O_2 in the presence of olefins (i.e., as an H-atom donor), thereby generating **2** via H-atom abstraction by a putative iron(III)-superoxo species (Scheme 1, pathway B).

Scheme 1. Formation of Iron(IV)-Oxo Complex by Oxidation of Iron(II) Complex with Oxygen in the Plesence of Source of Electron and Proton

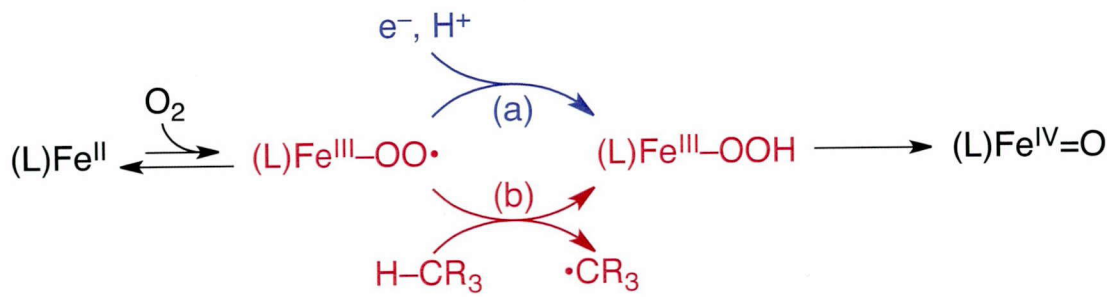

Experimental Section

Materials. Commercially available chemicals were used without further purification unless otherwise indicated. Solvents were dried according to published procedures and distilled under Ar prior to use.[9] Cyclohexene, cycloheptene, and cyclooctene were purchased from Aldrich Chemical Co. Cyclohexene-d_{10} was purchased from CDN Isotopes Inc. Olefins were refluxed and distilled under Ar, and filtered through a column of silica gel 60 and then filtered again through a column of active alumina prior to use.[9] $^{18}O_2$ (80% ^{18}O-enriched) was purchased from ICON Services Inc. (Summit, NJ, USA). TMC ligand was purchased from Aldrich Chemical Co. Iron(II) complex, $[Fe^{II}(TMC)(NCMe)_2](CF_3SO_3)_2$, was prepared by literature methods.[10]

Instrumentation. UV–vis spectra were recorded on a Hewlett Packard Agilent 8453 UV–visible spectrophotometer equipped with a circulating water bath or an UNISOKU cryostat system (USP-203; UNISOKU, Japan). Electrospray ionization mass spectra (ESI-MS) were collected on a Thermo Finnigan (San Jose, CA, USA) LCQTM Advantage MAX quadrupole ion trap instrument, by infusing samples directly into the source at 20 μL min^{-1} using a syringe pump. The spray voltage was set at 4.7 kV and the capillary temperature at 10°C. An ESI-MS sample of $[Fe^{IV}(O)(TMC)]^{2+}$ intermediate was generated in the reaction of $[Fe^{II}(TMC)(NCMe)_2](CF_3SO_3)_2$ (5.0×10^{-4} M) with cyclohexene (2.5×10^{-2} M) under air atmosphere in MeCN at 25°C. CW-EPR spectra were taken at 5 K using a X-band Bruker EMX-plus spectrometer equipped with a dual mode cavity (ER 4116DM). Low temperatures were achieved and controlled with an Oxford Instruments ESR900 liquid He quartz cryostat with an Oxford Instruments ITC503 temperature and gas flow controller. The experimental parameters for EPR spectra were as follows: Microwave frequency = 9.646 GHz, microwave power = 1 mW, modulation amplitude = 10 G, gain = 1×10^4, modulation frequency = 100 kHz, time constant = 40.96 ms and conversion time = 85.00 ms. Product analysis was performed with an Agilent Technologies 6890N gas chromatograph (GC) and Thermo Finnigan (Austin, Texas, USA) FOCUS DSQ (dual stage quadrupole) mass spectrometer interfaced with Finnigan FOCUS gas chromatograph (GC-MS). ^1H NMR spectra were measured with Bruker model digital AVANCE III 400 FT-NMR spectrometer. Quantitative analyses were made on the basis of comparison of NMR peak integration between products and authentic samples.

Kinetic Studies and Product Analysis. All reactions were followed by monitoring UV–vis spectral changes of reaction solutions with a Hewlett Packard 8453

spectrophotometer. Dioxygen activation by a nonheme iron(II) complex, $[Fe^{II}(TMC)]^{2+}$ (5.0×10^{-4} M), was examined with appropriate amounts of olefins (1.5×10^{-2}–1.0×10^{-1} M), by monitoring spectral changes in air-saturated MeCN at the given temperatures. Pseudo-first-order fitting of the kinetic data allowed the author to determine k_{obs} values for the formation of **2**. Reactions were run at least in triplicate, and the data reported represent the average of these reactions.

Products formed in the reaction of **1** and O_2 in the presence of olefins under air were analyzed by ^{1}H NMR spectroscopy. Quantitative analysis was done by comparing ^{1}H NMR peak areas of products with those of authentic samples. Four products, 2-cyclohexen-1-ol, 2-cyclohexen-1-one, 1,3-cyclohexadiene and benzene, were formed with the yields of 26(3)%, 21(2)%, 9(2)% and 5(2)%, respectively, in the reaction of cyclohexene. Products were also analyzed by GC and GC-MS. Products were identified by comparing with authentic samples, and product yields were determined by comparison against standard curves prepared with authentic samples and using decane as an internal standard. The ^{18}O-labeled experiment was performed with $^{18}O_2$ in a manner similar to that described above. The ^{16}O and ^{18}O compositions in allylic oxidation products were analyzed by GC-MS, by comparing the relative abundances of m/z = 83 and 98 for unlabeled 2-cyclohexen-1-ol and m/z = 85 and 100 for ^{18}O-labeled 2-cyclohexen-1-ol and m/z = 68 and 96 for unlabeled 2-cyclohexen-1-one and m/z = 68 and 96 for ^{18}O-labeled 2-cyclohexen-1-one.

Results and Discussion

As reported previously,[6b,8] **1** is air-stable in MeCN at 25°C (Scheme 2, pathway A). Interestingly, addition of olefins, such as cyclohexene, cycloheptene, and cyclooctene, to the solution of **1** gave a green intermediate within 1 min (Scheme 2, pathway B).[11] By UV–vis and ESI-MS analysis of the green intermediate (left panel of Figure 1a for UV–vis spectral changes; Figure 2 for ESI-MS), we confirmed the formation of **2** with a yield of >90% as determined from the absorbance at 820 nm (ε = 400 M^{-1} cm^{-1}).[10] In this reaction, the formation of **2** was observed because of the low reactivity of **2** toward olefins at 25°C. Pseudo-first-order fitting of the kinetic data allowed us to determine k_{obs} values (Figure 1a, right panel), and the first-order rate constants increased proportionally with the concentration of substrate (see the k_2 values in the Figure 1b caption).[12] The second-order rate constants were correlated with the C–H bond dissociation energies (BDEs) of the olefins;[13] the formation of **2** was faster with olefins having lower BDEs (Figure 1c).[14] In addition, through the use of deuterated cyclohexene as a substrate, a kinetic isotope effect (KIE) value of 6.3(3) in the

formation of **2** was obtained [Figure 1b; compare the plots for cyclohexene (black line) and cyclohexene-d_{10} (red line)].[15]

The reaction rates were also dependent on the reaction temperature; linear Eyring plots between 20 and 35°C were obtained, from which the activation parameters $\Delta H^{\ddagger}$ and $\Delta S^{\ddagger}$ were calculated (see Figures 3 and 4). *The large KIE value, with the dependence of the rate constants on the allylic C–H BDE of the olefin, indicates that C–H bond activation of the olefin is the rate-determining step for the formation of* ***2*** (see below).

Scheme 2. Formation of $[Fe^{IV}(O)(TMC)]^{2+}$ via Oxidation of $[Fe^{II}(O)(TMC)]^{2+}$ with Oxygen in the Presence of Cyclohexene

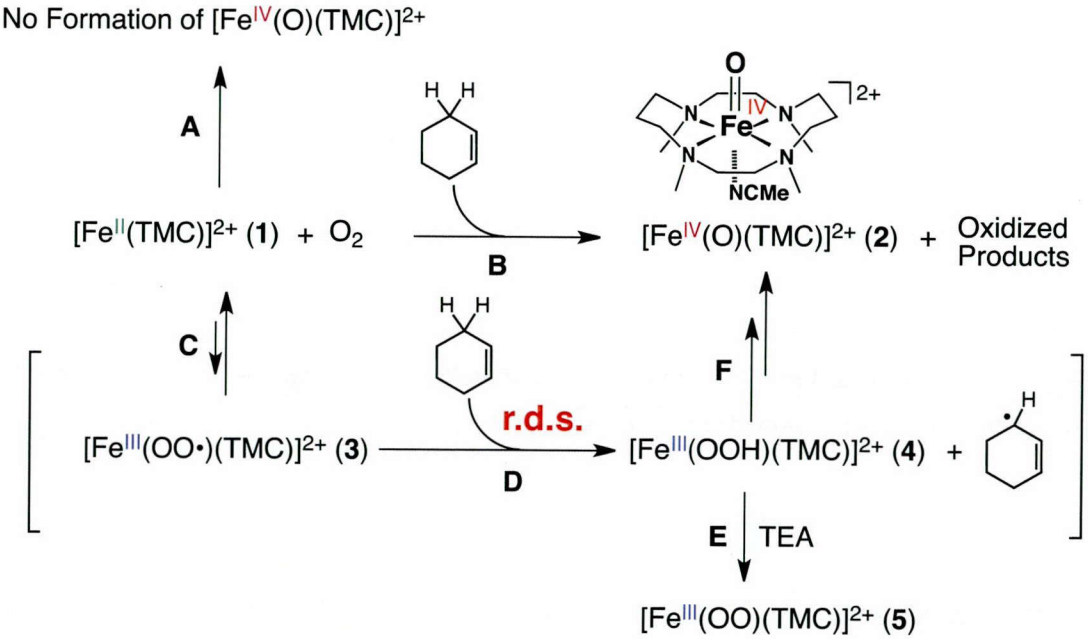

Product analysis of the reaction solutions was carried out using ^{1}H NMR spectroscopy, GC, and GC–MS after the complete formation of **2**. In the reaction of **1** and O_2 in the presence of cyclohexene, allylic oxidation products (i.e., 2-cyclohexen-1-ol and 2-cyclohexen-1-one) together with dehydrogenation products (i.e., 1,3-cyclohexadiene and benzene) were obtained, and the product yields were 26(4)% for 2-cyclohexen-1-ol, 21(3)% for 2-cyclohexen-1-one, 9(2)% for 1,3-cyclohexadiene, and 5(2)% for benzene (Figure 5). The reaction rates were also dependent on the reaction temperature; linear Eyring plots between 20 and 35°C were obtained, from which the activation parameters $\Delta H^{\ddagger}$ and $\Delta S^{\ddagger}$ were calculated (Figures 3 and 4). In addition, the source of oxygen in the allylic oxidation products was determined to be dioxygen on the basis of an ^{18}O-labeling experiment with $^{18}O_2$ (Figures 2b and 6 for ESI-MS of [^{18}O] **2** and product analysis, respectively).

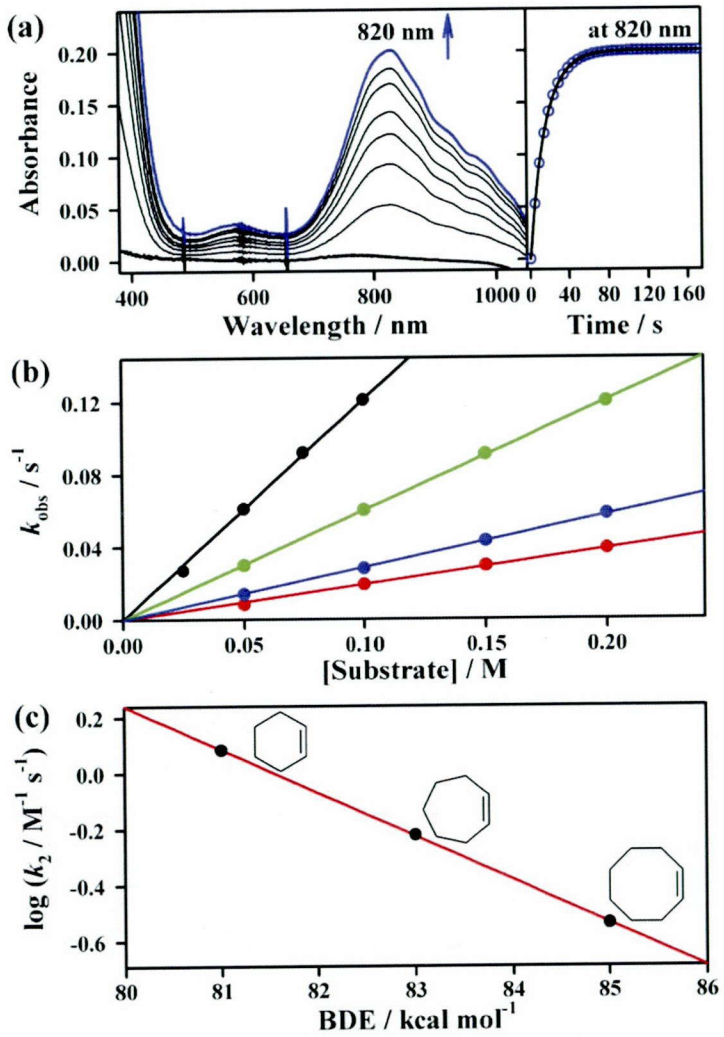

Figure 1. (a) UV–vis spectral changes (left panel) and time course (right panel) for the formation of **2** (blue line) in the reaction of **1** (0.5 mM) and O_2 in the presence of cyclohexene (50 mM) in MeCN at 25°C. (b) Plots of k_{obs} against substrate concentration to determine second-order rate constants for the formation of **2** with cyclohexene (black, $k_2 = 1.2$ M^{-1} s^{-1}), cycloheptene (green, $k_2 = 6.0 \times 10^{-1}$ M^{-1} s^{-1}), cyclooctene (blue, $k_2 = 2.9 \times 10^{-1}$ M^{-1} s^{-1}), and cyclohexene-d_{10} (red, $k_2 = 1.9 \times 10^{-1}$ M^{-1} s^{-1}). (c) Plot of log k_2 against olefin C–H BDE (cyclohexene, 81 kcal mol^{-1}; cycloheptene, 83 kcal mol^{-1}; cyclooctene, 85 kcal mol^{-1}).[13]

Although further studies are needed to elucidate the detailed mechanism of the product formation, what we can propose at this moment is that all of the oxidized products, such as allylic oxidation and dehydrogenation products, might be derived from a cyclohexenyl radical that was the initial product formed by H-atom abstraction of cyclohexene by an iron(III)-superoxo species (Scheme 2, pathways D and F).

One of the most important mechanistic points that deserve discussion here is the nature of an active oxidant that activates allylic C–H bonds of olefins. As the proposed

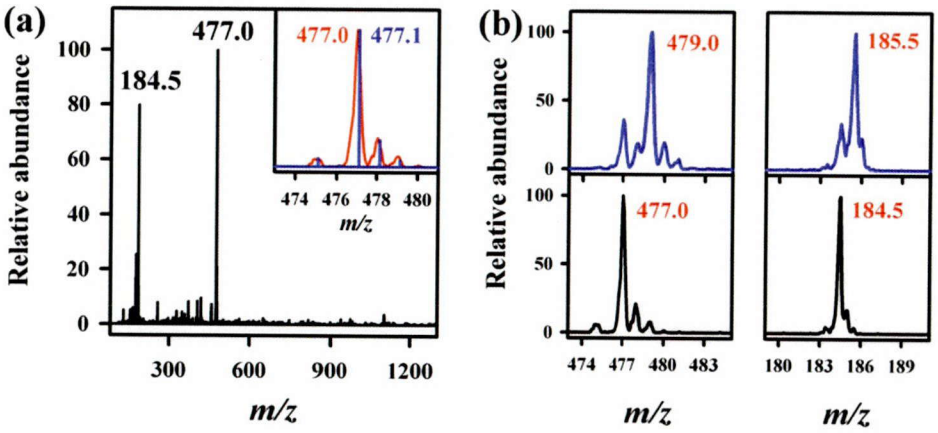

Figure 2. (a) ESI-MS spectrum of $[Fe^{IV}(O)(TMC)]^{2+}$ (2). Peaks at *m/z* of 184.5 and 477.0 correspond to $[Fe^{IV}(O)(TMC)(NCMe)]^{2+}$ and $[Fe^{IV}(O)(TMC)(CF_3SO_3)]^{+}$, respectively. Inset shows the observed (red) and calculated (blue) isotope distribution patterns of the peak at *m/z* of 477.0 (calculated *m/z* = 477.1). An ESI-MS sample of 2-^{16}O was generated in a reaction solution containing $[Fe^{II}(TMC)](CF_3SO_3)_2$ (5.0×10^{-4} M) and cyclohexene (2.5×10^{-2} M) under air in MeCN at 25°C. (b) ESI-MS spectra of 2-^{18}O (upper panel) and 2-^{16}O (lower panel). An ESI-MS sample of 2-^{18}O was generated in a reaction solution containing $[Fe^{II}(TMC)](CF_3SO_3)_2$ (5.0×10^{-4} M) and cyclohexene (2.5×10^{-2} M) under $^{18}O_2$ gas (80% ^{18}O-enriched) in MeCN at 25°C. The percentages of 2-^{18}O and 2-^{18}O in the upper panel were calculated to be 76% and 24%, respectively.

mechanism is depicted in Scheme 2, the reaction is initiated by binding of O_2 by **1**, which leads to the generation of an iron(III)-superoxo species (**3**) (pathway C).[16] Subsequently, **3** abstracts a H atom from the allylic C–H bond of the olefin, giving an iron(III)-hydroperoxo intermediate (**4**) and an alkenyl radical (pathway D).[17] Although **4** was not detected in the reaction solution,[18] we observed an iron(III)-peroxo species (**5**) when the reaction was carried out in the presence of base [e.g., triethylamine (TEA)] (pathway E) (Figures 7 and 8 for UV–vis and EPR spectra).[19] This result is indirect but compelling evidence that **4** was indeed generated in the reaction but could not be detected under the conditions.[17] In addition, the rate of the formation of **5** was dependent on the substrate, with the order of xanthene > cyclohexene > cyclohexene-d_{10}; this order indicates that the formation of **4** from the C–H bond activation of the substrate by **3** is the rate-determining step (pathway D).[20] In the final step of the proposed mechanism, which is the formation of **2** and oxidized products from **4** and an alkenyl radical (pathway F), allylic oxidation products might be formed from the rebound between **4** and the alkenyl radical or from the reaction of the alkenyl radical and O_2.[21]

In addition, the mechanism for the formation of dehydrogenation products is not clear at this moment, although such dehydrogenations have been observed in enzymatic reactions[22] as well as in non-heme iron models.

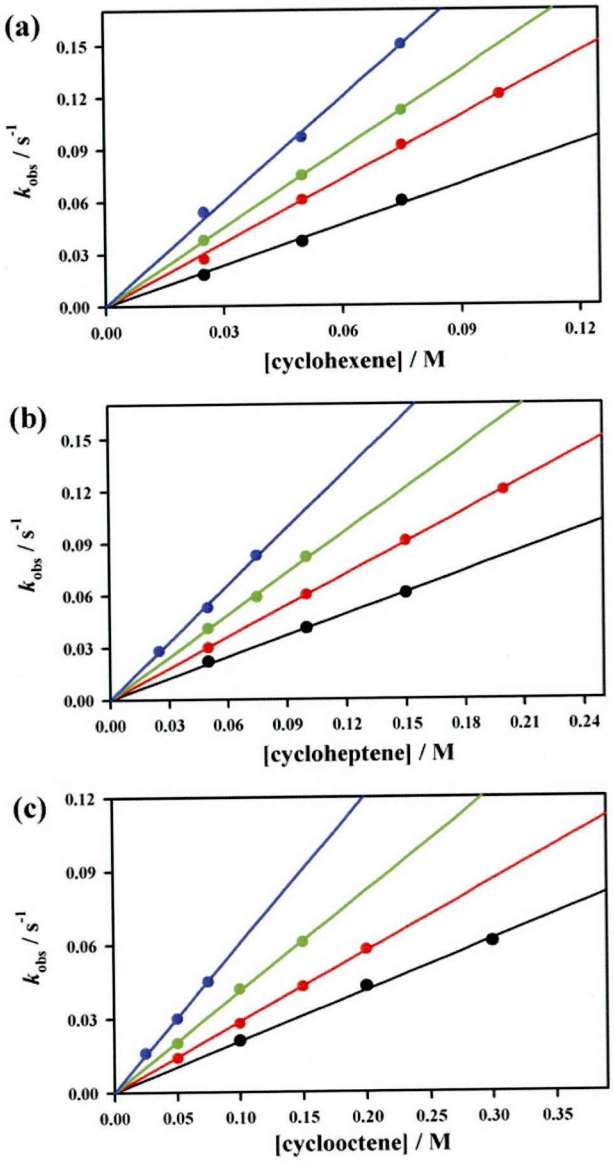

Figure 3. Plots of k_{obs} against olefin concentration to determine second-order rate constants in the reaction of 1 (5.0×10^{-4} M) and O_2 in the presence of (a) cyclohexene, (b) cycloheptene and (c) cyclooctene in MeCN at 20°C (black), 25°C (red), 30°C (green) and 35°C (blue).

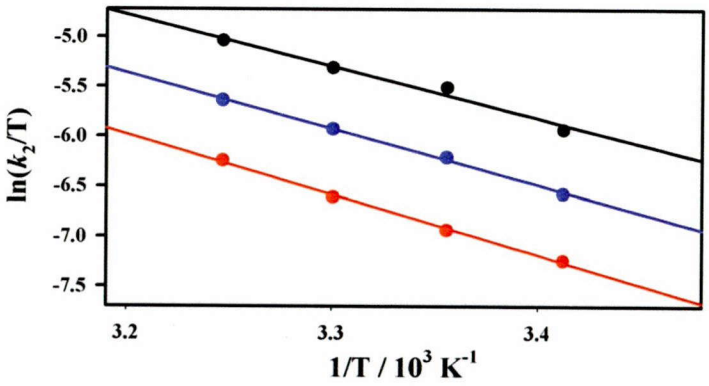

Figure 4. Eyring plots to determine activation parameters for the formation of 2 in the reaction of 1 (5.0×10^{-4} M) and O_2 in the presence of cyclohexene (black), cycloheptene (blue) and cyclooctene (red) in MeCN. The activation parameters calculated from the plots are as follows: $\Delta H^{\ddagger} = 43$ kJ mol^{-1} and $\Delta S^{\ddagger} = -99$ J mol^{-1} K^{-1} for cyclohexene, $\Delta H^{\ddagger} = 47$ kJ mol^{-1} and $\Delta S^{\ddagger} = -94$ J mol^{-1} K^{-1} for cycloheptene, and $\Delta H^{\ddagger} = 50$ kJ mol^{-1} and $\Delta S^{\ddagger} = -88$ J mol^{-1} K^{-1} for cyclooctene.

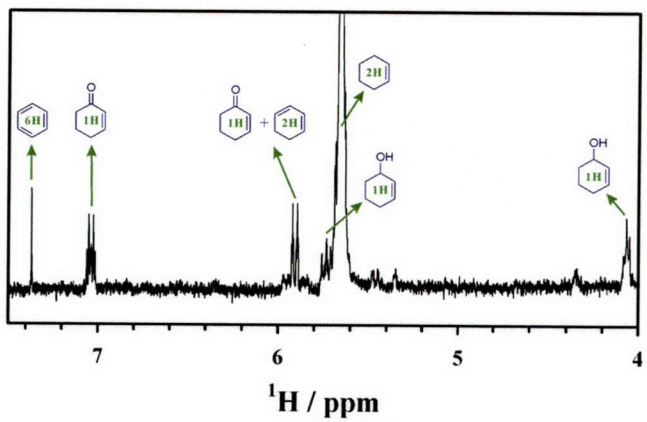

Figure 5. ^{1}H NMR spectrum of products formed in the reaction of 1 (2 mM) and O_2 in the presence of cyclohexene (20 mM, 10 equiv to 1) in MeCN-d_3 at 25°C. Reaction time was 10 min. Quantitative analyses were made on the basis of comparison of NMR peak integration between products and authentic samples. In this reaction, four products, 2-cyclohexen-1-ol, 2-cyclohexen-1-one, 1,3-cyclohexadiene and benzene, were obtained with the yields of 26(3)%, 21(2)%, 9(2)% and 5(2)%, respectively.

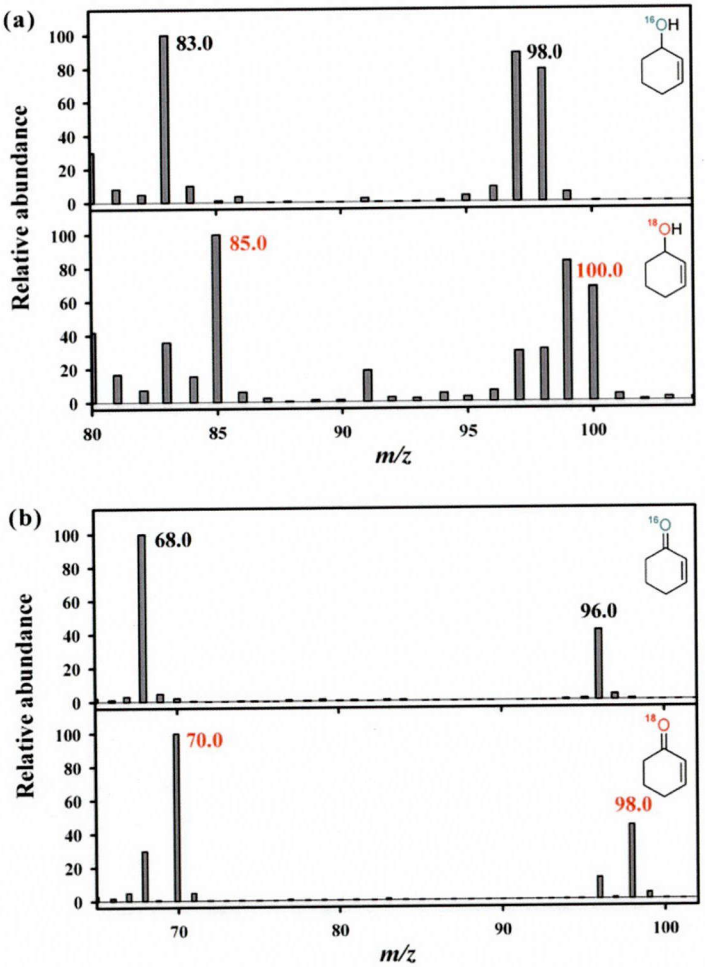

Figure 6. GC-MS spectra of allylic oxidation products, 2-cyclohexen-1-ol (a) and 2-cyclohexene-1-one (b), formed in a reaction solution containing $[Fe^{II}(TMC)](CF_3SO_3)_2$ (5.0×10^{-4} M) and cyclohexene (2.5×10^{-2} M) under $^{16}O_2$ (upper panels) and $^{18}O_2$ (80% ^{18}O-enriched) (lower panels) in MeCN at 25°C. The ^{16}O and ^{18}O compositions in 2-cyclohexen-1-ol and 2-cyclohexene-1-one formed under $^{18}O_2$ (80% ^{18}O-enriched) atmosphere were determined by the relative abundances of (a) m/z = 83.0 and 98.0 for unlabeled cyclohexen-1-ol and m/z = 85.0 and 100.0 for ^{18}O-labeled cyclohexen-1-ol and (b) m/z = 68.0 and 96.0 for unlabeled cyclohexen-1-one and m/z = 70.0 and 98.0 for ^{18}O-labeled cyclohexen-1-one. The ^{18}O percentages found in the cyclohexen-1-ol and cyclohexen-1-one products were 78%.

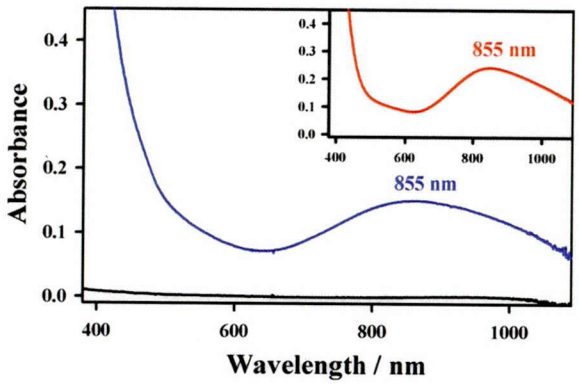

Figure 7. UV–vis spectra of 1 (black line) and $[Fe^{III}(O_2)(TMC)]^+$ (5) species (blue line) generated in the reaction of 1 (1.0 mM) and O_2 in the presence of triethylamine (TEA, 5.0 mM) and cyclohexene (50 mM) in MeCN at 25°C. Inset shows UV–vis spectrum of 5 (red line) prepared by reacting 1 (1.0 mM) with H_2O_2 (10 mM) in the presence of TEA (5.0 mM) in MeCN at 25°C. Although we were able to obtain the UV–vis spectrum of 5 with the yield of > 60% in the reaction of 1 and O2 in the presence of TEA and olefins, we were not able to follow the second-order kinetics due to the instability of 5 in MeCN. 5 decayed fast and disappeared within 5 min in MeCN at 25°C. However, initial rate of the formation of 5 was similar to that of the formation of 2, indicating that the intermediate 4 is generated in the reaction as a precursor to 2. In addition, although we were not able to follow the complete kinetics, we were able to observe the formation of 5 with the order of xanthene > cyclohexene > cyclohexene-d_{10}

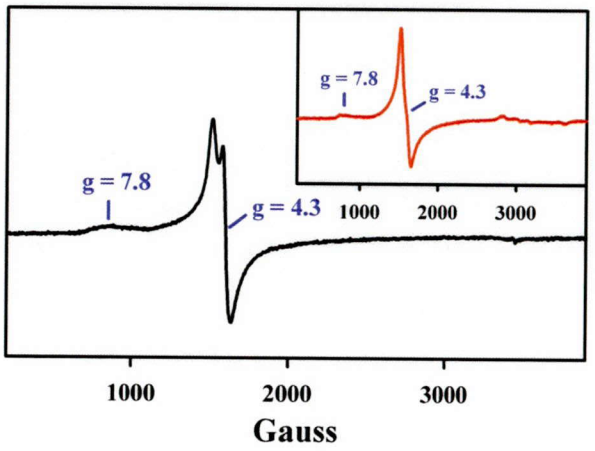

Figure 8. CW-EPR spectrum of 5 (black line) generated in the reaction of 1 (1.0 mM) and O_2 in the presence of triethylamine (TEA, 5.0 mM) and cyclohexene (50 mM) in MeCN at 25°C. Inset shows CW-EPR spectrum of 5 (red line) formed in the reaction of 1 (1.0 mM) and H_2O_2 (10 mM) in the presence of TEA (5.0 mM) in MeCN at 25°C. The experimental parameters for EPR spectra are as follows: Microwave frequency = 9.646 GHz, microwave power = 1 mW, modulation amplitude = 10 G, gain = 1×10^4, modulation frequency = 100 kHz, time constant = 40.96 ms, conversion time = 85.00 ms and measuring temperature = 7 K.

Conclusion

In conclusion, we have shown that a non-heme iron(II) complex activates O_2 in the presence of substrates with weak C–H bonds, thereby generating an iron(IV)-oxo complex. We have proposed that an iron(III)-superoxo intermediate is the active oxidant that abstracts a H atom from the substrate. The present results are probably relevant to the chemistry of mononuclear non-heme iron enzymes such as isopenicillin *N* synthase and 1-aminocyclopropane-1-carboxylic acid oxidase that initiate oxidation of their substrates by putative iron(III)-superoxo species (i.e., H-atom abstraction) and then generate iron(IV)-oxo species for further oxidation reactions.[2] Future studies, including theoretical calculations, will focus on elucidating the chemical properties of metal-superoxo species in oxidation reactions.

References

(1) Nam, W. *Acc. Chem. Res.* **2007**, *40*, 465.

(2) (a) Bruijnincx, P. C. A.; van Koten, G.; Klein Gebbink, R. J. M. *Chem. Soc. Rev.* **2008**, *37*, 2716. (b) Bollinger, J. M., Jr.; Krebs, C. *Curr. Opin. Chem. Biol.* **2007**, *11*, 151. (c) Xing, G.; Diao, Y.; Hoffart, L. M.; Barr, E. W.; Prabhu, K. S.; Arner, R. J.; Reddy, C. C.; Krebs, C.; Bollinger, J. M., Jr. *Proc. Natl. Acad. Sci. U.S.A.* **2006**, *103*, 6130.

(3) (a) Prigge, S. T.; Eipper, B. A.; Mains, R. E.; Amzel, L. M. *Science* **2004**, *304*, 864. (b) Chen, P.; Solomon, E. I. *Proc. Natl. Acad. Sci. U.S.A.* **2004**, *101*, 13105. (c) Klinman, J. P. *J. Biol. Chem.* **2006**, *281*, 3013. (d) Rolff, M.; Tuczek, F. *Angew. Chem., Int. Ed.* **2008**, *47*, 2344.

(4) (a) Maiti, D.; Fry, H. C.; Woertink, J. S.; Vance, M. A.; Solomon, E. I.; Karlin, K. D. *J. Am. Chem. Soc.* **2007**, *129*, 264. (b) Fujii, T.; Yamaguchi, S.; Hirota, S.; Masuda, H. *Dalton Trans.* **2008**, 164. (c) Maiti, D.; Lee, D.-H.; Gaoutchenova, K.; Würtele, C.; Holthausen, M. C.; Sarjeant, A. A. N.; Sundermeyer, J.; Schindler, S.; Karlin, K. D. *Angew. Chem., Int. Ed.* **2008**, *47*, 82. (d) Kunishita, A.; Kubo, M.; Sugimoto, H.; Ogura, T.; Sato, K.; Takui, T.; Itoh, S. *J. Am. Chem. Soc.* **2009**, *131*, 2788.

(5) (a) Mukherjee, A.; Cranswick, M. A.; Chakrabarti, M.; Paine, T. K.; Fujisawa, K.; Münck, E.; Que, L., Jr. *Inorg. Chem.* **2010**, *49*, 3618. (b) Zhao, M.; Helms, B.; Slonkina, E.; Friedle, S.; Lee, D.; DuBois, J.; Hedman, B.; Hodgson, K. O.; Fréchet, J. M. J.; Lippard, S. J. *J. Am. Chem. Soc.* **2008**, *130*, 4352. (c) Shan, X.; Que, L., Jr. *Proc. Natl. Acad. Sci. U.S.A.* **2005**, *102*, 5340.

(6) (a) Martinho, M.; Blain, G.; Banse, F. *Dalton Trans.* **2010**, *39*, 1630. (b) Hong, S.; Lee, Y.-M.; Shin, W.; Fukuzumi, S.; Nam, W. *J. Am. Chem. Soc.* **2009**, *131*, 13910. (c) Thibon, A.; England, J.; Martinho, M.; Young, V. G., Jr.; Frisch, J. R.; Guillot, R.; Girerd, J.-J.; Münck, E.; Que, L., Jr.; Banse, F. *Angew. Chem., Int. Ed.* **2008**, *47*, 7064.

(7) Nam, W. *Acc. Chem. Res.* **2007**, *40*, 522.

(8) Kim, S. O.; Sastri, C. V.; Seo, M. S.; Kim, J.; Nam, W. *J. Am. Chem. Soc.* **2005**, *127*, 4178.

(9) Armarego, W. L. F.; Chai, C. L. L. *Purification of Laboratory Chemicals*, 6th ed; Pergamon Press: Oxford, 2009.

(10) Rohde, J.-U.; In, J.-H.; Lim, M. H.; Brennessel, W. W.; Bukowski, M. R.; Stubna, A.; Münck, E.; Nam, W.; Que, L., Jr. *Science* **2003**, *299*, 1037.

(11) The substrates used in this study were thoroughly purified, and it was confirmed by iodometric titration that no peroxide (autoxidation initiator) was present in the olefins (<1 ppm). We thus conclude that **2** was not formed via an autoxidation process in the present case.

(12) The rates also increased with increasing concentrations of the iron complex and O_2, as expected from Scheme 2, pathway C.

(13) Luo, Y.-R. *Handbook of Bond Dissociation Energies in Organic Compounds*; CRC Press: Boca Raton, FL, 2003.

(14) **2** was formed at higher rates in the reactions of alkylaromatic compounds with weaker C–H bonds (BDEs of 75–78 kcal mol^{-1}), such as xanthene, 9,10-dihydroanthracene, and 1,4-cyclohexadiene. However, **2** disappeared after it was formed because it reacted with the substrates. See: Sastri, C. V.; Lee, J.; Oh, K.; Lee, Y. J.; Lee, J.; Jackson, T. A.; Hirao, H.; Que, L., Jr.; Shaik, S.; Nam, W. *Proc. Natl. Acad. Sci. U.S.A.* **2007**, *104*, 19181.

(15) For KIE values in C–H bond activation by iron(III)- and copper(II)–superoxo species in iron- and copper-containing enzymes, see: (a) Baldwin, J. E.; Abraham, E. *Nat. Prod. Rep.* **1988**, *5*, 129. (b) Francisco, W. A.; Merkler, D. J.; Blackburn, N. J.; Klinman, J. P. *Biochemistry* **1998**, *37*, 8244.

(16) Que and co-workers reported the dehydrogenation of cyclohexene in the reaction of an iron(II) complex and O_2, affording cycloxadiene as a major product. An iron(IV)-oxo complex was proposed as an active oxidant for the dehydrogenation reaction. See: Mukherjee, A.; Martinho, M.; Bominaar, E. L.; Münck, E.; Que, L., Jr. *Angew. Chem., Int. Ed.* **2009**, *48*, 1780.

(17) We failed to detect **3** in a solution containing **1** under an O_2 atmosphere using various spectroscopic methods, including EPR spectroscopy.

(18) We have recently shown that an isolated (TMC)Cr^{III}-superoxo complex is capable of abstracting a H atom from alkylaromatic compounds. See: Cho, J.; Woo, J.; Nam, W. *J. Am. Chem. Soc.* **2010**, *132*, 5958.

(19) The $[(TMC)Fe^{III}–OOH]^{2+}$ species has never been detected in any reactions, including the reaction of **1** and H_2O_2 in MeCN (see ref 10).

(20) (a) Annaraj, J.; Suh, Y.; Seo, M. S.; Kim, S. O.; Nam, W. *Chem. Commun.* **2005**, 4529. (b) Jensen, K. B.; McKenzie, C. J.; Nielsen, L. P.; Pedersen, J. Z.; Svendsen, H. M. *Chem. Commun.* **1999**, 1313.

(21) **4** can be ruled out as an active oxidant that abstracts H from a C-H bond of the substrate in the generation of **2**. See: Park, M. J.; Lee, J.; Suh, Y.; Kim, J.; Nam, W. *J. Am. Chem. Soc.* **2006**, *128*, 2630.

(22) Böttcher, A.; Grinstaff, M. W.; Labinger, J. A.; Gray, H. B. *J. Mol. Catal. A: Chem.* **1996**, *113*, 191.

(23) (a) Buist, P. H. *Nat. Prod. Rep.* **2004**, *21*, 249. (b) Kumar, D.; de Visser, S. P.; Shaik, S. *J. Am. Chem. Soc.* **2004**, *126*, 5072–5073. (c) Jin, Y.; Lipscomb, J. D. *J. Biol. Inorg. Chem.* **2001**, *6*, 717.

Chapter 7: Autocatalytic radical chain pathway in formation of an iron(IV)-oxo complex by oxidation of an iron(II) complex with dioxygen and isopropanol

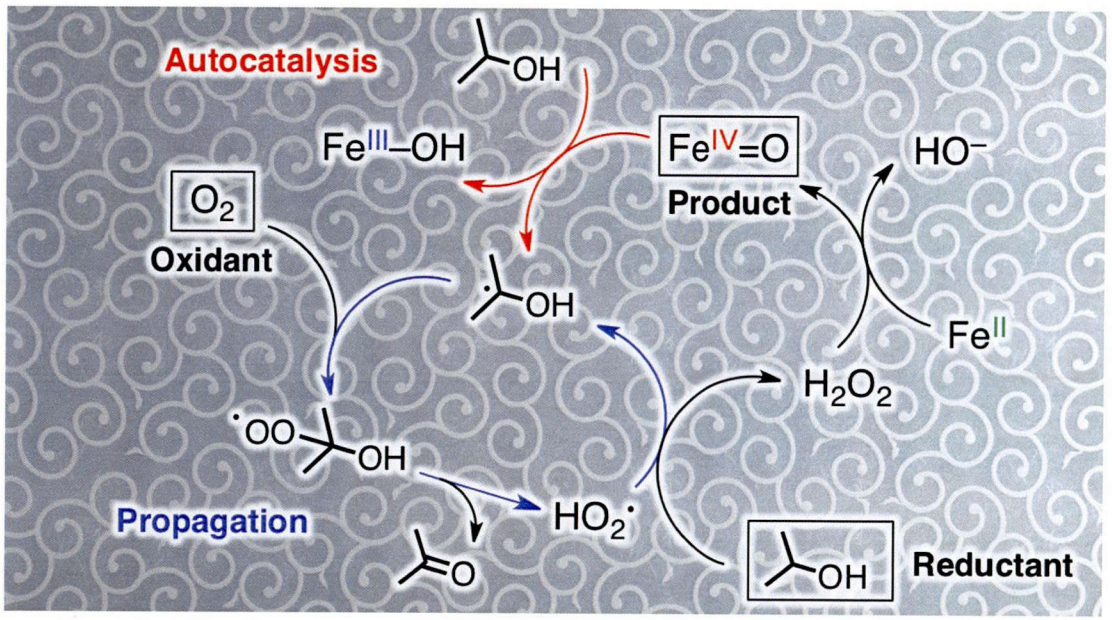

Abstract: Evidence of an autocatalytic radical chain pathway is demonstrated in formation of a non-heme iron(IV)-oxo complex by oxidation of an iron(II) complex with dioxygen and isopropanol in acetonitrile at 298 K. The radical chain reaction is initiated by hydrogen abstraction from isopropanol by the iron(IV)-oxo complex and the propagation step consists of formation of hydroperoxyl radical by the reaction of α-hydroxyisopropyl radical with dioxygen, followed by the rate-determining hydrogen abstraction from isopropanol by hydroperoxyl radical.

Introduction

Non-heme iron(IV)-oxo intermediates are known to act as active oxidizing species in the catalytic cycles of *Escherichia coli* taurine: α-ketoglutarate dioxygenase (TauD), prolyl-4-hydroxylase, and halogenase CytC3.[1,2] Iron(IV)-oxo intermediates in these enzymes are formed by the reductive activation of dioxygen (O_2) with two electrons and two protons.[1,2] Synthetic model compounds of such high-valent iron(IV)-oxo intermediates have usually been produced in the reactions of heme and non-heme iron complexes with artificial oxidants such as iodosylbenzene (PhIO), *m*-chloroperoxybenzoic acid (*m*-CPBA), and hydroperoxides (H_2O_2 and ROOH) via a "shunt" pathway.[3,4] Iron(IV)-oxo complexes have also been produced by two-electron oxidation of iron(II) complexes with water as an oxygen source, which is regarded as an oxidative activation of water.[5,6] With regard to a reductive activation of O_2 with hydrogen donors (hydrogen is equivalent to an electron and a proton),[7–9] formation of iron(IV)-oxo complexes ($Fe^{IV}(O)$) has been reported to occur via hydrogen abstraction from hydrogen donors (RH) by iron(III)-superoxo complexes ($Fe^{III}(O_2^{\bullet-})$), which are assumed to be produced by electron transfer from iron(II) complexes (Fe^{II}) to O_2, followed by the O–O bond cleavage of the iron(III)-hydroperoxo complexes ($Fe^{III}OOH$) by hydrogen abstracted radicals ($R^{\bullet}$) as shown (Scheme 1).[10]

Scheme 1. Formation of $Fe^{IV}(O)$ via Reductive Activation of O_2 with RH

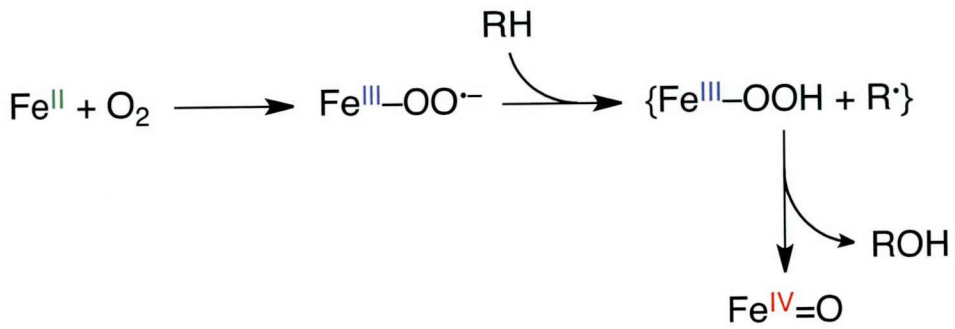

In Scheme 1, formation of $Fe^{IV}(O)$ by the O–O bond cleavage of $Fe^{III}OOH$ by radicals ($R^{\bullet}$) occurs within the cage without diffusion of free radicals. The produced $Fe^{IV}(O)$ can also abstract hydrogen from hydrogen donors to form iron(III)-hydroxo species (Fe^{III}–OH) and $R^{\bullet}$.[11–13] Once free radicals are formed, it is possible that $R^{\bullet}$ reacts rapidly with O_2 to produce the peroxyl radical ($RO_2^{\bullet}$).[14,15] In such a case, autoxidation of RH may occur via radical chain reactions as shown in Scheme 2. The hydroperoxide

(ROOH) produced in the autoxidation can generate iron(IV)-oxo species by oxidizing iron(II) species via a shunt pathway to start the initiation of the radical chain reactions. However, such an autocatalytic radical chain pathway has yet to be clarified in formation of iron(IV)-oxo complexes by reductive activation of O_2 with hydrogen donors.

Scheme 2. Radical Chain Reactions in Autoxidation of RH with O_2

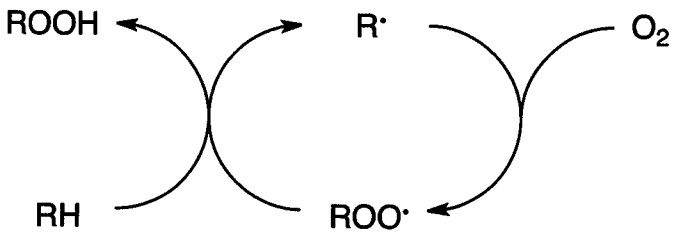

We report herein evidence of occurrence of autocatalytic radical chain reactions in formation of a nonheme iron(IV)-oxo complex, $[Fe^{IV}(O)(TMC)]^{2+}$ (TMC = 1,4,8,11-tetramethyl-1,4,8,11-tetraazacyclotetradecane),[16] from the corresponding iron(II) complex, $[Fe^{II}(TMC)]^{2+}$, with O_2 and isopropanol ($(CH_3)_2CHOH$) in acetonitrile (MeCN). The mechanism of formation of $[Fe^{IV}(O)(TMC)]^{2+}$ via radical chain reactions is elucidated by the mechanistic study including an inhibition effect of a radical scavenger and an acceleration effect of a catalytic amount of $[Fe^{IV}(O)(TMC)]^{2+}$ and hydrogen peroxide.

Experimental section

Materials. Commercially available chemicals were used without further purification unless otherwise indicated. Solvents were dried according to published procedures and distilled under N_2 prior to use.[18] Iodosylbenzene (PhIO) was prepared by a literature method.[19] Isopropanol and isopropanol-d_8 were purchased from Aldrich Chemical Co. and Chembridge Isotope Laboratories, Inc., respectively. Hydrogen peroxide (H_2O_2), 35 wt. % in water and galvinoxyl radical were purchased from Kishida Chemical Co., Ltd. and Tokyo Chemical Industry Co., Ltd., respectively. TMC ligand was purchased from Aldrich Chemical, and Iron complexes, $[Fe^{II}(TMC)(NCMe)_2](CF_3SO_3)_2$, and $[Fe^{IV}(O)(TMC)]^{2+}$, were prepared by literature methods.[16]

Kinetic measurements. Kinetic measurements were performed on a Hewlett Packard 8453 photodiode-array spectrophotometer at 298 K. Typically, the formation reaction of $[Fe^{IV}(O)(TMC)]^{2+}$ was started by adding solution of $[Fe^{II}(TMC)]^{2+}$ (5.0 mM) into air-saturated MeCN in the presence of isopropanol with other additives such as $[Fe^{IV}(O)(TMC)]^{2+}$, H_2O_2, and galvinoxyl radical. The reaction between $[Fe^{IV}(O)(TMC)]^{2+}$ and isopropanol was started by adding solution of $[Fe^{IV}(O)(TMC)]^{2+}$ into deaerated MeCN solution of isopropanol.

NMR measurements. Nuclear magnetic resonance (NMR) detection of acetone and H_2O was performed as follows: an air-saturated MeCN-d_3 solution of $[Fe^{IV}(O)(TMC)]^{2+}$ (1.0×10^3 M) was added to an air-saturated MeCN-d_3 solution of isopropanol (18 mM). After 5 h, ^1H NMR spectra were recorded on a JEOL JMN-AL-300 NMR spectrometer at room temperature.

EPR measurements. Electron paramagnetic resonance (EPR) detection of iron(III) complexes was performed as follows: an MeCN solution of isopropanol (2.6 M) in an EPR cell (3.0 mm i.d.) purged with N_2 for 5 min. Then, a deaerated MeCN solution of $[Fe^{IV}(O)(TMC)]^{2+}$ (1.0×10^{-3} M) was added to the solution. The EPR spectra of the iron(III) complexes were recorded on a JEOL JES-RE1XE spectrometer at 85 K. The magnitude of modulation was chosen to optimize the resolution and signal-to-noise (S/N) ratio of the observed spectra under non-saturating microwave power conditions. The g value was calibrated using an Mn^{2+} marker (g = 2.034 and 1.981).

Results and Discussion

$[Fe^{II}(TMC)]^{2+}$ is stable in the presence of O_2 in MeCN.[8] When isopropanol (0.26 M) was added to an air-saturated MeCN solution of $[Fe^{II}(TMC)]^{2+}$ (1.0 mM), $[Fe^{II}(TMC)]^{2+}$ was converted to $[Fe^{IV}(O)(TMC)]^{2+}$ as shown in Figure 1, where the absorption band at λ_{max} = 820 nm and 280 nm due to $[Fe^{IV}(O)(TMC)]^{2+}$ was observed. The stoichiometry of the reaction is given by eqn (1). The formation of acetone and water was confirmed by ^1H NMR spectroscopy (Figure 2).

$$[Fe^{II}(TMC)]^{2+} + O_2 + (CH_3)_2CHOH \longrightarrow [Fe^{IV}(O)(TMC)]^{2+} + (CH_3)_2CO + H_2O \quad (1)$$

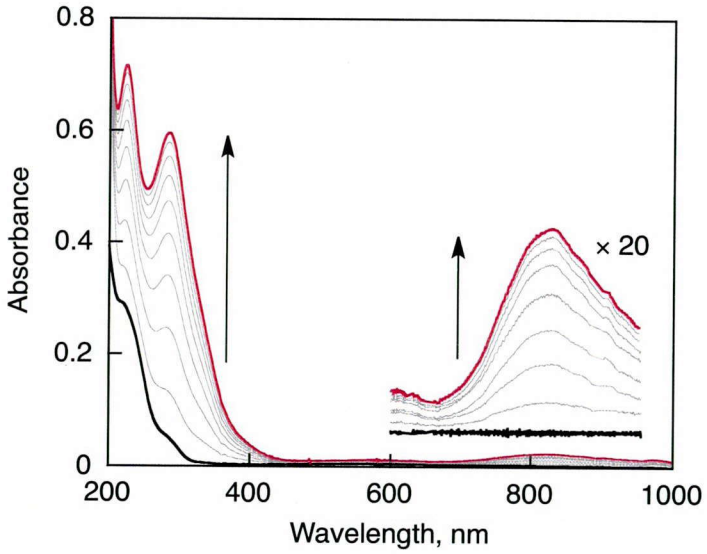

Figure 1. Absorption spectral change observed in formation of $[Fe^{IV}(O)(TMC)]^{2+}$ by the reaction of $[Fe^{II}(TMC)]^{2+}$ (0.10 mM) with isopropanol (0.26 M) in air-saturated MeCN at 298 K.

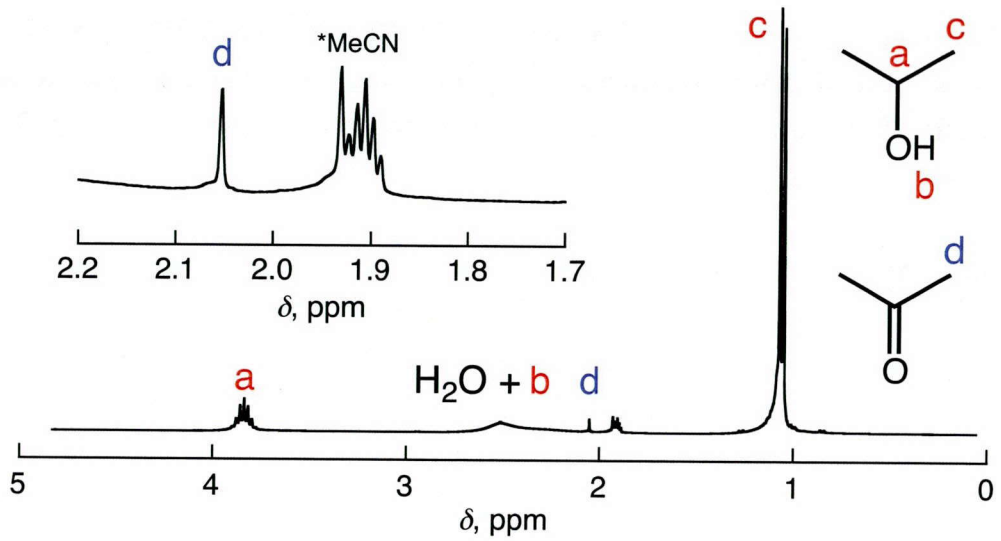

Figure 2. ^{1}H NMR spectrum of a resulting solution obtained in the reaction of $[Fe^{II}(TMC)]^{2+}$ (1.0 mM) and isopropanol (18 mM) to produce $[Fe^{II}(TMC)]^{2+}$ (0.49 mM) and acetone (0.8 mM) in air-saturated MeCN at 298 K.

The rate of formation of $[Fe^{IV}(O)(TMC)]^{2+}$ was monitored by an increase in absorbance at 280 nm. When a catalytic amount of $[Fe^{IV}(O)(TMC)]^{2+}$ was added to an air-saturated MeCN solution of isopropanol (0.26 M) and $[Fe^{II}(TMC)]^{2+}$ (0.10 mM), the induction period of the reaction was reduced and the rate of formation of $[Fe^{IV}(O)(TMC)]^{2+}$ increased with increasing concentration of added $[Fe^{IV}(O)(TMC)]^{2+}$ (Figure 3). The acceleration of sigmoidal generation of $[Fe^{IV}(O)(TMC)]^{2+}$ by the addition of the catalytic amount of itself clearly indicates the autocatalytic behavior.

The reduction of $[Fe^{IV}(O)(TMC)]^{2+}$ by isopropanol to produce $[Fe^{III}(OH)(TMC)]^{2+}$ (Figure 4) was also examined to understand the role of $[Fe^{IV}(O)(TMC)]^{2+}$ in the autocatalytic process.[19] The second-order rate of the reduction of $[Fe^{IV}(O)(TMC)]^{2+}$ by isopropanol in MeCN at 298 K was determined 1.0×10^{-3} M^{-1} s^{-1} (Figure 5), from which the initial rate of the decay of $[Fe^{IV}(O)(TMC)]^{2+}$ (1.0 mM) with isopropanol (0.26 M) was determined to be 2.6×10^{-10} M s^{-1}, which is much slower than the initial rate of formation of $[Fe^{IV}(O)(TMC)]^{2+}$ (3.3×10^{-8} M s^{-1}) with 1.0 mM in Figure 3. This indicates that the reduction of $[Fe^{IV}(O)(TMC)]^{2+}$ by isopropanol is the initiation step of an autocatalytic radical chain pathway (vide infra).

When a catalytic amount of hydrogen peroxide (H_2O_2) was added to an air-saturated MeCN solution of $[Fe^{II}(TMC)]^{2+}$ in the presence of isopropanol (0.26 M),

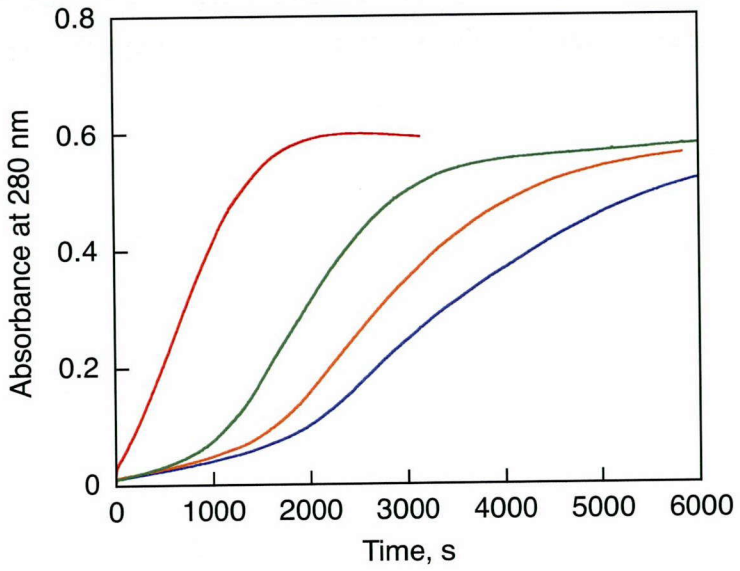

Figure 3. Time courses of the absorption change monitored at 280 nm during the formation reaction of $[Fe^{IV}(O)(TMC)]^{2+}$ from $[Fe^{II}(TMC)]^{2+}$ (0.10 mM) with isopropanol (0.26 M) in the absence and presence of a catalytic amount of $[Fe^{IV}(O)(TMC)]^{2+}$ (blue, 0 M; yellow, 0.050 mM ; green, 0.25 mM; red, 1.0 mM) in air-saturated MeCN at 298 K.

the induction period of the reaction was also reduced and the rate of formation of $[Fe^{IV}(O)(TMC)]^{2+}$ increased with increasing concentration of H_2O_2 (Figure 10). Because $[Fe^{IV}(O)(TMC)]^{2+}$ is produced by the reaction of $[Fe^{II}(TMC)]^{2+}$ with H_2O_2, the rate acceleration by H_2O_2 also indicates the autocatalytic behavior.

In contrast to the acceleration effects of $[Fe^{IV}(O)(TMC)]^{2+}$ (Figure 3) and H_2O_2 (Figure 6), addition of a catalytic amount of galvinoxyl radical, which is a typical radical scavenger, to an air-saturated MeCN solution of isopropanol (0.26 M) and $[Fe^{II}(TMC)]^{2+}$ (0.10 mM), resulted in significant increase in the induction period, which increased with increasing concentration of galvinoxyl radical (Figure 7). Such an inhibition effect of galvinoxyl radical is taken as evidence of involvement of a radical chain pathway in the formation of $[Fe^{IV}(O)(TMC)]^{2+}$.[20]

The rate of formation of $[Fe^{IV}(O)(TMC)]^{2+}$ also increased with increasing concentration of isopropanol (Figure 8). When $(CH_3)_2CHOH$ was replaced by $(CD_3)_2CDOH$, the rate of formation of $[Fe^{IV}(O)(TMC)]^{2+}$ was significantly slowed down as shown in Figure 9 (see also, Figure 8).

Based on the above results, the mechanism of formation of $[Fe^{IV}(O)(TMC)]^{2+}$ is proposed as shown in Scheme 3. The hydrogen abstraction from isopropanol by $[Fe^{IV}(O)(TMC)]^{2+}$ produces α-hydroxyisopropyl radical $[(CH_3)_2COH^{\bullet}]$. This is the autocatalytic initiation step of the radical chain reactions, in which α-hydroxyisopropyl radical reacts with O_2 to produce hydroperoxyl radical ($HO_2^{\bullet}$) and acetone. The reaction of α-hydroxyisopropyl radical with O_2 initially affords α-hydroxyisopropyl peroxyl radical,

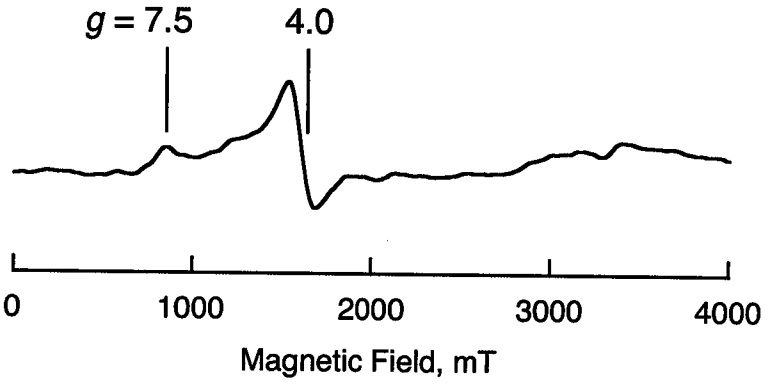

Figure 4. EPR spectrum of a resulting solution obtained in the reaction of $[Fe^{IV}(O)(TMC)]^{2+}$ (1.2 mM) and isopropanol (2.6 M) in deaerated MeCN at 298 K. The spectrum was recorded at 85 K.

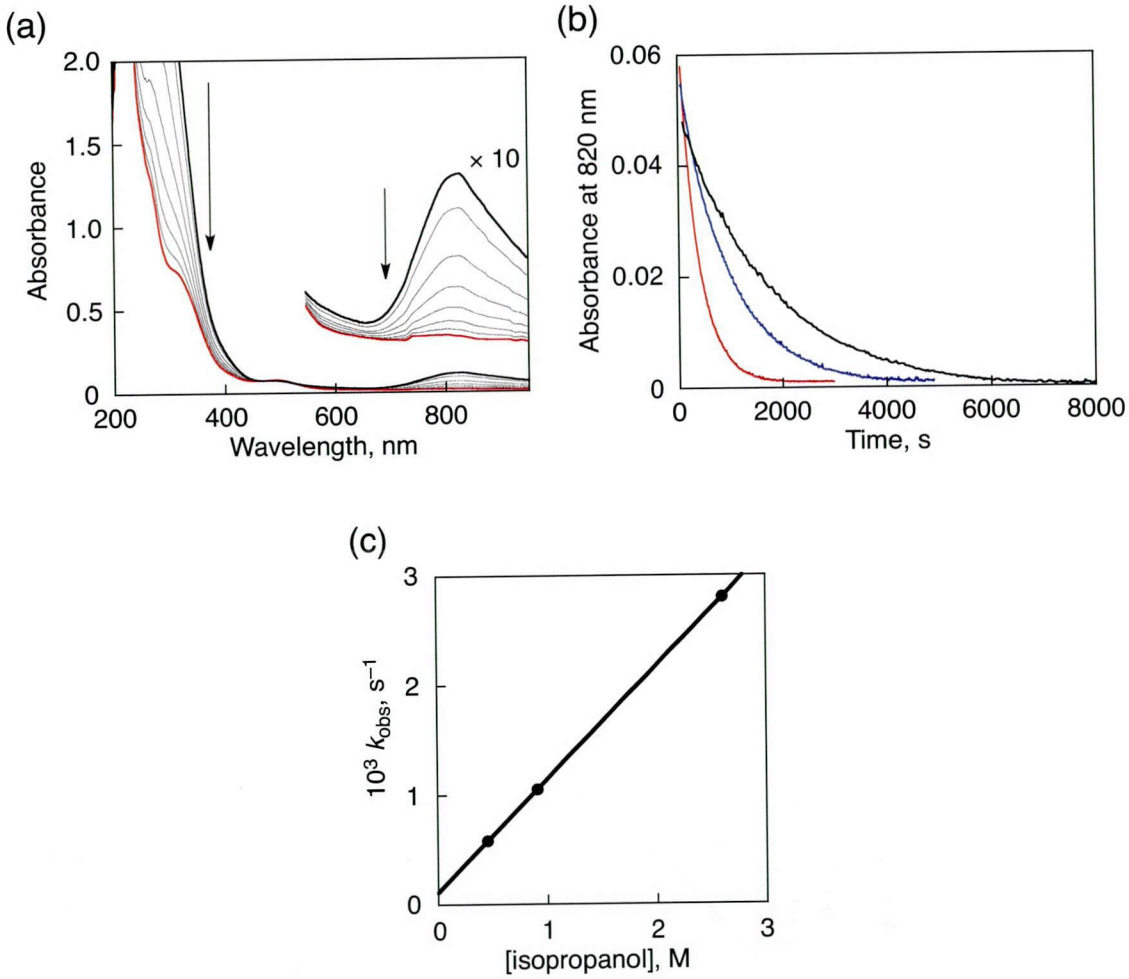

Figure 5. (a) UV–vis–NIR spectral changes observed in the oxidation of isopropanol (0.91 M) by $[Fe^{IV}(O)(TMC)]^{2+}$ (0.15 mM) in deaerated MeCN at 298 K. (b) Time courses of absorbance at 820 nm due to $[Fe^{IV}(O)(TMC)]^{2+}$ in the reaction of $[Fe^{IV}(O)(TMC)]^{2+}$ (0.15 mM) with isopropanol (red, 2.6 M; blue, 0.91 M; black, 0.46 M) in deaerated MeCN at 298 K. (c) Plot of pseudo-first-order rate constant vs. concentration of isopropanol.

but it is well known that α-hydroxyalkyl radical dissociates to $HO_2^{\bullet}$ and the ketone.[15,21] The $HO_2^{\bullet}$ radical thus produced abstracts hydrogen from isopropanol to produce hydrogen peroxide (H_2O_2), accompanied by regeneration of *a*-hydroxyisopropyl radical in the chain propagation step. This may be the rate-determining step of autoxidation of isopropanol with O_2, because the rate of formation of $[Fe^{IV}(O)(TMC)]^{2+}$ increased with increasing concentration of isopropanol (Figure 8) and a significant deuterium kinetic isotope effect (KIE) was observed when $(CH_3)_2CHOH$ was replaced by $(CD_3)_2CDOD$ (Figure 9). the product is used to initiate the radical chain reaction. The produced H_2O_2 reacts with $[Fe^{II}(TMC)]^{2+}$ to produce $[Fe^{IV}(O)(TMC)]^{2+}$. This is the reason why the

formation of $[Fe^{IV}(O)(TMC)]^{2+}$ exhibits autocatalytic behavior, because The termination step may be the disproportionation of hydroperoxyl radical ($HO_2^{\bullet}$) to produce H_2O and O_2 (Scheme 3).[15]

The initiation step without products of the propagation step in Scheme 3 ($[Fe^{IV}(O)(TMC)]^{2+}$ and H_2O_2) may be the reaction of $[Fe^{II}(TMC)]^{2+}$ with O_2 to produce the surperoxo complex ($Fe^{III}(O_2^{\bullet-})$), which is converted to the Fe^{IV}=O complex via the hydrogen abstraction from isopropanol as shown in Scheme 1 (green pathway in Scheme 3).[9,10] This initiation pathway (the reaction of $[Fe^{II}(TMC)]^{2+}$ with O_2) was supported by the increase in the rate of formation of $[Fe^{IV}(O)(TMC)]^{2+}$ with increasing concentration of O_2 (Figure 10).

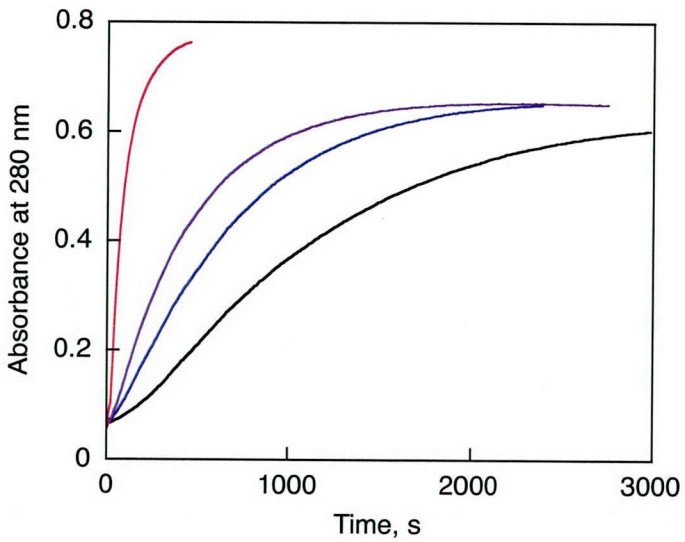

Figure 6. Time traces of the absorption change monitored at 280 nm during formation of $[Fe^{IV}(O)(TMC)]^{2+}$ in the reaction of $[Fe^{II}(TMC)]^{2+}$ (0.10 mM) with isopropanol (0.26 M) in the absence and presence of a catalytic amount of H_2O_2 (black, 0.0 M; blue 0.020 mM; purple 0.20 mM; red, 2.0 mM) in air-saturated MeCN at 298 K.

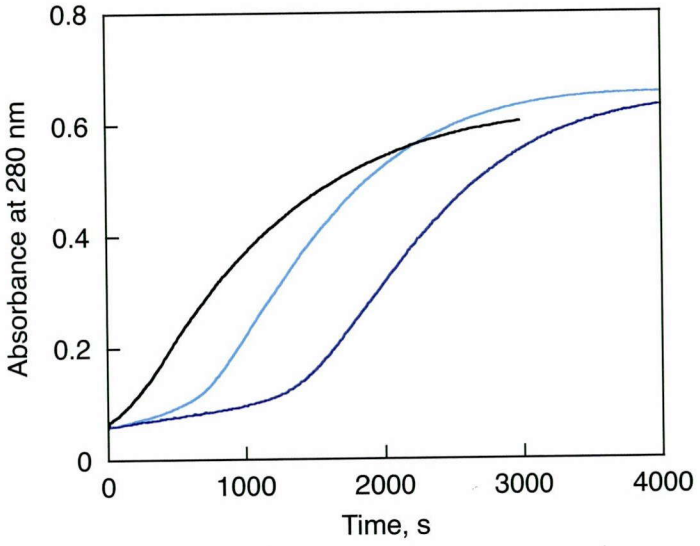

Figure 7. Time profiles of the absorbance at 280 nm in the reaction of $[Fe^{II}(TMC)]^{2+}$ (0.10 mM) with isopropanol (0.26 M) in the absence and presence of a catalytic amount of galvinoxyl radical (black, 0 M; sky blue, 2.5 μM; blue, 5 μM) in air-saturated MeCN at 298 K.

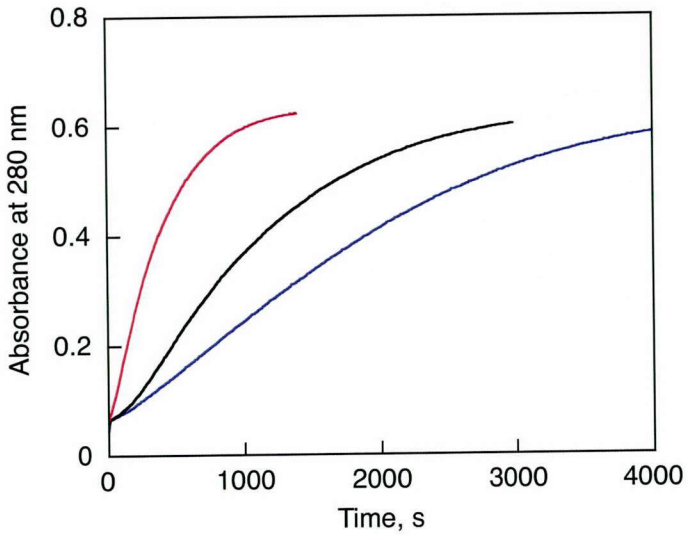

Figure 8. Time courses of the absorbance at 280 nm due to $[Fe^{IV}(O)(TMC)]^{2+}$ in the reaction of $[Fe^{II}(TMC)]^{2+}$ (0.10 mM) with various concentrations of isopropanol (blue, 0.13 M; black, 0.26 M; red 0.52 M) in air-saturated MeCN at 298 K.

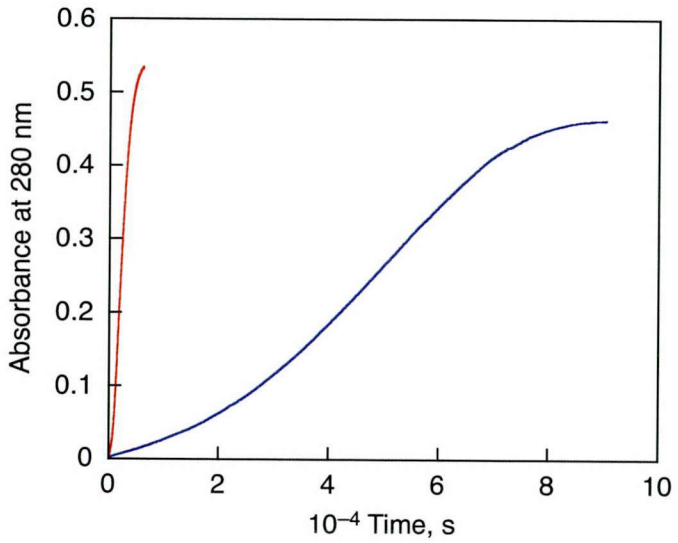

Figure 9. Time courses of the absorbance at 280 nm in the reaction of $[Fe^{II}(TMC)]^{2+}$ (0.10 mM) with isopropanol (red; 0.26 M) and deuterated isopropanol ($(CD_3)_2CDOH$) (blue; 0.26 M) in air-saturated MeCN at 298 K.

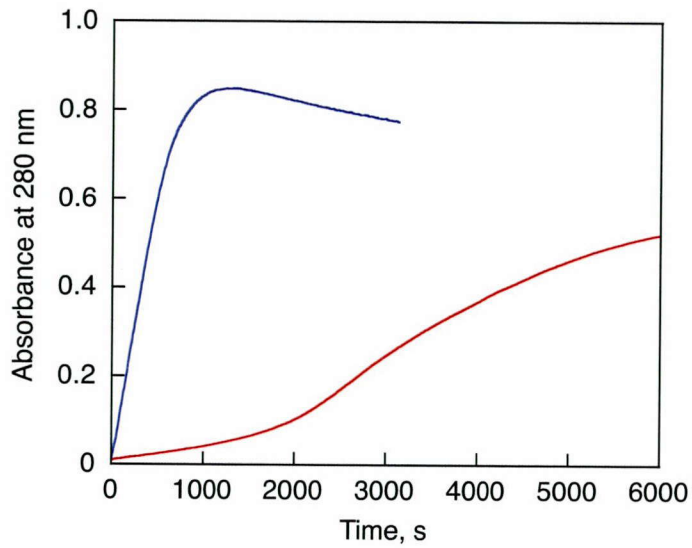

Figure 10. Time courses of the absorbance at 280 nm due to $[Fe^{IV}(O)(TMC)]^{2+}$ in the reaction of $[Fe^{II}(TMC)]^{2+}$ (0.10 mM) with isopropanol (0.26 M) in air-saturated (red) and O_2-saturated (blue) MeCN at 298 K.

Conclusion

In summary, we have demonstrated that formation of a non-heme iron(IV)-oxo complex by reductive O_2 activation with isopropanol proceeds via autocatalytic radical chain reactions in which hydroperoxyl radical is the chain carrier to produce hydrogen peroxide, which results in autocatalysis. The chain reactions are prohibited by a radical scavenger, which traps the chain carrier radical. This study provides a novel autocatalytic radical chain pathway for formation of high-valent metal-oxo complexes.

Scheme 3. Autocatalytic Radical Chain Mechanism for Formation of $[Fe^{IV}(O)(TMC)]^{2+}$ in Oxidation of $[Fe^{II}(TMC)]^{2+}$ with O_2 and Isopropanol

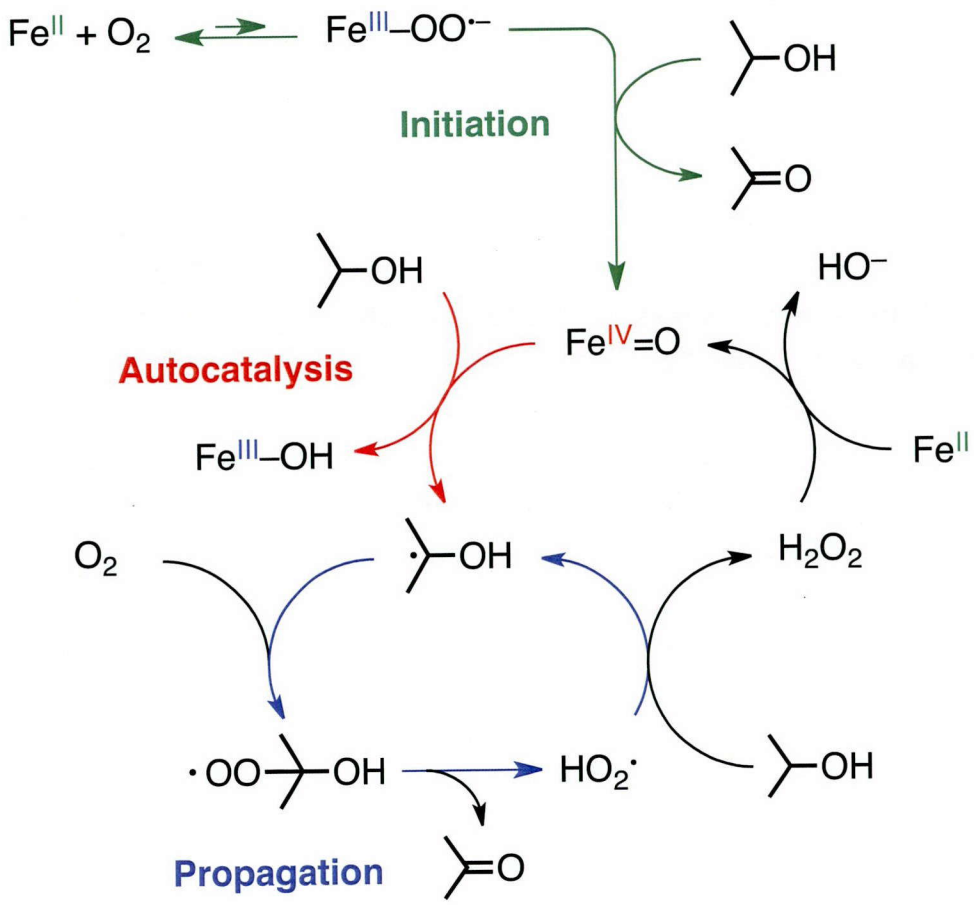

References

(1) (a) Krebs, C.; Fujimori, D. G.; Walsh, C. T.; Bollinger, J. M. Jr. *Acc. Chem. Res.* **2007**, *40*, 484. (b) Hoffart, L. M.; Barr, E. W.; Guyer, R. B.; Bollinger, J. M. Jr.; Krebs, C. *Proc. Natl. Acad. Sci. U.S.A.* **2006**, *103*, 14738. (c) Galonic, D. P.; Barr, E. W.; Walsh, C. T.; Bollinger, J. M. Jr.; Krebs, C. *Nat. Chem. Biol.* **2007**, *3*, 113.

(2) (a) Bruijnincx, P. C.; van Koten, G.; Gebbink, R. J. M. K. *Chem. Soc. Rev.* **2008**, *37*, 2716. (b) Kovaleva, E. G.; Lipscomb, J. D. *Nat. Chem. Biol.* **2008**, *4*, 186. (c) Kryatov, S. V.; Rybak-Akimova, E. V. *Chem. Rev.* **2005**, *105*, 2175. (d) Solomon, E. I.; Brunold, T. C.; Davis, M. I.; Kemsley, J. N.; Lee, S. K.; Lehnert, N.; Neese, F.; Skulan, A. J.; Yang, Y. S.; Zhou, J. *Chem. Rev.* **2000**, *100*, 235.

(3) (a) van Eldik, R. *Coord. Chem. Rev.* **2007**, *251*, 1649. (b) Groves, J. T. *Proc. Natl. Acad. Sci. U.S.A.* **2003**, *100*, 3569. (c) Cho, J.; Jeon, S.; Wilson, S. A.; Liu, L. V.; Kang, E. A.; Braymer, J. J.; Lim, M. H.; Hedman, B.; Hodgson, K. O.; Valentine, J. S.; Solomon, E. I.; Nam, W. *Nature*, **2011**, *478*, 502.

(4) (a) Que, L., Jr. *Acc. Chem. Res.* **2007**, *40*, 493. (b) Nam, W. *Acc. Chem. Res.* **2007**, *40*, 522. (c) Hohenberger, J.; Ray, K.; Meyer, K. *Nat. Commun.* **2012**, *3*, 720.

(5) Lee, Y.-M.; Dhuri, S. N.; Sawant, S. C.; Cho, J.; Kubo, M.; Ogura, T.; Fukuzumi, S.; Nam, W. *Angew. Chem., Int. Ed.* **2009**, *48*, 1803.

(6) Kotani, H.; Suenobu, T.; Lee, Y.-M.; Nam, W.; Fukuzumi, S. *J. Am. Chem. Soc.* **2011**, *133*, 3249.

(7) MacBeth, C. E.; Golombek, A. P.; Young, V. G. Jr.; Yang, C.; Kuczera, K.; Hendrich, M. P.; Borovik, A. S. *Science*, **2000**, *289*, 938.

(8) Kim, S. O.; Sastri, C. V.; Seo, M. S.; Kim, J.; Nam, W. *J. Am. Chem. Soc.* **2005**, *127*, 4178.

(9) Hong, S.; Lee, Y.-M.; Shin, W.; Fukuzumi, S.; Nam, W. *J. Am. Chem. Soc.* **2009**, *131*, 13910.

(10) Lee, Y.-M.; Hong, S.; Morimoto, Y.; Shin, W.; Fukuzumi, S.; Nam, W. *J. Am. Chem. Soc.* **2010**, *132*, 10668.

(11) Sono, M.; Roach, M. P.; Coulter, E. D.; Dawson, J. H. *Chem. Rev.* **1996**, *96*, 2841.

(12) Cho, K.; Leeladee, P.; McGown, A. J.; DeBeer, S.; Goldberg, D. P. *J. Am. Chem. Soc.* **2012**, *134*, 7392.

(13) Morimoto, Y.; Park, J.; Suenobu, T.; Lee, Y.-M.; Nam, W.; Fukuzumi, S. *Inorg. Chem.* **2012**, *51*, 10025.

(14) Kochi, J. K. Ed.; *Free Radicals*; Wiley: New York, 1973.

(15) Pestovsky, O.; Bakac, A. *J. Am. Chem. Soc.* **2004**, *126*, 13757.

(16) Rohde, J.-U.; In, J.-H.; Lim, M. H.; Brennessel, W. W.; Bukowski, M. R.; Stubna, A.; Münck, E.; Nam, W.; Que, L., Jr. *Science*, **2003**, *299*, 1037.

(17) Armarego, W. L. F.; Chai, C. L. L. *Purification of Laboratory Chemicals*, 6th ed; Pergamon Press: Oxford, 2009.

(18) Saltzman, H.; Sharefkin, J. G. *Organic Syntheses*; Collect. Vol. V; Wiley: New York, 1973, p 658.

(19) Lee, Y.-M.; Kotani, H.; Suenobu, T.; Nam, W.; Fukuzumi, S. *J. Am. Chem. Soc.* **2008**, *130*, 434.

(20) A similar inhibition effect of a radical scavenger on radical chain reactions has been reported; see: (a) Fukuzumi, S.; Hironaka, K.; Tanaka, T. *J. Am. Chem. Soc.* **1983**, *105*, 4722. (b) Fukuzumi, S.; Kochi, J. K. *J. Org. Chem.* **1980**, *45*, 2654.

(21) (a) Grieman, F. J.; Noell, A. C.; Atta, C. D.-V.; Okumura, M.; Sander, S. P. *J. Phys. Chem. A* **2011**, *115*, 10527. (b) da Silva, G.; Bozzelli, J. W.; Liang, L.; Farrell, J. T. *J. Phys. Chem. A* **2009**, *113*, 8923.

Concluding Remarks and Outlook

In this thesis, the author has described the effect of Lewis acids on iron(IV)-oxo complexes' structure and electron acceptability and the mechanisms of formation of iron(IV)-oxo complexes via reductive activation of oxygen molecule and oxidative activation of water. The results and findings in this work are summarized as follows:

The determination of the crystal structure of a Sc^{3+} ion bound iron(IV)-oxo complex ($[Fe^{IV}(O)(TMC)]^{2+}$–Sc^{3+}) in chapter 1 represented a significant breakthrough in metal-oxygen chemistry. Binding of a positively charged metal ion (Sc^{3+}) to the oxo group of the non-heme iron(IV)-oxo moiety facilitated further reduction. Once the one-electron reduction of a Sc^{3+} bound iron(IV)-oxo complex occurs, the resulting more electron rich iron(III)-oxo moiety binds the cation even more strongly, enhancing the effect of its positive charge and lowering the barrier to the further electron-transfer reduction. As discussed in chapter 1, these findings imply a possible key role that an auxiliary Lewis acid metal ion could play in the Mn_4Ca active-site cluster in PS II, facilitating the two-electron reduction of a Mn(V)-oxo group by water/hydroxide/oxide, i.e., O–O coupling to the peroxide level. Inspired by the findings in chapter 1, Ca^{2+} ion has been suggested to be involved in the modulation of the reduction potentials of the manganese centers in the OEC, localizing the charge and thus facilitating access to the higher oxidation states necessary for efficient O_2 production.[1–4]

In chapter 2, the effects of binding of metal ions to the oxo ligand of an iron(IV)-oxo complex on the redox potential of the iron(IV)-oxo complex and the electron-transfer reactivity have been quantitatively evaluated in light of the Marcus theory of electron transfer. Such control of electron-transfer reactions of metal-oxygen species by metal ion binding has been shown to be a general phenomenon as reported by later works.[5–7] Interestingly, in regard to reductive activation of oxygen, metal ions are also found to have novel activity due to its acidity.[8–10]

Based on the results in chapter 1 and 2, the reaction pathway and products of oxidation of benzyl alcohol derivatives by an iron(IV)-oxo complex was shown to be remarkably changed from a hydrogen atom transfer pathway in the absence of an acid to Sc^{3+} ion-coupled electron transfer pathway in the presence of Sc^{3+} ion depending on the one-electron oxidation potentials of benzyl alcohol derivatives in chapter 3. Such a switch of the reaction pathway by binding of acids (Sc^{3+} ion and proton) to an iron(IV)-oxo complex has later been shown to occur from an oxygen atom transfer pathway from an iron(IV)-oxo complex to thioanisole derivatives in the absence of an acid to proton-coupled electron transfer (PCET) and metal ion-coupled electron transfer

(MCET) pathways.[11,12]

In chapter 4, by examining the effects of proton and metal ions with the same counter anion on the electron-transfer reduction of an iron(IV)-oxo complex and also on the fluorescence spectrum of *N*-methylacridone, the rate enhancement in both PCET and MCET has been quantitatively correlated to the acidity of proton and metal ions. The replacement of proton with deuteron in the PCET reduction of a iron(IV)-oxo complex resulted in an inversed kinetic isotope effect. This is the first unequivocal evidence for the occurrence of concerted transfer of electron and proton to a iron(IV)-oxo complex to form the iron(III)-hydroxo complex.

From chapter 5 to chapter 7, environmental benign formation of high-valent metal-oxo species without peroxides has been established. In contrast to the conclusion in chapter 4, where Brønsted acids have been shown to accelerate the electron transfer reduction of an iron(IV)-oxo complex, Brønsted bases have been demonstrated to promote the formation of iron(IV)-oxo complex via the one-electron oxidation of the iron(III)-hydroxo complex both kinetically and thermodynamically in chapter 5. This is the first example describing proton acceptors effect on kinetics of PCET formation of high-valent metal-oxo species in non-aqueous medium.

In chapters 6 and 7, the formation mechanisms of a iron(IV)-oxo complex from a iron(II) complex by reductive activation of O_2 have been scrutinized. The hydrogen abstraction form a substrate by a iron(III)-superoxo complex, which is produced by electron transfer from a iron(II) complex to O_2, affords an iron(III)-hydroperoxo complex and a substrate radical, which react within the cage to yield an iron(IV)-oxo complex and the oxidized substrate as described in chapter 6. When a free radical is escaped from the cage, autocatalytic radical chain reactions are started to convert a iron(II) complex to the iron(IV)-oxo complex as demonstrated in chapter 7.

New findings about both the formation of a iron(IV)-oxo complex via reductive activation of O_2 and the remarkable enhancement of the oxidizing ability of a iron(IV)-oxo complex by binding of acids (metal ions and proton) in this thesis have paved a new way to develop efficient catalytic systems using environmentally benign oxidants.

References

(1) For structural model of OEC containing Ca^{2+}, see: Kanady, J. S.; Tsui, E. Y.; Day, M. W.; Agapie, T. *Science* **2011**, *333*, 733.

(2) For effect of metal ion on water oxidation reaction, see: Lie, D.; Zahl, A.; Wilson, E. F.; Streb, C.; Nye, L. C.; Meyer, K.; Ivanović-Burmazović, I. *Inorg. Chem.* **2011**, *50*, 9053.

(3) For effect of redox inactive metal ion in metal oxide on its water-oxidation activity, see: Yamada, Y Yano, K.; Hong, D.; Fukuzumi, S. *Phys. Chem. Chem. Phys.* **2012**, *14*, 5753.

(4) Karlin, K. D. *Nature Chem.* **2010**, *2*, 711.

(5) For binding between manganese(V)-oxo complex and zinc ion, see: Leeladee, P.; Baglia, R. A.; Prokop, K. A.; Latifi, R; de Visser, S. P.; Goldberg, D. P. *J. Am. Chem. Soc.* **2012**, *134*, 10397.

(6) For effect of scandium ion of the oxidation of cobalt complex, see: Pfaff, F. F.; Kundu, S.; Risch, M.; Pandian, S.; Heims, F.; Pryjomska-Ray, I.; Haack, P.; Metzinger, R.; Bill, E.; Dau, H.; Comba, P.; Ray, K. *Angew. Chem., Int. Ed.* **2011**, *50*, 1711.

(7) For effect of sodium ion on the electron-transfer property of molybdenum(V) complex, see: Matsumoto, T.; Wakizaka, M.; Yano, H.; Kobayashi, A.; Chang, H.-C.; Kato, M. *Dalton Trans.* **2012**, *41*, 8303.

(8) Park, Y. J.; Ziller, J. W.; Borovik, A. S. *J. Am. Chem. Soc.* **2011**, *133*, 9258.

(9) Lacy, D. C.; Park, Y. J.; Ziller, J. W.; Yano, J.; Borovik, A. S. *J. Am. Chem. Soc.* **2012**, *134*, 17526.

(10) Park, Y. J.; Cook, S. A.; Sickerman, N. S.; Sano, Y.; Ziller, J. W.; Borovik, A. S. *Chem. Sci.* 2012 DOI: 10.1039/c2sc21400h;

(11) For oxidation of thioanisoles in the presence of scandium ion, see: Park, J.; Morimoto, Y.; Lee, Y.-M.; Nam, W.; Fukuzumi, S. *J. Am. Chem. Soc.* **2011**, *133*, 5236.

(12) For oxidation of thioanisoles in the presence of proton, see: Park, J.; Morimoto, Y.; Lee, Y.-M.; Nam, W.; Fukuzumi, S. *J. Am. Chem. Soc.* **2012**, *134*, 3903.

Publication List

Original Papers

1. Crystal Structure of a Metal Ion-Bound Oxoiron(IV) Complex and Implications for Biological Electron Transfer
Shunichi Fukuzumi, Yuma Morimoto, Hiroaki Kotani, Panče Naumov, Yong-Min Lee and Wonwoo Nam
Nature Chem. **2010**, *2*, 756–759. (10.1038/NCHEM.731)

2. Dioxygen Activation by a Non-Heme Iron(II) Complex: Formation of an Iron(IV)-Oxo Complex Via C–H Activation by a Putative Iron(III)-Superoxo Species
Yong-Min Lee, Seungwoo Hong, Yuma Morimoto, Woonsup Shin, Shunichi Fukuzumi and Wonwoo, Nam
J. Am. Chem. Soc. **2010**, *132*, 10668–10670. (10.1021/ja103903c)

3. Metal Ion-Coupled Electron Transfer of a Nonheme Oxoiron(IV) Complex: Remarkable Enhancement of Electron-Transfer Rates by Sc^{3+}
Yuma Morimoto, Hiroaki Kotani, Jiyun Park, Yong-Min Lee, Wonwoo Nam and Shunichi Fukuzumi
J. Am. Chem. Soc. **2011**, *133*, 403–405. (10.1021/ja109056x)

4. Mechanistic Borderline of One-Step Hydrogen Atom Transfer Versus Stepwise Sc^{3+}-Coupled Electron Transfer from Benzyl Alcohol Derivatives to a Non-Heme Iron(IV)-Oxo Complex
Yuma Morimoto, Jiyun Park, Tomoyoshi Suenobu, Yong-Min Lee, Wonwoo Nam and Shunichi Fukuzumi
Inorg. Chem. **2012**, *51*, 10025–10036. (10.1021/ic3016723)

5. Effects of Proton Acceptors on Formation of a Non-Heme Iron(IV)-Oxo Complex via Proton-Coupled Electron Transfer
Yusuke Nishida, Yuma Morimoto, Yong-Min Lee, Wonwoo Nam and Shunichi Fukuzumi
Inorg. Chem. in press

6. Radical Chain Pathway in Formation of an Iron(IV)-Oxo Complex by Oxidation of an Iron(II) Complex with Dioxygen and Isopropanol
Yuma Morimoto, Yong-Min Lee, Wonwoo Nam and Shunichi Fukuzumi

Chem. Commun. ASAP (10.1039/c3cc38727e)

7. Proton-Coupled Electron Transfer vs. Metal Ion-Coupled Electron Transfer in Electron-Transfer Reduction of an Iron(IV)-Oxo Complex
Yuma Morimoto, Yong-Min Lee, Wonwoo Nam and Shunichi Fukuzumi
Submitted to Chem. Commun.

Perspective

Mechanisms of Metal Ion-Coupled Electron Transfer
Shunichi Fukuzumi, Kei Ohkubo and Yuma Morimoto
Phys. Chem. Chem. Phys. **2012**, *14*, 8472–8484. (10.1039/C2CP40459A)

Supplementary

1. Metal Ion Effect on the Switch of Mechanism from Direct Oxygen Transfer to Metal Ion-Coupled Electron Transfer in the Sulfoxidation of Thioanisoles by a Nonheme Iron(IV)-Oxo Complex
Jiyun Park, Yuma Morimoto, Yong-Min Lee, Wonwoo Nam and Shunichi Fukuzumi
J. Am. Chem. Soc. **2011**, *133*, 5236–5239. (10.1021/ja200901n)

2. Scandium Ion-Enhanced Oxidative Dimerization and *N*-Demethylation of *N,N*-Dimethylanilines by a Non-Heme Iron(IV)-Oxo Complex
Jiyun Park, Yuma Morimoto, Yong-Min Lee, Youngmin You, Wonwoo Nam and Shunichi Fukuzumi
Inorg. Chem. **2011**, *50*, 11612–11622. (10.1021/ic201545a)

3. Proton-Promoted Oxygen Atom Transfer vs Proton-Coupled Electron Transfer of a Non-Heme Iron(IV)-Oxo Complex
Jiyun Park, Yuma Morimoto, Yong-Min Lee, Wonwoo Nam and Shunichi Fukuzumi
J. Am. Chem. Soc. **2012**, *134*, 3903–3911. (10.1021/ja211641s)

4. Electron-Transfer Properties of a Nonheme Manganese(IV)-Oxo Complex Acting as a Stronger One-Electron Oxidant Than the Iron(IV)-Oxo Analogue
Heejung Yoon, Yuma Morimoto, Yong-Min Lee, Wonwoo Nam and Shunichi Fukuzumi
Chem. Commun. **2012**, *48*, 11187–11189. (DOI: 10.1039/c2cc36291k)

Presentations at International Conferences

ICBIC 14th: The 14th International Conference of Biological Inorganic Chemistry
Structure and reactivity of metal ion complexes of non-heme iron(IV)-oxo species
Yuma Morimoto, Hiroaki Kotani, Panče Naumov, Yong-Min Lee, Wonwoo Nam and Shunichi Fukuzumi
J. Biol. Inorg. Chem. **2009**, *14*, S108.

60CCCO: 60th Anniversary Conference on Coordination Chemistry in Osaka
Reaction Mechanism of Non-heme Oxoiron(IV) Species: Metal-Ion Coupled Electron Transfer and C-H bond Cleavage Reaction
Yuma Morimoto, Hiroaki Kotani, Yong-Min Lee, Wonwoo Nam and Shunichi Fukuzumi

Pacifichem 2010: International Chemical Congress of Pacific Basin Societies
Effect of Metal Ions on Electron-Transfer Properties of Oxoiron Species: Control of Reaction Mechanisms by Selecting Metal Ion
Yuma Morimoto, Hiroaki Kotani, Yong-Min Lee, Wonwoo Nam and Shunichi Fukuzumi

ICBIC 15th: The 15th International Conference of Biological Inorganic Chemistry
Scandium Ion-Coupled Electron Transfer Oxidation of Benzyl Alcohol Derivatives with a Non-Heme Oxoiron(IV) Complex
Yuma Morimoto, Hiroaki Kotani, Yong-Min Lee, Wonwoo Nam and Shunichi Fukuzumi
J. Biol. Inorg. Chem. **2011**, *16*, S691.

GCOEBEC-11: The 11th Global COE International Symposium: Bio-Environmental Chemistry
Mechanism Borderline between One-Step Hydrogen Atom Transfer and Stepwise Electron and Proton Transfer from Benzyl Alcohol Derivatives to Non-heme Oxoiron(IV) Species Activated by Sc^{3+}
Yuma Morimoto and Shunichi Fukuzumi

AsBIC IV: The 6th Asian Biological Inorganic Chemistry Conference
Formation of a non-heme iron(IV)-oxo complex by one-electron reduction of an

iron(III)-hydroperoxo complex
Yuma Morimoto, Wonwoo Nam and Shunichi Fukuzumi

Others

Awards

第 61 回錯体化学討論会 学生講演賞
「非ヘム鉄四価錯体によるヘンシルアルコール類のスカンシウムイオン共役電子移動酸化反応」

GCOEBEC-11 Excellent Presentation Award
''Mechanism Borderline between One-Step Hydrogen Atom Transfer and Stepwise Electron and Proton Transfer from Benzyl Alcohol Derivatives to Non-heme Oxoiron(IV) Species Activated by Sc^{3+}*''*

Invited Lecture

錯体化学若手の会　第 61 回近畿支部勉強会
「金属イオンを用いた高原子価鉄オキソ錯体の反応性の制御」

Acknowledgements

I would like to express my gratitude to Professor Shunichi Fukuzumi for his kind guidance, invaluable suggestions and encouragement throughout this study. What I have acquired under his direction, both material and immaterial, will be invaluable to me throughout my life.

My gratitude also goes to Dr. Tomoyoshi Suenobu and Dr. Hiroaki Kotani for their excellent suggestions and continuous encouragement throughout this study. They always listened to me, a fledgling chemist, and assisted me in many ways.

Similarly, I am deeply indebted to Prof. Takahiko Kojima, Dr. Yusuke Yamada, and Dr. Kei Ohkubo for taking time to give me useful suggestions.

I appreciate Prof. Wonwoo Nam, and Dr. Lee Yong-Min motivating me warmly and continually.

Special thanks to all the members of Fukuzumi laboratory for their help, valuable suggestions, useful discussions and friendship. There are not enough words to express how grateful I am to you all.

I am also grateful to the Global COE program "Global Education and Research Center for Bio-Environmental Chemistry" and JSPS of the ministry of Education, Culture, Sports, Science and Technology, Japan for their support through scholarships.

Finally, I wish to express my sincerest acknowledgement for continuous encouragement and support given by my friends and family, Hiromi Morimoto, Tatsuma Morimoto, Yae Morimoto, and Hiroyuki Morimoto.

Osaka, Japan
March, 2013

Yuma Morimoto

Laboratory of Physical Chemistry for Life Science at
Department of Material and Life Science,
Division of Advanced Science and Biotechnology,
Graduate School of Engineering, Osaka University